

Effective Interactions and Properties of Model Colloidal Suspensions: Integral Equation Theory and Molecular Dynamics Simulation Study

THESIS

Submitted in partial fulfillment
of the requirements for the degree of
DOCTOR OF PHILOSOPHY

by

UDAY KUMAR PADIDELA

Under the Supervision of
Dr. RAGHU NATH BEHERA



BITS Pilani
Pilani | Dubai | Goa | Hyderabad

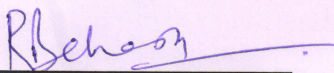
**BIRLA INSTITUTE OF TECHNOLOGY AND
SCIENCE PILANI (RAJASTHAN) INDIA
2018**

BIRLA INSTITUTE OF TECHNOLOGY AND SCIENCE, PILANI

CERTIFICATE

This is to certify that the thesis entitled **“Effective Interactions and Properties of Model Colloidal Suspensions: Integral Equation Theory and Molecular Dynamics Simulation Study”** submitted by Uday Kumar Padidela, ID No. 2012PHXF0406G for award of Ph.D. degree of the Institute embodies original work done by him under my supervision.

Signature of the Supervisor:



Name in capital letters:

Dr. RAGHU NATH BEHERA

Designation:

Associate Professor

Date: 25/02/2019

ACKNOWLEDGEMENTS

I express my deep sense of gratitude to my Supervisor and Mentor Dr. Raghu Nath Behera, Associate professor, at the Department of Chemistry, BITS-Pilani K.K. Birla Goa Campus, for his guidance, motivation and encouragement throughout the duration of my research work. His inputs have helped me a lot for the progress of my research work. Without his support this thesis wouldn't have shaped well and come to an end.

I would like to thank Hon'ble Vice Chancellor Professor Souvik Bhattacharya, BITS Pilani, the campus Director Professor G. Raghurama, Ex-Vice Chancellor Professor B.N. Jain, Prof. S.K. Verma, DEAN, ARD, BITS-Pilani, Prof. Sunil Bhand, Dean SRCD, Prof. P. K. Das, Former Associate Dean ARD, Prof. Bharat Deshpande, Associate Dean AGSRD and Prof. S. D. Manjare, former in-charge, RCED for all their support and help.

I sincerely thank my Doctor of Advisory Committee (DAC) members, Prof. Anjan Chattopadhyay and Prof. Ranjan Dey, Department of Chemistry, for their kind support and valuable suggestions. I would also like to thank Dr. Venkatesan Thimmakondur, former DAC member for the suggestions during his stay and tenure at BITS. I would like to thank DRC Convener Dr. Mainak Banerjee.

I'm indebted to the support provided by Dr. Ramprasad Joshi Assistant professor, Department of Computer Science, Faculty-In-Charge for Kosambi server (Computational facility)

My sincere thanks and acknowledgements to the CSIR for awarding me fellowship during my research work.

This work would not have been possible without the help and support of all the research scholars: Tarun Khanna, Selvaganapathy, Ashu Sharma, Gargi, Dayanand, Barani, Akanksha Saini, Praveen Saini, Pragnya, Vikas Kumar, Zigmee, Gokul, Dip Ratan Khandare, Shankar, Himank, Prasath, Priyadarshini Parakh, Souvik, Kanchanmala Deshpande, Subhenjit, Bhanu, Aruna, Barun, Moitra, Madhurya, , Monsoor, Ketaki, Oruganti Yasaswini, Riaz basha, Kanika, Divya, Nupur, Pallavee, Chitra, Mansi, Rakesh, Om Prakash, Shruti, Ansie, Geethanjali, Ram Ko, Rajesh, Gowdaman, Chandu, Kabilan, Angela, Akhila, Mouna,

Akanksha, Venkatesan, Anu Roshni, Dhiren, Vishnu, Saif, Praveen, Bharath, Shamanth, Lakshmi chechi, Bindu, Divya Nandamuri.

I also thank Non-teaching staff of Chemistry Department Digamber, Princy, Sunaina, Pratap for their help and support.

Venka Reddy, RDO (Warangal Urban District) for his support and timely help.

I am also thankful to my dearest friend Srikanth Venukanti for his constant help and motivation during this journey. A special mention to this lady Vidhyalakshmi for her timely help and who drove me hard with her inspiring words

I owe my warmest gratitude to my “ADUR” and “BLD” group, Ajay, Deepthi and Ramya for their belief, mental support, encouragement and inspiration which helped me to overcome my tough times.

I am grateful to my parents, my brothers Pranay, Arun and sister Ramya (Machi) for their belief, motivation and perseverance which helped me to complete this work successfully.

Uday Kumar Padidela

Abstract

Colloidal suspensions of charged macroparticles dissolved in electrolyte solutions have received long time scientific interests. They are quite complex systems consisting of mesoscopic polyions (the colloid) and the microscopic solvent molecules and ions. Under most physical conditions, there exists a clear separation of time/length-scales between the microscopic degrees of freedom (such as solvent particles, counter/co-ions and salt etc.) and the mesoscopically sized colloidal particles. This poses significant challenges for theoretical investigation of colloidal suspensions; but makes them excellent model systems to study many phenomena in soft-condensed matter physics, such as melting, freezing and glass transitions, etc. In this work, we study the colloidal suspensions using the description of solvent-solvent, solvent-colloid and colloid-colloid correlations from the formalism of statistical thermodynamics of liquids and asymmetrical mixtures. Molecular dynamic simulations and Integral equation theories have been used to find the correlation functions. Formulae expressing properties in terms of correlation functions are well known.

Chapter 1 introduces the importance and modelling of colloidal suspensions, basic statistical mechanics leading to pair correlation functions and property calculations, Integral Equation theory, Molecular Dynamics simulation, concept of effective pair potential etc. The gaps in existing research and objectives of this research work have also been discussed.

In Chapter 2, we studied asymmetric binary fluid mixtures using molecular dynamics simulation. The asymmetries are either in particle size, charge, or mass alone and their combinations. Systematic variations in the pair correlation functions and different properties have been observed as a function of size, charge and mass asymmetry. As the size and/or charge increases, the pair correlation functions shift to larger inter-particle distances indicating increase in repulsion between particles. Both the energy as well as the pressure of the system with neutral particles decreases with increase in size asymmetry, an effect similar to decrease in density of the system. With increase in the charge asymmetry, the interactions between the particles become long ranged and the magnitude of excess free energy increases. For a given charge asymmetry, higher excess free energy was found for size asymmetric mixture than that of size symmetric case, possibly due to reduction in charge density. The

self-diffusion coefficients were found to decrease with increase in size, charge and mass asymmetries. Arrhenius-type behavior was observed for the diffusion coefficient. Empirical relations expressing diffusion coefficients of systems having more than one-type of asymmetries in terms of diffusion coefficients of systems having asymmetry of only one-type, have been presented.

In chapter 3, we have extended our molecular dynamics simulation study to model colloidal suspensions in bulk solutions as well as in between two parallel walls. The simulations were carried out in a wide range of colloid charges ($10e$ - $100e$), diameters (20 nm-100 nm), concentrations ($0.484 \mu\text{M}$ - $2.42 \mu\text{M}$) using a two-component (salt free) and a three component (with added salt) ($1.9 \mu\text{M}$ - $7.7 \mu\text{M}$) primitive model. Systematic variations in pair correlation functions, effective colloid potentials, thermodynamic properties and self-diffusion coefficients were observed with system parameters. The depth of minima in the effective colloid-colloid pair potential were found to increase with increase in colloid charge, size and concentration. However, the positions of the minima shift to lower inter-colloid distances with increase in colloid size and concentration but remain more or less unaltered with increase in colloid charge. For the cases of colloid suspensions in between two parallel walls, the density profile functions become oscillatory indicating ordering/layering of colloids. The oscillatory behavior was found to be pronounced for colloid with neutral walls or one positive and one negative wall. Systematic variations in the density profile of small particles/ions were also observed. The self-diffusion coefficients of neutral colloids were found to be higher than those of charged ones, irrespective of the nature of the walls.

In Chapter 4, we have investigated the colloidal suspensions using the formalism of Integral equation theory. The Ornstein Zernike Equation have been solved along with three different closure approximations: Hypernetted Chain (HNC), Percus Yevick (PY) and Martynov Sarkisov (MS) using Newton-GMRES algorithm. The effective colloid potentials become repulsive with increase in colloid size for a two-component (salt free) system. However, on addition of salt (for a three-component system), the effective colloid potentials become attractive. With increase in colloid charge and concentration, the effective colloid potentials become attractive for both two-component as well as three-component systems. The potential of mean force becomes attractive with increase in size, charge and concentration of colloid in

HNC theory for two-component system. The three-component systems behave similar to those of two-component systems with variation in colloid size and concentration with opposite trends which were being observed with charge variation. With increase in size, charge and concentration of the colloidal particle, HNC theory performs better than PY and MS theory. HNC results show good agreement with MD simulation results for colloid size = 100nm and charge = $-25e$, whereas PY results shows good agreement only in three-component (added salt) systems. Generally, the integral equation results deviate substantially from those of simulation results. Among the studied systems and closures, HNC results seem to be closer to simulations than PY and MS results.

The overall conclusions and future scope of research have been given in chapter 5.

BRIEF CONTENTS

Chapter	Title	Page
1	Introduction and Review of Literature	1
2	Molecular Dynamics simulation study of asymmetric binary mixtures	34
3	Structure and effective interactions of model colloidal suspensions	62
4	Performance of HNC, PY and MS integral equations on model colloidal suspensions: Comparison with MD results	104

TABLE OF CONTENTS

	PAGE
Thesis title page (Annexure I)	
Certificate from Supervisor (Annexure II)	
Acknowledgements	
Abstract	i
Table of contents	iv
List of tables	xi
List of figures	xii
Chapter 1: Introduction and Review of Literature	
1.1 Introduction	2
1.2. Statistical Mechanics-Ensembles, Partition function & averages	3
1.3. Molecular Simulations	6
1.3.1. Monte Carlo Simulation	6
1.3.2. Molecular Dynamics Simulation	6
1.3.3. Reduced Units	7
1.3.4. System Size and periodic boundary conditions	7
1.3.5. Finite difference techniques	9
1.3.6. Pair Potential	10
1.4. Integral Equation Theory	11
1.4.1. Closure relations	12
1.4.1.1. Hypernetted Chain Approximation	12
1.4.1.2. Percus Yevick Approximation	13
1.4.1.3. Martynov Sarkisov Approximation	13
1.5. Pair potential and screening	14
1.6. Modeling of colloidal suspensions on different levels	17
1.7. Literature survey	19

1.8. Gaps in the existing research	21
1.9. Objectives of the Research Work	21
1.10. Summary of Thesis	21
1.11. References	22

Chapter 2: Molecular Dynamics simulation study of asymmetric binary mixtures

2.1. Introduction	35
2.2. Model and simulation details of asymmetric binary mixture	36
2.2.1. Details of simulation and choice of simulation parameters	38
2.3. Results and Discussions	40
2.3.1. Pair correlation functions	40
2.3.1.1. System with only size asymmetry	40
2.3.1.2. System with only charge asymmetry	43
2.3.1.3. System with only mass asymmetry	45
2.3.1.4. System with charge and size asymmetry	46
2.3.1.5. Thermodynamic properties	47
2.3.2. Self-diffusion coefficients	48
2.3.2.1. System with only mass asymmetry	49
2.3.2.2. System with only size/charge asymmetry	52
2.3.2.3. System with more than one type of asymmetry	52
2.3.2.4. Empirical relations	54
2.3.2.5. Estimation of System-size dependence of diffusion coefficient	55
2.4. Conclusion	56
2.5. References	56

Chapter 3: Structure and effective interactions of model colloidal suspensions

3.1. Introduction	63
A) Model of colloidal suspensions in bulk solution	
3.2. Model and simulation details	64
3.2.1. System studied	64

3.2.2. Calculation of effective potential	65
3.3. Results and discussions	67
3.3.1. Variation of colloidal charge	67
3.3.2. Variation of colloid size	72
3.3.3. Variation of colloid concentration	76
3.3.4. Effect of counterion valency	81
3.3.5. Effect of salt concentration	84
3.3.6. Variation in thermodynamic properties	86
3.3.6.1. Isothermal compressibility	87
3.3.7. Self-diffusion coefficients	88
B) Model of colloidal suspensions under confinement	
3.4. Overview	89
3.5. Model and simulation details	90
3.6. Density profile of colloids under confinement	91
3.7. Self-diffusion coefficients	95
3.8. Conclusion	97
3.9. References	97
Chapter 4: Performance of HNC, PY and MS integral equations on model colloidal suspensions: Comparison with MD results	
4.1. Introduction	105
4.2. Model and Methods	106
4.2.1. Integral Equation theory, HNC, PY and MS closures	106
4.2.2. Newton GMRES algorithm	107
4.3. Results and Discussions	109
4.3.1. Two-component colloidal system: HNC Results	109
4.3.1.1. Variation in size of colloid	109
4.3.1.1.1. Pair correlation functions	109
4.3.1.1.2. Direct Correlation functions	110
4.3.1.1.3. Effective potential and potential of mean force	111

4.3.1.1.4. Effective direct correlation functions	112
4.3.1.2. Variation in colloid charge	112
4.3.1.2.1. Pair correlation functions	112
4.3.1.2.2. Direct Correlation functions	113
4.3.1.2.3. Effective potential and potential of mean force	114
4.3.1.2.4. Effective direct correlation functions	115
4.3.1.3. Variation in colloid concentration	116
4.3.1.3.1. Pair correlation functions	116
4.3.1.3.2. Direct Correlation functions	117
4.3.1.3.3. Effective potential and potential of mean force	118
4.3.1.3.4. Effective direct correlation functions	118
4.3.2. Comparison of different closure approximations and molecular dynamics (MD) result in two-component colloidal system	119
4.3.2.1. Size Variation	119
4.3.2.1.1. Effective potential	119
4.3.2.1.2. Potential of mean force	120
4.3.2.1.3. Effective direct correlation function	121
4.3.2.2. Charge Variation	121
4.3.2.2.1. Effective potential	121
4.3.2.2.2. Potential of mean force	122
4.3.2.2.3. Effective direct correlation function	123
4.3.2.3. Concentration Variation	124
4.3.2.3.1. Effective potential	124
4.3.2.3.2. Effective direct correlation function	124
4.3.3. Three-component system: HNC Results	125
4.3.3.1. Variation in colloid size	125
4.3.3.1.1. Pair correlation functions	125
4.3.3.1.2. Direct correlation functions	126

4.3.3.1.3. Effective direct correlation function	127
4.3.3.1.4. Effective potential and potential of mean force	128
4.3.3.2. Variation in colloid charge	129
4.3.3.2.1. Pair correlation functions	129
4.3.3.2.2. Direct correlation functions & effective direct correlation function	130
4.3.3.2.3. Effective potential and potential of mean force	131
4.3.3.3. Variation in colloid concentration	131
4.3.3.3.1. Pair correlation functions	131
4.3.3.3.2. Direct correlation functions & Effective direct correlation function	132
4.3.3.3.3. Effective potential and potential of mean force	133
4.3.4. Comparison of different closures and MD result in three-component colloidal system	134
4.3.4.1. Size Variation	134
4.3.4.1.1. Effective direct correlation functions	134
4.3.4.1.2. Effective potential	135
4.3.4.1.3. Potential mean force	136
4.3.4.2. Charge Variation	136
4.3.4.2.1. Effective potential	136
4.3.4.2.2. Potential mean force	137
4.3.4.2.3. Effective direct correlation function	138
4.3.4.3. Concentration Variation	139
4.3.4.2.1. Effective potential	139
4.3.4.2.2. Effective direct correlation function	139
4.3.4.2.3. Potential mean force	140
4.4. Conclusion	141

4.5. References	141
-----------------	-----

Chapter 5

5.1. Conclusion & Future Scope of Work	144
--	-----

List of Publications and Presentations- Appendix I

Brief Biography of the Candidate- Appendix II

Brief Biography of the Supervisor- Appendix III

Copy Rights Permissions-Appendix IV

LIST OF TABLES

Table	Table Heading	Page
	Chapter 2	
Table 2.1	The peak height of pair-correlation functions for various mass asymmetries at different temperatures for neutral binary size-symmetric mixture. The packing fraction of the system is 0.0848. Note that $g_{00} = g_{10} = g_{11}$.	45
Table 2.2	Estimated Arrhenius parameters (Equation 2.9), the activation Energy and pre-factor (D_0), for different mass asymmetries (μ) for neutral binary size-symmetric mixture.	51
	Chapter 3	
Table 3.1	The position (r/σ_{00}) and depth of the minima of $\beta V^{eff}(r)$ and $\beta W_{00}(r)$ as a function of colloid charge for two component (salt free) and three component ($C_s = 4.484 \mu\text{M}$) systems. Fixed parameters: $\sigma_0 = 32\text{nm}$, $C_0 = 0.9681 \mu\text{M}$.	70
Table 3.2	The position (r/σ_{00}) and depth of the minima of $\beta V^{eff}(r)$ and $\beta W_{00}(r)$ as a function of colloid size for two-component (salt free) and three-component ($C_s = 4.484 \mu\text{M}$) systems. Fixed parameters: $Z_0 = -25e$, $C_0 = 0.9681 \mu\text{M}$.	75
Table 3.3	Comparison of peak positions and peak heights of structure factor $S_{00}(k)$ obtained experimentally by Cebula et al. [35] with our system parameters. The experimental parameters are $\sigma_0 = 32 \text{ nm}$, $Z_0 = -200e$ whereas our parameters are $\sigma_0 = 32 \text{ nm}$, $Z_0 = -25e$.	77
Table 3.4	The position (r/σ_{00}) and depth of the minima of $\beta V^{eff}(r)$ and $\beta W_{00}(r)$ as a function of colloid concentration for two component (salt free) and three component ($C_s = 4.484 \mu\text{M}$) systems. Fixed parameter: $\sigma_0 = 32\text{nm}$, $Z_0 = -25e$.	80

LIST OF FIGURES

Figure	Figure legend	Page
Chapter 1		
Figure 1.1	Schematic representation of periodic boundary conditions	8
Chapter 2		
Figure 2.1	Plot showing equilibration and production steps: a) reduced temperature vs time steps b) Total energy vs time steps with mass asymmetry ($\mu = 125$), size asymmetry ($\sigma_r = 1.0$) and box length of the system 180\AA .	39
Figure 2.2	Variation of the interaction potential with distance at different Bjerrum lengths (L_B) for the system with charge asymmetry ($z_r = 5.0$), size asymmetry ($\sigma_r = 5.0$) and no mass asymmetry ($\mu=1.0$); (a) Total potential (WCA + Coulomb), (b) Only the Coulomb potential.	40
Figure 2.3	Variation of pair-correlation functions with size asymmetry ($\sigma_r = 2.0$ to 10.0) for neutral binary mixture: (a) $g_{00}(r)$, (b) $g_{01}(r)$ and (c) $g_{11}(r)$. Other parameters: packing fraction (η) = 0.25 , no mass asymmetry ($\mu= 1.0$).	41
Figure 2.4	The variation of 0-0 structure factor with size asymmetry ($\sigma_r = 2.0$ to 10.0) for the neutral binary mixture. Other parameters are same as in figure 2.3.	42
Figure 2.5	Plot of pair-correlation function for size symmetric ($\sigma_r = 1.0$) and size asymmetric ($\sigma_r = 2.52$) neutral binary mixture. Other parameters: packing fraction (η) = 0.075 , no mass asymmetry ($\mu= 1.0$).	42
Figure 2.6	Variation of pair-correlation functions with different charge asymmetry ($z_r = 1.0$ to 10.0) for the binary mixture: (a) $g_{00}(r)$, (b) $g_{01}(r)$ and (c) $g_{11}(r)$. There is no mass asymmetry ($\mu=1.0$) and no size asymmetry ($\sigma_r=1.0$).	43
Figure 2.7	a) Plot of probability of finding a 0-type particle around another 0-	44

	type particle with different charge asymmetry ($z_r = 1.0$ to 10.0). b) Shift in the position of the first peak of the pair-correlation functions (g_{00} and g_{01}) for the charged system from the corresponding uncharged system. (diameter of both the particles = 10\AA , Charge Density is in $e/\text{\AA}^3$, $e = 1.6 \times 10^{-19}$ coulombs).	
Figure 2.8	Variation of the pair-correlation functions ($g(r)$) and 0-0 structure factor for size asymmetry ($\sigma_r = 5.0$) and different charge asymmetry ($z_r = 1.0$ to 3.0). There is no mass asymmetry ($\mu = 1.0$).	46
Figure 2.9	Variation of the reduced (a) energy (E^*) and (b) pressure (P^*) with size asymmetry for neutral binary system with mass symmetric ($\mu = 1.0$).	47
Figure 2.10	Variation of reduced excess free energy (\blacksquare) and osmotic coefficient (\bullet) with charge asymmetry (z_r) for the systems with size asymmetry ($\sigma_r = 5.0$, solid lines) and without size asymmetry ($\sigma_r = 1.0$, broken lines).	48
Figure 2.11	Plot of (a) mean square displacement (MSD) and (b) diffusion coefficient (D in $\text{\AA}^2/\text{ps}$) with mass asymmetry (μ) for size symmetric ($\sigma_r = 1.0$) neutral binary mixture at 300K with packing fraction ($\eta = 0.08481$).	49
Figure 2.12	The variation of diffusion coefficient (D) of heavier particle with mass asymmetry (μ) at different temperatures for size symmetric ($\sigma_r = 1.0$) neutral binary mixture with packing fraction ($\eta = 0.08481$).	50
Figure 2.13	Arrhenius plot ($\ln D$ vs $1/T$) of neutral binary mixture for different mass asymmetry (μ). Other parameters are same as given in figure 2.12.	51
Figure 2.14	The variation of diffusion coefficients of both the particles with size asymmetry ($\sigma_r = 2.5$ to 10.0) for the mass symmetric ($\mu = 1.0$) neutral binary mixture.	52

Figure 2.15	The variation of diffusion coefficients with charge asymmetry for binary mixture (a) with different size asymmetry ($\sigma_r = 1.0$ and 5.0), for 0-type particle (b) with mass asymmetry ($\mu = 125$), for both 0-type and 1-type particles. The diffusion coefficients of type 0 particles in figure (b) is multiplied by factor of 10.	53
Figure 2.16	Correlation plots of diffusion coefficients obtained from current simulation and predicted (a) by equation (2.10) and (b) by equation (2.11).	54
Figure 2.17	Variation of self-diffusion coefficient with different simulation box length (L) for the system with $z_r = 5.0$, $\sigma_r = 1.0$, $\mu = 1.0$ and packing fraction (η) = 0.067.	55
Chapter 3		
Figure 3.1	Variation of a) colloid-colloid radial distribution functions $g_{00}(r)$ b) colloid-counterion radial distribution functions $g_{01}(r)$ c) counterion-counterion radial distribution functions $g_{11}(r)$ with charge asymmetry at fixed $\sigma_0 = 32\text{nm}$, $C_0 = 0.968\mu\text{M}$ and $C_s = 0 \mu\text{M}$.	68
Figure 3.2	Variation of Structure factor $S_{00}(k)$ with charge of colloid. The parameters used are same as shown in Figure 3.1.	69
Figure 3.3	Variation of (a) $\beta W_{00}(r)$ and (b) $\beta V^{eff}(r)$ with charge asymmetry at fixed $\sigma_0 = 32\text{nm}$, $C_0 = 0.968\mu\text{M}$ and $C_s = 0 \mu\text{M}$	70
Figure 3.4	Variation of (a) $C_{00}^{eff}(r)$ and (b) $\beta v_s(r)$ with charge asymmetry at fixed $\sigma_0 = 32\text{nm}$, $C_0 = 0.968\mu\text{M}$ and $C_s = 0 \mu\text{M}$	72
Figure 3.5	Variation of a) colloid-colloid radial distribution functions $g_{00}(r)$ b) colloid-counterion radial distribution functions $g_{01}(r)$ c) counterion-counterion radial distribution functions $g_{11}(r)$ with size asymmetry at fixed $Z_0 = -25e$ and $C_0 = 0.968\mu\text{M}$	73
Figure 3.6	Variation of structure factor $S_{00}(k)$ with size of the colloid. The parameters used are same as in Figure 3.5.	74

Figure 3.7	Variation of (a) $\beta W_{00}(r)$ and (b) $\beta V^{eff}(r)$ with size of colloid. Two component system with $Z_0 = -25e$ and $C_0 = 0.968\mu\text{M}$.	74
Figure 3.8	Variation of (a) $c_{00}^{eff}(r)$ and (b) $\beta v_s(r)$ with colloid size. Two component systems with $Z_0 = -25e$ and $C_0 = 0.968\mu\text{M}$.	76
Figure 3.9	Variation of a) colloid-colloid radial distribution functions $g_{00}(r)$ b) colloid-counterion radial distribution functions $g_{01}(r)$ c) counterion-counterion radial distribution functions $g_{11}(r)$ with colloid concentration. Two-component system with $Z_0 = -25e$ and $\sigma_0 = 32\text{nm}$.	77
Figure 3.10	Variation of Structure factor $S_{00}(k)$ with colloid concentration. The parameters used are same as in Figure 3.9.	78
Figure 3.11	Variation of $S_{00}(k)$ with volume fraction (ϕ) for an ion exchanged latex (Cebula et al., [35]). black circle, $\phi = 0.04$; triangle, $\phi = 0.08$; circle, $\phi = 0.13$. with system parameters $\sigma_0 = 32\text{ nm}$, $Z_0 = -200e$. (Copy right is attached).	78
Figure 3.12	Variation of coordination number of colloid with its concentration. The system parameters used are same as in Figure 3.9.	79
Figure 3.13	Variation of (a) $\beta W_{00}(r)$ and (b) $\beta V^{eff}(r)$ with colloid concentration at fixed $Z_0 = -25e$, $\sigma_0 = 32\text{nm}$ and $C_s = 0$	80
Figure 3.14	Variation of (a) $c_{00}^{eff}(r)$ and (b) $\beta v_s(r)$ with colloid concentration at fixed $Z_0 = -25e$, $\sigma_0 = 32\text{nm}$ and $C_s = 0$.	81
Figure 3.15	Plot of radial distribution function a) colloid-colloid b) colloid-counterion c) counterion-counterion with variation of valency of counterion at fixed $\sigma_0 = 32\text{nm}$, $Z_0 = -25e$ and $C_0 = 1.936\mu\text{M}$.	82
Figure 3.16	Plot of radial distribution function a) colloid-colloid b) colloid-counterion c) counterion-counterion with variation of valency of counterion at fixed $\sigma_0 = 2\text{nm}$, $Z_0 = -12e$ and $C_0 = 0.0005\text{ mol dm}^{-3}$.	83

Figure 3.17	Effective potential $\beta V^{eff}(r)$ with variation in valency of counterion with same system parameters as in Figure 3.15.	83
Figure 3.18	Variation of a) colloid-colloid $g_{00}(r)$ b) colloid-counterion $g_{01}(r)$ c) counterion-counterion $g_{11}(r)$ with salt concentration at fixed $Z_0 = -50e$, $\sigma_0 = 32\text{nm}$ and $C_0 = 0.968\mu\text{M}$.	84
Figure 3.19	Variation of (a) $\beta W_{00}(r)$ and (b) $\beta V^{eff}(r)$ with salt concentration at fixed $Z_0 = -50e$, $\sigma_0 = 32\text{nm}$ and $C_0 = 0.968\mu\text{M}$.	85
Figure 3.20	Variation of (a) $c_{00}^{eff}(r)$ and (b) $\beta v_s(r)$ with salt concentration at fixed $Z_0 = -50e$, $\sigma_0 = 32\text{nm}$ and $C_0 = 0.968\mu\text{M}$.	85
Figure 3.21	Plot of reduced excess free energy ($\beta E^{ex}/\rho$) and the osmotic coefficient (Φ_v) with variation in size, charge and concentration of colloid.	86
Figure 3.22	Plot of isothermal compressibility χ_c with variation in (a) charge, (b) size and (c) concentration of colloid particle	87
Figure 3.23	Variation of self - diffusion coefficients of colloid (type 0) as well as counterion (type 1) with variation in (a) charge (b) size and (c) concentration of colloid. The solid line is for two-component system and the dotted line represents three-component system.	89
Figure 3.24	Schematic representation of the simulation box and the positions of walls at the top and bottom of the simulation box.	90
Figure 3.25	Variation of colloid density profiles ($\rho_0(z)$) in neutral colloidal suspensions of different diameters in between two walls: (a) neutral walls, (b) negatively charged walls (symbols: square denotes $\sigma_0 = 20\text{nm}$, triangle denotes $\sigma_0 = 40\text{nm}$ and star denotes $\sigma_0 = 60\text{nm}$).	92
Figure 3.26	Variation of small ion/particle density profiles ($\rho_1(z)$) in neutral colloidal suspensions of different diameters in between two negatively charged walls. Other parameters are same as in Figure 3.25.	92

Figure 3.27	Variation of colloid density profiles ($\rho_0(z)$) with different colloidal charges for the colloidal suspensions of diameter $\sigma_0 = 32\text{nm}$: (a) between two neutral walls, b) between two negatively charged walls (symbols: square indicates $Z_0 = 0$ (neutral), circle indicates $Z_0 = -10e$ and star indicates $Z_0 = -25e$)	93
Figure 3.28	Variation of counterion density profiles ($\rho_1(z)$) with different colloidal charges for the colloidal suspensions of diameter $\sigma_0 = 32\text{nm}$ between two negatively charged walls. Other parameters are same as in Figure 3.27.	94
Figure 3.29	Variation of colloid density profiles ($\rho_0(z)$) with different types of walls for the colloidal suspensions of diameter $\sigma_0 = 20\text{nm}$ and charge $Z_0 = -25e$. (symbols: circle indicates neutral wall on both sides, star indicates negatively charged wall on both sides (- -) and inverted triangle indicates oppositely charged wall on both sides (+ -)).	94
Figure 3.30	Representative plots for variation of (a) colloid-colloid, (b) counterion-counterion, mean-square displacement (MSD) with simulation time for the colloidal suspension ($\sigma_0 = 20\text{nm}$, $Z_0 = -25e$) with different confinement. (the first two lines from the top are for systems with neutral colloid in neutral and charged walls, next three lines are for systems with charged colloid with three kinds of wall described in Figure 3.21).	95
Figure 3.31	Self-diffusion coefficient of colloid (square) and small ion/particle (star) for various colloidal suspensions under confinement: (a) variation with colloid size, (b) variation with colloid charge, (c) variation with different types of walls. The wall types are same as in Fig 3.21	96

Chapter 4

Figure 4.1	Variation of pair correlation functions (a) $g_{00}(r)$, (b) $g_{01}(r)$ and (c)	109
-------------------	---	-----

	$g_{11}(r)$ with colloid diameter at fixed $Z_0 = -25e$ and $C_0 = 0.968 \mu\text{M}$.	
Figure 4.2	Plots of direct correlation functions (a) colloid-colloid $c_{00}(r)$, (b) colloid-counterion $c_{01}(r)$ and (c) counterion-counterion $c_{11}(r)$, as a function of colloid diameter at a fixed $Z_0 = -25e$ and $C_0 = 0.968 \mu\text{M}$.	110
Figure 4.3	Plots of (a) $\beta V^{eff}(r)$ and (b) $\beta W_{00}(r)$, as a function of colloid diameter at fixed $Z_0 = -25e$ and $C_0 = 0.968 \mu\text{M}$.	111
Figure 4.4	Plot of $c_{00}^{eff}(r)$, as a function of colloid diameter at fixed $Z_0 = -25e$ and $C_0 = 0.968 \mu\text{M}$.	112
Figure 4.5	Plots of pair correlation functions (a) colloid-colloid $g_{00}(r)$, (b) colloid-counterion $g_{01}(r)$, (c) counterion-counterion $g_{11}(r)$, as a function of colloid charge at fixed $\sigma_0 = 32\text{nm}$ and $C_0 = 0.968 \mu\text{M}$	113
Figure 4.6	Plots of direct correlation functions (a) colloid-colloid $c_{00}(r)$, (b) colloid-counterion $c_{01}(r)$ and (c) counterion-counterion $c_{11}(r)$, as a function of colloid charge at fixed $\sigma_0 = 32\text{nm}$ and $C_0 = 0.968 \mu\text{M}$.	114
Figure 4.7	Variation of (a) $\beta V^{eff}(r)$ and (b) $\beta W_{00}(r)$ as a function of colloid charge at fixed $\sigma_0 = 32\text{nm}$ and $C_0 = 0.968 \mu\text{M}$.	115
Figure 4.8	Plot of $c_{00}^{eff}(r)$ as function of colloid charge at fixed $\sigma_0 = 32\text{nm}$ and $C_0 = 0.968 \mu\text{M}$.	115
Figure 4.9	Plots of pair correlation functions (a) $g_{00}(r)$, (b) $g_{01}(r)$, (c) $g_{11}(r)$, as a function colloid concentration at fixed $\sigma_0 = 32\text{nm}$ and $Z_0 = -25e$.	116
Figure 4.10	Plots of direct correlation functions (a) colloid-colloid $c_{00}(r)$, (b) colloid-counterion $c_{01}(r)$, (c) counterion-counterion $c_{11}(r)$, as a function of colloid concentration at fixed $\sigma_0 = 32\text{nm}$ and $Z_0 = -25e$.	117
Figure 4.11	Plots of (a) $\beta V^{eff}(r)$ and (b) $\beta W_{00}(r)$, as a function of colloid concentration at fixed $\sigma_0 = 32\text{nm}$ and $Z_0 = -25e$.	118
Figure 4.12	Plot of $c_{00}^{eff}(r)$ as a function of colloid concentration at fixed $\sigma_0 = 32\text{nm}$ and $Z_0 = -25e$.	119

Figure 4.13	Comparison of $\beta V^{eff}(r)$ with different closures: HNC, PY, MS and MD result for two-component system at fixed $Z_0 = -25e$ and $C_0 = 0.9681\mu\text{M}$. (a) $\sigma_0 = 20nm$ (b) $\sigma_0 = 100nm$.	120
Figure 4.14	Comparison of $\beta W_{00}(r)$ with different closures: HNC, PY, MS and MD result for two-component system. Other parameters are same as in Figure 4.13.	120
Figure 4.15	Comparison of $c_{00}^{eff}(r)$ with different closures: HNC, PY, MS and MD result for two-component system. Other parameters are same as in Figure 4.13.	121
Figure 4.16	Comparison of $\beta V^{eff}(r)$ with different closures: HNC, PY, MS and MD result for two-component system at fixed $\sigma_0 = 32nm$ and $C_0 = 0.9681\mu\text{M}$. (a) $Z_0 = -10e$ and (b) $Z_0 = -25e$.	122
Figure 4.17	Comparison of $\beta W_{00}(r)$ with different closures: HNC, PY and MS for two-component system. Other parameters are same as in Figure 4.16.	123
Figure 4.18	Comparison of $c_{00}^{eff}(r)$ with different closures: HNC, PY and MS for two component system. Other parameters are same as in Figure 4.16.	123
Figure 4.19	Comparison of $\beta V^{eff}(r)$ with different closures: HNC, PY and MS for two-component system at fixed $\sigma_0 = 32nm$ and $Z_0 = -25e$. (a) $C_0 = 0.9681\mu\text{M}$ (b) $C_0 = 4.84\mu\text{M}$	124
Figure 4.20	Comparison of $c_{00}^{eff}(r)$ with different closures: HNC, PY and MS for two-component system. Other parameters are same as in Figure 4.19.	125
Figure 4.21	Variation of pair correlation functions (a) $g_{00}(r)$, (b) $g_{01}(r)$ and (c) $g_{11}(r)$ (d) $g_{20}(r)$, (e) $g_{21}(r)$ and (f) $g_{22}(r)$, as a function of colloid diameter at fixed $Z_0 = -25e$, $C_0 = 0.968\mu\text{M}$ and $C_s = 4.84\mu\text{M}$.	126
Figure 4.22	Plots of direct correlation functions (a) $c_{00}(r)$, (b) $c_{01}(r)$ and (c)	127

	$c_{11}(r)$, as a function of colloid diameter. Other parameters are same as in Figure 4.21.	
Figure 4.23	Plot of $c_{00}^{eff}(r)$ as a function colloid diameter. Other parameters are same as in Figure 4.21.	128
Figure 4.24	Plots of (a) $\beta V^{eff}(r)$ and (b) $\beta W_{00}(r)$, as function of colloid diameter. Other system parameters are same as in Figure 4.21.	128
Figure 4.25	Plots of pair correlation functions (a) $g_{00}(r)$, (b) $g_{01}(r)$, (c) $g_{11}(r)$, as a function colloid charge at fixed $\sigma_0 = 32\text{nm}$, $C_0 = 0.968 \mu\text{M}$ and $C_s = 4.84 \mu\text{M}$.	129
Figure 4.26	Plots of direct correlation functions (a) $c_{00}(r)$, (b) $c_{01}(r)$, (c) $c_{11}(r)$ and (d) $c_{00}^{eff}(r)$, as a function of colloid charge. Other parameters are same as in Figure 4.25.	130
Figure 4.27	Plots of (a) $\beta V^{eff}(r)$ and (b) $\beta W_{00}(r)$, as a function of colloid charge. Other parameters are same as in Figure 4.25.	131
Figure 4.28	Plots of pair correlation functions (a) $g_{00}(r)$, (b) $g_{01}(r)$, (c) $g_{11}(r)$, as a function of colloid concentration at fixed $\sigma_0 = 32\text{nm}$ and $Z_0 = -25e$.	132
Figure 4.29	Plot of direct correlation functions (a) $c_{00}(r)$, (b) $c_{01}(r)$, (c) $c_{11}(r)$, and effective direct correlation function (d) $c_{00}^{eff}(r)$ as a function of colloid concentration. Other parameters are same as in Figure 4.28.	133
Figure 4.30	Plots of (a) $\beta V^{eff}(r)$ and (b) $\beta W_{00}(r)$ as function of colloid concentration. Other parameters are same as in Figure 4.28.	134
Figure 4.31	Comparison of $c_{00}^{eff}(r)$ with different closures: HNC, PY and MS for three-component system at fixed $Z_0 = -25e$, $C_0 = 0.968 \mu\text{M}$ and $C_s = 4.836 \mu\text{M}$. (a) $\sigma_0 = 20\text{nm}$ (b) $\sigma_0 = 100\text{nm}$	135
Figure 4.32	Comparison of $\beta V^{eff}(r)$ with different closures: HNC, PY and MS for three-component system. Other system parameters are same as mentioned in Figure 4.31.	135
Figure 4.33	Comparison of $\beta W_{00}(r)$ with different closures: HNC, PY and MS for	136

	three-component system. Other parameters are same as in Figure 4.31.	
Figure 4.34	Comparison of $\beta V^{eff}(r)$ with different closures: HNC, PY and MS for three-component system at fixed $\sigma_0 = 32nm$, $C_0 = 0.9681\mu M$ and $C_s = 4.836 \mu M$. (a) $Z_0 = -10e$ and (b) $Z_0 = -25e$	137
Figure 4.35	Comparison of $\beta W_{00}(r)$ with different closures: HNC, PY and MS for three-component system. Other parameters are same as in Figure 4.34.	138
Figure 4.36	Comparison of $c_{00}^{eff}(r)$ with different closures: HNC, PY and MS for three-component system. Other parameters are same as in Figure 4.34.	138
Figure 4.37	Comparison of $\beta V^{eff}(r)$ with different closures: HNC, PY and MS for three-component system at fixed $\sigma_0 = 32nm$ and $Z_0 = -25e$. (a) $C_0 = 0.9681\mu M$ (b) $C_0 = 9.681\mu M$	139
Figure 4.38	Comparison of $c_{00}^{eff}(r)$ with different closures: HNC, PY and MS for three-component system. Other parameters are same as in Figure 4.37.	140
Figure 4.39	Comparison of $\beta W_{00}(r)$ with different closures: HNC, PY and MS for three-component system. Other parameters are same as in Figure 4.37.	140

Chapter 1
Introduction and Review of Literature

1.1. Introduction

Colloidal suspensions are abundant in everyday experience and are used in countless industrial applications in the chemical, pharmaceutical, biological and food industries. They are quite complex systems consisting of mesoscopic polyion, (the colloid, in nm- μ m range) and the microscopic solvent molecules and counterion/co-ions. The presence of solute components makes it possible to modify at will and on a large scale the static and dynamic macroscopic properties of the whole solution [1]. Different types of macroion interactions, such as long-range repulsive, short-range attractive, hard-sphere-like and dipolar, can be realized simply by changing the system parameters (e.g. quality of solvent, salt concentration etc). Thus colloidal suspensions serve as excellent model systems to study a variety of phenomena (such as melting, freezing and glass transitions, etc.) in soft-condensed matter physics [2] and for making advanced materials [3,4].

The structure of a solution or a suspension of charged macroparticles (colloids) has been of considerable recent interest because of a variety of reasons. They show quite complex phase behavior analogous to simple gases, liquids, solids and glasses. Due to this complex phase behavior colloidal fluids, crystals and glasses have been identified. Mixture of spheres of different size and charge show interesting phase separation. Colloidal suspensions have interesting mechanical and rheological properties [5–7]. They are usually viscoelastic and show marked non-linear responses such as yield stress, shear thinning, shear thickening and dilatancy [8–10]. Their response to external electric field, commonly called electrorheological response is interesting from a fundamental point of view and has considerable technological applications. Electrorheological fluids have found applications as vibration isolators, brakes and clutches [11,12]. In addition, the biological importance of these polymeric fluids brings them to the centerstage of today's research[13].

A basic understanding of these important fluids from a microscopic viewpoint uses methods of statistical mechanics [14,15]. The method we propose to use is to solve an integral equation, the Ornstein-Zernike equation using an approximation in the form of a "closure" relation. An alternative approach for calculation of physical properties is to use the technique of computer simulation [16]. Averages over accessible states are calculated by Monte Carlo

and by Molecular Dynamics simulation. Below we summarize some basic concept of statistical mechanics.

1.2. Statistical Mechanics- Ensembles, Partition function & average [15,17]

Statistical mechanics provides methods of calculating properties of systems with many interacting particles. The mechanical state of such system is not completely specified. The preparation of the system specifies the range of accessible mechanical states in the phase space. For calculation of properties, one assigns weight factors to every point in the accessible region in phase space. The equilibrium property of the system is calculated as a statistically weighted average over the accessible energy eigenstates of the system. If A designates a property, then the average value is

$$\langle A \rangle = \sum_i p_i A_i \quad (1.1)$$

where p_i is the weight factor of the i^{th} accessible energy eigenstate (diagonal elements of density matrix) and A_i is the expectation value of the operator A in this state.

To calculate properties of systems in thermal equilibrium, statistical mechanics uses several classes of accessible states over which averaging is done [18,19]. They are called “ensembles”. A statistical-mechanical ensemble is an arbitrarily large collection of imaginary systems, each of which is a replica of the physical system of interest and characterized by the same macroscopic parameters. The systems of the ensemble differ from each other in the assignment of the coordinates and momenta of the particles. The most widely used are microcanonical, canonical and grand canonical ensembles, although other types are also in use. If E, V (the energy & volume of the system) are fixed, i.e., if the system is isolated, the ensemble that represents the system is microcanonical. The accessible states differ from one another, but share the same E and V . If T, V (the temperature & volume) are fixed, i.e., if the system is mechanically isolated, but thermally interact with a heat bath, then the ensemble that represents the system is called canonical. The members of the canonical ensemble do not have a fixed value of energy but conservation of energy states that they can have any value of energy between zero and the total energy of the heat bath, which is so large that no error is committed if we set it to be infinitely large. Energy is a variable, but number of particles is kept fixed in

a canonical ensemble. In grand canonical ensemble, the quantities that assume a fixed value in every member are μ , V , T (the chemical potential, volume & temperature), the variables now include number of particles. Thus, open systems in thermal equilibrium are represented by grand canonical ensemble.

The weight factor of the members of a microcanonical ensemble is a constant, that of a canonical ensemble is proportional to the Boltzmann factor, $\exp(-\beta E)$, that of a grand canonical ensemble is proportional to the factor, $\exp[-\beta(E - \mu N)]$, where $\beta = 1/kT$ is the inverse temperature. The sum of these weight factors with respect to an arbitrary (and unimportant) zero are called partition functions. The canonical partition function Q_N is given by

$$Q_N = \sum_n \exp(-\beta E_n) \quad (1.2)$$

where n labels an energy eigenstate. The grand canonical partition function Ξ is given by

$$\Xi = \sum_{n,N} \exp[-\beta(E_n - \mu N)] \quad (1.3)$$

Where N specifies the number of particles that can vary. Ξ can be written in terms of Q_N as

$$\Xi = \sum_N \exp(\beta \mu N) Q_N \quad (1.4)$$

The weight factors of accessible energy eigenstates in canonical ensemble is given as

$$p_n = \frac{\exp(-\beta E_n)}{Q_N} \quad (1.5)$$

and those in grand canonical ensemble is given as

$$p_{n,N} = \frac{\exp[-\beta(E_n - \mu N)]}{\Xi} \quad (1.6)$$

Weight factors of a subset of accessible states, when summed, is useful in statistical mechanics. For example, the n -particle distribution function p_n is the sum of weight factors of accessible states which share the characteristics of having fixed location for n -particles:

$$\rho^{(n)}(\mathbf{r}_1, \dots, \mathbf{r}_n) = \frac{N!}{(N-n)!Z_N} \int \dots \int \exp[-\beta U_N(\mathbf{r}^N)] d\mathbf{r}_{n+1} d\mathbf{r}_{n+2} \dots d\mathbf{r}_N \quad (1.7)$$

Where, $Z_N = \int \dots \int \exp[-\beta U_N(\mathbf{r}^N)] d\mathbf{r}_1 d\mathbf{r}_2 \dots d\mathbf{r}_N$, is the configurational integral and $U_N(\mathbf{r}^N)$ is the potential energy of the system. Thus, the quantity $\rho^{(n)}(\mathbf{r}_1, \mathbf{r}_2, \dots, \mathbf{r}_n) d\mathbf{r}_1 \dots d\mathbf{r}_n$ gives the probability of simultaneously finding particle 1 in $d\mathbf{r}_1$ around \mathbf{r}_1 , particle 2 in $d\mathbf{r}_2$ around \mathbf{r}_2 , ..., particle n in $d\mathbf{r}_n$ around \mathbf{r}_n , irrespective of the positions of the remaining $(N-n)$ particles. Because U_N depends on relative coordinates, the positions and orientations of particles is not random. The detail of such molecular interactions determines the structure and dynamics of the system.

For $n = 1$, the one-particle density distribution, or the density profile gives $\rho^{(1)}(\mathbf{r}_1) = \rho = N/V$, the mean number density. In a similar way, the pair density distribution $\rho^{(2)}(\mathbf{r}_1, \mathbf{r}_2)$ can be written. The n -particle correlation function $g^{(n)}$ is expressed in terms of $\rho^{(n)}$ as

$$g^{(n)}(\mathbf{r}^n) = \frac{\rho^{(n)}(\mathbf{r}^n)}{\prod_{i=1}^n \rho^{(n)}(\mathbf{r}_i)} \quad (1.8)$$

For example, the *pair correlation function* $g^{(2)}(r_1, r_2)$ is defined as ($n = 2$)

$$g^{(2)}(\mathbf{r}_1, \mathbf{r}_2) = \frac{\rho^{(2)}(\mathbf{r}_1, \mathbf{r}_2)}{\rho^2} \quad (1.9)$$

For homogeneous, isotropic systems the pair distribution function depends only on the separation $r = |\mathbf{r}_1 - \mathbf{r}_2|$ between the two particles. In this special case, it is then called the *radial distribution function* and written as $g(r)$. A variety of properties has been related to pair correlation function $g(r)$. Some examples are:

(1) Internal energy U :

$$\frac{U}{NkT} = \frac{3}{2} + \frac{\rho}{2kT} \int_0^\infty u(r)g(r)4\pi r^2 dr \quad (1.10)$$

(ρ : number density, $u(r)$: interparticle central potential)

(2) Pressure P :

$$P = \frac{NkT}{V} - \frac{N}{6} \rho \int_0^\infty r \frac{du(r)}{dr} g(r) 4\pi r^2 dr \quad (1.11)$$

(3) Chemical potential μ :

$$\mu = kT \ln \rho \Lambda^3 + \rho \int_0^1 \int_0^\infty u(r) g(r, \xi) 4\pi r^2 d\xi dr \quad (1.12)$$

Where ξ is coupling parameter and has a value 1 for real fluid and $\Lambda = \left(\frac{2\pi mkT}{h^3}\right)^{\frac{3}{2}}$.

1.3. Molecular Simulations

1.3.1. Monte Carlo Simulation

The computer simulation of liquids [16] was carried out to get a detailed information at the microscopic level and this information is converted into macroscopic level is the domain of statistical mechanics. The first computer simulation of the liquid was carried out at Los Alamos National Laboratories in the United States [20]. The Los Alamos computer, called MANIAC, was at that time one of the most powerful computers. Metropolis laid foundations for Monte Carlo (MC) simulations. This method was applied initially to hard discs and spheres [21,22]. MC generates configurations of the system by random sampling. Averages are taken over the configurations, each weighted by the corresponding normalized Boltzmann factor. Uniform sampling of the configurations is impractical, since the Boltzmann factor is negligible but for a few typical configurations of the system, so the so-called importance sampling is used, where configurations are sampled according to the value of the Boltzmann factor; so, the important configurations are generated and contribute to the average. The most popular sampling method is Metropolis algorithm [23,24], which is asymptotic but enjoys the advantageous feature is partition function is not needed.

1.3.2. Molecular Dynamics Simulation

Another indispensable tool used to obtain the accurate solutions for various model systems is Molecular Dynamics (MD) simulation [25]. This describe the solution of the classical

Newton's equations of motion for all particles in fluid. This was first carried out for a system of hard spheres, by Alder and Wainwright in 1957 [26]. Later on, successful attempt was made to solve the equations of motion for Lennard-Jones particles [27–30]. The classical molecular dynamic simulation is a deterministic procedure where the molecular dynamic simulation [16,31] of colloidal suspension is performed by integrating the Newton's equations of motion over time

$$F_i(t) = m_i a_i = m_i \frac{\partial^2 r_i(t)}{\partial t^2}, i = 1, \dots, N \quad (1.13)$$

where m_i is the mass of the particle i , $r_i(t)$ its position at time t , F_i the force acting on particle i and N is the number of particles.

1.3.3. Reduced Units

In simulations, [16] it is necessary to introduce the variables in reduced units. The energies are scaled by characteristic energy in the system ε . The lengths are scaled by the characteristic length σ i.e. particle diameter. The reduced variables are defined as: the reduced density $\rho^* = \rho \sigma^3$, the reduced temperature $T^* = k_B T / \varepsilon$, the reduced pressure $P^* = P \sigma^3 / \varepsilon$ and the reduced time in $t^* = t / \sigma \sqrt{(\varepsilon / M)}$. The reason for introducing the reduced units in simulations is that the many combinations of ρ , ε , T and σ correspond to the same state in reduced units. The use of reduced units minimizes the effects of round off errors and has technical advantage if the given value is in unity. The simulation box is scaled by these lengths which yields a unit box and useful to treat minimum image convention and periodic boundary conditions (section 1.4.4).

1.3.4. System Size and periodic boundary conditions [16,25]

Simulations were usually carried out with thousands of particles to sometimes millions packed in cubic box with periodic boundary conditions. It is important to choose periodic boundary conditions which replicates the infinite bulk surroundings to simulate the bulk systems. The simulation box is replicated throughout the space to form an infinite lattice (Figure 1.1). The surface effects problem can be overcome by implementing periodic boundary conditions [32]. The commonly used simulation box is cubic box. The volume $V = L^3$ of the box together with

number of particles N , defines the number density $n = N/V$. The number density in the central box and hence in entire system, is conserved. It is not necessary to store the coordinates of all images, just the particles in central box have to be stored.

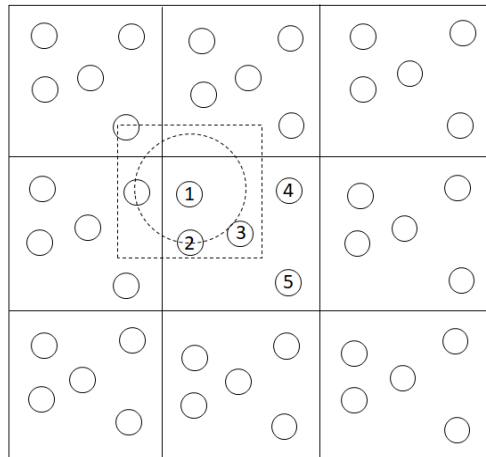


Figure 1.1: Schematic representation of periodic boundary conditions.

When a particle leaves the central box, attention can be shifted to the image just entering or one can follow the motion of the particle leaving the central box. A given particle will interact with all other particles in infinite periodic system i.e. all other particles in the same periodic cell as well as all particles in all other cells, including its own periodic images. The boundary of the periodic box itself has no special significance. The periodic lattice origin of the primitive cells can be chosen anywhere, and this choice will not affect any property of the model system under study. In contrast, what is fixed is the shape of the periodic cell and its orientation. When it is dealt with short-range pair potential, as in instance of Lennard Jones potential, it is admissible to truncate the inter-atomic interaction at finite radial cutoff distance r_c and particles are now allowed only to interact with the finite number of surrounding particles. If $r_c < L/2$, the particle at the center interacts with the nearest periodic image of the surrounding particle. This is called minimum image convention (MIC). The use of periodic boundary conditions proves to be effective method to simulate the homogeneous bulk systems. However, it inhibits the occurrence of long wavelength fluctuations.

1.3.5. Finite difference techniques

These methods are used to generate the trajectories using continuous potentials, assumed to be pairwise additive. The basic idea of integration is divided into small steps, each separated in time by a fixed time Δt . The total force on each particle in the configuration at time t is calculated as vector sum of the particle interactions with the other particles. From this force we can determine the accelerations of the particles, which are combined with the velocities and positions at time t to calculate the velocities and positions at time $t + \Delta t$. The forces on the particles in their new positions are determined which leads to the new velocities and positions at time $t + 2\Delta t$, etc. The integration step is not time-consuming, but it is important because the conservation of energy or time reversibility is determined using this method. There are many algorithms for integrating the equations of motions used in molecular dynamics simulation calculations.

In 1967 Loup Verlet introduced a central difference-based algorithm into molecular simulations [33]. In many cases, this simple algorithm has turned out to be the best to use in MD simulations and it is extensively used. The Velocity Verlet algorithm is the most common algorithm used to integrate the equations of motion and computes position of particles $r(t)$, velocity of particles $v(t)$, accelerations $a(t)$, Δt is the time step in the numerical scheme and previous positions of the particles $r(t - \Delta t)$. The algorithm is derived by using Taylor expansion of the position coordinate both forward and backward time.

$$r(t + \Delta t) = r(t) + v(t)\Delta t + \frac{1}{2}\Delta t^2 a(t) + \dots \quad (1.14)$$

$$r(t - \Delta t) = r(t) - v(t)\Delta t + \frac{1}{2}\Delta t^2 a(t) + \dots \quad (1.15)$$

By adding the above two equations we obtain

$$r(t + \Delta t) = 2r(t) - r(t - \Delta t) + a(t)\Delta t^2 \quad (1.16)$$

This equation is known as verlet algorithm. The velocities do not enter explicitly in the algorithm; however, they are needed to estimate kinetic energy and temperature. The numerical stability, ease and simplicity makes the velocity Verlet algorithm suitable for MD simulations and highly recommended.

Another integration method which is common used in MD simulation is leap frog algorithm [34]. The positions are computed by using velocities at half-integer time step.

$$\vec{v}(t - \Delta t / 2) \equiv \frac{\vec{r}(t) - \vec{r}(t - \Delta t)}{\Delta t}, \quad (1.17)$$

$$\vec{v}(t + \Delta t / 2) \equiv \frac{\vec{r}(t + \Delta t) - \vec{r}(t)}{\Delta t} \quad (1.18)$$

The velocities are not calculated at the same time as the positions, using leap frog algorithm. Once the new positions of all the particles are computed using equations of motion, the whole procedure of calculating the forces and consequently the new positions and velocities are repeated as often as needed and thus the system evolves in time. The properties can be time averaged once the system is equilibrated. The properties of interest can then be time-averaged after the system is equilibrated.

1.3.6. Pair Potential

The simple and convenient pair potentials used in simulations are: Hard sphere potential [35] [36], the potential between the hard spheres of diameter σ , i.e.

$$u(r) = \begin{cases} \infty & r < \sigma \\ 0 & r \geq \sigma \end{cases} \quad (1.19)$$

Lennard-Jones potential [37] provides a good description of interactions between the pairs of noble gases atoms like argon, krypton and xenon.

It was originally proposed for liquid argon for a pair of atoms i and j at r_i and r_j

$$u_{ij}(r) = \begin{cases} 4\epsilon \left[\left(\frac{\sigma}{r_{ij}} \right)^{12} - \left(\frac{\sigma}{r_{ij}} \right)^6 \right] & r_{ij} < r_c \\ 0 & r_{ij} \geq r_c \end{cases} \quad (1.20)$$

Where $r_{ij} = r_i - r_j$, the parameter \mathcal{E} directs the strength of the interaction and well depth, σ determines the length scale. The potential has a long-range attractive part in the form of $-1/r^6$ and the repulsive part in the form of $-1/r^{12}$. The cutoff distance of separation is r_c .

The Lennard-Jones potential turns to Weeks-Chandler-Andersen (WCA) [38] potential when cutoff is minimum, $r_c = 2^{1/6} \sigma$ which is purely repulsive.

The ionic charged systems are quite well represented by sum of pair potentials. The particles are charged, and interactions are dominated by the Coulombs interaction. These represent the long-range interactions

$$u_{ij}^C(r) = \beta L_B z_i z_j / r \quad (1.21)$$

z_i, z_j are charges, $L_B = \beta e^2 / \epsilon$ is the Bjerrum length, $\beta = 1/(k_b T)$ is the inverse temperature, k_b is the Boltzmann constant, T is the temperature.

1.4. Integral Equation Theory:

The pair correlation function (for an m -component system) is calculated by solving the OZ equation [39]

$$h_{ab}(r_{12}) = c_{ab}(r_{12}) + \sum_{n=0}^m \rho_n \int d^3 r_3 c_{an}(r_{13}) h_{nb}(r_{32}), \quad (1.22)$$

where $r_{ab} = |r_a - r_b|$, $\rho_n = \text{number density}$

Equation 1.22 can be written in the matrix form as [31]

$$H = C + C * R H \quad (1.23)$$

Where H and C are $n \times n$ matrix correlation functions and R is the diagonal matrix of densities.

$$H = \begin{pmatrix} h_{11} & h_{12} & \dots \\ h_{21} & h_{22} & \dots \\ \dots & \dots & \dots \end{pmatrix}, \quad C = \begin{pmatrix} c_{11} & c_{12} & \dots \\ c_{21} & c_{22} & \dots \\ \dots & \dots & \dots \end{pmatrix}, \quad R = \begin{pmatrix} \rho_1 & 0 & \dots \\ 0 & \rho_2 & \dots \\ \dots & \dots & \dots \end{pmatrix}$$

Along with closure, we written it without any approximation [40] as

$$h_{ij}(r) = \exp[-\beta u_{ij}(r) + h_{ij}(r) - c_{ij}(r) + B_{ij}(r)] - 1, \quad (1.24)$$

Where ρ_n is the number density of particle species n , $h_{ij}(r) = g_{ij}(r) - 1$ is the total correlation function, $c_{ij}(r)$ is the direct correlation function and $B_{ij}(r)$ is the bridge diagram sum.

Bridge diagrams are difficult to evaluate and most of the time it is approximated, leading to different closure relations. For example, by setting $B_{ij}(r) = 0$, in Eq. 1.24 we obtained HNC closure [41], PY closure [42] is obtained by setting $B_{ij}(r) = \ln[1 + h_{ij}(r) - c_{ij}(r)] - h_{ij}(r) - c_{ij}(r)$ and MS closure [43] is obtained when $B_{ij}(r) = [1 + 2(h_{ij}(r) - c_{ij}(r))]^{1/2} - (h_{ij}(r) - c_{ij}(r)) - 1$.

1.4.1. Closure Relations [31] [40]

We discuss now different closure relations which express $c(r)$ approximately in terms of $h(r)$ and pair interaction potential $u(r)$. These relations are derived from a cluster diagrammatic analysis [44] that reads

$$h(r) + 1 = \exp[-\beta u(r) + h(r) - c(r) + B(r)] \quad (1.25)$$

The term $h(r) - c(r) + B(r)$ is called as negative excess potential of mean force [45,46]. The bridge function $B(r)$ was shown to be the sum of the infinite number of terms, each consisting of intervals whose kernel are products, of increasing order, of correlation functions. This infinite series is represented diagrammatically by “bridge” diagram [47,48]. In combination with OZ equation, the closure relations to calculation of $g(r)$. These equations have been found, in comparison with molecular simulation data and scattering data, to be useful in calculating the $g(r)$ and various properties of liquids.

1.4.1.1. Hypernetted Chain (HNC) Approximation

An analysis of clusters expansion to higher orders leads to hypernetted-chain (HNC) approximation [44]. The total correlation function is given by

$$h(r) = \exp[-\beta u(r) + h(r) - c(r)] - 1 \quad (1.26)$$

Implying that the bridge function $B(r)$ is identically equal to 0. HNC is not analytically solvable [49–55] and requires iterational procedure starting with a guess for either of the functions h or c . The easiest method is to use (equation 1.27) between Fourier transforms of h and c [40,56,57].

$$\hat{h}(k) = \frac{\hat{c}(k)}{1 - \rho \hat{c}(k)} \quad (1.27)$$

An initial guess, $c_0(r)$ is made and its Fourier transform is substituted in (equation 1.27). An inverse transform of it yields $h(r)$. The improved guess $c_1(r)$ is obtained using closure relation between h and c . The process is repeated, with $c_1(r)$ replacing $c_0(r)$ as input, and the iteration continues until convergence is achieved. HNC is more accurate than PY for systems governed by long range potentials.

1.4.1.2. Percus-Yevick (PY) Approximation [58]

The PY approximation is expressed in pair correlation function for a simple fluid as

$$g(r) = \exp[-\beta u(r)][1 + h(r) - c(r)] \quad (1.28)$$

The bridge function corresponding to PY relation reads

$$B(r) = \ln[1 + h(r) - c(r)] - h(r) + c(r) \quad (1.29)$$

Equation 1.28 and 1.29 are both solved iteratively to obtain the solution of the system [59–66]. The PY closure is recovered by linearizing the HNC closure. In this aspect the HNC is expected to be more accurate than the PY.

1.4.1.3. Martynov Sarkisov (MS) Approximation

This approximation was proposed by Martynov and Sarkisov (MS) and sets the bridge function as

$$B(r) = [1 + 2(h(r) - c(r))]^{1/2} - (h(r) - c(r)) - 1 \quad (1.30)$$

In the dense regime, it has been shown that MS improved the PY and HNC results, by reducing considerably the thermodynamic inconsistency of the two latter ones [67–71]. The MS approximation, which has been originally applied to hard sphere system, has no adjustable parameter.

Liquid state integral equations have been an active area of research from some years. The numerical solution of these equations was found out initially using Picard iterations, however, the hybrid Picard/Newton-Raphson methods of Gillan [72,73] and Labík [74] had

dominated the field. A number of problem specific generalizations of these algorithms have been developed [75–77]. Some matrix methods for solution of integral equations which describe inhomogeneous fluids was carried out by Chen and Pettit [78]. Homeier and coworkers used vector extrapolation technique and illustrated the iterative solution of bulk Ornstein Zernike (OZ) type integral equations [79], provides standard against which to compare the Newton-GMRES algorithm. Zerah [80] described the use of a Newton method for the numerical solution of the fluid integral equations in which the linear system is solved efficiently using an iterative conjugate gradient (CG) technique [81]. The CG algorithm is usually intended for the solution of symmetric positive definite systems. It is generalized to nonsymmetric linear systems as carried out by Zerah. The examples considered by Zerah are the solution of the Percus-Yevick equation for an inverse twelfth power potential and the hypernetted chain (HNC) equation for a Lennard Jones (LJ) potential. Zerah illustrate that the stability and efficiency of a Newton iterative method (Newton-CG).

1.5. Pair Potential and screening [82,83]

Several different classes of pair potentials have been used to describe interaction between a macroion pair in solution. The first is the interaction potential between two macroions in vacuum. This potential depends on only the macroion charges and their relative co-ordinates. If the pair is suspended in a solvent, then the interaction of the macroions with solvent molecules will show up in the expression of “effective interaction” between the pair [84,85]. This complex many body screening effect is taken into account by a single parameter, the dielectric constant of the solvent. This is a very good approximation, unless the distances are very small. The screening constant alters in the presence of other macromolecules and salt. Potential of average force $w_{12}(r)$, as defined in statistical mechanics, takes into account this additional screening. The negative of the gradient is the ensemble averaged force, $w_{12}(r)$ is calculated from the pair correlation function by the formula

$$w_{12}(r) = -kT \ln g_{12}(r) \quad (1.31)$$

In thermodynamic equilibrium, states are incompletely specified. In these states $w_{12}(r_{12})$ is the equivalent of $u_{12}(r_{12})$ in the completely specified mechanical state. So we use $w_{12}(r)$ as the pair potential in an incompletely specified state [86].

In the closure equation of the hypernetted chain approximation $\beta w_{12}(r)$ is related to $\beta u_{12}(r)$ by the following expression

$$\begin{aligned} h_{12}(r) &= c_{12}(r) + \ln(1 + h_{12}(r)) + \beta u_{12}(r) \\ &= c_{12}(r) - \beta w_{12}(r) + \beta u_{12}(r) \end{aligned} \quad (1.32)$$

or

$$\beta w_{12}(r) - \beta u_{12}(r) = c_{12}(r) - h_{12}(r). \quad (1.33)$$

$u_{12}(r)$ includes the effect of screening by solvent alone. The ratio w_{12}/u_{12} therefore gives additional screening due to macroions and salt. We denote it by \mathcal{E}_{eff} .

$$\mathcal{E}_{eff} - 1 = \frac{c_{12}(r) - h_{12}(r)}{\beta u_{12}(r)} \quad (1.34)$$

In Chapter 3, we define, following Adelman [87], a one component equivalent of a multicomponent solution, in which the particle pairs interact through an effective pair potential such that pair correlation function in this one component model is the same as that of this component in the multicomponent system. The pair potential enters the theory in the following manner. We define an effective macroion-macroion $c_{12}^{eff}(r)$ denoted as $c_{mm}^{eff}(r)$ as that function which through an one component O-Z equation gives the macroion-macroion $h_{12}(r)$ denoted as $h_{mm}(r)$, which is obtained by solving the multicomponent O-Z equation. The closure equation of the one component model (the single component is macroion ‘m’)

$$h_{mm}(r) = c_{mm}^{eff}(r) + \log(1 + h_{mm}(r)) + \beta V_{mm}^{eff}(r) \quad (1.35)$$

$h_{mm}(r)$ remains the same as that of the multicomponent model. $c_{mm}^{eff}(r)$ and $\beta V_{mm}^{eff}(r)$ are different from their counterparts in multicomponent model, in which the closure relation are not mixed up and remain separate for each component, i.e., for a macroion pair it is

$$h_{mm}(r) = c_{mm}(r) + \log(1 + h_{mm}(r)) + \beta u_{mm}(r) \quad (1.36)$$

So, $c_{mm}(r) + \beta u_{mm}(r) = c_{mm}^{eff}(r) + \beta V_{mm}^{eff}(r)$.

It is shown in Chapter 3 that $c_{mm}^{eff}(r) = c_{mm}(r) + \beta v_s(r)$, where $v_s(r)$ is called the screening function and is expressed in terms of all direct pair correlation functions other than macroion-macroion. The $\beta V_{mm}^{eff}(r)$ differs from $\beta u_{mm}(r)$ by the same screening term, i.e., $\beta V_{mm}^{eff}(r) = \beta u_{mm}(r) + \beta v_s(r)$. $\beta V_{mm}^{eff}(r)$ plays the role of $\beta u_{mm}(r)$ in the one component model. It is the pair potential between an isolated pair of macroions, in the absence of other macroions, but in the solvent environment that prevails at finite macroion concentration and finite salt concentration. As macroion concentration decreases the environment approaches that of an infinitely dilute solution and may expect DLVO potential [88–90] to be represented by $\beta V_{mm}^{eff}(r)$. In contrast to $\beta w_{12}(r)$, $\beta V_{mm}^{eff}(r)$ retains screening due to finite macroion concentration only through the solvent environment that it creates. If however the calculation is done in an infinitely dilute solution $h(r) = c(r)$ or $c^{eff}(r)$ (in one component model) [82] and therefore $w(r) = u(r)$ or, $V_{eff}(r)$ (in one component model). The screening in such a case is only due to the salt present. The environment is entirely that of an infinitely dilute solution and is completely free from the effect of a finite macroion concentration. This potential should be the DLVO potential, as calculated by statistical mechanics. Calculation of correlation function by methods of statistical mechanics is therefore a route to understanding DLVO potential and deviation from it.

From a theoretical point of view, analytical and numerical methods from classical statistical mechanics (due to mesoscopic size of colloid, quantum effect is small) are the appropriate tool for predicting properties of these suspensions [85]. However, an explicit description of these highly asymmetric, multicomponent, many-particle systems is formidable. One way to deal with this problem is coarse-graining approaches where certain degrees of freedom are integrated out, resulting in an effective interaction/potential [83]. Significant progress has emerged from exploiting the analogy between these (effective) potentials and the potentials of atomic and molecular fluids. In other words, colloidal suspensions can be treated as a multi-component fluid mixture, and the well-established machinery of liquid state can be exploited.

1.6. Modeling of colloidal suspensions on different levels [91]

The theoretical model for the description of charged colloidal particles can be done on five different levels [85]. The higher the level, the more realistic the model is, and, at the same time, the more complicated the computational effort. Any higher level includes the lower levels as special cases.

The simplest approach is the linear counterion screening theory, resulting analytical Yukawa pair potential for the effective interaction between colloids, as given by the Deraguin–Landau–Verwey–Overbeek (DLVO) theory [92,93]. On this level, only the colloidal particles are considered explicitly. The next level is the nonlinear Poisson–Boltzmann (PB) approach, which includes a full treatment of the counterion entropy but still works on a mean-field level. On the PB level, the colloids and the averaged counterion density field are considered explicitly. In the ‘primitive’ model (PM), one treats the counterions explicitly. This approach includes full counterion correlations. The solvent only enters via a continuous dielectric background. Models treating solvent explicitly are also known, e.g. Hard sphere solvent model (HSSM) [77] and dipolar solvent model [94,95] or a Stockmayer liquid [96]. With quantum chemistry, one may even reach a higher level with a full microscopic description of the solvent interactions [97].

As mentioned, in the Primitive Model (PM) one treats the polyions and small ions explicitly while the solvent is considered as a dielectric continuum (degrees of freedom are integrated out). Even the PM level of description may be challenging when polyion-microion asymmetry (in size and charge) is large. So, in the linear counterion screening theory, only the colloidal particles are considered explicitly while the degrees of freedom of solvent as well as remaining microions are integrated out, resulting in an analytical Yukawa pair potential for the effective interaction between colloids. This is the famous Deraguin-Landau-Verwey-Overbeek (DLVO) potential [98]. The concepts of coarse-graining and effective potential are also natural in experiments, e.g. the experimental techniques like light, x-ray or neutron scattering view the colloidal suspensions at length scales where only the colloids (macroparticles) are visible and the microscopic ions and solvent plays the role of a background and their effects are not considered explicitly [99]. The experimental profiles have to be then interpreted by means of

an effective interaction between the colloids, which indirectly includes all the effects of the remaining constituents. The nature, strength and even the sign of this effective potential are not obvious and depend on the details of the solvent-solvent and solvent-colloid direct interactions [82].

The DLVO which is a purely repulsive effective pair-potential between colloids was very successful in explaining colloidal potential since five decades. However, recent experimental study on effective potential of a like charged pair of colloids, a pair of dielectric plates, and a plate and a sphere embedded in an electrolyte solution show [85,100] an attractive minimum at small as well as large interparticle distance in bulk solution and at large interparticle distance in a confined fluid. These observations contradict the DLVO theory and are difficult to explain even in the context of the more sophisticated theoretical schemes, since they predict different length scales for the attractive interaction. Since the concept of the effective interactions of colloids is applied in the determination of the parameters of the system (e. g. colloid size & its charge, ionic strength of supporting electrolyte etc.), the question of its proper definition and the accuracy of approximations involved are of considerable practical interest.

Electrostatic colloid crystals obtained at low concentration in highly deionized conditions (monovalent counterions) studied by direct visualization using confocal laser scanning microscopy and by ultra-small-angle x-ray scattering reveal the presence of apparently empty regions or voids inside the crystal (evidence for a long-range attraction) [101]. However, advanced experimental techniques (video microscopy in combination with optical tweezers) predict a purely repulsive interaction in bulk suspension [102]. Thus, direct measurement of forces acting between charged polyions contrasts with indirect determinations of effective forces via small-angle x-ray measurements of static structure factors [103]. Clearly, experimental evidence of ion mediated effective attraction between spherical colloids is still an open and controversial issue.

In view of the above, studying of effective interactions between a pair of colloids in a systematic and quantitative way is quite important. A clear understanding of this effective

interaction potential and its dependence on system parameters will give new insights to the structure and properties of colloidal suspensions.

1.7. Literature Survey:

Most of the studies on asymmetric electrolytes were done using fluid integral theory [104]. An asymmetry (in size and charge) around 10 can be early handled with in PM description using the fluid integral equation with Hypernetted Chain approximation (HNC). Using HNC equation, Das et al. [105] studied asymmetric macroionic systems and found that as the size and charge asymmetry increases the HNC solution tends to be unstable. For the simple planar geometry of two parallel dielectric walls (infinite dilution) enclosing an ionic solution of 2:2 electrolyte or a bivalent counter-ion, both Monte Carlo (MC) simulations [106,107] and inhomogeneous HNC calculations [108] within the primitive model have proven without ambiguity the existence of attraction between the plates (negative pressure) at high electrostatic coupling. The MC result was also verified experimentally. However, for bulk systems of spherical colloids, the situation is not so clear. Theoretical evidences of effective attraction have been first obtained following the integral equation approach. Patey [51] solved the Ornstein-Zernike (OZ) equation [39] using HNC approximation in primitive model and found a negative potential of mean force at a small interparticle between a pair of highly charged colloids at infinite dilution embedded in the bulk of a 1:1 electrolyte solution at high particle charge and salt concentration. However, Teubner [109] pointed out that the minima of Patey may very well be an artifact of HNC approximation (i.e., a result of ignoring bridge diagrams) as applied to the colloid - colloid correlation and should disappear if neglected bridge diagrams are included. Patey's attraction disappears for monovalent ions but subsists for divalent ions when including the first bridge diagram. A similar result supporting Teubner's point was obtained by Behera [110] when a self-consistent integral equation theory was used. Behera et al. reported that the potential function obtained from Zerah and Hansen (ZH) closure at higher salt concentration, although repulsive over the whole range of distance, shows significant deviation from DLVO potential. Brukhno [111] reported that addition of simple monovalent salt gradually lowers the effective macroion charge and reduces the solution solubility. The concentration of multivalent salt that exceeds the macroion concentration causes macroion charge inversion and electrostatically driven macroion aggregation in both

60:3 and 60:5 charge asymmetry system. This aggregation of colloids leads to phase separation. Allahyarov [112] identified a salt driven attraction between like-charge mesoscopic colloid which occurs only for low or moderate dielectric constants of the solvent such that salt ions form pairs which are depleted around the colloidal surface. Gutierrez-Valladares [113] reported that the size asymmetric 1:1 electrolyte considered does not dramatically affect the performance of the HNC theory in applied concentration range of $0.0001 \text{ mol dm}^{-3}$ to 1.5 mol dm^{-3} . Leger et al. [114] studied the system of size ratio equal to 80 and charge ratio between 1 and 4000 using OZ equation and HNC approximation and found a fair agreement with effective potential obtained from Poisson Boltzmann (PB) theory when charge is smaller than 1000. With larger charges the PB and HNC values differ. MC simulation was carried out by Cuetos [115] for a system of two colloidal particles in presence of monovalent co and counterions (size asymmetry of 1:40 and charge asymmetry upto 1:1000) in the primitive model. They found that whereas the internal energy becomes attractive at high colloidal charges, free energy (which corresponds to the true effective colloid-colloid interaction) remains always repulsive. The effective force between the charged spherical colloids induced by the presence of smaller charged spheres using MC simulations were studied [116–118]. Later on Dullens [119] measured chemical potential, pressure of colloidal suspensions using confocal microscopy and came out with a concept that from particle configurations the available volume to insert an additional sphere of that volume was determined which provides direct relations between geometry of colloidal particles and thermodynamics. When it comes to tunability of colloids Van Gruijthuijsen [120] synthesized and characterized colloidal suspensions that behave as effective hard spheres at very high salt concentration and show electrostatic repulsions at lower salt content that can be tuned by further decrease in the salt concentration using small-angle neutron and small-angle x-ray scattering experiments.

We planned to use the formalism of statistical mechanical theory of asymmetrical mixtures, namely the Integral Equation Theory (IET) and molecular dynamics (MD) simulation to get the pair correlation functions, which are related to the properties.

1.8. Gaps in Existing Research

1. The nature and strength of the effective interaction potential of colloidal suspensions is still an open and challenging problem. A clear understanding of this potential in a systematic way is important.
2. Although Integral equation theory is quite successful for simple liquids and mixtures, they become increasingly unreliable for asymmetric systems and their numerical solution tends to become unstable.
3. Simulation data on colloidal systems are very less. The simulation of colloidal suspensions has been mostly done either with lesser number of polyions or with lesser charge asymmetry (typically for micellar system). Full simulation even within PM level is rare.

1.9. Objectives

1. To calculate and properties of asymmetric binary mixtures using molecular dynamics simulation.
2. To calculate the effective potential and thermodynamic properties of model colloidal suspensions using both molecular dynamics simulation and Integral equation theory with different closures. A systematic variation of these properties will be carried out with variation in the system parameters, which would enable in understanding the colloidal stability.
3. To compare the results of Integral equation theory with different closures and molecular dynamics simulation for model colloidal suspensions.

1.10. Summary of Thesis:

With this background, Chapter 1 of the thesis introduces the importance and modelling of colloidal suspensions, basic statistical mechanics leading to pair correlation function and property calculation, Integral Equation theory, Molecular Dynamics simulation, concept of effective pair potential etc. The gaps in existing research and objectives of this research work have also been discussed.

In Chapter 2, we studied binary mixtures asymmetric in size, charge and mass and their combinations using molecular dynamics simulation. A systematic variations of pair correlation functions and different properties as a function of size, charge and mass asymmetry have been observed. Empirical relations expressing diffusion coefficient of systems having more than one type of asymmetry in terms of diffusion coefficient of systems having asymmetry of only one type, have been presented.

In chapter 3, we have extended our molecular dynamics simulations study to model colloidal suspensions in bulk solutions as well as in between two walls. Systematic variation in pair correlation functions, effective colloid potential, thermodynamic properties and self-diffusion coefficient were observed with system parameters. The density profiles and diffusion coefficients of the colloidal suspensions under confinement was studied as a function of colloid size, colloid charge and type of walls.

In Chapter 4, we studied the performance of different integral equation theories for model colloidal suspensions and compared with the simulation results of chapter 3. The Newton-GMRES algorithm was used to solve the Ornstein Zernike equation with three different closure approximations: Hypernetted Chain (HNC), Percus Yevick (PY) and Martynov Sarkisov (MS). The pair correlation functions, effective colloid potential were systematically studied with variation in size, charge and concentration of the colloid. The overall conclusion and scope of future research work is presented in chapter 5.

1.11. References

- [1] S. Das, J. Riest, R.G. Winkler, G. Gompper, J.K.G. Dhont and G. Nägele, *Clustering and dynamics of particles in dispersions with competing interactions: Theory and simulation*, Soft Matter 14 (2017), pp. 92–103.
- [2] A.-M. Philippe, D. Truzzolillo, J. Galvan-Myoshi, P. Dieudonné-George, V. Trappe, L. Berthier et al., *Glass transition of soft colloids*, Phys. Rev. E 97 (2018), pp. 40601.
- [3] S.A. Mallory, C. Valeriani and A. Cacciuto, *An Active Approach to Colloidal Self-Assembly*, Annu. Rev. Phys. Chem. 69 (2018), pp. 59–79.
- [4] S. Sacanna, W.T.M. Irvine, P.M. Chaikin and D.J. Pine, *Lock and key colloids*, Nature

- 464 (2010), pp. 575.
- [5] Y. Jin and D. Stephan, *Colloidal interaction between vinylacetate ethylene latex stabilized by polyvinyl alcohol and portland cement*, SN Appl. Sci. 1 (2019), pp. 129.
- [6] G. Li, T. Zhao, P. Zhu, Y. He, R. Sun, D. Lu et al., *Structure-property relationships between microscopic filler surface chemistry and macroscopic rheological, thermo-mechanical, and adhesive performance of SiO₂ filled nanocomposite underfills*, Compos. Part A Appl. Sci. Manuf. 118 (2019), pp. 223–234.
- [7] W.J. Frith, T.A. Strivens and J. Mewis, *Dynamic mechanical properties of polymerically stabilized dispersions*, J. Colloid Interface Sci. 139 (1990), pp. 55–62.
- [8] M. Wei, L. Sun, C. Zhang, P. Qi and J. Zhu, *Shear-thickening performance of suspensions of mixed ceria and silica nanoparticles*, J. Mater. Sci. 54 (2019), pp. 346–355.
- [9] C.D. Cwalina and N.J. Wagner, *Material properties of the shear-thickened state in concentrated near hard-sphere colloidal dispersions*, J. Rheol. (N. Y. N. Y). 58 (2014), pp. 949–967.
- [10] Y.S. Lee and N.J. Wagner, *Dynamic properties of shear thickening colloidal suspensions*, Rheol. Acta 42 (2003), pp. 199–208.
- [11] J.E. Martin, D. Adolf and T.C. Halsey, *Electrorheology of a model colloidal fluid*, J. Colloid Interface Sci. 167 (1994), pp. 437–452.
- [12] A. Yethiraj and A. van Blaaderen, *A colloidal model system with an interaction tunable from hard sphere to soft and dipolar*, Nature 421 (2003), pp. 513.
- [13] H. Löwen, *Colloidal soft matter under external control*, J. Phys. Condens. Matter 13 (2001), pp. R415.
- [14] B. Bagchi, *Statistical Mechanics for Chemistry and Materials Science*, CRC Press, 2018.
- [15] T.L. Hill, *Statistical Mechanics: Principles and Selected Applications*, Dover

- Publications, 1987.
- [16] M.P. Allen and D.J. Tildesley, *Computer Simulation of Liquids*, Oxford university press, 2017.
- [17] D.A. McQuarrie, *Statistical mechanics. 2000*, Sausalito, Calif. Univ. Sci. Books 12 (2004), pp. 641.
- [18] P. Attard, *Entropy Beyond the Second Law; Thermodynamics and statistical mechanics for equilibrium, non-equilibrium, classical, and quantum systems*, Entropy Beyond Second Law; Thermodyn. Stat. Mech. equilibrium, non-equilibrium, Class. quantum Syst. by Attard, Phil. ISBN 978-0-7503-1590-6. IOP ebooks. Bristol, UK IOP Publ. 2018 (2018), .
- [19] W. Sung, *Statistical Mechanics of Fluids and Solutions*, in *Statistical Physics for Biological Matter*, Springer, 2018, pp. 51–73.
- [20] N. Metropolis, A.W. Rosenbluth, M.N. Rosenbluth, A.H. Teller and E. Teller, *Equation of state calculations by fast computing machines*, J. Chem. Phys. 21 (1953), pp. 1087–1092.
- [21] I.K. Snook and D. Henderson, *Monte Carlo study of a hard-sphere fluid near a hard wall*, J. Chem. Phys. 68 (1978), pp. 2134–2139.
- [22] J.A. Barker and D. Henderson, *Monte Carlo values for the radial distribution function of a system of fluid hard spheres*, Mol. Phys. 21 (1971), pp. 187–191.
- [23] H. Gould, J. Tobochnik and W. Christian, *An Introduction to Computer Simulation Methods*, Vol. 1, Addison-Wesley New York, 1988.
- [24] M. Mezei, S. Swaminathan and D.L. Beveridge, *Convergence characteristics of Monte Carlo--Metropolis computer simulations on liquid water*, J. Chem. Phys. 71 (1979), pp. 3366–3373.
- [25] D.C. Rapaport and D.C.R. Rapaport, *The Art of Molecular Dynamics Simulation*, Cambridge university press, 2004.

- [26] B.J. Alder and T.E. Wainwright, *Phase transition for a hard sphere system*, J. Chem. Phys. 27 (1957), pp. 1208–1209.
- [27] A. Geiger, A. Rahman and F.H. Stillinger, *Molecular dynamics study of the hydration of Lennard-Jones solutes*, J. Chem. Phys. 70 (1979), pp. 263–276.
- [28] A.F. Bakker, C. Bruin, F. Van Dieren and H.J. Hilhorst, *Molecular dynamics of 16000 Lennard-Jones particles*, Phys. Lett. A 93 (1982), pp. 67–69.
- [29] A.A. Galata, S.D. Anogiannakis and D.N. Theodorou, *Thermodynamic analysis of Lennard-Jones binary mixtures using Kirkwood-Buff theory*, Fluid Phase Equilib. 470 (2018), pp. 25–37.
- [30] V.G. Baidakov, S.P. Protsenko and V.M. Bryukhanov, *Relaxation processes at liquid-gas interfaces in one-and two-component Lennard-Jones systems: Molecular dynamics simulation*, Fluid Phase Equilib. 481 (2019), pp. 1–14.
- [31] J.-L. Barrat and J.-P. Hansen, *Basic Concepts for Simple and Complex Liquids*, Cambridge University Press, 2003.
- [32] M. Born and T. von Karman, *On fluctuations in spatial grids*, Phys. Zeitschrift 13 (1912), pp. 18.
- [33] L. Verlet, *Computer" experiments" on classical fluids. I. Thermodynamical properties of Lennard-Jones molecules*, Phys. Rev. 159 (1967), pp. 98.
- [34] W.F. Van Gunsteren and H.J.C. Berendsen, *A leap-frog algorithm for stochastic dynamics*, Mol. Simul. 1 (1988), pp. 173–185.
- [35] P. Atkins and J. De Paula, *Elements of Physical Chemistry*, Oxford University Press, USA, 2013.
- [36] N.I. Levine, *Physical Chemistry, 3-nd Ed*, Chem. Dep. Brooklyn Coll. City Univ. New York (1988), pp. 371–373.
- [37] J.E. Lennard-Jones, *The equation of state of gases and critical phenomena*, Physica 4 (1937), pp. 941–956.

-
- [38] J.D. Weeks, D. Chandler and H.C. Andersen, *Role of repulsive forces in determining the equilibrium structure of simple liquids*, J. Chem. Phys. 54 (1971), pp. 5237–5247.
- [39] L.S. Ornstein and F. Zernike, *Integral equation in liquid state theory*, in Proc. Acad. Sci. Amsterdam, 17 (1914), pp. 793.
- [40] R.O. Watts, *Statistical Mechanics Volume 1*, (1988), .
- [41] J.M.J. van Leeuwen, J. Groeneveld and J. de Boer, *New method for the calculation of the pair correlation function. I*, Physica 25 (1959), pp. 792–808.
- [42] J.K. Percus and G.J. Yevick, *Analysis of classical statistical mechanics by means of collective coordinates*, Phys. Rev. 110 (1958), pp. 1.
- [43] G.A. Martynov and G.N. Sarkisov, *Exact equations and the theory of liquids. V*, Mol. Phys. 49 (1983), pp. 1495–1504.
- [44] H.L. Friedman, *A Course in Statistical Mechanics*, Prentice-Hall, 1985.
- [45] G.A. Martynov, *Fundamental Theory of Liquids: Method of Distribution Functions*, Hilger, 1992.
- [46] J.-M. Bomont, *Recent advances in the field of integral equation theories: bridge functions and applications to classical fluids*, Adv. Chem. Phys. 139 (2008), pp. 1–84.
- [47] L. Belloni, *Exact molecular direct, cavity, and bridge functions in water system*, J. Chem. Phys. 147 (2017), pp. 164121.
- [48] D. Yokogawa, *Toward accurate solvation free energy calculation with the reference interaction site model self-consistent field: introduction of a new bridge function*, J. Chem. Theory Comput. 14 (2018), pp. 3272–3278.
- [49] D. Henderson, L. Blum and W.R. Smith, *Application of the hypernetted chain approximation to the electric double layer at a charged planar interface*, Chem. Phys. Lett. 63 (1979), pp. 381–383.
- [50] P.J. Rossky and H.L. Friedman, *Accurate solutions to integral equations describing*

- weakly screened ionic systems*, J. Chem. Phys. 72 (1980), pp. 5694–5700.
- [51] G.N. Patey, *The interaction of two spherical colloidal particles in electrolyte solution. An application of the hypernetted-chain approximation*, J. Chem. Phys. 72 (1980), pp. 5763–5771.
- [52] P.H. Fries and G.N. Patey, *The solution of the hypernetted-chain approximation for fluids of nonspherical particles. A general method with application to dipolar hard spheres*, J. Chem. Phys. 82 (1985), pp. 429–440.
- [53] H. Greberg and R. Kjellander, *Electric double-layer properties calculated in the anisotropic reference hypernetted chain approximation*, Mol. Phys. 83 (1994), pp. 789–801.
- [54] M. Lukšič, E. Slejko and B. Hribar-Lee, *The influence of the poly (ethylene glycol) on the mean activity coefficients of NaCl aqueous solutions. The application of the MSA and HNC method*, J. Mol. Liq. 270 (2018), pp. 40–45.
- [55] Ü. Akdere, S.D. Günay and Ç. Taçsseven, *Ordering and diffusion in liquid magnesium antimonide (Mg₃Sb₂) from hypernetted-chain theory and molecular dynamics simulation*, Ionics (Kiel). (2018), pp. 1–7.
- [56] F. Lado, *Pressure-Consistent Integral Equation for Classical Fluids: Hard-Sphere Solutions*, J. Chem. Phys. 47 (1967), pp. 4828.
- [57] A.A. Broyles, *Radial Distribution Functions from the Born-Green Integral Equation*, J. Chem. Phys. 33 (1960), pp. 456–458.
- [58] J.-P. Hansen and I.R. McDonald, *Theory of Simple Liquids*, Elsevier, 1990.
- [59] A. Ben-Naim, *Application of an Approximate Percus--Yevick Equation for Liquid Water*, J. Chem. Phys. 52 (1970), pp. 5531–5541.
- [60] R.O. Watts, D. Henderson and R.J. Baxter, *Hard Spheres with Surface Adhesion: The Percus-Yevick Approximation and the Energy Equation*, Adv. Chem. Phys. Chem. Dyn. Pap. Honor Henry Eyring (1971), pp. 421–430.

- [61] H.C. Andersen and D. Chandler, *Optimized Cluster Expansions for Classical Fluids. I. General Theory and Variational Formulation of the Mean Spherical Model and Hard Sphere Percus-Yevick Equations*, J. Chem. Phys. 57 (1972), pp. 1918–1929.
- [62] J. Fischer, *A fluid in contact with a wall: The Percus-Yevick versus the superposition approximation*, Mol. Phys. 33 (1977), pp. 75–81.
- [63] D. Henderson, S. Sokolowski and D. Wasan, *Second-order Percus-Yevick theory for a confined hard-sphere fluid*, J. Stat. Phys. 89 (1997), pp. 233–247.
- [64] E. Katzav, R. Berdichevsky and M. Schwartz, *Random close packing from hard-sphere Percus-Yevick theory*, Phys. Rev. E 99 (2019), pp. 12146.
- [65] F. De Francqueville, P. Gilormini and J. Diani, *Representative volume elements for the simulation of isotropic composites highly filled with monosized spheres*, Int. J. Solids Struct. 158 (2019), pp. 277–286.
- [66] S. Jang, G.R. Shin and S.-C. Kim, *Electrostatic Adsorption of Uniformly Charged Sphere Ions Confined between Two Charged Plates*, J. Korean Phys. Soc. 74 (2019), pp. 30–35.
- [67] A. Tani, D. Henderson, J.A. Barker and C.E. Hecht, *Application of perturbation theory to the calculation of the dielectric constant of a dipolar hard sphere fluid*, Mol. Phys. 48 (1983), pp. 863–869.
- [68] L. Lue and D. Blankschtein, *Liquid-state theory of hydrocarbon-water systems: application to methane, ethane, and propane*, J. Phys. Chem. 96 (1992), pp. 8582–8594.
- [69] L. Sarkisov and P.R. Van Tassel, *Integral equation theory of adsorption in templated materials: Influence of molecular attraction*, J. Phys. Chem. C 111 (2007), pp. 15726–15735.
- [70] G. Pellicane, R.L.C. Vink, C. Caccamo and H. Löwen, *Colloid--polymer mixtures in the presence of quenched disorder: a theoretical and computer simulation study*, J. Phys. Condens. Matter 20 (2008), pp. 115101.

- [71] A. Kovalenko, A.E. Kobryn, S. Gusarov, O. Lyubimova, X. Liu, N. Blinov et al., *Molecular theory of solvation for supramolecules and soft matter structures: application to ligand binding, ion channels, and oligomeric polyelectrolyte gelators*, *Soft Matter* 8 (2012), pp. 1508–1520.
- [72] M.J. Gillan, *A new method of solving the liquid structure integral equations*, *Mol. Phys.* 38 (1979), pp. 1781–1794.
- [73] G.M. Abernethy and M.J. Gillan, *A new method of solving the HNC equation for ionic liquids*, *Mol. Phys.* 39 (1980), pp. 839–847.
- [74] S. Labik, A. Malijevsky and P. Vovnka, *A rapidly convergent method of solving the OZ equation*, *Mol. Phys.* 56 (1985), pp. 709–715.
- [75] M. Kinoshita and M. Harada, *Numerical solution of the RHNC theory for water-like fluids near a macroparticle and a planar wall*, *Mol. Phys.* 81 (1994), pp. 1473–1488.
- [76] S. Labik, R. Pospivsil, A. Malijevsky and W.R. Smith, *An efficient Gauss-Newton-like method for the numerical solution of the Ornstein-Zernike integral equation for a class of fluid models*, *J. Comput. Phys.* 115 (1994), pp. 12–21.
- [77] M. Kinoshita and D.R. Bérard, *Analysis of the bulk and surface-induced structure of electrolyte solutions using integral equation theories*, *J. Comput. Phys.* 124 (1996), pp. 230–241.
- [78] Z.-M. Chen and B.M. Pettitt, *Non-isotropic solution of an OZ equation: matrix methods for integral equations*, *Comput. Phys. Commun.* 85 (1995), pp. 239–250.
- [79] H.H.H. Homeier, S. Rast and H. Krienke, *Iterative solution of the Ornstein-Zernike equation with various closures using vector extrapolation*, *Comput. Phys. Commun.* 92 (1995), pp. 188–202.
- [80] G. Zerah, *An efficient Newton's method for the numerical solution of fluid integral equations*, *J. Comput. Phys.* 61 (1985), pp. 280–285.
- [81] C.T. Kelley, *Iterative Methods for Linear and Nonlinear Equations (Frontiers in*

-
- Applied Mathematics vol 16*(Philadelphia: SIAM), (1995), .
- [82] L. Belloni, *Colloidal interactions*, J. Phys. Condens. Matter 12 (2000), pp. R549–R587.
- [83] C. Likos, *Effective Interactions in Soft Condensed Matter Physics*, Vol. 348, 2001.
- [84] B. Beresford-Smith, D.Y.. Chan and D.J. Mitchell, *The electrostatic interaction in colloidal systems with low added electrolyte*, J. Colloid Interface Sci. 105 (1985), pp. 216–234.
- [85] J.-P. Hansen and H. Löwen, *Effective interactions between electric double layers*, Annu. Rev. Phys. Chem. 51 (2000), pp. 209–242.
- [86] D.A. McQuarrie, D.A. McQuarrie, D.A. McQuarrie and D.A. McQuarrie, *Statistical Thermodynamics*, Harper & Row New York, 1973.
- [87] S. a. Adelman, *The effective direct correlation function: An approach to the theory of liquid solutions*, J. Chem. Phys. 64 (1976), pp. 724.
- [88] H. Löwen and G. Kramposthuber, *Optimal effective pair potential for charged colloids*, EPL (Europhysics Lett. 23 (1993), pp. 673.
- [89] D.G. Grier, *Optical tweezers in colloid and interface science*, Curr. Opin. Colloid Interface Sci. 2 (1997), pp. 264–270.
- [90] T. Missana and A. Adell, *On the applicability of DLVO theory to the prediction of clay colloids stability*, J. Colloid Interface Sci. 230 (2000), pp. 150–156.
- [91] H. Lowen, E. Allahyarov, J. Dzubiella, C. Von Ferber, A. Jusufi, C.N. Likos et al., *Interactions and phase transitions of colloidal dispersions in bulk and at interfaces*, Philos. Trans. R. Soc. London A Math. Phys. Eng. Sci. 359 (2001), pp. 909–920.
- [92] B. V Deraguin and L. Landau, *Theory of the stability of strongly charged lyophobic sols and of the adhesion of strongly charged particles in solution of electrolytes*, Acta Physicochim USSR 14 (1941), pp. 633–662.

- [93] *Theory of Stability of Lyophobic Colloids* 'Elsevier Publishing' Co. Amsterdam Holland, 1948.
- [94] J. Zhao, X. Wang, N. Jiang, T. Yan, Z. Kan, P.M. Mendes et al., *Polarization effect and electric potential changes in the stimuli-responsive molecular monolayers under an external electric field*, J. Phys. Chem. C 119 (2015), pp. 22866–22881.
- [95] K. Okada and A. Satoh, *Quasi-2D Monte Carlo simulations of the regime change in the aggregates of magnetic cubic particles on a material surface*, Mol. Phys. 115 (2017), pp. 683–701.
- [96] B. Groh and S. Dietrich, *Long-ranged orientational order in dipolar fluids*, Phys. Rev. Lett. 72 (1994), pp. 2422.
- [97] I. Poltavsky, R.A. DiStasio Jr and A. Tkatchenko, *Perturbed path integrals in imaginary time: Efficiently modeling nuclear quantum effects in molecules and materials*, J. Chem. Phys. 148 (2018), pp. 102325.
- [98] E.J.W. Verwey and J.T.G. Overbeek, *Theory of the Stability of Hydrophobic Colloids* Elsevier, New York, NY (1948), .
- [99] A. Thuresson, M. Ullner and M. Turesson, *Interaction and aggregation of charged platelets in electrolyte solutions: A coarse-graining approach*, J. Phys. Chem. B 118 (2014), pp. 7405–7413.
- [100] K. Bohinc, J. Reščič, S. Maset and S. May, *Debye-Hückel theory for mixtures of rigid rodlike ions and salt*, J. Chem. Phys. 134 (2011), .
- [101] H. Zhou, S. Xu, W. Ouyang, Z. Sun and L. Liu, *Influence of the surface charge on the homogeneity of colloidal crystals*, J. Chem. Phys. 139 (2013), pp. 64904.
- [102] N. Helfricht, A. Mark, L. Dorwling-Carter, T. Zambelli and G. Papastavrou, *Extending the limits of direct force measurements: colloidal probes from sub-micron particles*, Nanoscale 9 (2017), pp. 9491–9501.
- [103] B. Leahy, N. Lin and I. Cohen, *Quantitative Light Microscopy of Dense Suspensions:*

- Colloid Science at the Next Decimal Place*, Curr. Opin. Colloid Interface Sci. (2018), .
- [104] M. Borowko, W. Rzyzko, S. Sokolowski and T. Staszewski, *Integral equations theory for two-dimensional systems involving nanoparticles*, Mol. Phys. 115 (2017), pp. 1065–1073.
- [105] B. Das and P. Gupta-Bhaya, *Hypernetted chain calculation of static correlation function of macroions in solution using Allnatt equation*, Mol. Phys. 86 (1995), pp. 1397–1418.
- [106] C. Contreras-Aburto, C.A. B'aez, J.M. M'endez-Alcaraz and R. Castaneda-Priego, *Long-time self-diffusion of charged spherical colloidal particles in parallel planar layers*, J. Chem. Phys. 140 (2014), pp. 244116.
- [107] F.J.M. Ruiz-Cabello, M. Moazzami-Gudarzi, M. Elzbieciak-Wodka, P. Maroni, C. Labbez, M. Borkovec et al., *Long-ranged and soft interactions between charged colloidal particles induced by multivalent coions*, Soft Matter 11 (2015), pp. 1562–1571.
- [108] F.J.M. Ruiz-Cabello, G. Trefalt, Z. Csendes, P. Sinha, T. Oncsik, I. Szilagyi et al., *Predicting aggregation rates of colloidal particles from direct force measurements*, J. Phys. Chem. B 117 (2013), pp. 11853–11862.
- [109] M. Teubner, *On the applicability of the HNC approximation to highly charged polyelectrolytes*, 75 (1981), pp. 1907–1911.
- [110] R.N. Behera and P. Gupta-Bhaya, *On attractive interaction of a colloid pair of like charge at infinite dilution*, J. Chem. Phys. 126 (2007), .
- [111] A. V Brulkhno, T. Akesson and B. Jonsson, *Phase Behavior in Suspensions of Highly Charged Colloids*, J. Phys. Chem. B 113 (2009), pp. 6766–6774.
- [112] E. Allahyarov, E. Zaccarelli, F. Sciortino, P. Tartaglia and H. Löwen, *Interaction between charged colloids in a low dielectric constant solvent*, Epl 78 (2007), pp. 1–5.
- [113] E. Gutiérrez-Valladares, M. Luksic, B. Millán-Malo, B. Hribar-Lee and V. Vlachy,

-
- Primitive model electrolytes. A comparison of the HNC approximation for the activity coefficient with Monte Carlo data*, arXiv Prepr. arXiv1202.4259 (2012), .
- [114] D. Léger and D. Levesque, *Effective interactions in the colloidal suspensions from hypernetted-chain theory*, J. Chem. Phys. 123 (2005), pp. 124910.
- [115] A. Cuetos, J. a. Anta and A.M. Puertas, *Internal and free energy in a pair of like-charged colloids: Monte Carlo simulations*, J. Chem. Phys. 133 (2010), .
- [116] M. Peláez-Fernández, J. Callejas-Fernández and a. Moncho-Jordá, *Effective interaction in asymmetric charged binary mixtures: The non-monotonic behaviour with the colloidal charge*, Eur. Phys. J. E 35 (2012), .
- [117] G.J. Ojeda-Mendoza, A. Moncho-Jordá, P. González-Mozuelos, C. Haro-Pérez and L.F. Rojas-Ochoa, *Evidence of electrostatic-enhanced depletion attraction in the structural properties and phase behavior of binary charged colloidal suspensions*, Soft Matter 14 (2018), pp. 1355–1364.
- [118] G. Bareigts and C. Labbez, *Effective pair potential between charged nanoparticles at high volume fractions*, Phys. Chem. Chem. Phys. 19 (2017), pp. 4787–4792.
- [119] R.P.A. Dullens, W.K. Kegel and D. Aarts, *Direct measurement of thermodynamic properties of colloidal hard spheres*, Oil Gas Sci. Technol. l'IFP 63 (2008), pp. 295–303.
- [120] K. Van Gruijthuijsen, M. Obiols-Rabasa, M. Heinen, G. Nägele and A. Stradner, *Sterically stabilized colloids with tunable repulsions*, Langmuir 29 (2013), pp. 11199–11207.

Chapter 2

Molecular dynamics simulation study of asymmetric binary mixtures

Structural and thermodynamic properties as well as diffusion coefficients of binary fluid mixtures have been investigated. The diameter, charge and mass of the fluid mixture are in the range 6Å-60Å, $1e-10e$ and 1amu-500amu, respectively, corresponding to typical micellar solutions. Variations in different properties with the size, charge and mass ratio of the particles are presented.

*Reproduced in part with permission from

Uday Kumar Padidela, Tarun Khanna, and Raghu Nath Behera, "Structure, thermodynamics and diffusion in asymmetric binary mixtures: A molecular dynamics simulation study", *Physics and Chemistry of Liquids*, 56(5), 685-701, 2018. Copy right attached

2.1. Introduction

The study of structural and dynamic properties of fluids and their mixtures has been of great importance for both basic as well as applied research [1–7]. Binary fluid mixtures where one species differs from others in mass, size and/or charge serve as simple models for a wide range of systems, ranging from electrolyte, molten salts, classical plasma, polyelectrolytes, micellar solutions to colloidal dispersions, and are subject of many studies, both with respect to their static [8–12] as well as dynamic [13–19] properties. A popular theoretical model which mimics these systems is the so called “primitive model” [1] where both the species are treated explicitly on equal footing, while the solvent is treated as a structure-less dielectric continuum. From a theoretical point of view, investigating properties of such systems possess significant challenge due to size, charge and mass asymmetry leading to spatial correlations on different length and time scales, but makes them excellent model systems to study a variety of phenomena such as phase and glass transitions (dynamic arrest and cage effect, anomalous diffusion) etc [20]. Many of these studies are based on hard-sphere type model (defined by an interaction potential that considers only the repulsive forces among the molecules) [21], which facilitates one to study the structure and properties of the systems by performing computer simulations [22]. For example, the Weeks Chandler and Andersen (WCA) potential [23] has been quite successful in describing the structure and properties of liquid systems [23].

The equilibrium structure (local order as well as the long-range order) and thermodynamic properties of a fluid is provided by the pair correlations. Local properties, e.g. the way in which molecules are arranged in a neighborhood of a given molecule of the fluid, is obtained by the pair-correlation function ($g(r)$), while the long-ranged properties, e.g. the compressibility, is better described in the reciprocal space (Fourier space) with the structure factor ($S(k)$) [1]. There are several approaches to the study of diffusion phenomena (transport phenomena, in general). The hydrodynamic theory (continuum theory approach) [24] is quite successful for systems where the solute size is much greater than the solvent particles. The Enskog kinetic theory [25] is successful in predicting the diffusion constant in the low-density regime, but overestimates in the high-density regime, and also shows strong mass dependence for mixture. The mode coupling theory [26] seems to be quite successful in

describing the diffusion behavior for dense gases and liquids. Alternatively, molecular simulations play key role to describe them [27], as it is possible to observe the motion of the particles at atomic length and time scales during the simulation. Diffusion coefficient of noble gases, Lennard Jones fluids and their binary mixtures at various temperatures has been interest of study from years [3,4,28]. Further the diffusion coefficient of the binary mixtures was studied in slit shaped nanochannels [29,30], rectangular nanotubes [31].

Systems with asymmetry in mass, size or charge are difficult to analyze and model. These systems have been studied less widely. For example, a binary system asymmetric with respect to size has two length scales in which the properties can be calculated; either in the length scale of smaller particle or the length scale of the larger particle. The difficulty increases with increase in the size asymmetry of the mixture. Similar problem occurs in the system with mass asymmetry. In case of charged particles, the long-range coulombic interaction in combination with Periodic Boundary Condition [1] provide a great difficulty in computer simulations because of the slow convergence of the algorithms like P3M [32] at large particle charges. The problem is further compounded in a system with more than one type of asymmetry. We tried to study the relative effect of asymmetry in size, mass, charge and their combinations on the equilibrium and transport properties of the particles. We have investigated two component fluids consisting of spherical particles with asymmetry in size (6Å:60Å), charge (1e:10e) and mass (1amu:500amu) with total volume fractions in the range 0.02 to 0.62. The system parameter taken in this study mimics typical micellar solutions.

2.2. Model and Simulation Details of Asymmetric Binary Mixture

We consider a two-component mixture of spherical fluid particles of types 0 and 1 with mass m_i , number N_i , (density $\rho_i = N_i/V$) and diameter σ_i , ($i = 0, 1$), interacting with the pair potential.

$$u_{ij}(r) = u_{ij}^{WCA} + u_{ij}^C \quad (2.1)$$

Where the truncated and shifted Lennard-Jones potential (also known as Weeks-Chandler-Anderson potential) given by

$$u_{ij}^{WCA}(r) = \begin{cases} u_{ij}^{LJ}(r) - u_{ij}^{LJ}(r_c), & r < r_c \\ 0, & r > r_c \end{cases} \quad (2.2)$$

With, $u_{ij}^{LJ}(r) = 4\varepsilon_{ij}[(\sigma_{ij}/r)^{12} - (\sigma_{ij}/r)^6]$. The Coulomb potential (only for particles having charges) is given by $u_{ij}^C(r) = \beta L_B z_i z_j / r$. In the above expressions, the cut-off distance, $r_c = 2^{1/6} \sigma_{ij}$, $\sigma_{ij} = (\sigma_i + \sigma_j)/2$, $\varepsilon_{ij} = \sqrt{\varepsilon_i \varepsilon_j}$, r is the inter particle distance, z_i are charges, $L_B = \beta e^2 / \varepsilon$ is the Bjerrum length, $\beta = 1/(k_b T)$ is the inverse temperature, k_b is the Boltzmann constant, T is the temperature, ε is the dielectric constant of the medium. The total number of particle is $N = N_I + N_0$ and the total density is $\rho = \rho_I + \rho_0$. All the simulations were carried out in NVT ensemble. The Langevin Thermostat [33] was used to maintain a constant temperature, which also provided the surrounding solvent conditions implicitly. Velocity Verlet scheme [34] was used for integrating the equation of motion using ESPResSO molecular dynamics simulation package [35]. P3M algorithm [32] was used for the columbic interactions in case of charged particles. The parameters needed for P3M algorithm were determined by solving the inbuilt rms error function “tuneV2” [36,37] (with accuracy 10^{-5}) of the ESPResSO package.

Simulations were carried out for binary mixtures with total number of particles N (600 to 1000) packed in a cubic box under periodic boundary conditions with total density in the range 4×10^{-6} atoms/Å³ to 4.3×10^{-4} atoms/Å³ (corresponding to total packing fraction $\eta = \eta_0 + \eta_I$ between 0.01554 and 0.61571, with $\eta_i = (\pi/6)\rho_i\sigma_i^3$). The box sizes and/or number of particles were adjusted for the desire density $\rho = N/V$. Simulations were carried out for at least 1.4×10^6 steps (8.4 ns). All the properties were calculated from the configurations stored in the production step of at least 1.0×10^6 steps (6.0 ns) with the integration steps of at most 300 steps (1.8 ps). This production step is preceded by equilibration steps of at least 4×10^5 steps (2.4 ns) (Note: Here all the times are with respect to lighter particle).

The pair-correlation function which is proportional to the probability of finding a particle at a given distance r from a given particle, is calculated from

$$g(r) = \frac{\langle N(r, r + \Delta r) \rangle}{4\pi\rho^2\Delta r} \quad (2.3)$$

where ρ is the density of the fluid, $\langle N(r, r + \Delta r) \rangle$ is the average number of particles in a spherical shell of radius r and thickness Δr around a given particle. The structure factor ($S(k)$) is the density response of a system, initially in equilibrium, to a weak, external perturbation of wavelength $2\pi/k$. It is determined by

$$S(k) = 1 + \rho \int g(r) \exp(-ik \cdot r) dr \quad (2.4)$$

Thermodynamic properties, e.g., osmotic coefficient Φ_V , excess free energy E^{ex} are calculated using the standard formulae [1].

$$\Phi_V = 1 - \frac{\beta}{6\rho} \sum_{ij} \rho_i \rho_j \int_0^\infty dr 4\pi r^3 g_{ij}(r) \left(\frac{du_{ij}}{dr} \right) \quad (2.5)$$

$$\frac{\beta E^{ex}}{\rho} = \frac{\beta}{2\rho} \sum_{ij} \rho_i \rho_j \int_0^\infty dr 4\pi r^2 g_{ij}(r) u_{ij}(r) \quad (2.6)$$

The diffusion coefficient of particle α , D_α , is calculated from the slope of mean square displacement (MSD) at large times according to Einstein relation [38]

$$D_\alpha = \lim_{t \rightarrow \infty} \frac{\langle [\mathbf{r}_\alpha(t) - \mathbf{r}_\alpha(0)]^2 \rangle}{6t} \quad (2.7)$$

Where, $\mathbf{r}_\alpha(t)$ is the position of the particle α at time t , and $\langle \dots \rangle$ denotes the ensemble averaging.

2.2.1. Details of simulation and choice of simulation parameters:

During initialization of molecular dynamics (MD) simulation, the number of particles, the size of simulation box and the initial positions and velocities of the particles were selected. For a crystalline solid the atoms are placed corresponding to the lattice structure. And for a liquid, the atoms were placed on the lattice to avoid the overlap between the atoms. The initial positions and velocities of particles are assigned randomly to obtain the kinetic energy

of the system. During the initial phase of run, the system is relaxed from its initial condition and the energy is exchanged between the potential and kinetic modes; eventually the temperature of the system drifts from its set point. However, to attain equilibration we run the simulation to certain number of time steps in integration procedure. Figure 2.1a displays that the temperature of the system drops down during equilibration of the system and slowly the temperature attains equilibrium after certain time steps.

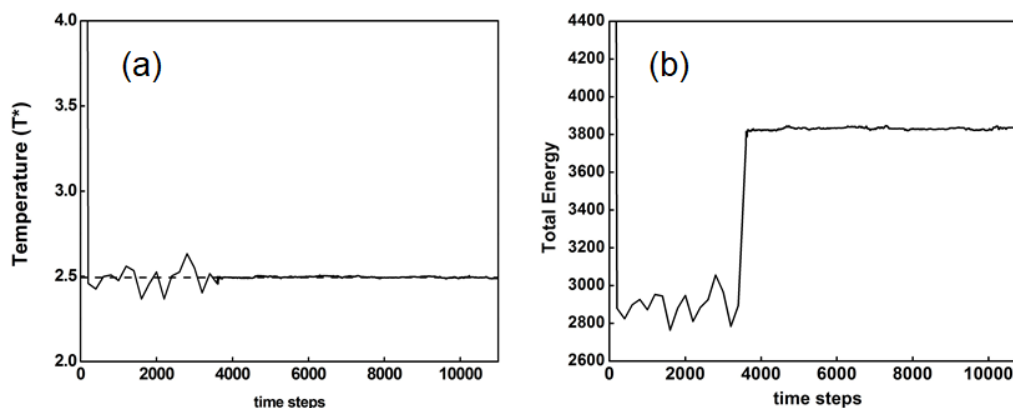


Figure 2.1: Plot showing equilibration and production steps: a) reduced temperature vs time steps b) Total energy vs time steps with mass asymmetry ($\mu = 125$), size asymmetry ($\sigma_r = 1.0$) and box length of the system 180\AA .

The total energy of the system (Figure 2.1b) with respect to the time steps doesn't show more fluctuations and the system is stable. Similarly, we have carried out simulations using different box lengths (300\AA , 375\AA) the temperature and the total energy is nearly similar without more fluctuations and attains equilibrium.

We have tested the simulation by varying time steps also in order to find a suitable time step to perform the simulations. After testing the system by monitoring the system parameters for equilibration we obtained the above properties of the system which concludes that the system attains the equilibration state and further carried out simulations to calculate properties like pair correlation functions, structure factor, diffusion coefficient etc.

2.3. Results and Discussions

We have studied neutral as well as ionic binary mixtures (of types 0 and 1) from the viewpoint of their equilibrium structural arrangement (pair correlation function) and their transport properties (self-diffusion coefficient) with size asymmetry ($\sigma_r = \sigma_0/\sigma_1$) from 1.0 to 10.0, charge asymmetry ($z_r = z_0/z_1$) from 1.0 to 10.0 and mass asymmetry ($\mu = m_0/m_1$) from

1.0 to 500. The size/mass/charge of type 0 particle is varied (while those of particle 1 is kept constant at $\sigma_1 = 6\text{\AA}$, $m_1 = 1\text{amu}$ (1.0 g/mole) and $z_1 = -1e$) to achieve the desire σ_r , z_r and μ . The variation of the interaction potential (WCA + Coulomb) for a typical system studied is shown in Figure 2.2.

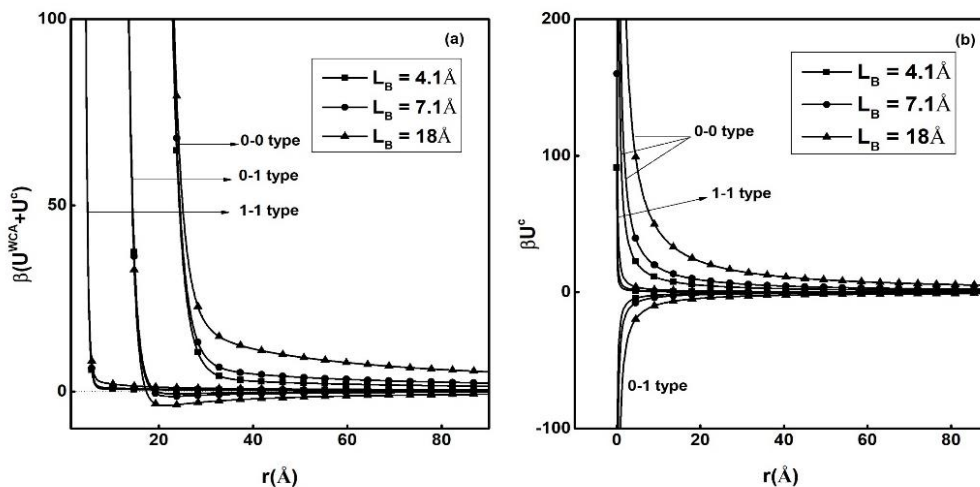


Figure 2.2: Variation of the interaction potential with distance at different Bjerrum lengths (L_B) for the system with charge asymmetry ($z_r = 5.0$), size asymmetry ($\sigma_r = 5.0$) and no mass asymmetry ($\mu=1.0$); (a) Total potential (WCA + Coulomb), (b) Only the Coulomb potential.

2.3.1. Pair-correlation functions

2.3.1.1. System with only Size Asymmetry

We simulated a binary mixture of neutral particles with size of type 0 particle varying from 6\AA to 60\AA and size of type 1 particle fixed at 6\AA . The mass of both the particles were held constant at 1amu . The variation of pair-correlation function and the structure factor with different size asymmetry are displayed in Figure 2.3 and Figure 2.4, respectively.

As the size of the type 0 particle increases (σ_r increases), the peak positions in the pair-correlation function $g_{00}(r)$ and $g_{01}(r)$ shifts towards larger inter-particle distance. In all cases, the first peak positions appear near the inter-particle contact, i.e. at around $r/\sigma_{ij} \approx 1$. For $g_{11}(r)$, the trend is somewhat opposite. As the size of type 0 particles increase, they displace the smaller (type 1) particles to a greater extent and thus the probability of finding type 1 particles around another type 1 particle increases, the peak position in $g_{11}(r)$ shifts to smaller inter-particle distance.

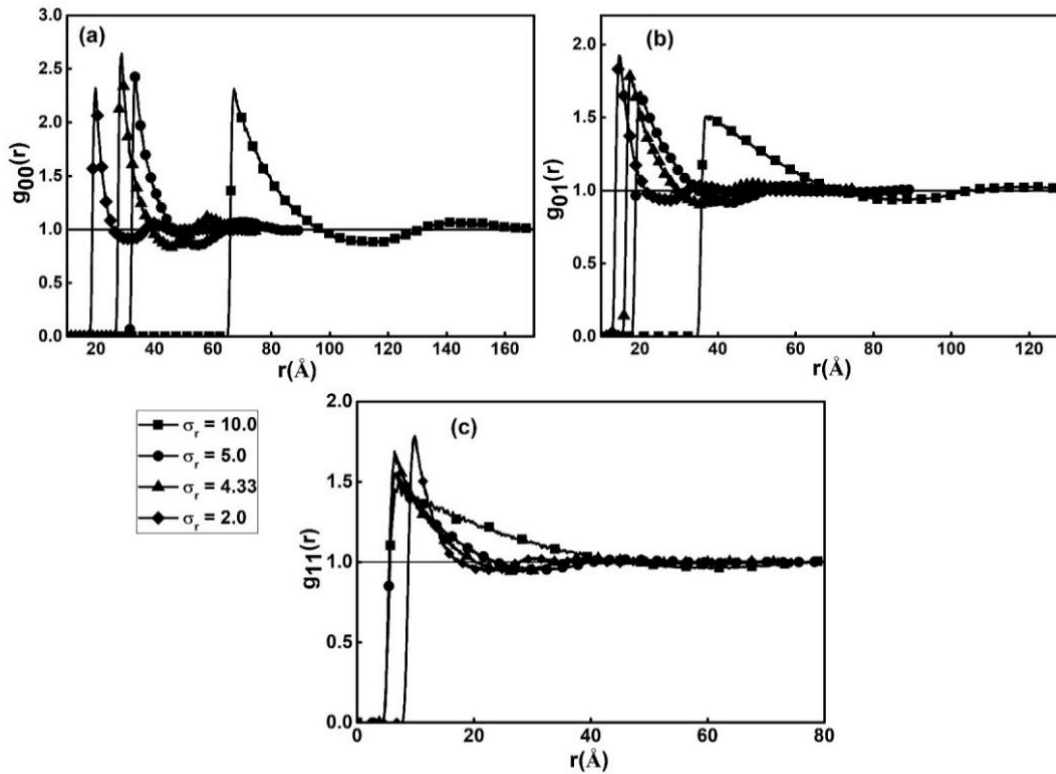


Figure 2.3: Variation of pair-correlation functions with size asymmetry ($\sigma_r = 2.0$ to 10.0) for neutral binary mixture: (a) $g_{00}(r)$, (b) $g_{01}(r)$ and (c) $g_{11}(r)$. Other parameters: packing fraction (η) = 0.25, no mass asymmetry ($\mu = 1.0$).

With increase in the size asymmetry, the peak positions in the 0-0 structure factor $S_{00}(k)$ shift towards the lower wave vector k (larger inter-particle distance) consistent with $g_{00}(r)$ (Figure 2.4).

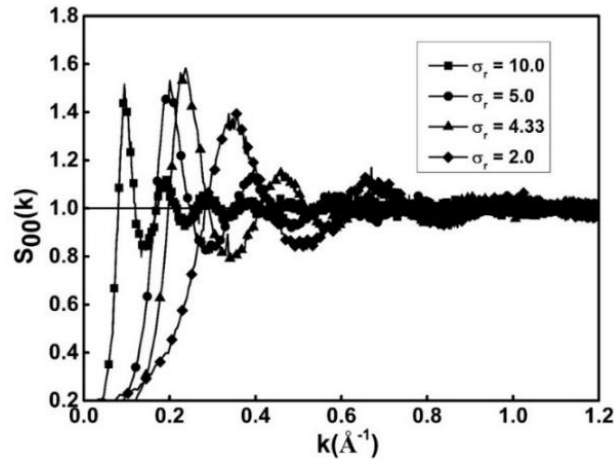


Figure 2.4: The variation of 0-0 structure factor $S_{00}(k)$ with size asymmetry ($\sigma_r = 2.0$ to 10.0) for the neutral binary mixture. Other parameters are same as in figure 2.3.

The values of pair-correlation function at contact distances decrease with increase in size asymmetry. This trend is clearly observed in $g_{0l}(r)$ and roughly observed in the other correlation functions. In addition to the first peak, a second peak (coordination shell) is observed in most of the correlation functions. This behaviour is quite expected, as the systems with particles more tightly packed have more long-range correlations and are closer to the solid state as compared with the particles which are loosely packed and are much nearer to the gaseous phase. The location of this second peak (coordination shell) is observed around $r/\sigma_{ij} \approx 2$ for low size asymmetry and this value keep on increase as the size of the bigger particle increases. For systems with lower packing fraction (lesser than 0.2), only the first peak is observed. A representative plot with a packing fraction 0.075 is shown in Figure 2.5.

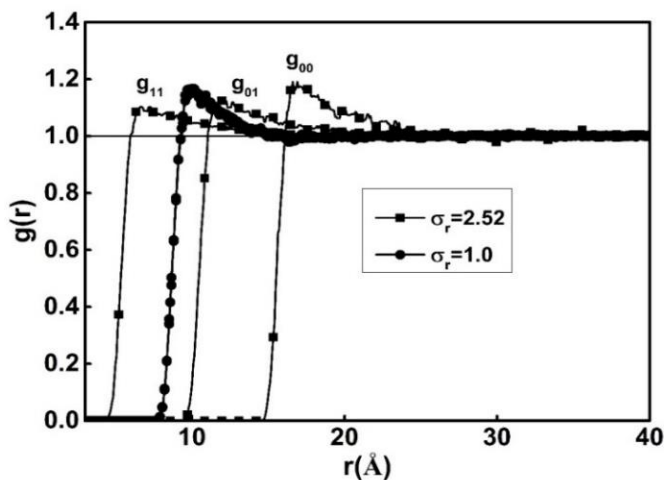


Figure 2.5: Plot of pair-correlation function $g(r)$ for size symmetric ($\sigma_r = 1.0$) and size asymmetric ($\sigma_r = 2.52$) neutral binary mixture. Other parameters: packing fraction (η) = 0.075, no mass asymmetry ($\mu = 1.0$).

2.3.1.2. System with only Charge Asymmetry

In this case, we simulated a binary mixture of charged particles with charge of type 0 particle varying from $-1e$ to $-10e$ and charge of type 1 particle fixed at $1e$. The mass and size of both the particles were held fixed at 1amu and 10\AA , respectively. The number of type 0 and type 1 particles are adjusted to make the whole system electro-neutral.

As the charge (of type 0 particle) increases (z_r increases), the repulsion between two type 0 particles increases much more than the attraction between a type 0 and a type 1 particle. This is clearly visible in the plot of pair correlation of functions for different charge asymmetry displayed in Figure 2.6.

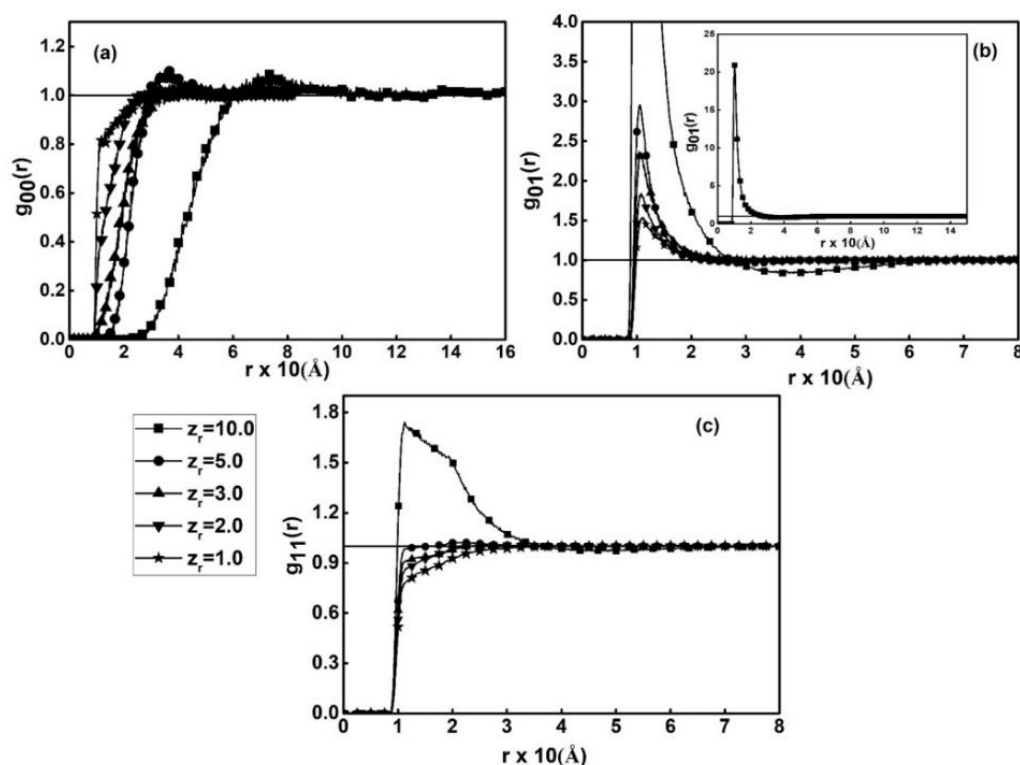


Figure 2.6: Variation of pair-correlation functions with different charge asymmetry ($z_r = 1.0$ to 10.0) for the binary mixture: (a) $g_{00}(r)$, (b) $g_{01}(r)$ and (c) $g_{11}(r)$. There is no mass asymmetry ($\mu=1.0$) and no size asymmetry ($\sigma_r = 1.0$).

As the repulsion between two type 0 particles increases, the peak position as well as the position of first non-zero value in $g_{00}(r)$ curves shift towards larger interparticle distances. For example, the first non-zero value in g_{00} (probability finding a type 0 particle

around another type 0 particle) occurs around $r/\sigma \approx 1$ (at the inter-particle-contact) for $z_r = 1.0$ to 3.0, and changes to $r/\sigma \approx 1.5$ and 3.0 for $z_r = 5.0$ and 10.0, respectively. Similarly, the peak positions in g_{00} appear around $r/\sigma \approx 2, 3, 6$ for $z_r = 3.0, 5.0$ and 10.0, respectively (Figure 2.6(a)). Further we have also discussed the g_{00} for big colloids i.e. colloid-colloid type in chapter 3. We have plotted the probability of finding particles of type 0 around another particle of same type within a sphere of diameter $\sigma, 2\sigma, \dots$ etc in Figure 2.7(a). This probability decreases nearly up to 50% as the charge on the type 0 particle increases from $1e$ to $10e$ (from $z_r = 1.0$ to 10.0). This indicates that the accumulation of counter-ions (type 1 particles) on the surface of type 0 particles (counter-ion condensation) may not be significant. However, as the charge (on particle of type 0) increases, probability of finding the number of counter-ions (type 1 particles) around this particle increases. This is supported by an increase in the value of the pair-correlation function $g_{01}(r)$ (which is proportional to the number of nearest neighbours) as we move towards the highly asymmetric case (Figure 2.6(b)). The peak heights increase with increase in charge on the type 0 particles with the peak positions nearly same around $r/\sigma \approx 1$. This increase is quite drastic in case of system with asymmetry 10:1 ($z_r = 10.0$). With increase in charge on type 0 particle, the $g_{11}(r)$ (Figure 2.6(c)) peak becomes broad and peak height increases, peak positions shift to lower inter-particle distance. The value of correlation function $g_{11}(r)$ is nearly unity in case of system with lower charge asymmetries ($z_r = 1.0$ to 3.0). This may be due to the loose packing of the system and a relatively weak long-range interaction as compared to a system with larger charge asymmetry, say $z_r = 5.0$ and 10.0.

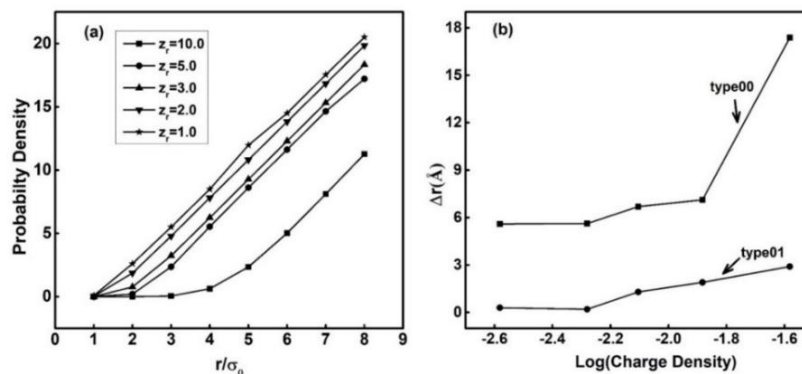


Figure 2.7: a) Plot of probability of finding a 0-type particle around another 0-type particle with different charge asymmetry ($z_r = 1.0$ to 10.0). b) Shift in the position of the first peak of

the pair-correlation functions (g_{00} and g_{01}) for the charged system from the corresponding uncharged system. (diameter of both the particles = 10\AA , Charge Density is in $e/\text{\AA}^3$, $e=1.6 \times 10^{-19}$ coulombs).

For selected cases, we have compared the peak positions of pair-correlation functions of the charged systems with the corresponding neutral systems in Figure 2.7(b). This plot shows how the shift in the position of the first peak for various neutral system from that of corresponding charged system in $g_{00}(r)$ and $g_{01}(r)$ as a function of the charge density of the bigger particle. The shift in the peak positions increase as the charge asymmetry increases, and the shift is about an order of magnitude more for $g_{00}(r)$.

2.3.1.3. System with only Mass Asymmetry

Here, we simulated a neutral system with asymmetry in mass ($\mu = m_0/m_1$) varying from $\mu = 1.0$ to $\mu = 500$. The size of both the particles are same ($\sigma = 10\text{\AA}$). The packing fraction of the system is 0.08481.

The pair correlation functions (radial distribution functions and the structure factor) for the different mass asymmetry are nearly superimposable to one another (not shown here) with the first peak occurring around $r = 2^{1/6} \sigma$ (at the minimum of the interacting potential). The peak heights of all the pair-correlation functions for different mass asymmetry are collected in Table 2.1.

Table 2.1. The peak height of pair-correlation functions for various mass asymmetries at different temperatures for neutral binary size-symmetric mixture. The packing fraction of the system is 0.0848. Note that $g_{00} = g_{10} = g_{11}$.

Mass asymmetry (μ)	120K	300K	500K
2	1.254	1.183	1.155
10	1.254	1.184	1.154
50	1.255	1.183	1.153
84	1.253	1.182	1.153
125	1.257	1.182	1.153
250	1.254	1.184	1.154
500	1.253	1.183	1.153

The values are nearly same for a given temperature and decrease as the temperature increases. Thus, mass asymmetry has almost negligible effect on the equilibrium structure

arrangement of the system. This behaviour is expected because the potential of interaction between the particles which determines the equilibrium arrangement of the system is independent of the mass of the particle. However, the mass influences diffusion coefficient.

In addition to above, we simulated binary mixtures with asymmetry in (a) both size and mass, as well as (b) both charge and mass. The pair-correlation functions and structure factors (not shown here) are found to be similar to the cases, respectively, with (a) only size asymmetry, and (b) only charge asymmetry, hence supporting the claim that mass of the particles have negligible effect on the equilibrium structure arrangement of the studied systems.

2.3.1.4. System with charge and size asymmetry

This is an interesting case as both charge and size asymmetry effects the equilibrium structure arrangement of the particles individually. In this set of simulations, we took binary mixture of size ratio (σ_r) = 5.0 with the charge asymmetry (z_r) = 3.0 to 10.0.

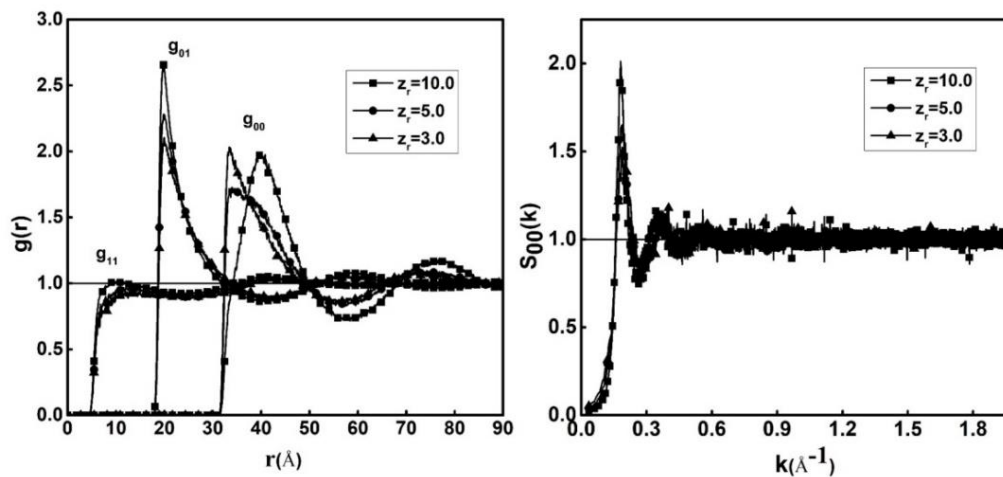


Figure 2.8: Variation of the pair-correlation functions ($g(r)$) and 0-0 structure factor $S_{00}(k)$ for size asymmetry ($\sigma_r = 5.0$) and different charge asymmetry ($z_r = 10.0$ to 3.0). There is no mass asymmetry ($\mu=1.0$).

The pair correlation functions for this mixture are plotted in Figure 2.8. On increasing the charge and size of type 0 particle in the mixture, the $g_{00}(r)$ show a trend closer to the systems with only charge asymmetry (than system with only size asymmetry) - the peak shifts

towards larger inter-particle distances. The $g_{01}(r)$ shows similar trend like that of only charge asymmetry, i.e. the peak height increases with increasing charge asymmetry. The $g_{11}(r)$ peak increases as the charge of bigger particle increases. The structure factor $S_{00}(k)$ shifts towards lower wave vector k with increase in charge asymmetry.

2.3.1.5. Thermodynamic Properties

The variation of reduced energy and pressure with size asymmetry (σ_r) for neutral binary mixture is displayed in Figure 2.9. The reduced energy as well the pressure of the system decreases with increasing the size asymmetry (increasing σ_r). This variation is similar to decreasing the density of the system.

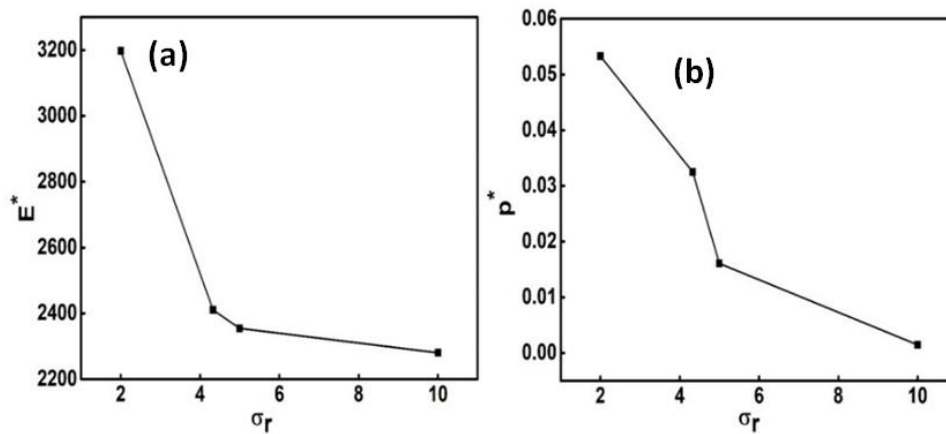


Figure 2.9: Variation of the reduced (a) energy (E^*) and (b) pressure (P^*) with size asymmetry for neutral binary system with mass symmetric ($\mu = 1.0$).

The variation of reduced excess free energy ($\beta E^{ex}/\rho$) and the osmotic coefficient (Φ_V) as a function of charge asymmetry (z_r) for the size-symmetric ($\sigma_r = 1.0$) as well as size-asymmetric ($\sigma_r = 5.0$) binary mixtures are plotted in Figure 2.10. The equation 2.5 and equation 2.6 can be written as

$$\Phi_V = 1 + \frac{\beta E^{ex}}{3\rho} + \frac{2\pi}{3\rho} \sum_{ij} \rho_i \rho_j \sigma_{ij}^3 g_{ij}(\sigma_{ij} + 0) \quad (2.8)$$

$$\frac{\beta E^{ex}}{\rho} = \frac{2\pi L_B}{\rho} \sum_{ij} \rho_i \rho_j Z_i Z_j \int_0^{\infty} h_{ij}(r) r dr \quad (2.9)$$

$$= \frac{L_B}{\pi\rho} \sum_{ij} \rho_i \rho_j Z_i Z_j \int_0^{\infty} \tilde{h}_{ij}(k) dk \quad (2.10)$$

is the excess energy per ion. This expression is valid for hard-sphere plus coulomb potential. But the WCA potential we used to be purely repulsive which often can be used to mimic hard-sphere potential.

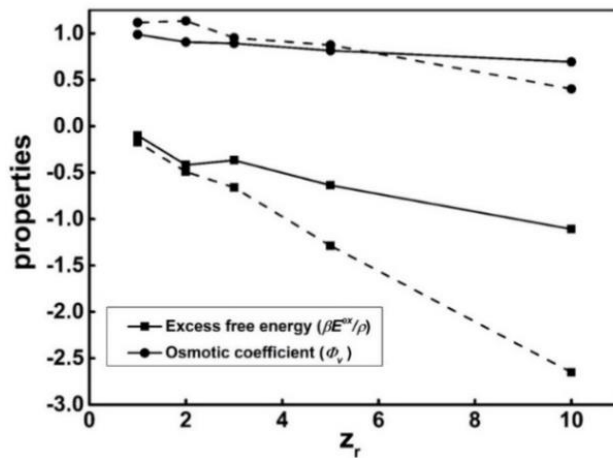


Figure 2.10: Variation of reduced excess free energy (■) and osmotic coefficient (●) with charge asymmetry (z_r) for the systems with size asymmetry ($\sigma_r = 5.0$, solid lines) and without size asymmetry ($\sigma_r = 1.0$, broken lines).

$\beta E^{\text{ex}}/\rho$ increases (in magnitude) as the charge asymmetry increases (z_r increases), and the rate of increase is more after $z_r > 3.0$. As z_r increases the coulomb interactions between the particles increases and become long range. This results in increase of excess free energy ($\beta E^{\text{ex}}/\rho$). As the size (σ) of the particle increases (for a given charge asymmetry), the charge density decreases and so the long-range interactions. This brings the system close to ideal and so magnitude of excess free energy decreases. The osmotic coefficient (Φ_V) decreases as the charge asymmetry increases (z_r increases). The values of size symmetric case are found to be greater than those corresponding size asymmetric systems at lower charge asymmetry. This trend becomes opposite at higher charge ($z_r > 5$).

2.3.2 Self-Diffusion coefficients

As mentioned previously, the self-diffusion coefficients of our studied systems are calculated from the slope of the mean-square displacement at long time limit.

2.3.2.1. System with only mass asymmetry

The mean square displacement (MSD) for type 0 particle as a function of simulation time for different mass asymmetry ($\mu = m_0/m_1$) at 300 K is plotted in Figure 2.11(a). The MSD decreases with increase in the mass asymmetry (increase in μ). The self-diffusion coefficients for both type 0 (D) as well as type 1 particles (D_1), obtained from the corresponding MSD, are presented in Figure 2.11(b).

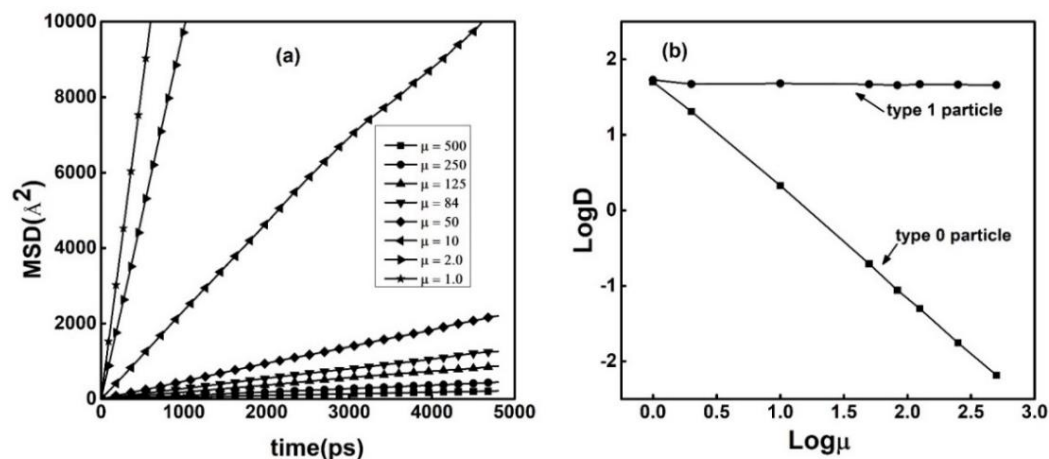


Figure 2.11: Plot of (a) mean square displacement (MSD) and (b) diffusion coefficient (D in $\text{\AA}^2/\text{ps}$) with mass asymmetry (μ) for size symmetric ($\sigma_r = 1.0$) neutral binary mixture at 300K with packing fraction ($\eta = 0.08481$).

The values of D decrease sharply while the values of D_1 are nearly constant with increase in the mass asymmetry (increase in μ) of the mixture. The value of D changes from $50.1091 \text{ \AA}^2/\text{ps}$ at $\mu = 1$ to $0.0065 \text{ \AA}^2/\text{ps}$ at $\mu = 500$ at 300K. The corresponding values of D_1 are $53.551 \text{ \AA}^2/\text{ps}$ to $45.832 \text{ \AA}^2/\text{ps}$, respectively. A similar trend in the diffusion coefficients with the mass asymmetry (μ) is obtained for other temperatures. The variation of D with mass asymmetry is shown in the isotherms of Figure 2.12. The isotherms are found to be parallel following the equation ($R^2 = 0.99$)

$$\text{Log}(D) = F - 1.45 \times \text{Log}(\mu) \quad (2.11)$$

The values of the intercept F increase with the temperature and were estimated to be 1.34, 1.74 and 1.97 for 120K, 300K and 500K respectively.

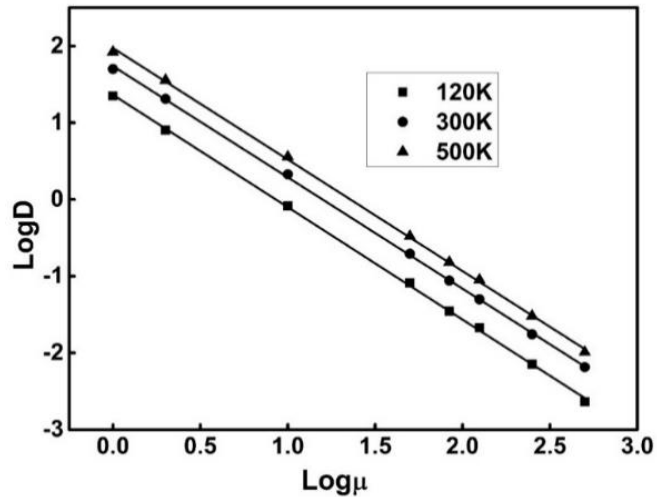


Figure 2.12: The variation of diffusion coefficient (D) of heavier particle with mass asymmetry (μ) at different temperatures for size symmetric ($\sigma_r = 1.0$) neutral binary mixture with packing fraction ($\eta = 0.08481$).

Further insight is obtained from the Macedo-Litovitz theory [39,40] which is quite successful in describing the diffusion behaviour for glass transition of fluids [41] and in polymers [42,43]. This theory is based upon the assumption that diffusion in liquids is controlled by two simultaneous events: (1) the existence of an adjacent local free volume of certain size into which the molecule can jump, and (2) the acquisition of sufficient energy by the molecule in order to escape from the force field of its neighbours. Accordingly, the diffusion coefficient is expressed in the following form:

$$D = D'_0 \exp\{-[(\gamma v_0 / v_f) + (E_a / RT)]\} \quad (2.12)$$

Where, v_0 and v_f are, respectively, the molar volume and the average free volume per molecule, γ is a numerical factor between 0.5 and 1. For our case of mass asymmetry, the ratio v_0/v_f is nearly constant as the size of the particles is constant. For example, the ratio v_0/v_f is found to be 0.68 for the packing fraction of 0.0848 using the Carnahan-Starling equation of state [44]. In view of nearly constant free volume term (which can be absorbed in the pre-factor D_0), the the Macedo-Litovit equation reduces to the Arrhenius relationship

$$D = D_0 \exp\{-(E_a / RT)\} \quad (2.13)$$

The plot between $\ln D$ and the inverse temperature is displayed in Figure 2.13 and the extracted activation energy (E_a) and D_0 (from the slope and intercept of the plot, respectively) for the heavier particle are summarized in Table 2.2.

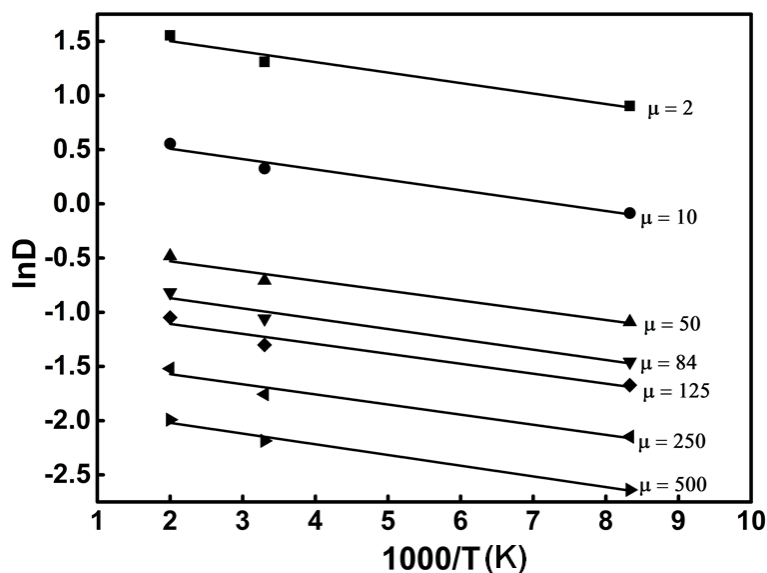


Figure 2.13: Arrhenius plot ($\ln D$ vs $1/T$) of neutral binary mixture for different mass asymmetry (μ). Other parameters are same as given in figure 2.12.

Table 2.2: Estimated Arrhenius parameters (Equation 2.13), the activation Energy and pre-factor (D_0), for different mass asymmetries (μ) for neutral binary size-symmetric mixture.

Mass asymmetry (μ)	Activation Energy(J/mol)	D_0
2	804.17	49.545
10	796.39	5.012
50	750.65	0.447
84	791.04	0.209
125	763.61	0.119
250	775.94	0.041
500	821.18	0.015

The values of activation energy vary from 750.6 to 821.2 J/mol (minimum for $\mu = 50$) and the pre-factor D_0 (which is proportional to the collision frequency of the particles) decreases with increase in mass asymmetry. The obtained values of the activation energy are comparable to reported values for similar system but with full LJ potential [45].

2.3.2.2. System with only size/charge asymmetry

The variation of diffusion coefficients with only size asymmetry is shown in Figure 2.14.

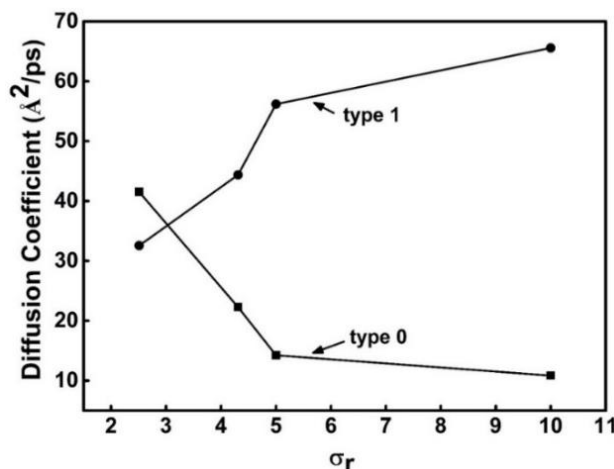


Figure 2.14: The variation of diffusion coefficients of both the particles with size asymmetry ($\sigma_r = 2.5$ to 10.0) for the mass symmetric ($\mu = 1.0$) neutral binary mixture.

With increase in size of type 0 particle (with increase in σ_r), the values of the diffusion coefficient of type 0 particle (D) decrease (in agreement with the Stoke-Einstein relationship [36] and that of type 1 particle (D_1) increases. Similarly, with increasing the charge on the type 0 particle (with keeping the charge of type 1 particle fixed) the diffusion coefficient value of the type 0 particle decreases (Figure 2.15(a), $\sigma_r = 1.0$ curve).

2.3.2.3. System with more than one type of asymmetry

The variation of self-diffusion coefficients (D) studied till now can be summarized as follows: the diffusion coefficient value decreases with increase in (i) mass, (ii) size, and (iii) charge, of the particle. It will be interesting to see the variation of D with a combination of size, charge and mass. Figure 2.15(a) shows the variation of diffusion coefficient (of type 0 particle) with charge asymmetry for a size symmetric ($\sigma_r = 1.0$) and a size asymmetric ($\sigma_r = 5.0$) system. In both the cases, the diffusion coefficients decrease with increase in charge asymmetry (increase in z_r). However, the value of D is smaller (about 15%) for the system with size asymmetry than the size-symmetric system. Representative results for systems with asymmetry in both mass and charge is displayed in Figure 2.15(b). For the system with mass

asymmetry $\mu = 125$, the values of diffusion coefficients are closer to the system with only mass asymmetry and also the effect of charge comes into picture only for systems with $z_r > 3.0$. This may be due to the fact that the electrostatic interactions in systems with $z_r < 3.0$ may not be able to bring much of momentum change for a particle with mass 125amu ($\mu = 125$) as compared to particle of 1amu mass. This is supported by about two-fold increase in the diffusion coefficient values of the lighter (type 1) particle (whose mass is held constant at 1amu). Although, the diffusion coefficient steadily decreases when either μ or σ_r increases, but the maximum value was found with $\mu = 1$, $\sigma_r = 2.5$ (and not with $\sigma_r = 1$) when both mass as well as size of the particles vary simultaneously. Almost similar results are obtained for the case with both mass and size asymmetry. The diffusion coefficients follow the trend for only mass asymmetry, but the decrease in D is more for the system with additional size asymmetry.

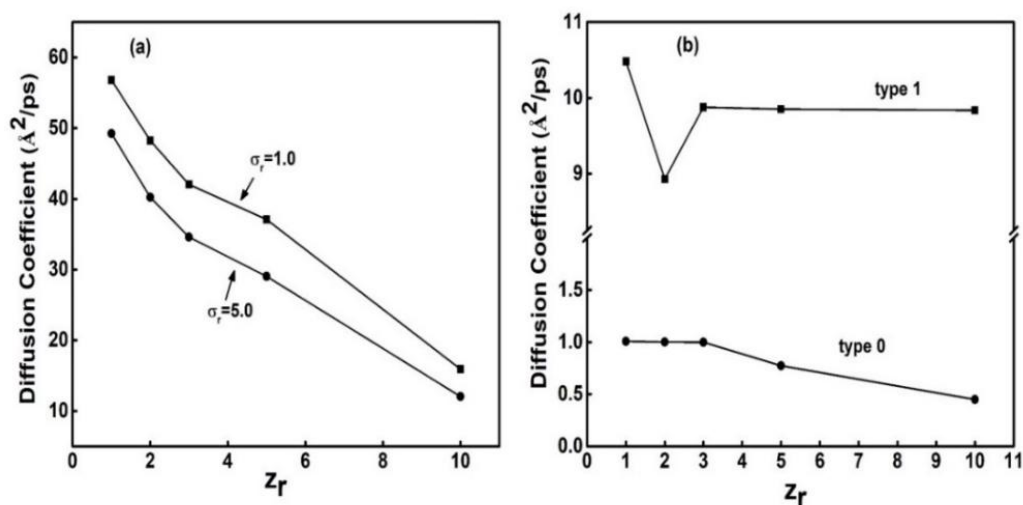


Figure 2.15: The variation of diffusion coefficients with charge asymmetry for binary mixture (a) with different size asymmetry ($\sigma_r = 1.0$ and 5.0), for 0-type particle (b) with mass asymmetry ($\mu = 125$), for both 0-type and 1-type particles. The diffusion coefficients of type 0 particles in figure (b) is multiplied by factor of 10.

2.3.2.4. Empirical relations

We have obtained an empirical relation (Equation 2.14) to predict the diffusion coefficient (D) for the systems with asymmetry in both size as well as mass in terms of the diffusion coefficients of systems with only mass asymmetry (D_M) and diffusion coefficient of system with only size asymmetry (D_S). The expression is ($\mu = \sigma_r \neq 1.0$):

$$D = \left(\frac{\log \mu}{\log(\mu \times \sigma_r)} \right)^a \times D_M + \left(\frac{\log \sigma_r}{\log(\mu \times \sigma_r)} \right)^b \times D_S \quad (2.14)$$

With $a = 1.9$, $b = 4.99$ for $84 < \mu < 1.0$, where as $a = 4.49$, $b = 5.79$ for $500 < \mu < 84$. The prediction of Equation (2.14) is compared with the simulation results in Figure 2.16(a).

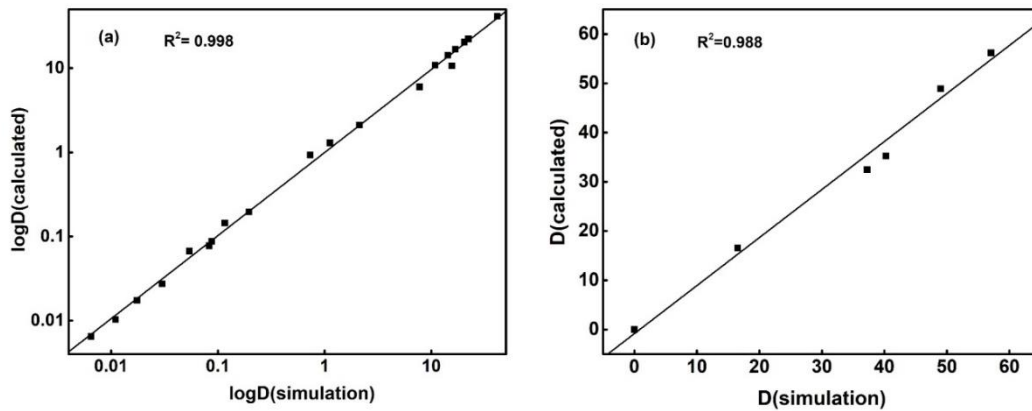


Figure 2.16: Correlation plots of diffusion coefficients obtained from current simulation and predicted (a) by equation (2.14) and (b) by equation (2.15).

We have tried to express the diffusion coefficients of charged system (D_C) in terms of those of corresponding neutral systems (D_N). The following empirical relation was obtained:

$$D_C = \frac{(\eta_C)^{0.27}}{(\eta_N)^{0.37}} \frac{D_N}{z^{0.4}} \quad (2.15)$$

Where z is the charge on the particle, η_N and η_C are the packing fraction of the neutral and the charged particle, respectively. This empirical equation (Equation 2.15) reproduces the simulation result quite well (Figure 2.16(b)).

2.3.2.5 Estimation of System-Size Dependence of diffusion coefficient

We have estimated the system-size dependence on the diffusion coefficients calculated, using Yeh and Hummer equation [46]

$$D_{PBC} = D_0 - 2.837297 k_B T / (6\pi\zeta L) \quad (2.16)$$

Where, D_{PBC} is the diffusion coefficient calculated in the simulation, D_0 is the diffusion coefficient of the particle in an infinite system, k_B the Boltzmann constant, T the absolute temperature, and ζ the shear viscosity of the solvent. We have calculated the diffusion coefficients of a representative system ($z_r = 5.0$, $\sigma_r = 1.0$, $\mu = 1.0$ and $\eta = 0.067$) with different simulation box lengths (L). The values of diffusion coefficients obtained are 37.07, 38.66, 39.33 and 40.05 $\text{\AA}^2/\text{ps}$, for $L = 150, 180, 300$ and 375\AA , respectively. This variation of self-diffusion coefficient with simulation box lengths is also plotted in Figure 2.17.

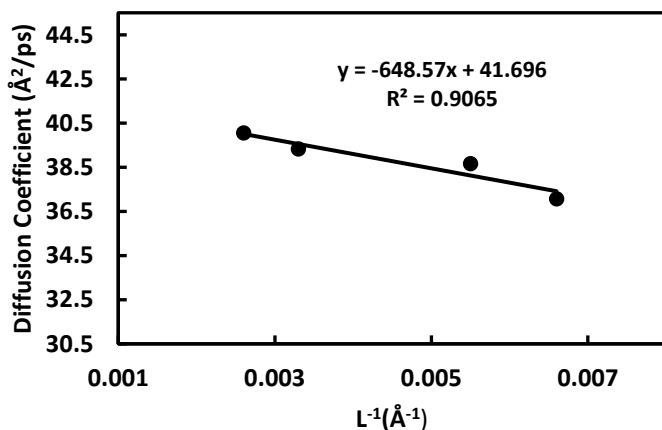


Figure 2.17: Variation of self-diffusion coefficient with different simulation box length (L) for the system with $z_r = 5.0$, $\sigma_r = 1.0$, $\mu = 1.0$ and packing fraction (η) = 0.067.

The diffusion coefficient in the limit of infinite box length (D_0), estimated from the intercept of this plot (Eq. 2.16), is found to be 41.69 $\text{\AA}^2/\text{ps}$. The estimated deviations of the simulated diffusion coefficients from that of D_0 for the system considered are about 11% (for $L = 150 \text{\AA}$), 7% (for $L = 180 \text{\AA}$), 5% (for $L = 300 \text{\AA}$) and 4% (for $L = 375 \text{\AA}$). Thus, our values reported mostly at $L = 180 \text{\AA}$ (and few cases 300\AA and 375\AA) have a system-size dependence error within 7% (or less). Accordingly, we expect a similar deviation (4%–7%) in the values of D as well as D_M and D_S in Eq. (2.14), and D_C as well as D_N in Eq. (2.15), and probably, the numerical constants in these equations may be hardly affected.

2.4 Conclusion

We have reported the molecular dynamics simulation results for binary fluid mixtures having asymmetry in size, mass, charge and their combinations. A systematic variations in different properties as a function of charge, size and mass asymmetries have been observed. Possible explanation for these trends is presented in many cases. The pair correlation functions shift to larger inter-particle distances as the size and/or charge increases indicating increase in repulsion between particles. The mass variation has practically no effect. This may be due to the fact that mass doesn't appear explicitly in the expression for pair potential (Equation 2.1). With increase in size asymmetry, both the energy and pressure of the neutral systems decreases, an effect similar to decrease in density of the system. As the charge asymmetry increases, the interactions between the particles become long ranged and the magnitude of excess free energy increases. For a given charge asymmetry, higher excess free energy is found for size symmetric mixture than those of size symmetric case, possibly due to reduction in charge density. The self-diffusion coefficients are found to decrease with increase in size, charge and mass asymmetries. Arrhenius-type behavior is found for the diffusion coefficient. Empirical relations expressing diffusion coefficient of systems having more than one type of asymmetry in terms of diffusion coefficient of systems having asymmetry of only one type, have been presented.

2.5. References

- [1] J.-L. Barrat and J.-P. Hansen, *Basic Concepts for Simple and Complex Liquids*, Cambridge University Press, 2003.
- [2] D. Chandler, *From 50 Years Ago, the Birth of Modern Liquid-State Science*, Annu. Rev. Phys. Chem. 68 (2017), pp. 19–38.
- [3] F. Betaouaf, F. Cailliez, B. Rousseau and F. Ould-Kaddour, *Molecular simulation of the thermodynamics, structural and transport properties of the liquid binary mixture methane + nitrogen*, J. Mol. Liq. 200 (2014), pp. 298–304.
- [4] I. Shvab and R.J. Sadus, *Thermodynamic properties and diffusion of water+ methane*

- binary mixtures*, J. Chem. Phys. 140 (2014), pp. 104505.
- [5] S. Ghimire and N.P. Adhikari, *Study of structural and transport properties of argon, krypton, and their binary mixtures at different temperatures*, J. Mol. Model. 23 (2017), pp. 94.
- [6] J. Wang, H. Zhong, H. Feng, W. Qiu and L. Chen, *Molecular dynamics simulation of diffusion coefficients and structural properties of some alkylbenzenes in supercritical carbon dioxide at infinite dilution*, J. Chem. Phys. 140 (2014), pp. 104501.
- [7] N.A.T. Miller, P.J. Daivis, I.K. Snook and B.D. Todd, *Computation of thermodynamic and transport properties to predict thermophoretic effects in an argon-krypton mixture*, J. Chem. Phys. 139 (2013), pp. 144504.
- [8] V. Lobaskin and P. Linse, *Accurate simulation of highly asymmetric electrolytes with charge asymmetry 20:1 and 20:2*, J. Chem. Phys. 109 (1998), pp. 3530–3541.
- [9] B. Rotenberg, O. Bernard and J.-P. Hansen, *Underscreening in ionic liquids: a first principles analysis*, J. Phys. Condens. Matter 30 (2018), pp. 54005.
- [10] M. Andreev, J.J. de Pablo, A. Chremos and J.F. Douglas, *Influence of ion solvation on the properties of electrolyte solutions*, J. Phys. Chem. B 122 (2018), pp. 4029–4034.
- [11] H. Jiang and H. Adidharma, *Study of thermodynamic properties of symmetric and asymmetric electrolyte systems in mixture with neutral components: Monte Carlo simulation results and integral equation predictions*, Mol. Simul. 41 (2015), pp. 727–734.
- [12] L.E. Sánchez-Díaz, G.A. Méndez-Maldonado, M. González-Melchor, H. Ruiz-Estrada and M. Medina-Noyola, *Equilibrium structure of the multi-component screened charged hard-sphere fluid*, J. Chem. Phys. 135 (2011), pp. 14504.
- [13] K.R. Harris, *H-Bonding in 2, 2, 2-Trifluoroethanol: Application of the Stokes--Einstein--Sutherland Equation to Self-Diffusion and Viscosity at High Pressures*, J. Chem. Eng. Data 63 (2018), pp. 1443–1453.

- [14] W.Z. Li, C. Chen and J. Yang, *Molecular dynamics simulation of self-diffusion coefficient and its relation with temperature using simple Lennard-Jones potential*, Heat Transf. - Asian Res. 37 (2008), pp. 86–93.
- [15] W. Fenz, I.M. Mryglod, O. Prytula and R. Folk, *Concentration and mass dependence of transport coefficients and correlation functions in binary mixtures with high mass asymmetry*, Phys. Rev. E 80 (2009), pp. 21202.
- [16] M. Sharma and S. Yashonath, *Size dependence of solute diffusivity and Stokes-Einstein relationship : effect of van der Waals interaction*, Diffus. Fundam. 7 (2007), pp. 1–15.
- [17] S. Bastea, *Diffusion and conduction in a salt-free colloidal suspension via molecular dynamics simulations*, Soft Matter 6 (2010), pp. 4223–4228.
- [18] R. Sharma, K. Tankeshwar and S. Ranganathan, *Mass dependence of mutual diffusion coefficient: computer simulation study*, Phys. Chem. Liq. 49 (2011), pp. 206–218.
- [19] G. Feng, M. Chen, S. Bi, Z.A.H. Goodwin, E.B. Postnikov, M. Urbakh et al., *Kinetics of Ion Transport in Ionic Liquids: Two Dynamical Diffusion States*, arXiv Prepr. arXiv1805.00697 (2018), .
- [20] H. Lowen, E. Allahyarov, J. Dzubiella, C. Von Ferber, A. Jusufi, C.N. Likos et al., *Interactions and phase transitions of colloidal dispersions in bulk and at interfaces*, Philos. Trans. R. Soc. London A Math. Phys. Eng. Sci. 359 (2001), pp. 909–920.
- [21] A. Mulero, C.A. Galán, M.I. Parra and F. Cuadros, *Equations of state for hard spheres and hard disks*, in *Theory and Simulation of Hard-Sphere Fluids and Related Systems*, Springer, 2008, pp. 37–109.
- [22] V. Lobaskin and P. Linse, *Accurate simulation of highly asymmetric electrolytes with charge asymmetry 20: 1 and 20: 2*, J. Chem. Phys. 109 (1998), pp. 3530–3541.
- [23] D.M. Heyes and H. Okumura, *Some physical properties of the Weeks--Chandler--Andersen fluid*, Mol. Simul. 32 (2006), pp. 45–50.

- [24] J.P. Boon and S. Yip, *Molecular Hydrodynamics*, Courier Corporation, 1980.
- [25] K. Miyazaki, G. Srinivas and B. Bagchi, *The Enskog theory for transport coefficients of simple fluids with continuous potentials*, J. Chem. Phys. 114 (2001), pp. 6276–6285.
- [26] P. Banerjee and B. Bagchi, *A mode-coupling theory analysis of the observed diffusion anomaly in aqueous polyatomic ions*, J. Chem. Phys. 147 (2017), pp. 124502.
- [27] G. Guevara-Carrion, T. Janzen, Y.M. Muñoz-Muñoz and J. Vrabec, *Mutual diffusion of binary liquid mixtures containing methanol, ethanol, acetone, benzene, cyclohexane, toluene, and carbon tetrachloride*, J. Chem. Phys. 144 (2016), pp. 124501.
- [28] N. Ohtori and Y. Ishii, *Explicit expressions of self-diffusion coefficient, shear viscosity, and the Stokes-Einstein relation for binary mixtures of Lennard-Jones liquids*, J. Chem. Phys. 143 (2015), pp. 164514.
- [29] R. Bhadauria and N.R. Aluru, *A multiscale transport model for Lennard-Jones binary mixtures based on interfacial friction*, J. Chem. Phys. 145 (2016), pp. 74115.
- [30] U. Marini Bettolo Marconi, P. Malgaretti and I. Pagonabarraga, *Tracer diffusion of hard-sphere binary mixtures under nano-confinement*, J. Chem. Phys. 143 (2015), pp. 184501.
- [31] R. Devi, S. Srivastava and K. Tankeshwar, *Static and dynamic effects of confinement on self-diffusion*, Phys. Chem. Liq. 52 (2014), pp. 636–649.
- [32] T. Darden, D. York and L. Pedersen, *Particle mesh Ewald: An $N \log(N)$ method for Ewald sums in large systems*, J. Chem. Phys. 98 (1993), pp. 10089–10092.
- [33] P.H. Hünenberger, *Thermostat algorithms for molecular dynamics simulations*, in *Advanced computer simulation*, Springer, 2005, pp. 105–149.
- [34] M.P. Allen and D.J. Tildesley, *Computer Simulation of Liquids*, Oxford university press, 2017.

- [35] H.-J. Limbach, A. Arnold, B.A. Mann and C. Holm, *ESPReso an extensible simulation package for research on soft matter systems*, Comput. Phys. Commun. 174 (2006), pp. 704–727.
- [36] M. Deserno and C. Holm, *How to mesh up Ewald sums. I. A theoretical and numerical comparison of various particle mesh routines*, J. Chem. Phys. 109 (1998), pp. 7678–7693.
- [37] M. Deserno and C. Holm, *How to mesh up Ewald sums. II. An accurate error estimate for the particle-particle-particle-mesh algorithm*, J. Chem. Phys. 109 (1998), pp. 7694–7701.
- [38] *Investigations on the Theory of Brownian Motion. Reprint of the 1st English edition (1926)*. Dover, New-York, 1956.
- [39] H.S. Chung, *On the Macedo Litovitz hybrid equation for liquid viscosity*, J. Chem. Phys. 44 (1966), pp. 1362–1364.
- [40] P.B. Macedo and T.A. Litovitz, *On the relative roles of free volume and activation energy in the viscosity of liquids*, J. Chem. Phys. 42 (1965), pp. 245–256.
- [41] G.L. Hunter and E.R. Weeks, *The physics of the colloidal glass transition*, Reports Prog. Phys. 75 (2012), pp. 66501.
- [42] A. Farajnezhad, O.A. Afshar, M.A. Khansary and S. Shirazian, *Binary mutual diffusion coefficients of polymer/solvent systems using compressible regular solutions theory and free volume theory*, J. Non-Equilibrium Thermodyn. 41 (2016), pp. 215–223.
- [43] Q.-L. Liu and H.-Q. Gao, *Prediction of mutual-diffusion coefficients in polymer solutions using a simple activity coefficient model*, J. Memb. Sci. 214 (2003), pp. 131–142.
- [44] N.F. Carnahan and K.E. Starling, *Equation of state for nonattracting rigid spheres*, J. Chem. Phys. 51 (1969), pp. 635–636.

- [45] L. Wei-Zhong, C. Cong and Y. Jian, *Molecular dynamics simulation of self-diffusion coefficient and its relation with temperature using simple Lennard-Jones potential*, Heat Transf. Res. Co-sponsored by Soc. Chem. Eng. Japan Heat Transf. Div. ASME 37 (2008), pp. 86–93.
- [46] I.-C. Yeh and G. Hummer, *System-size dependence of diffusion coefficients and viscosities from molecular dynamics simulations with periodic boundary conditions*, J. Phys. Chem. B 108 (2004), pp. 15873–15879.

Chapter 3

Structure and effective interactions of model colloidal suspensions

Structure and properties of model colloidal suspensions (salt free cases as well as with added salt) in bulk solutions as well as under confinement have been investigated using molecular dynamics simulations. The diameter of colloid ranges from $\sigma_0 = 20 - 100$ nm, charge of colloid $Z_0 = 10-100e$, concentration of colloid $C_0 = 0.484-2.42$ μM and concentration of salt $C_s = 0 - 7.7$ μM . Variation of different properties with system parameters (colloid size, charge, concentration etc.) have been investigated.

*Reproduced in part with permission from

P. Udaykumar, R. N. Behera, "Molecular dynamics simulation study of colloidal suspensions under confinement", *Asian Journal of Chemistry*, 30(11), 2450-2454, 2018. Copy right CC BY-NC 4.0 license.

3.1. Introduction

The study of highly asymmetric multicomponent colloidal systems remains a challenge from last few decades, as different length and time scales are involved for the different constituents. This problem is dealt by coarse graining method which requires elimination of degrees of freedom of some of the smaller particles. The multicomponent colloidal system is treated as monodisperse system [1,2] i.e. the effective one-component system (OCS) of colloidal particles as primitive model (PM). This model contains asymmetric colloids, counterions and co-ions which depicts the electrostatic attraction and repulsion between them and this level of description is stated as multicomponent primitive model. This model is employed to study the colloidal systems by standard techniques like molecular simulations and liquid-state theories based on Ornstein Zernike Equation (OZE).

By employing the primitive model, the attractive potential between the charged colloids arising from electrostatic interactions have been found in various theories [3–7] and computer simulations [8–10]. In these simulation studies and various theories, the attractive force appears to be short range and in few other theoretical studies a long-range attraction is present at certain conditions [11]. Simulations have confirmed a presence of short-range attraction, which is obtained from spatial correlations between the ions present on surface of colloids. The reports on attractive pair potential of a like charged pair of colloids in bulk solution and infinite dilution, a pair of plates and a sphere in an electrolyte solution came into existence [12–16]. Guldbrand [17] confirmed the attraction between the like-charged surfaces immersed in divalent ions in the limit of high surface charge density. Other Monte Carlo (MC) simulations [9,18] also showed that attractive interactions between the charged wall and spherical poly-ion (both monovalent and divalent). They found that attraction is favored by high surface charge density, if counterion is polyvalent, relative permittivity and temperature are low. Linse et al. demonstrated that an aqueous solution with colloid charge of 60 at strong electrostatic coupling, the effective attraction between the like-charged colloids may lead to phase separation [19,20] MC simulations recently proved that the existence of attractive interactions between like-charged surfaces is strongly conditioned by finite size of ions [21]. Further a simulation method was developed based on a homogeneous background charge density to estimate the density dependent effective pair potential between

charged colloids and reported by Bareigts et al [22]. This method works in diluted and concentration regimes as well as at low and high electrostatic coupling.

We employed the molecular dynamics simulations on highly asymmetric colloidal suspensions. We present the systematic variations of pair correlation functions, diffusion coefficients along with thermodynamic properties, effective potential and potential of mean force as a function of charge, size and concentration of colloid in multicomponent colloidal system which give insights about the type of interactions which occur at different system parameters which resemble and mimic the real colloidal systems like micelles, polystyrene latex particles, surfactants etc. We have investigated multicomponent spherical colloidal systems in bulk solution with diameter of colloidal particle $\sigma_0 = 20 \text{ nm}-100 \text{ nm}$, charge of colloid $Z_0 = 10e-100e$, colloid concentrations $C_0 = 0.484 \mu\text{M} - 2.42 \mu\text{M}$ and salt concentrations $C_s = 0 - 7.7 \mu\text{M}$. The surface charge densities $\sigma_e = Z_0 e / \pi r^2$ (r is the radius of colloid) and the diameter used here nearly resemble those of synaptic vesicles (SV) [23] from brain cortex and brush- border- membrane vesicles (BBMV) [24] from small intestine, whose diameters are 45nm and 84nm.

We have divided this chapter into A) Model of colloidal suspensions in bulk solution. B) Effect of confinement on model colloidal suspensions. To study the effective interactions of colloidal suspensions we present a general definition of effective potential of colloid particles of a multicomponent system. In experiments, basically only a set of components are observed out of a complex system. This set of components are considered and the pair correlations among these are assumed to produce the effective pair potentials. This process is paralleled by considering the pair correlations from simulations and using the set of Ornstein Zernike equations and reduced to relevant set of equations where correlations appear.

A) Model of colloidal suspensions in bulk solution

3.2. Model and Simulation Details

3.2.1. System Studied

We have studied spherical anionic colloid (type 0) of molar concentration C_0 (charge Z_0 , diameter σ_0) with monovalent counterion (type 1) obeying electroneutrality condition

$Z_0C_0 + Z_1C_1 = 0$. In addition to these two component (salt free) cases, we have also investigated systems with added salt using a three-component model. To make the system trackable for simulation, we have used monovalent 1:1 salt (type 2) with that of same counterion (type 1). The electroneutrality condition becomes $Z_1C_1 = Z_0C_0 + Z_2C_2$.

We have studied both the static properties (pair correlation function), effective direct correlation function, effective pair potentials, thermodynamic properties and transport property of asymmetric multicomponent colloidal suspensions with the diameter of colloid σ_0 (in nm) = 20, 32, 40, 60, 100, charge of colloid Z_0 (in e) = 10, 15, 25, 50, 75, 100, and concentration of colloid C_0 (in μM) = 0.484, 0.968, 1.452, 1.936 ($\mu M = 10^{-6}$ molar) and concentration of salt C_s (in μM) = 0.484, 0.968, 1.452, 1.936, 2.42, 4.84, 7.7. The diameters and the magnitude of charge of the counterion and co-ions were fixed, respectively at 0.3 nm and $1e$.

Classical molecular dynamics simulations were carried out for the above-mentioned systems with WCA + Coulomb interaction potential. The details of interaction potentials and the simulations were given in chapter 2 (section 2.2). The simulation consisted of total number of particles N (2200 to 20200) packed in a cubic box under periodic boundary conditions with density in the range 6.413×10^{-6} atoms/ nm^3 to 5.889×10^{-5} atoms/ nm^3 . The box sizes were adjusted for the desired density $\rho = N/V$. The total simulation time is 20.4ns, but the properties are calculated from the last 10.4ns of the trajectory with the integration steps of at most 300 steps (1.8 ps). The static, thermodynamic and transport property (self-diffusion coefficient) of the colloidal suspensions were calculated using the standard formulae already described in chapter 2 (section 2.2).

3.2.2. Calculation of effective one-component potential:

The multicomponent OZ equation in Fourier space given by

$$\hat{h}_{ab}(k) - \hat{c}_{ab}(k) = \sum_{s=1}^m \hat{c}_{as}(k) \rho_s \hat{h}_{sb}(k) \quad (3.1)$$

can be solved along with a closure relation which can be written as

$$h_{ab}(r) = \exp[-\beta u_{ab}(r) + h_{ab}(r) - c_{ab}(r) + B_{ab}(r)] - 1, \quad (3.2)$$

Where $\beta u_{ab}(r)$ and $B_{ab}(r)$ are the pair potential and bridge diagram sum, respectively.

Equation 3.1 can be written as that of an effective one component (colloid only) OZ equation [25] as

$$\hat{h}_{00}(k) = \hat{c}_{00}^{eff}(k) + \rho_0 \hat{h}_{00}(k) \hat{c}_{00}^{eff}(k) \quad (3.3)$$

Where the direct correlation function of the effective one component fluid, $\hat{c}_{00}^{eff}(k)$ is given by

$$\hat{c}_{00}^{eff}(k) = \hat{c}_{00}(k) + \beta v_s(k) \quad (3.4)$$

$$\text{with } \beta v_s(k) = \hat{c}_0^T \cdot (1 - \hat{c}^*)^{-1} \cdot \hat{c}_0 \quad (3.5)$$

The elements of the column vector \hat{c}_0 and that of matrix \hat{c}^* in above equations are given by $[\hat{c}_0]_a = \sqrt{\rho_a} \hat{c}_{a0}(k)$ and $[\hat{c}^*]_{ab} = \sqrt{\rho_a \rho_b} \hat{c}_{ab}(k)$, ($a, b \neq 0$). The $\hat{c}_{00}^{eff}(k)$ includes the terms as colloid-colloid direct correlation function ($c_{00}(k)$) and the screening function ($v_s(r)$) which includes the contributions of particles other than colloid, i.e. counterions and/or co-ions.

The exact closure of the one component fluid can be given by

$$h_{00}(r) = \exp[-\beta V^{eff}(r) + h_{00}(r) - c_{00}^{eff}(r) + B_{00}^{eff}(r)] - 1 \quad (3.6)$$

Where $V^{eff}(r)$ is the pair potential of the effective one component system which reproduces the $h_{00}(r)$ of the multicomponent system.

In the view of Eq. (3.3) and the fact that h_{00} of Eq. (3.6) is same as that for multicomponent one (Eq. 3.2), V^{eff} can be found out as follows. Equating Eq. 3.6 and Eq. 3.2 ($a = 0 = b$, colloid-colloid part) gives

$$-\beta V^{eff}(r) + h_{00}(r) - c_{00}^{eff}(r) + B_{00}^{eff}(r) = -\beta u_{00} + h_{00}(r) - c_{00}(r) + B_{00}(r) \quad (3.7)$$

$$-\beta V^{eff}(r) + B_{00}^{eff}(r) - B_{00}(r) = -\beta u_{00}(r) + c_{00}^{eff}(r) - c_{00}(r)$$

Assuming $B_{00}^{eff}(r) \approx B_{00}(r)$ which is quite a good approximation, the above equation gives

$$\begin{aligned} -\beta V^{eff}(r) &= -\beta u_{00}(r) + c_{00}^{eff}(r) - c_{00}(r) \\ &= -\beta u_{00}(r) + \beta v_s(r) \end{aligned} \quad (3.8)$$

For a two-component system (consisting of type 0 and 1 particles), Equation 3.5 gives

$$\beta v_s(k) = \frac{\rho_1 c_{10}^2(k)}{1 - \rho_1 c_{11}(k)} \quad (3.9)$$

And for a three-component system consisting of type 0, type 1 and type 2 particle

$$\beta v_s(k) = \frac{\rho_1 \hat{c}_{01}^2 - \rho_1 \hat{c}_{01}^2 \rho_2 \hat{c}_{22} + 2\sqrt{\rho_1 \rho_2} \hat{c}_{01} \hat{c}_{02} \hat{c}_{12} + \rho_2 \hat{c}_{02}^2 - \rho_2 \hat{c}_{02}^2 \rho_1 \hat{c}_{11}}{((1 - \rho_1 \hat{c}_{11})(1 - \rho_2 \hat{c}_{22}) - \hat{c}_{12}^2)} \quad (3.10)$$

The $\beta v_s(k)$ from the Equation 3.9 and 3.10 is inverse Fourier transformed to get $\beta v_s(r)$.

3.3. Results and discussions

3.3.1. Variation of Colloid Charge

The effect of increasing colloid charge (at a fixed $\sigma_0 = 32nm$ and $C_0 = 0.968\mu M$) on various RDFs (colloid-colloid $g_{00}(r)$, colloid-counterion $g_{01}(r)$ and counterion-counterion $g_{11}(r)$) are displayed in Figure 3.1. For $Z_0 = 10e$, the $g_{00}(r)$ increases smoothly and levels up to unity without any peak as the inter colloid distance r increases (Figure 3.1a). This resembles closely a vapor like system. As Z_0 increases, the value of $g_{00}(r)$ increases, exceeding one and peaks start appearing indicating a liquid like structure. The initial slope has increased (stiffer) indicating increasing in repulsive force between the particles. The starting of the $g_{00}(r)$ (the distance of closest approach of two colloids) curves shift towards larger inter-particle distances. The peak height of the first neighbouring peak of $g_{00}(r)$ (the probability of finding colloids around another colloid) increases. As the charge of the colloid increases, the concentration of counterions increases (for electroneutrality). The effective repulsions between the colloids decreases due to screening of the counterions. Thus, the probability of

finding a colloid around another colloid (peak height) increases. This is supported by colloid-counterion RDFs $g_{01}(r)$, showed in Figure 3.1b.

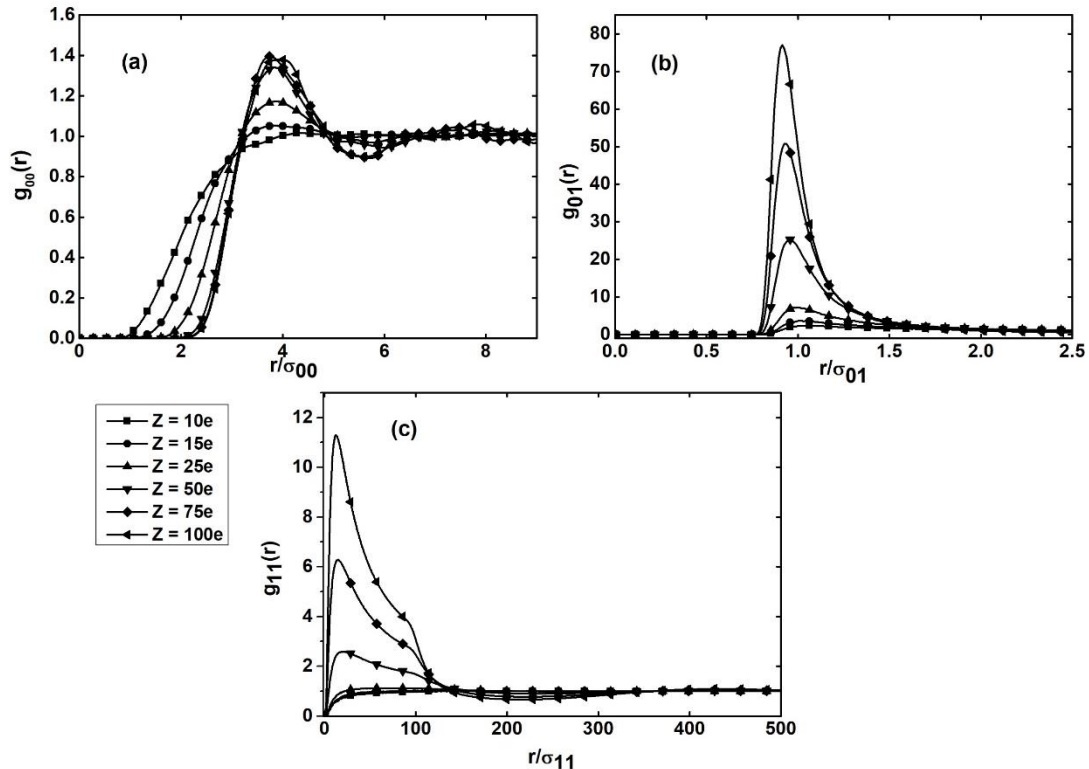


Figure 3.1. Variation of a) colloid-colloid radial distribution functions $g_{00}(r)$ b) colloid-counterion radial distribution functions $g_{01}(r)$ c) counterion-counterion radial distribution functions $g_{11}(r)$ with charge asymmetry at fixed $\sigma_0 = 32\text{nm}$, $C_0 = 0.968\mu\text{M}$ and $C_s = 0\mu\text{M}$.

The peak height (probability of finding counterions around a colloid) increases substantially as the colloid charge increases. The peak position is roughly at $r = \sigma_{01}$ indicating counterion accumulation on the surface of colloid, resulting decrease in the effective charge of the colloid. With increase in Z_0 , the broad maxima of counterion-counterion RDFs $g_{11}(r)$ (Figure 3.1c) increase and the peak positions shift towards lower r/σ_{11} , the peak becomes sharper owing to increase in counterion accumulation.

Almost similar trends in the radial distribution functions with macroion charge has been found using MC simulations [26,27], although the system parameters are different than those

used here. For example, Linse group [26] have used $Z_0 = 10e - 80e$, $\sigma_0 = 2\text{nm}$ and volume fraction $\phi = 0.01$. In their studies the peak heights and peak positions are (from 1.05 - 1.25, $r/\sigma_{00} \sim 3.5$) for $g_{00}(r)$, (2.3 - 6, $r/\sigma_{01} \sim 1$) for $g_{01}(r)$, (1 -17, $r/\sigma_{11} \sim 1$) for $g_{11}(r)$. The corresponding values for the present case are (1 - 1.4, $r/\sigma_{00} \sim 4$) for $g_{00}(r)$, (2.2 - 7.6, $r/\sigma_{01} \sim 1.0$) for $g_{01}(r)$, (0.84 - 11.1, $r/\sigma_{11} \sim 22.1$) for $g_{11}(r)$. A similar behavior is also reported by us using integral equation theory [28].

The variation of colloid-colloid structure factor $S_{00}(k)$ as a function of Z_0 is displayed in Figure 3.2. As colloid charge increases, the peak height of $S_{00}(k)$ increases slightly while the peak position remains more or less same. A secondary peak starts appearing with increase in charge, indicating particle arrangement in which there is considerable short-range order. These behaviors are in consistent with those obtained by the RDFs just discussed.

It is worth mentioning the results on $S_{00}(k)$ obtained by Fushiki [29] using HNC theory i.e. $S_{00}(k) = 1.6$ and $S_{00}(k)$ obtained by Beresford [30] using Jellium approximation i.e. $S_{00}(k) = 1.5$, our $S_{00}(k)$ obtained by MD simulation is underestimated with their theories. The peak height of the first peak is obtained at $S_{00}(k) = 1.26$. The system parameters of our simulations are $\sigma_0 = 32\text{nm}$, $Z_0 = -100e$, $C_0 = 0.968\mu\text{M}$ and $C_s = 0\mu\text{M}$.

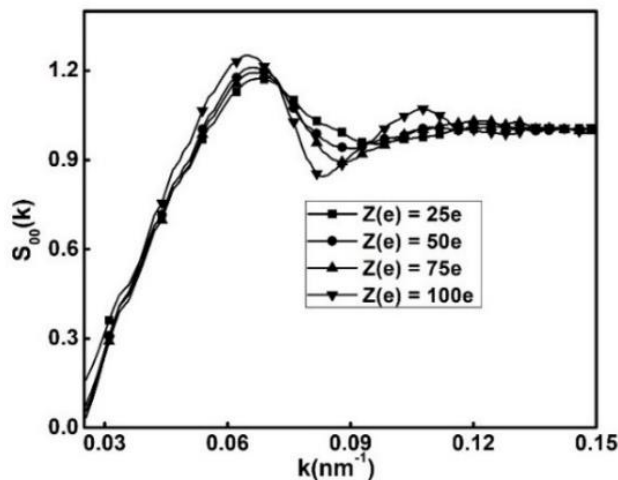


Figure 3.2. Variation of Structure factor $S_{00}(k)$ with charge of colloid. The parameters used are same as in Figure 3.1.

The variation of potential of mean force ($\beta W_{00}(r) = -\log(g_{00}(r))$) with increasing the colloid charge Z_0 , is displayed in Figure 3.3a. $\beta W_{00}(r)$ is stiffer (repulsive) at large inter-colloid

distance. As the colloid charge increases, the $\beta W_{00}(r)$ decreases, becomes negative (attractive) and becomes positive (repulsive) with increase in the inter-colloid separation. A secondary peak start appearing when the colloid charge increases [31]. The position (r/σ_{00}) and depth of the minima as a function of charge are summarized in Table 3.1. With increase in colloid charge, the depth at minima of $\beta W_{00}(r)$ increases and peak position slightly decreases.

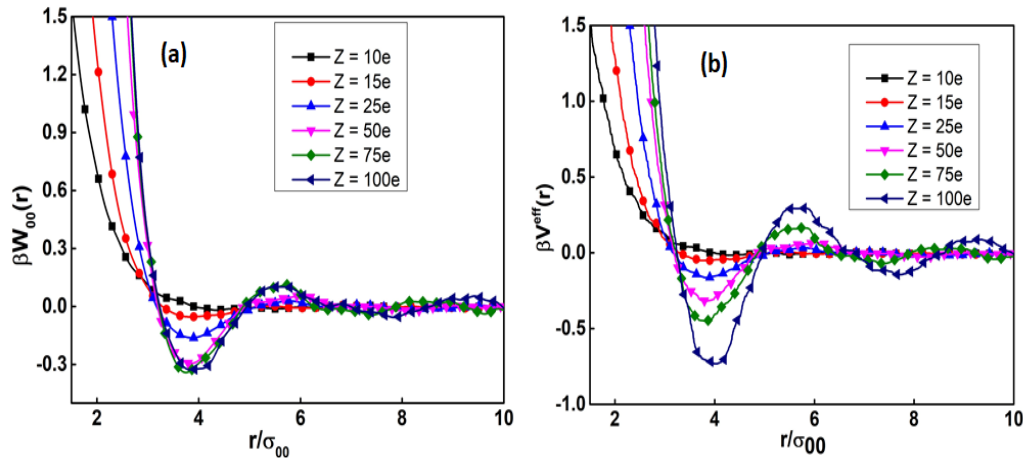


Figure 3.3. Variation of (a) $\beta W_{00}(r)$ and (b) $\beta V^{eff}(r)$ with charge asymmetry at fixed $\sigma_0 = 32\text{nm}$, $C_0 = 0.968\mu\text{M}$ and $C_s = 0\mu\text{M}$.

Table 3.1: The position (r/σ_{00}) and depth of the minima of $\beta V^{eff}(r)$ and $\beta W_{00}(r)$ as a function of colloid charge for two component (salt free) and three component ($C_s = 4.484\mu\text{M}$) systems. Fixed parameters: $\sigma_0 = 32\text{nm}$, $C_0 = 0.9681\mu\text{M}$.

Z_0 (e)	$\beta V^{eff}(r)$				$\beta W_{00}(r)$			
	r/σ_{00}	Two component system	r/σ_{00}	Three component system	r/σ_{00}	Two component system	r/σ_{00}	Three component system
10	3.939	0.008	3.623	-0.005	4.172	-0.012	3.681	-0.003
15	3.922	-0.056	3.593	-0.039	3.856	-0.053	3.681	-0.045
25	3.822	-0.163	3.765	-0.139	3.843	-0.167	3.727	-0.142
50	3.823	-0.323	3.686	-0.232	3.838	-0.295	3.712	-0.237
75	3.822	-0.460	3.577	-0.275	3.858	-0.317	3.602	-0.279
100	4.038	-0.771	3.593	-0.333	3.801	-0.321	3.602	-0.345

The variation of effective colloid-colloid potential $\beta V^{eff}(r)$ with colloid charge is almost similar to that of potential of mean force and is displayed in Figure 3.3b. However, the magnitude at the minima are larger corresponding to the case of $\beta W_{00}(r)$. This is probably due to the fact that additional screening due to other colloids are included in $\beta V^{eff}(r)$, but absent in $\beta W_{00}(r)$. The minima obtained (Table 3.1) are qualitatively similar to those obtained by Lobaskin [32] and Anta [33]. The particle charges they used are $20e$ and $60e$. The diameter of colloid is significantly larger in our work, viz., 20nm to 100nm as compared to 4nm in Anta's work. The minima get deeper with increase in charge of the colloidal particle, for $100e$ it reaches -0.77 at $r/\sigma_{00} = 4.038$.

The effective colloid-colloid direct correlation function $c_{00}^{eff}(r)$ is studied with increasing colloid charge (Figure 3.4a). The effective colloid-colloid direct correlation function $c_{00}^{eff}(r)$ (expressed in Equation 3.4 and 3.5) includes the terms as colloid-colloid direct correlation function ($c_{00}(r)$) and the screening function ($v_s(r)$) which includes the contributions of other particles i.e. counterions and/or co-ions. The $c_{00}^{eff}(r)$ increases from -0.999 for charge $Z_0 = 10e$ to 4.932 for $Z_0 = 100e$ in salt free colloidal system. The magnitude of screening function $\beta v_s(r)$ is positive at smaller r , becomes negative and finally tends to zero as r increases (Figure 3.4b). With increase in Z_0 , the magnitude of $\beta v_s(r)$ increases. The $\beta v_s(r)$ at $r = 71.22 \text{ nm}$ for charge $Z_0 = -10e$ is -4.2×10^{-4} and at $r = 71.22 \text{ nm}$ for charge $Z_0 = -100e$ is -1.180 .

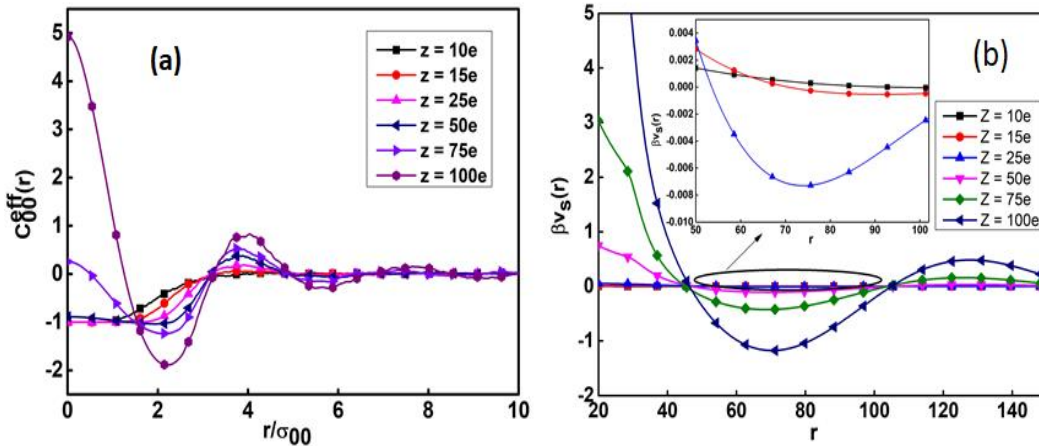


Figure 3.4. Variation of (a) $c_{00}^{eff}(r)$ and (b) $\beta v_s(r)$ with charge asymmetry at fixed $\sigma_0 = 32\text{nm}$, $C_0 = 0.968\mu\text{M}$ and $C_s = 0\mu\text{M}$.

3.3.2. Variation of Colloid Size:

The radial distribution function as a function of colloid diameter at a fixed $Z_0 = -25e$ and $C_0 = 0.9681\mu\text{M}$ is illustrated in Figure 3.5. As the diameter of the colloid increases, the peak height of $g_{00}(r)$ (Figure 3.5a) increases steadily from 1.14 for $\sigma_0 = 20\text{ nm}$ to 1.56 for $\sigma_0 = 100\text{ nm}$ and the peak positions are shifted towards the lower r/σ_{00} : from 6.01 for $\sigma_0 = 20$ to 1.1 for $\sigma_0 = 100\text{ nm}$. Almost similar trends in the radial distribution functions with colloid size has been found experimentally and using MC simulations, although the system parameters are different than ours [34]. This shifting of peak positions towards the colloid surface with increasing σ_0 indicates that colloids with smaller diameter show larger repulsion (larger colloid charge density). And as the diameter of colloidal particle increases, the broad peak becomes narrower indicating accumulation of increasing number of counterions on colloid surface.

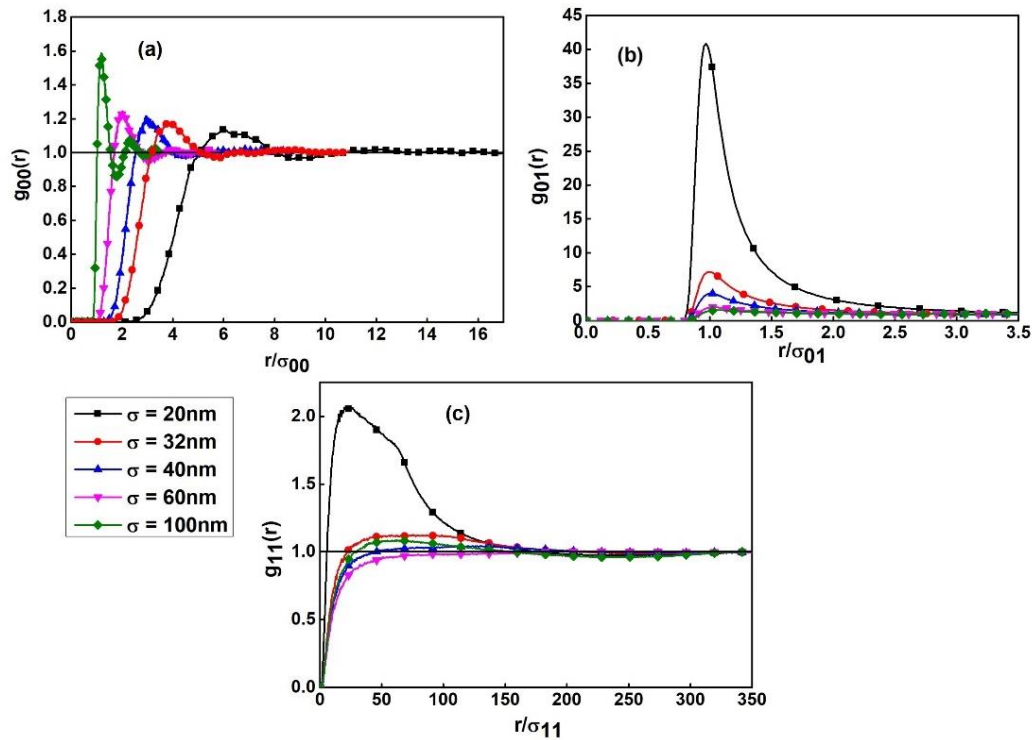


Figure 3.5. Variation of a) colloid-colloid radial distribution functions $g_{00}(r)$ b) colloid-counterion radial distribution functions $g_{01}(r)$ c) counterion-counterion radial distribution functions $g_{11}(r)$ with size asymmetry at fixed $Z_0 = -25e$ and $C_0 = 0.968\mu\text{M}$.

The accumulation of counterion on macroion (colloid) surface is supported by the colloid-counterion correlation function $g_{01}(r)$ (Figure 3.5b). The peak appearing around $r = \sigma_{01}$ and the peak height (probability of finding counterion around a colloid) decreases, as the diameter of colloid increases. The accumulation of counter-ions near a colloid surface is determined by the product of surface area and the probability of finding the counterion at the colloid surface. The contact value of $g_{11}(r)$ in Figure 3.5c decreases as the diameter of colloidal particle increases showing repulsions among the counter-ions. The colloid-colloid structure factor in Figure 3.6 shows increase in peak height with increasing size of colloidal particle which is similar to $g_{00}(r)$.

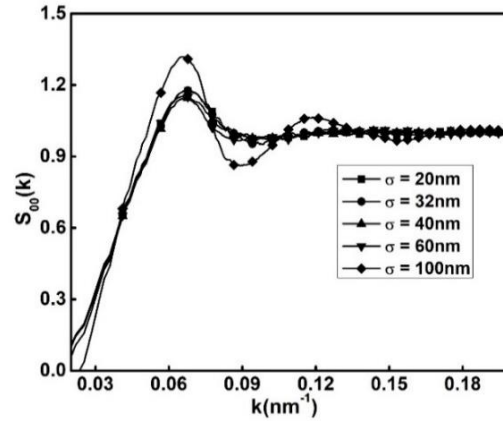


Figure 3.6. Variation of colloid-colloid structure factor $S_{00}(k)$ with size of the colloid. The parameters used are same as in Figure 3.5.

As diameter of colloidal particle increases, both $\beta W_{00}(r)$ (Figure 3.7a) and $\beta V^{eff}(r)$ (Figure 3.7b) become less repulsive, probably due to reduction in colloid charge density. The depth of the potential minima increases and shift towards lower inter-colloid distance ($r/\sigma_{00} = 6.030$ for $\sigma_{00} = 20\text{nm}$ to $r/\sigma_{00} = 1.160$ for $\sigma_{00} = 100\text{nm}$). The relevant numerical data is given in Table 3.2 for the two-component (salt free) and the three-component (with salt) systems.

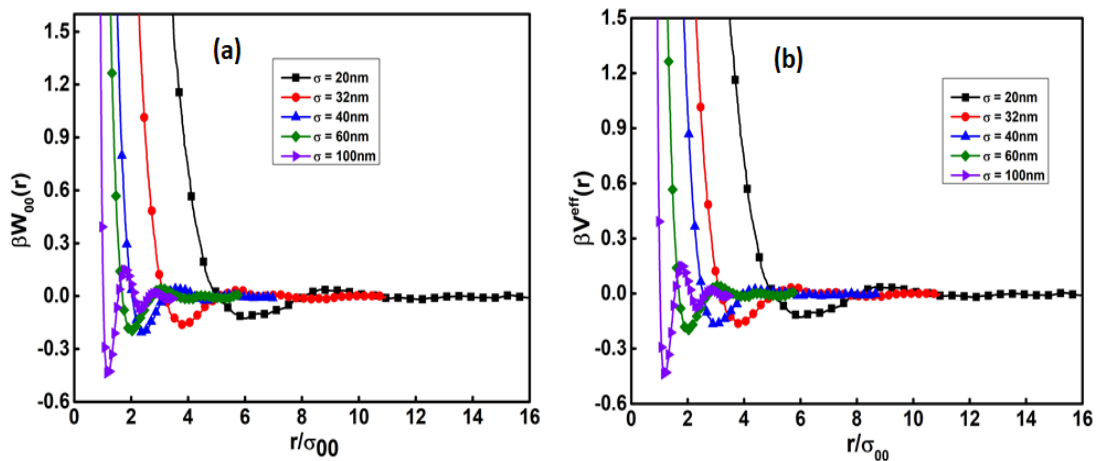


Figure 3.7. Variation of (a) $\beta W_{00}(r)$ and (b) $\beta V^{eff}(r)$ with size of colloid. Two component system with $Z_0 = -25e$ and $C_0 = 0.968\mu\text{M}$.

Table 3.2: The position (r/σ_{00}) and depth of the minima of $\beta V^{eff}(r)$ and $\beta W_{00}(r)$ as a function of colloid size for two-component (salt free) and three-component ($C_s = 4.484 \mu\text{M}$) systems. Fixed parameters: $Z_0 = -25e$, $C_0 = 0.9681 \mu\text{M}$.

σ_0 (nm)	$\beta V^{eff}(r)$				$\beta W_{00}(r)$			
	r/σ_{00}	Two component system	r/σ_{00}	Three component system	r/σ_{00}	Two component system	r/σ_{00}	Three component system
20	6.030	-0.126	6.030	-0.120	6.037	-0.130	6.072	-0.121
32	3.822	-0.163	3.765	-0.139	3.843	-0.167	3.727	-0.142
40	2.963	-0.176	3.137	-0.151	2.372	-0.210	3.148	-0.142
60	1.989	-0.188	1.989	-0.195	2.038	-0.210	1.993	-0.193
100	1.160	-0.445	1.160	-0.432	1.151	-0.447	1.140	-0.424

The effective direct correlation function $c_{00}^{eff}(r)$ and the screening function $\beta v_s(r)$ are studied with increase in colloidal size and the plots are displayed in Figure 3.8a & b. Its value decreases from -1.004 for $\sigma_0 = 20\text{nm}$ to -0.976 for $\sigma_0 = 100\text{nm}$ in salt free colloidal system. As the colloid size increases, the peak height in $c_{00}^{eff}(r)$ increases and the peak position shift towards lower inter-colloid distance. This behavior is similar to the variation in $g_{00}(r)$, though the values in the former are negative at lower inter-colloid distance. The screening functions $\beta v_s(r)$ are positive at lower inter-colloid distance, become negative and level upto zero as inter-colloid distance increases. They show non-monotonic variation with variation in colloid diameters. With increase in diameter of the colloidal particle, the magnitude of $\beta v_s(r)$ decreases.

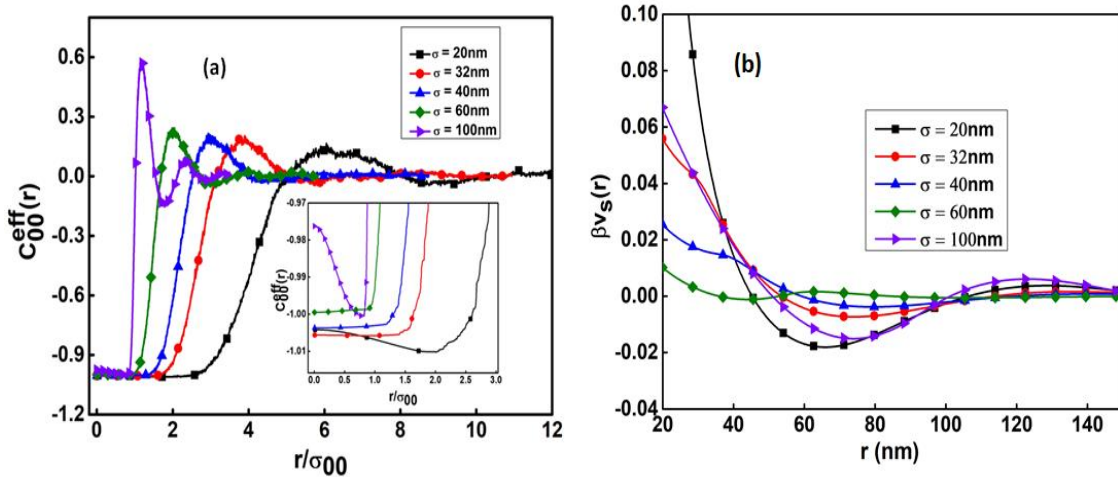


Figure 3.8. Variation of (a) $c_{00}^{eff}(r)$ and (b) $\beta v_s(r)$ with colloid size. Two component systems with $Z_0 = -25e$ and $C_0 = 0.968\mu\text{M}$.

3.3.3. Variation of Colloid concentration:

The effect of varied concentration of colloid (at a fixed parameter of $Z_0 = -25e$ and $\sigma_0 = 32\text{nm}$) on different RDFs are presented in Figure 3.9. Increase in colloid concentration has the combined effect of increasing counterion concentration (due to electroneutrality) as well as increasing the volume fraction. As the concentration of colloid in the solution increases, the first neighboring peak of $g_{00}(r)$ (Figure 3.9a) shifts toward the shorter separations with slight increase in the peak heights. The $g_{01}(r)$ (Figure 3.9b) is sharply peaked roughly at $r/\sigma_{11} = 1.0$ and the peak height decreases with increase in the colloid concentration. The $g_{11}(r)$ (Figure 3.9c) show a broad maxima, probably due to correlations between counterions condensed in the surface of same colloid. The colloid-colloid structure factors $S_{00}(k)$ are plotted in Figure 3.10. The peak height slightly increases and the peak position shifts towards higher interparticle distance with increasing concentration of colloidal particles. The variations are quite similar to those obtained experimentally. For example, the $S_{00}(k)$ data reported by Cebula et al [35] using small-angle neutron scattering (SANS) is displayed in Figure 3.11. Although the parameters considered in this study are somewhat different from our simulations, the trends are well reproduced (Table 3.3).

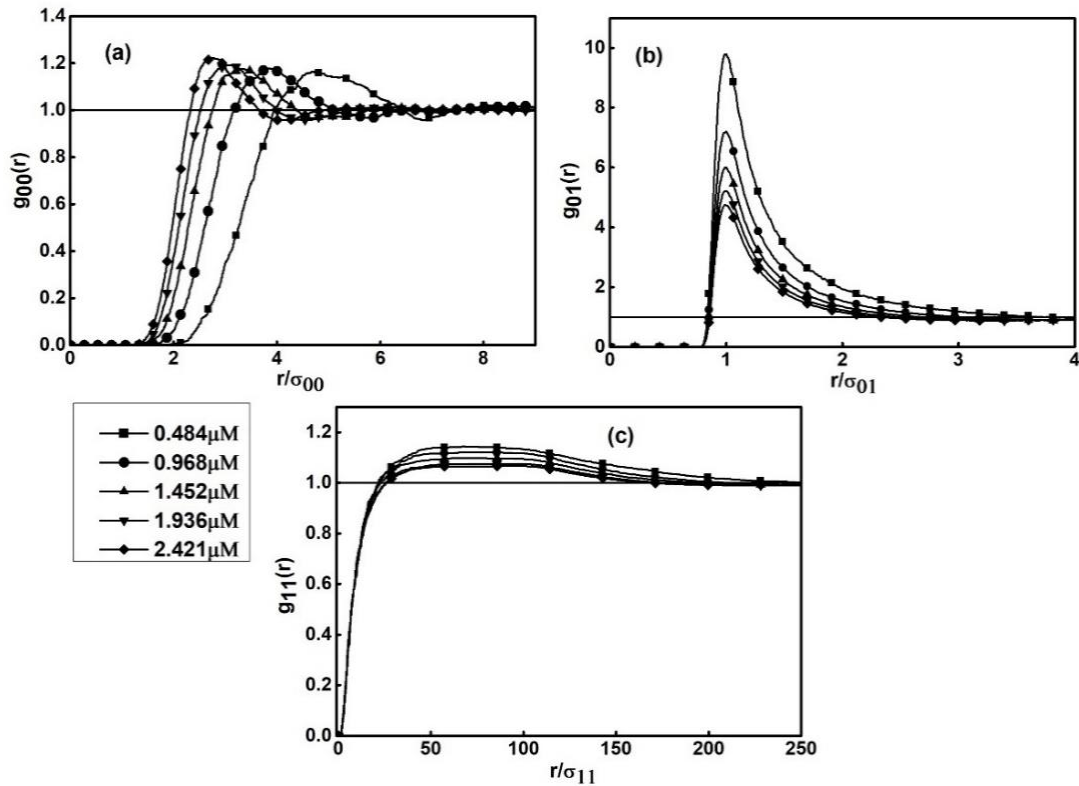


Figure 3.9. Variation of a) colloid-colloid radial distribution functions $g_{00}(r)$ b) colloid-counterion radial distribution functions $g_{01}(r)$ c) counterion-counterion radial distribution functions $g_{11}(r)$ with colloid concentration. Two-component system with $Z_0 = -25e$ and $\sigma_0 = 32\text{nm}$.

Table 3.3: Comparison of peak positions and peak heights of structure factor $S_{00}(\mathbf{k})$ obtained experimentally by Cebula et al. [35] with our system parameters. The experimental parameters are $\sigma_0 = 32\text{ nm}$, $Z_0 = -200e$ whereas our parameters are $\sigma_0 = 32\text{ nm}$, $Z_0 = -25e$.

ϕ_{exp}	$\mathbf{k}_{\text{exp}} (\text{\AA}^{-1})$	$S_{00}(\mathbf{k})_{\text{exp}}$	ϕ_{sim}	$\mathbf{k}_{\text{sim}} (\text{\AA}^{-1})$	$S_{00}(\mathbf{k})_{\text{sim}}$
0.04	0.009	1.65	0.01	0.0067	1.174
0.08	0.0116	2.06	0.015	0.0072	1.186
0.13	0.014	2.50	0.02	0.0077	1.204

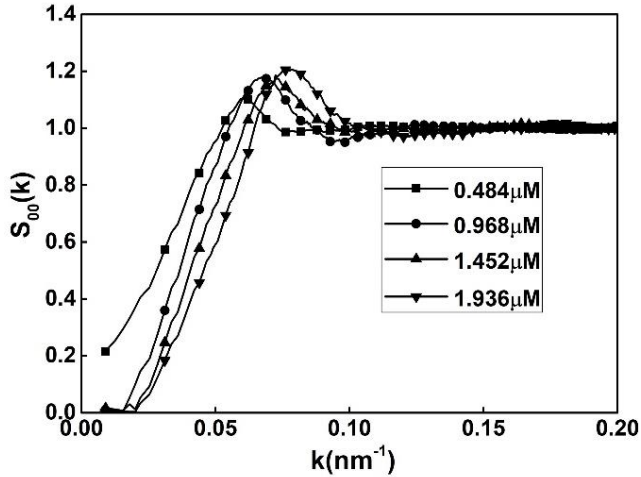


Figure 3.10. Variation of Structure factor $S_{00}(k)$ with colloid concentration. The parameters used are same as in Figure 3.9.

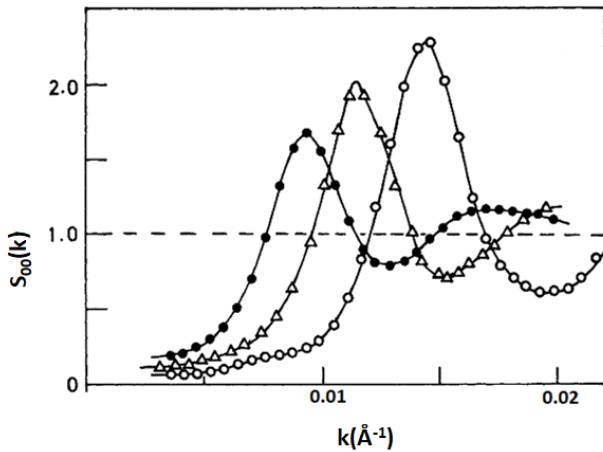


Figure 3.11. Variation of $S_{00}(k)$ with volume fraction (ϕ) for an ion exchanged latex (Cebula et al., [35]). black circle, $\phi = 0.04$; triangle, $\phi = 0.08$; circle, $\phi = 0.13$. with system parameters $\sigma_0 = 32$ nm, $Z_0 = -200e$. (Copy right is attached)

We have estimated the coordination number (n) of colloid by integrating the corresponding radial distribution function $n = 4\pi\rho \int_0^{\infty} r^2 g(r) dr$ and is displayed in Figure 3.12. With increase in concentration of colloid (for a fixed volume), the colloids are packed more, the probability of finding a colloid around another colloid increases and so the coordination number increases. The coordination number increases from 1.3 for $C_0 = 0.484$ μM and 5.5 for $C_0 = 1.936$ μM .

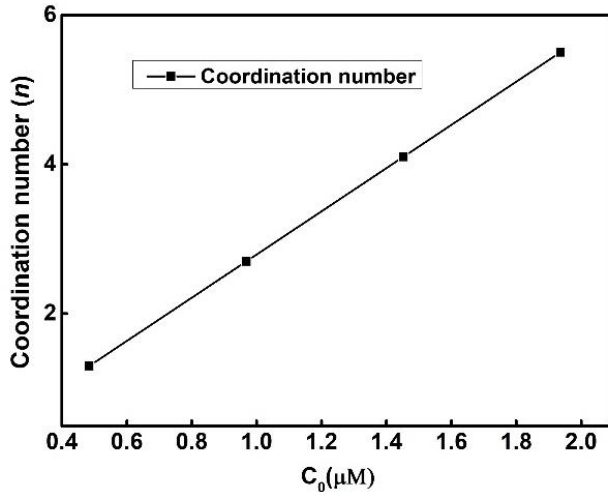


Figure 3.12. Variation of coordination number of colloid with its concentration. The system parameters used are same as in Figure 3.9.

With increasing the colloid concentration, the general features of $\beta W_{00}(r)$ (Figure 3.13a) is similar to variation in charge and size. However, the positions of the minima shift towards lower inter-colloid distance as colloid concentration increases. The relevant numerical data is given in Table 3.4. With increase in the colloid concentration, the effective potential $\beta V^{eff}(r)$ become less repulsive (Figure 3.13b), show attractive minima (negative) and shift towards the lower inter-colloidal particle distance. The depth for minima varies from -0.151 for $C_0 = 0.484\mu\text{M}$ at $r/\sigma_{00} = 4.69$ to -0.197 for $C_0 = 2.42\mu\text{M}$ at $r/\sigma_{00} = 2.717$ (Table 3.4). Unlike the attractive minima obtained at very low packing fractions in the current study, Bareigts et al. [22] obtained purely repulsive effective pair potential at high packing fractions with colloid diameter 4 nm and charge $-60e$. However, recent experimental and simulation results by Ojeda Mendoza et al [16] with colloid diameter 110 nm and charge $-603e$ shows attractive effective potentials similar to the current study. As the volume fraction increases there is decrease in repulsive tail and at the same time the attractive minima develop. The attractive well is obtained for all the concentrations with gradual decrease in the repulsive tail. As the concentration of the colloidal particle increases, attractive well is followed by the secondary repulsive barrier. Such behavior is caused by structural arrangement of smaller particles around the colloids due to the repulsion among small ions.

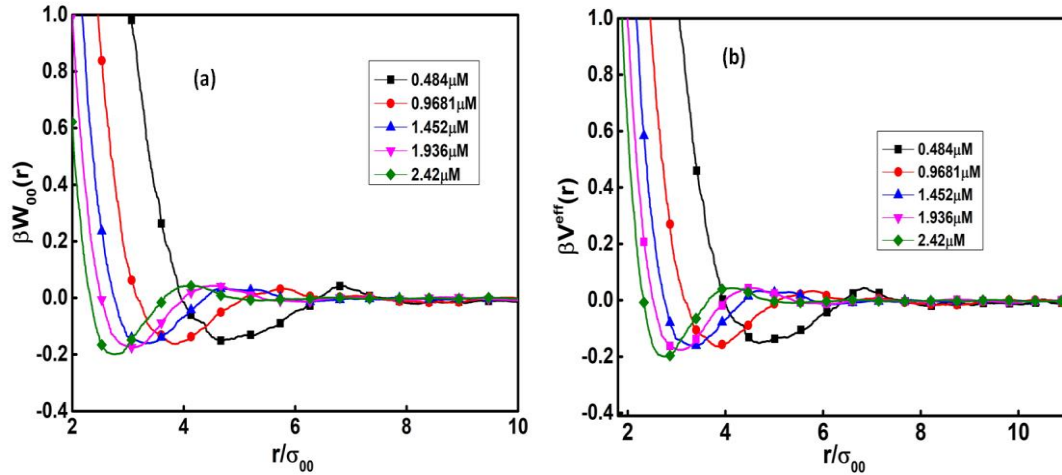


Figure 3.13. Variation of (a) $\beta W_{00}(r)$ and (b) $\beta V^{eff}(r)$ with colloid concentration at fixed $Z_0 = -25e$, $\sigma_0 = 32\text{nm}$ and $C_s = 0$.

Table 3.4: The position (r/σ_{00}) and depth of the minima of $\beta V^{eff}(r)$ and $\beta W_{00}(r)$ as a function of colloid concentration for two component (salt free) and three component ($C_s = 4.484 \mu\text{M}$) systems. Fixed parameter: $\sigma_0 = 32\text{nm}$, $Z_0 = -25e$.

C_0 (μM)	$\beta V^{eff}(r)$				$\beta W_{00}(r)$			
	r/σ_{00}	Two comp system	r/σ_{00}	Three comp system	r/σ_{00}	Two Comp system	r/σ_{00}	Three comp system
0.484	4.475	-0.151	4.472	-0.111	4.693	-0.151	4.455	-0.106
0.968	3.822	-0.163	3.765	-0.139	3.843	-0.167	3.727	-0.142
1.452	3.334	-0.161	3.268	-0.165	3.306	-0.161	3.329	-0.164
1.936	3.054	-0.172	3.004	-0.175	3.079	-0.168	3.005	-0.174
2.421	2.746	-0.201	2.856	-0.192	2.745	-0.197	2.796	-0.188

The effective direct correlation function $c_{00}^{eff}(r)$ and screening function $\beta v_s(r)$ are studied with increase in colloid concentration and the results are plotted in Figure 3.14.

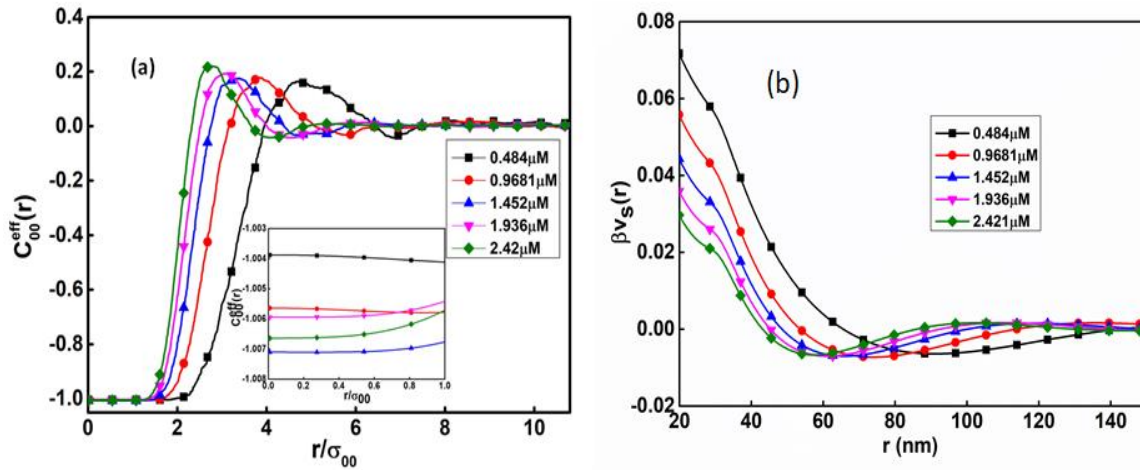


Figure 3.14. Variation of (a) $c_{00}^{eff}(r)$ and (b) $\beta v_s(r)$ with colloid concentration at fixed $Z_0 = -25e$, $\sigma_0 = 32\text{nm}$ and $C_s = 0$.

The increase in colloid number density of the colloidal system is accompanied by an increase in counterion concentration which results in an increase in screening between the particles. The magnitude of $\beta v_s(r)$ decreases and become negative and level upto zero. The range of screening function (r at which the function is negative) becomes shorter with increase in colloid concentration. Because of increasing repulsions between the counterions with increase in colloid concentration, the counterions are pushed away nearer to the colloid resulting in increased screening.

3.3.4. Effect of counterion valency

We varied the counterion charge from $+1e$ to $+3e$ and studied the effect on RDF and effective potential. The counterion size was kept constant at 0.3nm . The variation of radial distribution functions with counterion valency for system with $\sigma_0 = 32\text{nm}$, $Z_0 = -25e$ and $C_0 = 1.936 \mu\text{M}$ is displayed in Figure 3.15. With increase in valency of counterion, the effective charge density of the colloid decreases (counterion condensation) and the colloid-colloid repulsion decreases. The probability of finding a counterion around colloid increases. The counterion-counterion interaction become more repulsive, the displacement of counterion by

another counterion increases, result in a broad peak in $g_{11}(r)$. The peak heights in the colloid-colloid RDFs $g_{00}(r)$ decreases and shows less structured for trivalent counterion. while opposite trends were observed in the case of colloid-counterion and counterion-counterion RDF.

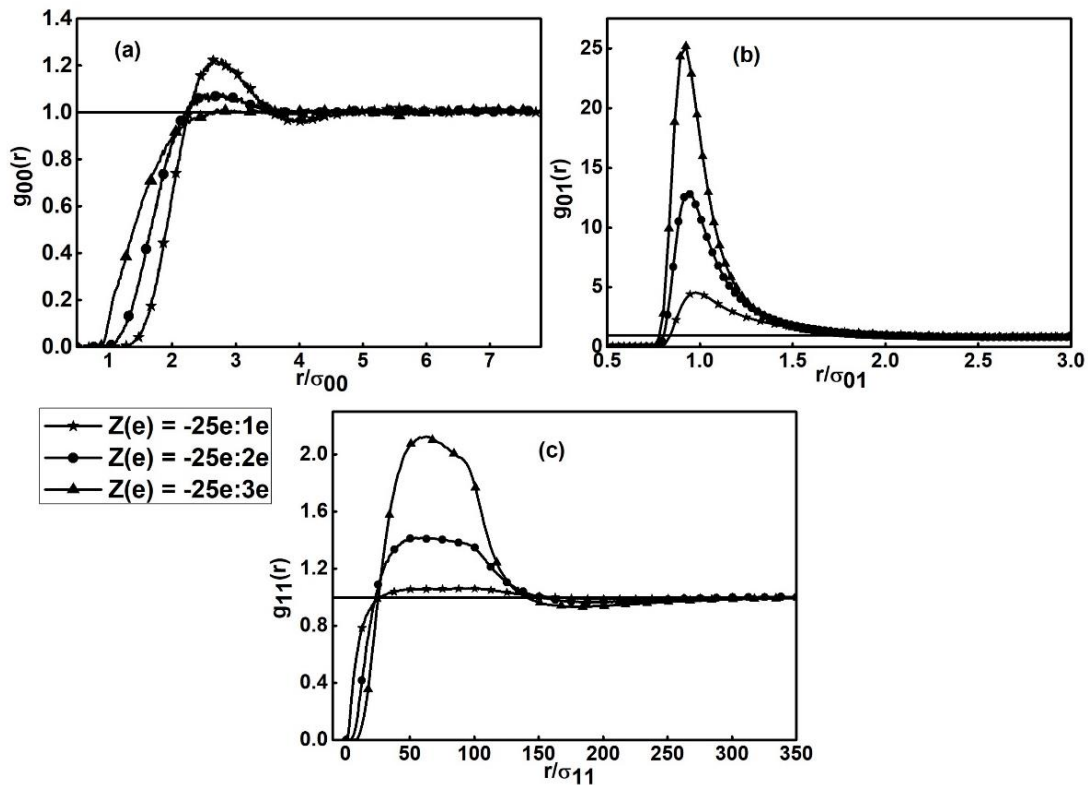


Figure 3.15. Plot of radial distribution function a) colloid-colloid b) colloid-counterion c) counterion-counterion with variation of valency of counterion at fixed $\sigma_0 = 32\text{nm}$, $Z_0 = -25e$ and $C_0 = 1.936\mu\text{M}$.

Similar trends in RDF with counterion valency have been observed using Monte Carlo (MC) simulations by Hribar and Vlachy [27,36] and Linse and Lobaskin [20]. We have simulated a system with parameters more similar to those used by Hribar and Vlachy and obtained a similar trend. The results are given in (Figure 3.16).

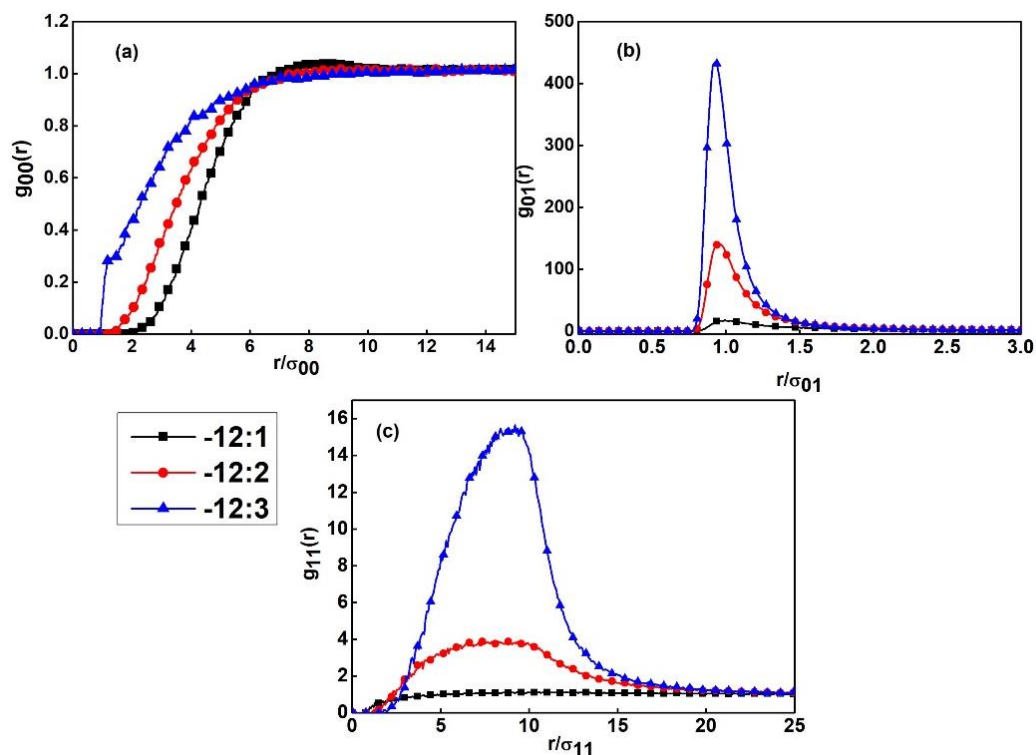


Figure 3.16. Plot of radial distribution function a) colloid-colloid b) colloid-counterion c) counterion-counterion with variation of valency of counterion at fixed $\sigma_0 = 2\text{ nm}$, $Z_0 = -12e$ and $C_0 = 0.0005\text{ mol dm}^{-3}$.

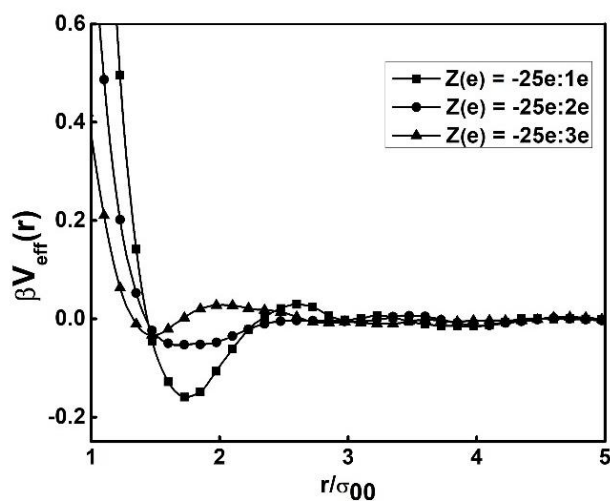


Figure 3.17. Effective potential $\beta V_{\text{eff}}(r)$ with variation in valency of counterion with same system parameters as in Figure 3.15.

The effective potential $\beta V_{\text{eff}}(r)$ (Figure 3.17) becomes more repulsive and less attractive with increase in counterion valency. The peak position of minima shift towards the lower

interparticle distance. This weakening of attractive behavior in charge colloid due to increase in counterion valency was reported recently [11].

3.3.5. Effect of Salt Concentration

The effect of salt concentration on various RDFs is displayed in Figure 3.18. With increase in salt concentration, the peak height of colloid-colloid radial distribution function $g_{00}(r)$ slightly decreases (Figure 3.18a). The $g_{01}(r)$ plots in Figure 3.18b shows larger values at the colloidal surface and the values decreases with increase in salt concentration. The $g_{11}(r)$ (Figure 3.18c) shows decrease in peak height with increase in salt concentration. The peaks are broader in this case. The magnitude of change in RDF due to colloid concentration is much smaller than those due to colloid charge and size.

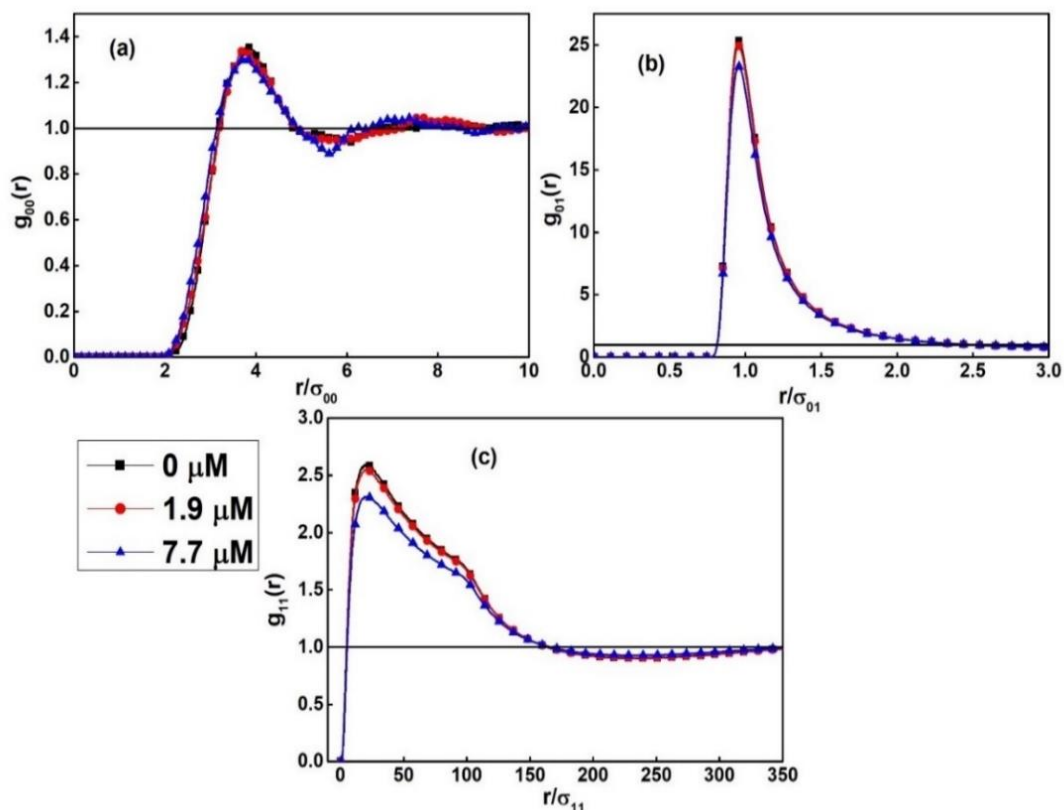


Figure 3.18. Variation of a) colloid-colloid $g_{00}(r)$ b) colloid-counterion $g_{01}(r)$ c) counterion-counterion $g_{11}(r)$ with salt concentration at fixed $Z_0 = -50e$, $\sigma_0 = 32\text{nm}$ and $C_0 = 0.968\mu\text{M}$.

The variation of $\beta W_{00}(r)$ and $\beta V^{eff}(r)$ with salt concentration is plotted in Figure 3.19. The depth of the minima decreases, and the positions shift towards lower interparticle distance in both cases; from -0.303 at $r/\sigma_{00} = 3.86$ to -0.242 at $r/\sigma_{00} = 3.67$ for $\beta W_{00}(r)$ and $r/\sigma_{00} = 3.75$ is -0.323 for $C_s = 0\mu\text{M}$ to -0.239 at $r/\sigma_{00} = 3.75$ for $C_s = 7.7\mu\text{M}$ for $\beta V^{eff}(r)$.

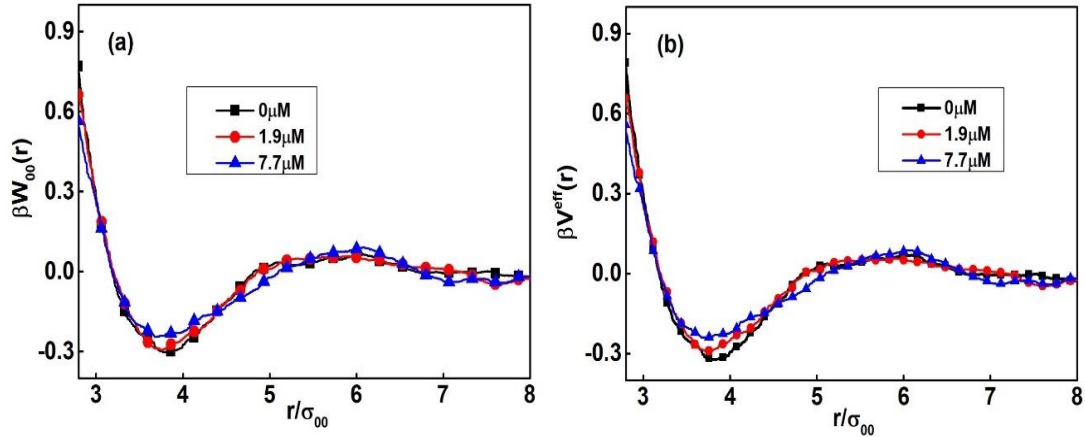


Figure 3.19. Variation of (a) $\beta W_{00}(r)$ and (b) $\beta V^{eff}(r)$ with salt concentration at fixed $Z_0 = -50e$, $\sigma_0 = 32\text{nm}$ and $C_0 = 0.968\mu\text{M}$.

The effective colloid-colloid direct correlation function $c_{00}^{eff}(r)$ is studied with salt concentration (Figure 3.20a).

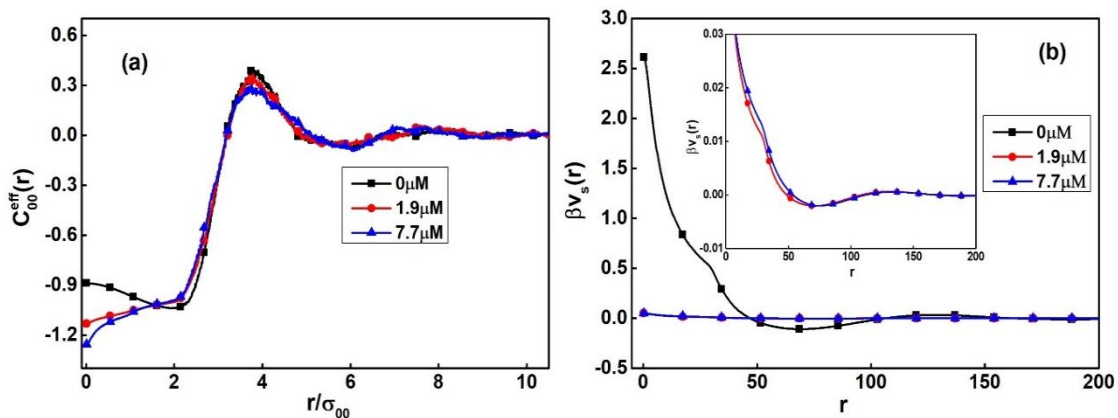


Figure 3.20. Variation of (a) $c_{00}^{eff}(r)$ and (b) $\beta v_s(r)$ with salt concentration at fixed $Z_0 = -50e$, $\sigma_0 = 32\text{nm}$ and $C_0 = 0.968\mu\text{M}$.

The $c_{00}^{eff}(r)$ varies from -0.901 for $C_s = 0\mu\text{M}$ to -1.260 for $C_s = 7.7\mu\text{M}$. The variation of screening function $\beta v_s(r)$ with salt concentration is illustrated in Figure 3.20b. With increase in salt concentration, the screening of counterions increases and $\beta v_s(r)$ decreases (less negative).

3.3.6. Variation in Thermodynamic Properties

The variation of reduced excess free energy ($\beta E^{ex}/\rho$) and the osmotic coefficient (Φ_V) as a function of colloid charge, size and concentration is plotted in Figure 3.21.

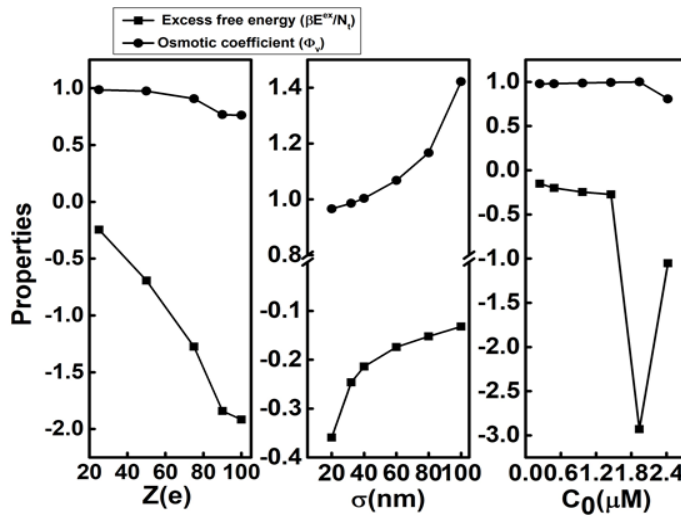


Figure 3.21. Plot of reduced excess free energy ($\beta E^{ex}/\rho$) and the osmotic coefficient (Φ_V) with variation in size, charge and concentration of colloid.

The magnitude of excess free energy ($\beta E^{ex}/\rho$) increases when charge as well as concentration of colloid particle increases, and as the diameter of the colloidal particle decreases. Similar trends with charge and size asymmetry have been explained in chapter 2. Osmotic coefficient shows opposite trend with variation in charge and diameter of the colloid, but it follows similar trend with increase in concentration of the colloidal particle. Similar trends have been reported in the literature [28] including aqueous protein solutions [37].

3.3.6.1 Isothermal Compressibility

The direct correlation function is also associated to the thermodynamic properties of liquids, e.g. the isothermal compressibility χ_c [38,39]

$$\chi_c = \left[1 - \frac{1}{\rho} \sum_{ij} \rho_i \rho_j \int_0^{\infty} dr 4\pi r^2 c_{ij}^s(r) \right]^{-1}, \quad (3.8)$$

Where $c_{ij}^s(r) = c_{ij}(r) + \frac{z_i z_j L_B}{r}$, $c_{ij}^s(r)$ is defined as the short-ranged part of direct correlation functions which tends to zero when $r \rightarrow \infty$.

The variation of isothermal compressibility in charge, size, concentration of colloidal particle is displayed in Figure 3.22.

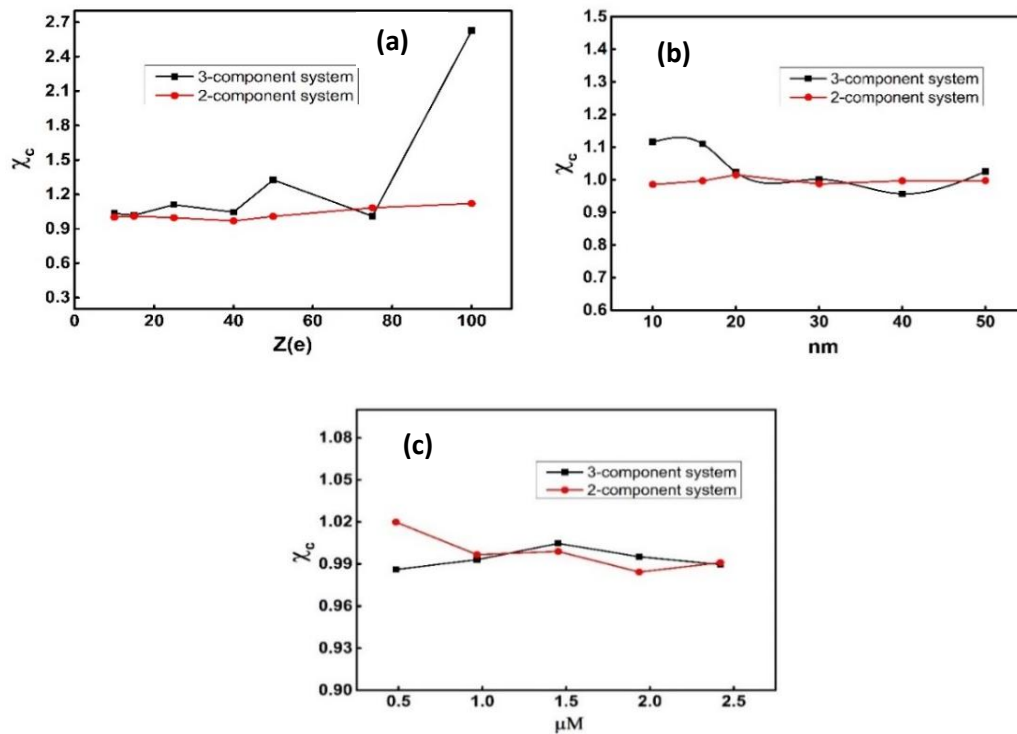


Figure 3.22. Plot of isothermal compressibility χ_c with variation in (a) charge, (b) size and (c) concentration of colloid particle.

For two-component (salt free) systems, χ_c value starts at 1.002 for $Z_m = -10e$ and increases to 1.121 for $Z_m = -100e$. In presence of salt (4.48 μM) the value changes from 1.033 for $Z_m = -10e$ to 2.627 for $Z_m = -100e$. With variation in size, the χ_c values almost remain constant (0.985 for 20nm colloid to 0.998 for 100nm colloid). These values change from 1.115 for 20nm to 1.025 for 100nm in presence of added salt (4.48 μM). With increase in colloid concentration χ_c ranges between 1.02 for 0.48 μM colloid concentration to 0.99 for 2.42 μM colloid concentration.

3.3.7. Self -Diffusion Coefficients

We have studied the variation of self-diffusion coefficient as a function of colloid charge, size and concentration. The self-diffusion coefficients of colloid (type 0) D_0 as well as counterion (type 1) D_1 for two-component and three-component systems are presented in Figure 3.23.

In case of two-component system (without salt), with increase in charge of colloid (Figure 3.23a), the D_0 decreases initially and becomes steady at larger colloid charge. With addition of salt (three-component), the D_0 behaves similar but the value decreases slightly at lower colloid charge. In two-component system, the D_1 (type 1) slightly increase at lower charge and then decreases with increase in charge of the colloid, whereas for the three-component system the D_1 value more or less remains constant.

With increase in colloid diameter, D_0 increases steadily till $\sigma_0 = 60\text{nm}$ and then decreases (Figure 3.23b). At lower colloid size the D_1 increases, becomes steady and decreases with increase in size of the colloid. With addition of salt the D_1 value decreases than increases at $\sigma_0=60\text{nm}$ and steadily decreases as the size of the colloid further increases. The D_0 decreases with increase in concentration of colloid for both two-component and three-component systems (Figure 3.23c). The D_1 value slightly increases with colloid concentration in case of two-component system and in case of three-component system D_1 steadily increases and then decreases when the concentration is high.

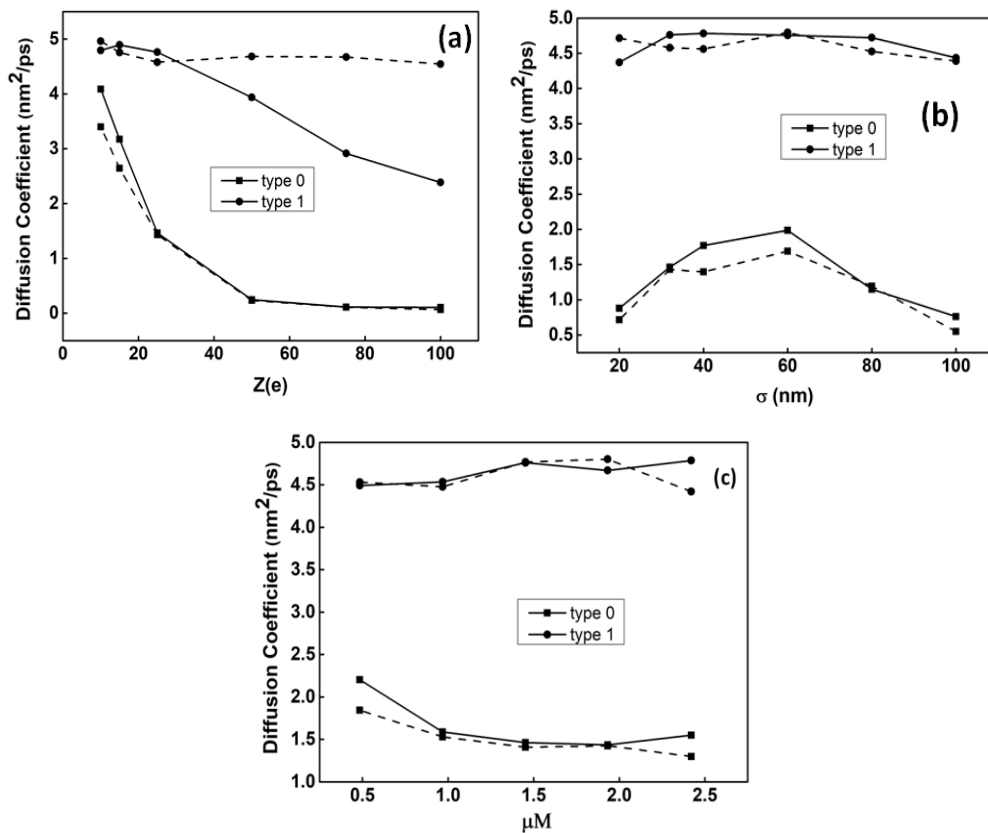


Figure 3.23. Variation of self - diffusion coefficients of colloid (type 0) as well as counterion (type 1) with variation in (a) charge (b) size and (c) concentration of colloid. The solid line is for two-component system and the dotted line represents three-component system.

B) Effect of confinement on model colloidal suspensions

3.4. Overview

The colloidal suspensions under confinement can have very interesting properties [40]. When the confining length (the distance between opposing boundaries) becomes comparable to the intrinsic length scale of the colloid particle, the confined suspension can behave quite differently from an identical suspension in the bulk [41–44]. Narrow confinement tends to lower the particle entropy and induces microscopic ordering of colloids into layers parallel to the confining walls [45]. This ordering is usually characterized by the density profile $\rho(z)$

across the confining walls. This density profile gives the distribution of particles across the walls and depends on the particle-particle and particle-wall interactions. The effects of confinement on structural and dynamics properties of colloids have given rise to many interesting phenomena [46–51]. Both simulation [52] and experimental [53] studies show the shift of the glass transition relative to bulk glass transition. Also, the diffusion coefficient of the binary colloidal mixtures has been studied in confined geometries [54] slit shaped nanochannels [55,56] cylindrical pores [57], rectangular nanotubes [58,59] and within spherical cavity [60].

We have employed the molecular dynamics simulations to study the molecular distribution and diffusion of model colloidal suspensions confined between two parallel walls. The walls are separated by a distance h along z -axis and are placed on the top and bottom of the simulation box (Figure 3.24 shows schematic representation of the confinement). We have focused on the density profiles which are related to the interactions.

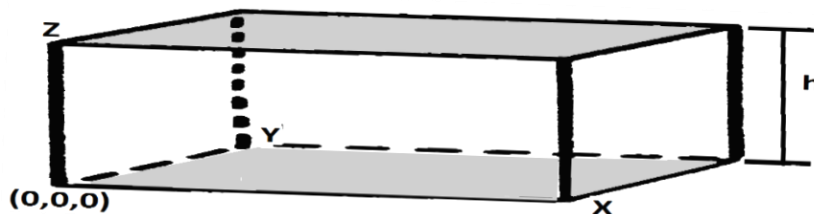


Figure 3.24: Schematic representation of the simulation box and the positions of walls at the top and bottom of the simulation box.

3.5. Model and simulation details:

The pair potential we used is of similar to the bulk solution. All the simulations were carried out with two confining parallel walls, one at the bottom and the other at the top of the simulation box (normal of the wall pointing up and down along z -axis), are created using the inbuilt function “constraint wall” of the ESPResSO package. Partial periodic boundary conditions (along x and y directions) are used. The type of the wall is used like a particle type to define the interaction of the walls with the particles. MMM2D algorithm was used for confined systems [61]. Simulations were carried out for colloidal suspensions with total number of particles N (2100 to 5600) packed in an asymmetric box of dimension $L_X = L_Y =$

1414nm, $L_z = 500nm$, under partial periodic boundary conditions (along X and Y directions) with density in the range 2×10^{-7} atoms/nm³ to 5.6×10^{-6} atoms/nm³. The number of colloids, counterions and the wall charges were adjusted to maintain the electroneutrality condition of the entire system. The simulation time taken here are similar to the simulations performed for bulk solutions.

We simulated the colloidal suspensions under the confinement of two parallel walls placed at the bottom and top of the simulation box (walls are parallel to xy plane). Both charged as well as neutral colloidal suspensions are considered. The diameters and charge used for the colloid (type 0 particle) are $\sigma_0 = 20, 32, 40, 60nm$, and $Z_0 = 0$ (neutral), $-10e$, $-25e$. The diameter and charge of counter ion (type 1 particle) are fixed at $\sigma_1 = 0.30nm$, and $Z_1 = 0$ (neutral) or $1e$. We use three types of walls: (i) both neutral, (ii) both negatively charged ($-1e$), and (iii) one positively charged ($1e$) and one negatively charged ($-1e$). We report the variations of density distribution $\rho_i(z)$ and the self-diffusion coefficient (along the xy plane) D_i of the constituent particles ($i = 0, 1$) as a function of colloid diameter (σ_0) and colloid charge (Z_0) in the above chosen systems.

3.6. Density Profile of Colloids under confinement:

The density profile of particle α is calculated by expression [62]

$$\rho_\alpha(z) = \frac{\langle N_\alpha(z, z + \Delta z) \rangle}{A \Delta z} \quad (3.6)$$

Where $\langle N_\alpha(z, z + \Delta z) \rangle$ is the average number of particles in a layer of thickness Δz around z , and A is the area of the walls. In our case, $\Delta z = L_z / 20$. We have reported our results in terms of reduced density $\rho^* = \rho \sigma^3$. In Figure 3.25(a), we have compared the variations of colloid density profile ($\rho_0(z)$) for the systems with neutral colloid of different sizes confined between neutral walls. For the colloid with $\sigma_0 = 20nm$, the density is more or less uniform except a small build up close to the walls (around 73 & 445nm). As the colloid size increases (to 40 and 60nm), there is a clear building up of density at various distances within the walls ($z = \sim 50, 200, 400, 450nm$), indicating a layered distribution of colloid.

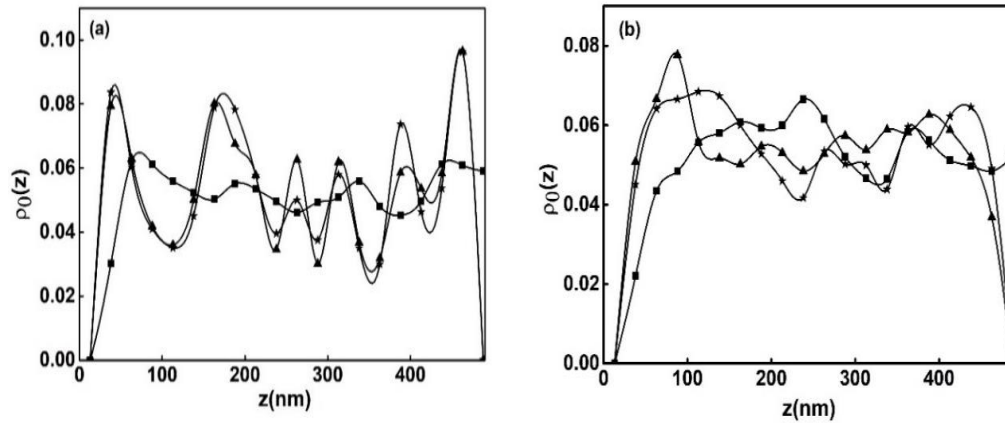


Figure 3.25. Variation of colloid density profiles ($\rho_0(z)$) in neutral colloidal suspensions of different diameters in between two walls: (a) neutral walls, (b) negatively charged walls (symbols: square denotes $\sigma_0 = 20$ nm, triangle denotes $\sigma_0 = 40$ nm and star denotes $\sigma_0 = 60$ nm).

The density is found to be at minimum at around layer of 250 to 300nm (around the middle of the walls) and maximum close to the walls ($z = 60$ and 440nm). Replacing the neutral walls with negatively charged walls, the density profile for the colloid (Figure 3.25b) become less structured, the peak for $\sigma_0 = 20$ nm has moved away from the walls.

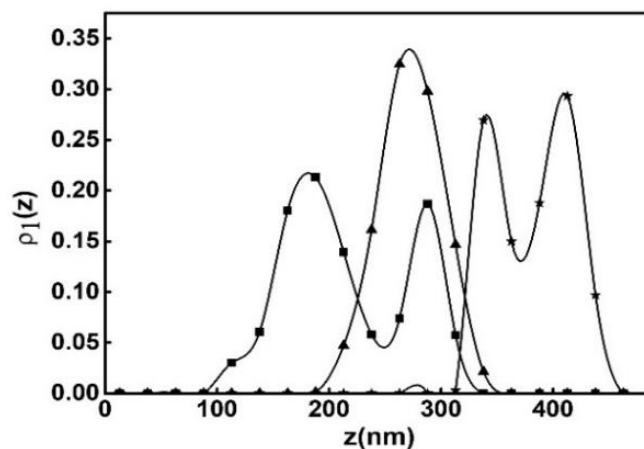


Figure 3.26: Variation of small ion/particle density profiles ($\rho_1(z)$) in neutral colloidal suspensions of different diameters in between two negatively charged walls. Other parameters are same as in Figure 3.25.

The density distributions for the counterions (Figure 3.26) show layered distributions, shifting toward the upper wall with increase in colloid diameters.

The variation of colloid density profile with its charge confined between neutral walls (with $\sigma_0 = 32nm$) is shown in Figure 3.27a, and for the charged walls is shown in Figure 3.28b. We have taken colloid charge of $-10e$ and $-25e$ along with a neutral one (charge zero) for comparison. As clear from the plots, the neutral colloid density profile is more structured with build-up of density (roughly around $32, 300$ and $450nm$). As the charge increases from zero to $-10e$ (Figure 3.28a), the colloids are pushed away from the walls (more from the bottom wall); two broad peaks (below $z = 250nm$) merge to one, and the profile becomes smooth. On further increase of charge to $-25e$ (Figure 3.27b), a similar build-up of density near walls appear. As the charge increases, the density is more of less symmetrical with average values at the middle of the walls and maxima around $1/4^{\text{th}}$ from both the walls.

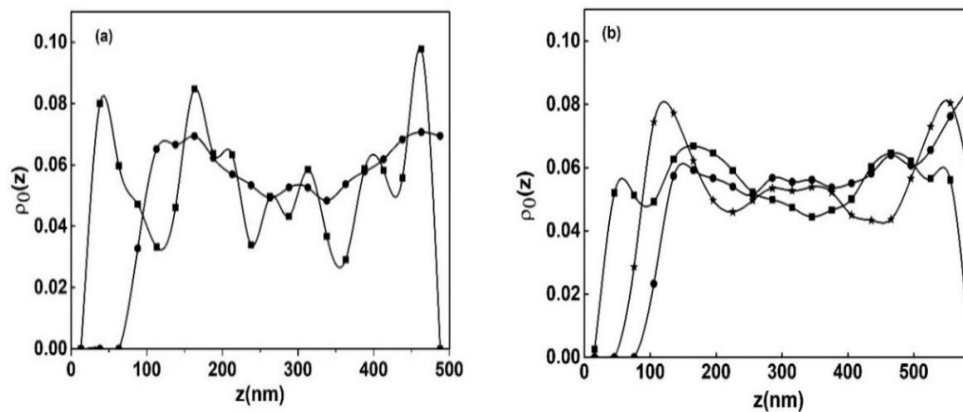


Figure 3.27: Variation of colloid density profiles ($\rho_0(z)$) with different colloidal charges for the colloidal suspensions of diameter $\sigma_0 = 32nm$: (a) between two neutral walls, b) between two negatively charged walls (symbols: square indicates $Z_0 = 0$ (neutral), circle indicates $Z_0 = -10e$ and star indicates $Z_0 = -25e$)

The counter-ion density profile for the charged colloids between charged walls is displayed in Figure 3.28. The counterion is distributed in layer roughly in the midway between the two walls and shift towards the upper wall as the colloid charge increases.

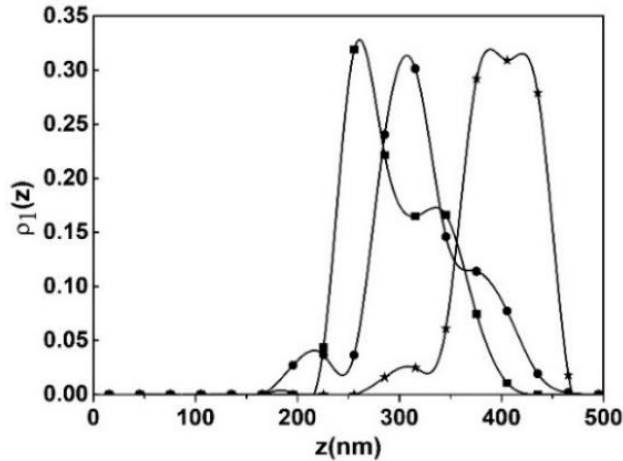


Figure 3.28: Variation of counterion density profiles ($\rho_1(z)$) with different colloidal charges for the colloidal suspensions of diameter $\sigma_0 = 32\text{nm}$ between two negatively charged walls. Other parameters are same as in Figure 3.27.

In order to see the effects of different kinds of walls (described in the beginning of the section) on colloid profile, we carry out simulations for a colloidal suspension with $\sigma_0 = 20\text{nm}$ and $Z_0 = -25e$. The result is shown in Figure 3.29.

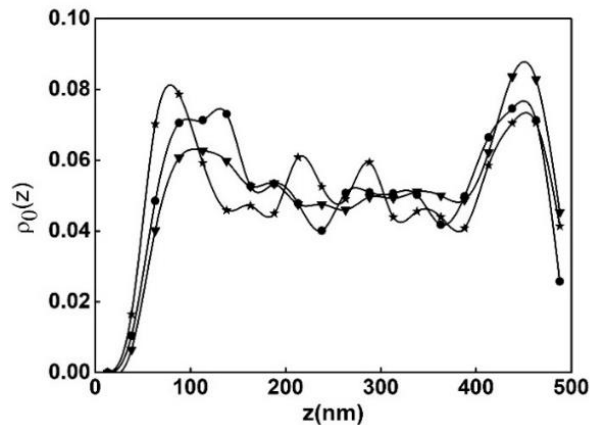


Figure 3.29: Variation of colloid density profiles ($\rho_0(z)$) with different types of walls for the colloidal suspensions of diameter $\sigma_0 = 20\text{nm}$ and charge $Z_0 = -25e$. (symbols: circle indicates neutral wall on both sides, star indicates negatively charged wall on both sides (- -) and inverted triangle indicates oppositely charged wall on both sides (+ -)).

For the case of neutral walls, the density profile increases from zero reaches maxima and then fall to an average value as we go away from the wall. For the case of charged walls, we find a similar trend in density profile, but the values of maxima differ. For the case of both negatively charged walls, the magnitude of maxima close to bottom wall is less and that close to upper wall is more compared to the corresponding case for neutral walls; whereas

for the case of (bottom positively and top negatively) charged walls, the peak height closer to positive wall increase (peak position closer to wall) and that close to negative wall slightly decreases. Also, appearance of additional density distributions are found in the midway between the walls for oppositely charged walls.

3.7. Self-diffusion coefficient:

The diffusion coefficient of particle α is calculated from the slope of mean square displacement (MSD) at large times (along xy direction) according to Einstein relation

$$D_\alpha = \lim_{t \rightarrow \infty} \frac{\langle [\mathbf{r}_\alpha(t) - \mathbf{r}_\alpha(0)]^2 \rangle}{6t} \quad (3.7)$$

Where, $\mathbf{r}_\alpha(t)$ is the position of the particle in the xy plane at time t , and $\langle \dots \rangle$ denotes the ensemble averaging.

Representative plots for the mean-square displacement (MSD) for type 0 (colloid) and type 1 (small ion) particle as a function of simulation time is displayed in Figure 3.30. The MSD decreases in case of charged colloidal system/charged walls, as compared to the neutral colloidal system/neutral walls. The decrease in type 0 particle (colloid) is more compared to that for smaller ion (type 1 particle).

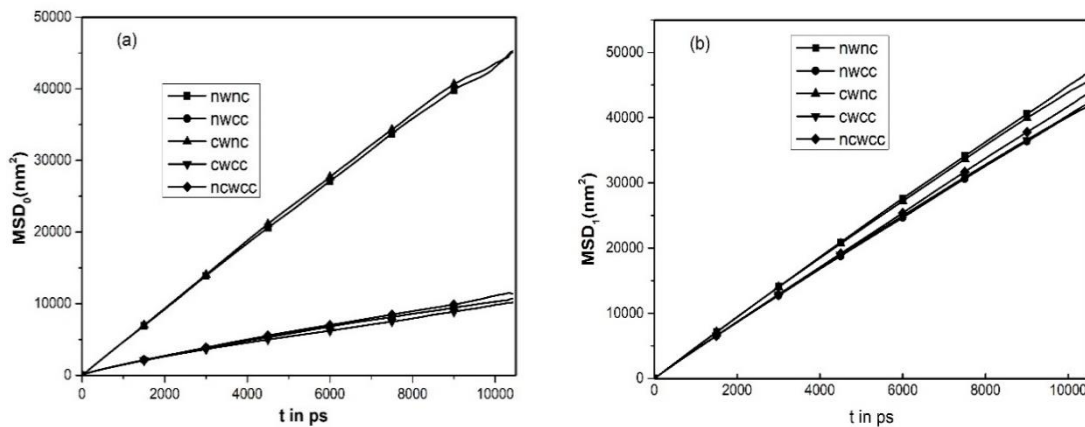


Figure 3.30: Representative plots for variation of (a) colloid-colloid, (b) counterion-counterion, mean-square displacement (MSD) with simulation time for the colloidal suspension ($\sigma_0 = 20\text{nm}$, $Z_0 = -25e$) with different confinement. (the first two lines from the

top are for systems with neutral colloid in neutral and charged walls, next three lines are for systems with charged colloid with three kinds of wall described in Figure 3.29).

The self-diffusion coefficient of both the colloid and small ion/particle (D_0 and D_1) for various systems are presented in Figure 3.31. The variation of D_i ($i = 0, 1$) as a function of colloid diameter for neutral colloid confined in charged walls is plotted in Figure 3.31(a). As the colloid diameter increases, the value of D_0 systematically decreases while the value of D_1 increases and finally levels up. The variations in D_i ($i = 0, 1$) are much similar with increase in the charge of colloid (Fig. 3.31b) though the decrease of D_0 with Z_0 is more drastic. Finally, we have compared (in Figure 3.31c) the diffusion coefficients D_i for different types of colloidal suspensions in different types of walls studied. It is clear from the graph that, the value of D_0 of neutral colloid is higher than those of charged colloid, irrespective of the types of wall. A similar trend in D_1 is observed, although the decrease in magnitude is very small.

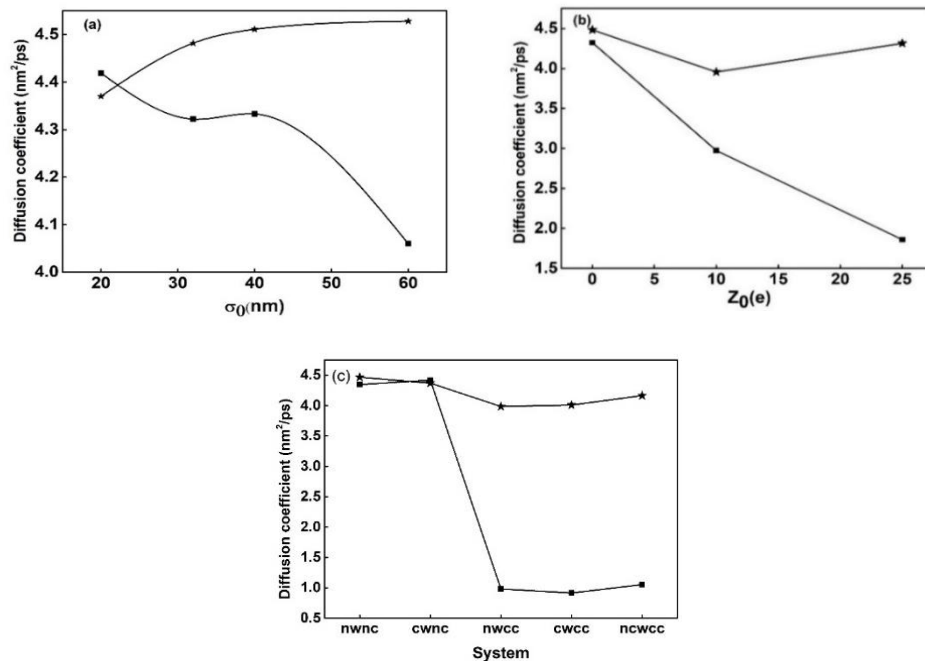


Figure 3.31: Self-diffusion coefficient of colloid (square) and small ion/particle (star) for various colloidal suspensions under confinement: (a) variation with colloid size, (b) variation with colloid charge, (c) variation with different types of walls. The wall types are same as in Fig 3.29

Self-diffusion coefficient of type 0 particle for charged colloidal particle with uncharged wall is less compared to the neutral colloidal particle of uncharged wall and the trend is same in charged colloid with charged wall when compared to neutral colloid with charged wall. The self-diffusion coefficient of type 1 particle for charged colloid system with charged and neutral wall is nearly same. However, for neutral colloidal system with charged wall the self-diffusion coefficient is less compared to neutral wall.

3.8. Conclusion:

We studied the model colloidal suspensions in bulk solutions as well as in between two walls using molecular dynamics simulations. The studies were carried out in a wide range of colloid charge ($10e$ - $100e$), diameter (20 nm-100 nm), concentration ($0.484 \mu\text{M}$ - $2.42 \mu\text{M}$) using a two-component (salt free) and a three component (with added salt) ($1.9 \mu\text{M}$ - $7.7 \mu\text{M}$). A systematic variations in radial distribution functions and effective colloid-colloid potential with colloid charge, size and concentration was observed. With increase in colloid charge, size and concentration, the peak height in $g_{00}(r)$ systematically increases. The depth of minima in the effective colloid-colloid potential are found to increase with increase in colloid charge, size and concentration. However, the position of the minima shift to lower inter-colloid distance with increase in colloid size and concentration but remain more or less unaltered with increase in colloid charge. The effect of salt (in the range investigated) has very little effect. With the increase in counterion valency, the effective colloid-colloid potential becomes less attractive. For the cases of colloid suspensions in between two parallel walls, the density profiles functions for colloid become oscillatory indicating ordering/layering of particles. The oscillatory behavior is found to be pronounced for colloid with neutral walls or one positive and one negative wall. A systematic variation in the density profile of small particle/ion is also observed. The self-diffusion coefficient of neutral colloid is found to be higher than that of charged one irrespective of the nature of walls.

3.9. References

- [1] L. Belloni, *Colloidal interactions*, J. Physics-Condensed Matter 12 (2000), pp. R549–R587.
- [2] C. Likos, *Effective Interactions in Soft Condensed Matter Physics*, Phys. Reports. Vol.

- 348, 2001.
- [3] R. Kjellander and S. Marčvelja, *Correlation and image charge effects in electric double layers*, Chem. Phys. Lett. 112 (1984), pp. 49–53.
- [4] I. Rouzina and V.A. Bloomfield, *Macroion attraction due to electrostatic correlation between screening counterions. I. Mobile surface-adsorbed ions and diffuse ion cloud*, J. Phys. Chem. 100 (1996), pp. 9977–9989.
- [5] Y. Li, M. Girard, M. Shen, J.A. Millan and M.O. De La Cruz, *Strong attractions and repulsions mediated by monovalent salts*, Proc. Natl. Acad. Sci. 114 (2017), pp. 11838–11843.
- [6] R. van Roij and J.-P. Hansen, *Van der Waals--like instability in suspensions of mutually repelling charged colloids*, Phys. Rev. Lett. 79 (1997), pp. 3082.
- [7] A.R. Denton, *Effective electrostatic interactions in colloid-nanoparticle mixtures*, Phys. Rev. E 96 (2017), pp. 1–14.
- [8] B. Hribar and V. Vlachy, *Macroion - Macroion Correlations in Presence of Divalent Counterions*, (2000), pp. 4218–4221.
- [9] P. Linse, *Simulation of charged colloids in solution*, in *Advanced computer simulation approaches for soft matter sciences II*, Springer, 2005, pp. 111–162.
- [10] P. Gonzalez-Mozuelos, G.I. Guerrero-Garcia and M. de la Cruz, *An exact method to obtain effective electrostatic interactions from computer simulations: The case of effective charge amplification*, J. Chem. Phys. 139 (2013), pp. 64709.
- [11] Y.-Y. Wu, F.-H. Wang and Z.-J. Tan, *Calculating potential of mean force between like-charged nanoparticles: a comprehensive study on salt effects*, Phys. Lett. A 377 (2013), pp. 1911–1919.
- [12] D.G. Grier and J.C. Crocker, *Comment on Monte Carlo study of structural ordering in charged colloids using a long-range attractive interaction*, Phys. Rev. E 61 (2000), pp. 980.

- [13] A.E. Larsen and D.G. Grier, *Like-charge attractions in metastable colloidal crystallites*, Nature 385 (1997), pp. 230.
- [14] B.V.R. Tata, P.S. Mohanty and M.C. Valsakumar, *Bound pairs: Direct evidence for long-range attraction between like-charged colloids*, Solid State Commun. 147 (2008), pp. 360–365.
- [15] A.H. Jalil and U. Pyell, *Quantification of Zeta-Potential and Electrokinetic Surface Charge Density for Colloidal Silica Nanoparticles Dependent on Type and Concentration of the Counterion: Probing the Outer Helmholtz Plane*, J. Phys. Chem. C 122 (2018), pp. 4437–4453.
- [16] G.J. Ojeda-Mendoza, A. Moncho-Jordá, P. González-Mozuelos, C. Haro-Pérez and L.F. Rojas-Ochoa, *Evidence of electrostatic-enhanced depletion attraction in the structural properties and phase behavior of binary charged colloidal suspensions*, Soft Matter 14 (2018), pp. 1355–1364.
- [17] L. Gulbrand, B. Jönsson, H. Wennerström and P. Linse, *Electrical double layer forces. A Monte Carlo study*, J. Chem. Phys. 80 (1984), pp. 2221–2228.
- [18] B. Svensson and B. Jönsson, *The interaction between charged aggregates in electrolyte solution. A Monte Carlo simulation study*, Chem. Phys. Lett. 108 (1984), pp. 580–584.
- [19] P. Linse, *On the convergence of simulation of asymmetric electrolytes with charge asymmetry 60: 1*, J. Chem. Phys. 110 (1999), pp. 3493–3501.
- [20] P. Linse and V. Lobaskin, *Electrostatic attraction and phase separation in solutions of like-charged colloidal particles*, J. Chem. Phys. 112 (2000), pp. 3917–3927.
- [21] A. Martín-Molina, J.G. Ibarra-Armenta, E. González-Tovar, R. Hidalgo-Álvarez and M. Quesada-Pérez, *Monte Carlo simulations of the electrical double layer forces in the presence of divalent electrolyte solutions: Effect of the ion size*, Soft Matter 7 (2011), pp. 1441–1449.
- [22] G. Bareigts and C. Labbez, *Effective pair potential between charged nanoparticles at*

- high volume fractions*, Phys. Chem. Chem. Phys. 19 (2017), pp. 4787–4792.
- [23] K. Ohsawa, H. Oshima and S. Ohki, *Surface potential and surface charge density of the cerebral-cortex synaptic vesicle and stability of vesicle suspension*, Biochim. Biophys. Acta (BBA)-Biomembranes 648 (1981), pp. 206–214.
- [24] K. Ohsawa, M. Murata and H. Ohshima, *Zeta potential and surface charge density of polystyrene-latex; comparison with synaptic vesicle and brush border membrane vesicle*, Colloid Polym. Sci. 264 (1986), pp. 1005–1009.
- [25] S.A. Adelman, *The effective direct correlation function: An approach to the theory of liquid solutions*, J. Chem. Phys. 64 (1976), pp. 724–731.
- [26] P. Linse, *Structure, phase stability, and thermodynamics in charged colloidal solutions*, J. Chem. Phys. 113 (2000), pp. 4359–4373.
- [27] B. Hribar and V. Vlachy, *Evidence of Electrostatic Attraction between Equally Charged Macroions Induced by Divalent Counterions*, J. Phys. Chem. B 101 (1997), pp. 3457–3459.
- [28] P. Udaykumar, T. Khanna and R.N. Behera, *Equilibrium Structure and Properties of Model Colloidal Suspensions*, 2 (2013), pp. 61–66.
- [29] M. Fushiki, *A hypernetted chain structure factor for charged colloidal dispersions*, J. Chem. Phys. 89 (1988), pp. 7445–7453.
- [30] B. Beresford-Smith, D.Y.C. Chan and D.J. Mitchell, *The electrostatic interaction in colloidal systems with low added electrolyte*, J. Colloid Interface Sci. 105 (1985), pp. 216–234.
- [31] U.K. Padidela and R.N. Behera, *Interactions in charged colloidal suspensions: A molecular dynamics simulation study*, in AIP Conference Proceedings, 1859 (2017), pp. 20111.
- [32] V. Lobaskin, A. Lyubartsev and P. Linse, *Effective macroion-macroion potentials in asymmetric electrolytes*, Phys. Rev. E 63 (2001), pp. 20401.

- [33] J.A. Anta, F. Bresme and S. Lago, *Integral equation studies of charged colloids: non-solution boundaries and bridge functions*, J. Phys. Condens. Matter 15 (2003), pp. S3491.
- [34] B.V.R. Tata, R.G. Joshi, I.S. Sogami and M. Carlo, *Long-range Attraction between Like-charged Colloids : Simulations and Microgravity Experiments*, 32 (2015), pp. 1–6.
- [35] D.J. Cebula, J.W. Goodwin, G.C. Jeffrey, R.H. Ottewill, A. Parentich and R.A. Richardson, *Properties of concentrated polystyrene latex dispersions*, Faraday Discuss. Chem. Soc. 76 (1983), pp. 37–52.
- [36] B. Hribar and V. Vlachy, *Clustering of macroions in solutions of highly asymmetric electrolytes*, Biophys. J. 78 (2000), pp. 694–698.
- [37] M. Druchok, Y. Kalyuzhnyi, J. Rescic and V. Vlachy, *Analysis of osmotic pressure data for aqueous protein solutions via a multicomponent model*, J. Chem. Phys. 124 (2006), pp. 114902.
- [38] L. Belloni, *A hypernetted chain study of highly asymmetrical polyelectrolytes*, Chem. Phys. 99 (1985), pp. 43–54.
- [39] G.M. Abernethy and M.J. Gillan, *A new method of solving the HNC equation for ionic liquids*, Mol. Phys. 39 (1980), pp. 839–847.
- [40] J. Klafter and J.M. Drake, *Molecular Dynamics in Restricted Geometries*, Wiley-Interscience, 1989.
- [41] P. Pieranski, L. Strzelecki and B. Pansu, *Thin colloidal crystals*, Phys. Rev. Lett. 50 (1983), pp. 900.
- [42] J.A. Weiss, D.W. Oxtoby, D.G. Grier and C.A. Murray, *Martensitic transition in a confined colloidal suspension*, J. Chem. Phys. 103 (1995), pp. 1180–1190.
- [43] W. Qi, Y. Peng, Y. Han, R.K. Bowles and M. Dijkstra, *Nonclassical nucleation in a solid-solid transition of confined hard spheres*, Phys. Rev. Lett. 115 (2015), pp.

185701.

- [44] M. Heinen, T. Palberg and H. Löwen, *Coupling between bulk-and surface chemistry in suspensions of charged colloids*, J. Chem. Phys. 140 (2014), pp. 124904.
- [45] C. Stubenrauch and R. Von Klitzing, *Disjoining pressure in thin liquid foam and emulsion films new concepts and perspectives*, J. Phys. Condens. matter 15 (2003), pp. R1197.
- [46] A. Schlaich, E.W. Knapp and R.R. Netz, *Water dielectric effects in planar confinement*, Phys. Rev. Lett. 117 (2016), pp. 48001.
- [47] R. Hayes, G.G. Warr and R. Atkin, *Structure and nanostructure in ionic liquids*, Chem. Rev. 115 (2015), pp. 6357–6426.
- [48] S.H.L. Klapp, D. Qu and R. V. Klitzing, *Long-range interactions between soft colloidal particles in slit-pore geometries*, J. Phys. Chem. B 111 (2007), pp. 1296–1303.
- [49] Y. Zeng, S. Grandner, C.L.P. Oliveira, A.F. Thunemann, O. Paris, J.S. Pedersen et al., *Effect of particle size and Debye length on order parameters of colloidal silica suspensions under confinement*, Soft Matter 7 (2011), pp. 10899–10909.
- [50] K. Stratford, O. Henrich, J.S. Lintuvuori, M.E. Cates and D. Marenduzzo, *Self-assembly of colloid-cholesteric composites provides a possible route to switchable optical materials*, Nat. Commun. 5 (2014), pp. 3954.
- [51] Y. Zeng, S. Grandner, C.L.P. Oliveira, A.F. Thünemann, O. Paris, J.S. Pedersen et al., *Effect of particle size and Debye length on order parameters of colloidal silica suspensions under confinement*, Soft Matter 7 (2011), pp. 10899–10909.
- [52] A.M. Puertas, F.J. de las Nieves and A. Cuetos, *Computer simulations of charged colloids in confinement*, J. Colloid Interface Sci. 440 (2015), pp. 292–298.
- [53] C.R. Nugent, K. V Edmond, H.N. Patel and E.R. Weeks, *Colloidal glass transition observed in confinement*, Phys. Rev. Lett. 99 (2007), pp. 25702.

- [54] K. Nygård, *Colloidal diffusion in confined geometries*, Phys. Chem. Chem. Phys. 19 (2017), pp. 23632–23641.
- [55] R. Bhadauria and N.R. Aluru, *A multiscale transport model for Lennard-Jones binary mixtures based on interfacial friction*, J. Chem. Phys. 145 (2016), pp. 74115.
- [56] U. Marini Bettolo Marconi, P. Malgaretti and I. Pagonabarraga, *Tracer diffusion of hard-sphere binary mixtures under nano-confinement*, J. Chem. Phys. 143 (2015), pp. 184501.
- [57] S.T. Cui, *Molecular self-diffusion in nanoscale cylindrical pores and classical Ficks law predictions*, J. Chem. Phys. 123 (2005), pp. 54706.
- [58] R. Devi, S. Srivastava and K. Tankeshwar, *Static and dynamic effects of confinement on self-diffusion*, Phys. Chem. Liq. 52 (2014), pp. 636–649.
- [59] P.K. Yuet, *Simulation study of charged nanoparticles confined in a rectangular tube with discrete wall charges*, Langmuir 22 (2006), pp. 2979–2985.
- [60] C. Aponte-Rivera, Y. Su and R.N. Zia, *Equilibrium structure and diffusion in concentrated hydrodynamically interacting suspensions confined by a spherical cavity*, J. Fluid Mech. 836 (2018), pp. 413–450.
- [61] A. Arnold and C. Holm, *MMM2D: A fast and accurate summation method for electrostatic interactions in 2D slab geometries*, Comput. Phys. Commun. 148 (2002), pp. 327–348.
- [62] J. Alejandre, M. Lozada-Cassou, E. González-Tovar and G.A. Chapela, *Molecular dynamics of a hard-sphere fluid between two walls: a comparison with the three-point extension hypernetted chain approximation*, Chem. Phys. Lett. 175 (1990), pp. 111–116.

Chapter 4
Performance of HNC, PY and MS
integral equations on model colloidal
suspensions : Comparison with MD
results

Numerical results on the structure and equilibrium properties of model colloidal suspensions have been presented using integral equation theory. The Ornstein Zernike Equation (OZE) has been solved with three different closures, viz. Hypernetted-chain (HNC), Percus Yevick (PY) and Martynov Sarkisov (MS) using Newton-GMRES algorithm. Comparison of the results among different closures as well as with those of MD simulation have been carried out.

4.1. Introduction:

Integral equation theory based on Ornstein-Zernike (OZ) equation provides standard route to the structure of fluids [1]. The OZ equation is a basic non-linear Fredholm second-kind integral equation employed in the statistical mechanics of fluids to compute the microscopic structure from description of the underlying intermolecular forces. Theories based on the OZ equation with different closures such as hypernetted chain (HNC), Percus-Yevick (PY) etc. have been quite successful in studying different fluids. They are computationally less expensive than molecular simulations. However, availability of efficient algorithms that improve and accelerate the convergence of the solution of such non-linear integral equations are limited. Over the years several attempts were made to improve the performance of the theories and extend the validity of the integral equation theory to wide range of parameters.

Some matrix methods for solution of integral equations which describe inhomogeneous fluids was carried out by Chen and Pettit [2]. Homeier and coworkers used vector extrapolation technique and illustrated the iterative solution of bulk Ornstein Zernike (OZ) type integral equations [3], provides standard against which to compare the Newton-GMRES algorithm. Zerah [4] described the use of a Newton method for the numerical solution of the fluid integral equations in which the linear system is solved efficiently using an iterative conjugate gradient (CG) technique [5]. The CG algorithm is usually intended for the solution of symmetric positive definite systems. It is generalized to nonsymmetric linear systems as carried out by Zerah. The examples considered by Zerah are the solution of the Percus-Yevick equation for an inverse twelfth power potential and the hypernetted chain (HNC) equation for a Lennard Jones (LJ) potential. Zerah illustrate that the stability and efficiency of a Newton iterative method (Newton-CG). With variation in volume fractions the effective pair potential for binary mixtures were obtained using HNC approximation, which yields attractive well at about $-0.5k_B T$ [6].

Several methods that have been developed for solving very large systems of non-linear equations include Newton-iterative methods (also known as truncated Newton methods). The crucial ingredient in this type of Newton method is that the linear system arising in every iteration of the newton method is not solved by a direct method (which require the matrix of coefficients and a significant amount of arithmetic) but by an iterative

method. Thus, a truncated Newton method solves a nonlinear system by an outer nonlinear iteration, each step of which solves a linear approximation to the problem by an inner linear iteration. In this work, we use the Newton-GMRES (Generalized Minimum RESidual) algorithm of Saad and Schultz [7] as the linear solver.

In this chapter, we present numerical calculations of correlation functions of model colloidal suspensions using three different closures: HNC, PY and Martynov Sarkisov (MS) for a wide range of system parameters. In few cases, we compared with the MD simulation results.

4.2. Model and Methods

4.2.1. Integral equation theory, HNC, PY and MS closures

We studied the multicomponent asymmetric colloidal system using primitive model. It contains negatively charged spherical colloidal particles (as type 0), positively charged counter-ions (as type 1) and negatively charged co-ions (as type 2) interacting with the pair potential as described earlier in chapter 2 of section 2.2.

The pair correlation function (for an m -component system) is calculated by solving the OZ equation [8].

$$h_{ab}(r_{12}) = c_{ab}(r_{12}) + \sum_{n=1}^m \rho_n \int d^3r_3 c_{an}(r_{13}) h_{nb}(r_{32}), \quad (4.1)$$

$$\text{where } r_{ab} = |r_a - r_b|, \rho_n = \text{number density}$$

Along with the closure, which can be written without any approximation as

$$h_{ij}(r) = \exp[-\beta u_{ij}(r) + h_{ij}(r) - c_{ij}(r) + B_{ij}(r)] - 1, \quad (4.2)$$

where ρ_n is the number density of particle species n , $h_{ij}(r) = g_{ij}(r) - 1$ is the total correlation function, $c_{ij}(r)$ is the direct correlation function and $B_{ij}(r)$ is the bridge diagram sum.

By setting $B_{ij}(r) = 0$, in Eq. 4.3 we obtained HNC closure [9], PY closure [10] is obtained by setting $B_{ij}(r) = \ln[1 + h_{ij}(r) - c_{ij}(r)] - h_{ij}(r) - c_{ij}(r)$ and MS closure [11] is obtained when $B_{ij}(r) = [1 + 2(h_{ij}(r) - c_{ij}(r))]^{1/2} - (h_{ij}(r) + c_{ij}(r)) - 1$.

4.2.2. Newton GMRES algorithm [12]

The Newton-Raphson method solves non-linear equations in the form $F(x) = 0$. An initial guess estimate x_n is required, one can find the next guess x_{n+1} , using the equation below.

$$x_{n+1} = x_n - \frac{F(x_n)}{F'(x_n)}$$

Because of iteration steps required at each step, the convergence was a problem. To overcome the drawback of this method, a new specialized and matrix free method was implemented called Newton-GMRES method. It is an inexact Newton method.

It approximates the solution of linear equation and uses the Newton step as a vector s that satisfies the inexact Newton condition. The termination criterion for linear iteration is the standard inexact Newton condition

$$\|F'(x_n)s + F(x_n)\| \leq \eta \|F(x_n)\|$$

The parameter η can be varied as the Newton iteration progresses. The global and local convergence properties of algorithm is influenced by the choice of forcing term (η) called Eisenstat-Walker forcing term. We set $\eta = 10^{-4}$ for all computations, is a very small forcing term which leads to rapid quadratic convergence near the solution. The maximum number of nonlinear iterations used are 40.

The HNC closure (Eq 4.2 with $B_{ij}=0$) and OZ equation (Eq 4.1) can be written as

$$h_{ab}(r_{12}) + 1 - \exp(-\beta u_{ab}(r_{12}) + h_{ab}(r_{12}) - c_{ab}(r_{12})) = 0 \quad (4.3)$$

$$c_{ab}(r_{12}) + 1 - \exp(-\beta u_{ab}(r_{12}) + h_{ab}(r_{12}) - c_{ab}(r_{12}) + \rho(c * h)(r_{12})) = 0 \quad (4.4)$$

Equation 4.4 is a result of adding Eq 4.1 and 4.2.

The Newton-GMRES iteration scheme expresses the above two equations in the general form [13].

$$F = M - K = 0 \quad M = \begin{pmatrix} h - c \\ \exp(-\beta u + h - c - h - 1) \end{pmatrix} \quad K = - \begin{pmatrix} 0 \\ \rho(c * h) \end{pmatrix} \quad (4.5)$$

We set

$$N(h, c)(r) = \exp(-\beta u_{ab}(r_{12}) + h_{ab}(r_{12}) - c_{ab}(r_{12}))$$

And N defined is substituted in equation

$$M(r) = \begin{pmatrix} h_{ab}(r_{12}) + 1 - N(h, c)(r) \\ c_{ab}(r_{12}) + 1 - N(h, c)(r) \end{pmatrix}, \text{ and}$$

$$K(r) = - \begin{pmatrix} 0 \\ \rho(c * h)(r) \end{pmatrix}$$

The convolution $c * h$ can be computed using spherical-Bessel transform. The h was defined

$$\hat{h}(k) = H(h)(k) = 4\pi \int_0^{\infty} \frac{\sin(kr)}{kr} h(r) r^2 dr \quad (4.6)$$

and

$$h(r) = H^{-1}(\hat{h})(r) = \frac{1}{2\pi^2} \int_0^{\infty} \frac{\sin(kr)}{kr} \hat{h}(k) k^2 dk \quad (4.7)$$

$c * h$ was computed by discretizing the formula

$$c * h = H^{-1}(\hat{c}\hat{h}) \quad (4.8)$$

Where $\hat{c}\hat{h}$ is the pointwise product of functions.

We used MATLAB (version R2012b) to solve the required equations using the Newton-GMRES algorithm. All the functions are evaluated within the range of $(0, L)$. The range is then divided into $N-1$ intervals of equal size Δr and all the functions are evaluated at each mesh point. The periodic nature of sine and cosine functions utilized by imposing the condition $\Delta r \Delta k = \pi / (N-1)$, Δk is the mesh size in the Fourier space. We used $N = 2049$. The iteration is assumed to be converged as the tolerances $\tau_a = \tau_r = 10^{-8}$.

4.3. Results and Discussions

We have studied the static properties (pair correlation function), direct correlation functions, effective pair potentials of model colloidal suspensions with the diameter of colloid (type 0 particle) σ_0 (in nm) = 20, 32, 40, 60, 100, charge of colloid Z_0 (in e) = -10, -15, -20, -25, -30, and concentration of colloid C_0 (in μM) = 0.9681, 1.9362, 2.42, 4.836, 9.681, 12.091 (μM = 10^{-6} molar) and concentration of salt C_s (in μM) = 4.836, 9.681. The diameters of the counterion and co-ion were fixed as $0.3 nm$ and the charge of the counterion (type 1) and co-ion (type 2) $1e$ and $-1e$. We used the temperature = 298.15K, the Bjerrum length $L_B = 0.715nm$.

4.3.1. Two-component colloidal system: HNC Result

4.3.1.1. Variation in size of colloid

4.3.1.1.1. Pair correlation functions

The diameter of the colloid particle is varied from $\sigma_0 = 20$ to $100 nm$ at a fixed colloid charge $Z_0 = -25e$ and concentration of colloid $C_0 = 0.968\mu M$.

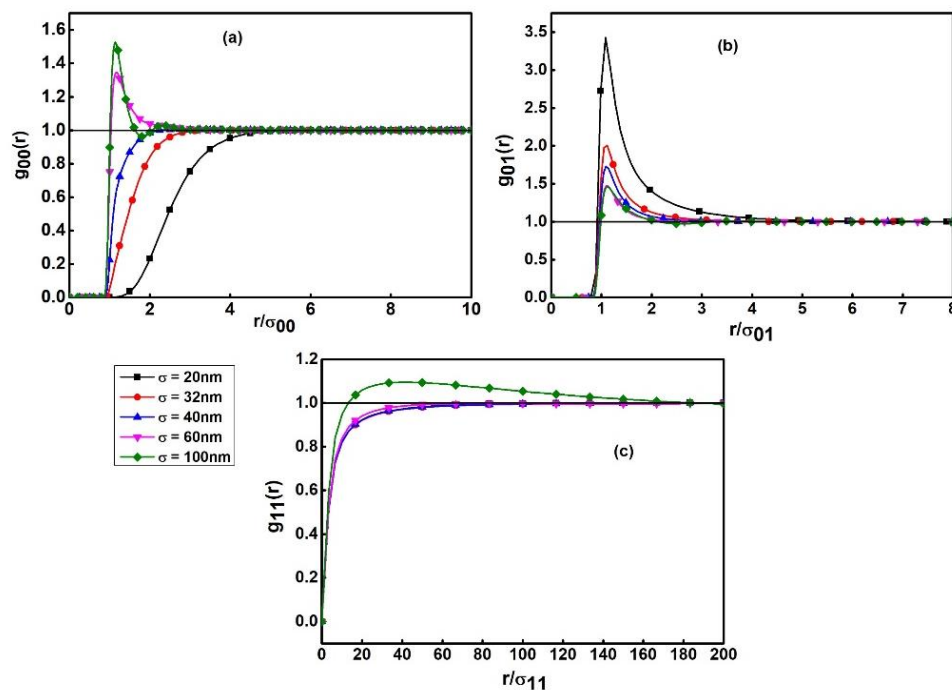


Figure 4.1: Variation of pair correlation functions (a) $g_{00}(r)$, (b) $g_{01}(r)$ and (c) $g_{11}(r)$ with colloid diameter at fixed $Z_0 = -25e$ and $C_0 = 0.968 \mu M$.

The colloid-colloid ($g_{00}(r)$), colloid-counterion ($g_{01}(r)$) and counterion-counterion ($g_{11}(r)$) pair correlation functions are plotted in Figure 4.1 as a function of colloidal diameter. With increase in the size of the colloidal particle, the peak height (probability of finding colloid around another colloid) increases and the peak shifts towards the shorter interparticle distance. The colloid-counterion (Figure 4.1b) contact value decreases as the diameter of the colloid increases. This indicates the accumulation of counterions on the surface decreases. The counterion-counterion (Figure 4.1c) peaks are broader and peak height increases with increase in diameter of the colloid particle. Thus, the HNC results are very similar to those obtained by MD simulation in chapter 3.

4.3.1.1.2. Direct correlation functions

The variation of direct correlation functions $c_{00}(r)$, $c_{01}(r)$, $c_{11}(r)$ with colloidal diameter is shown in Figure 4.2.

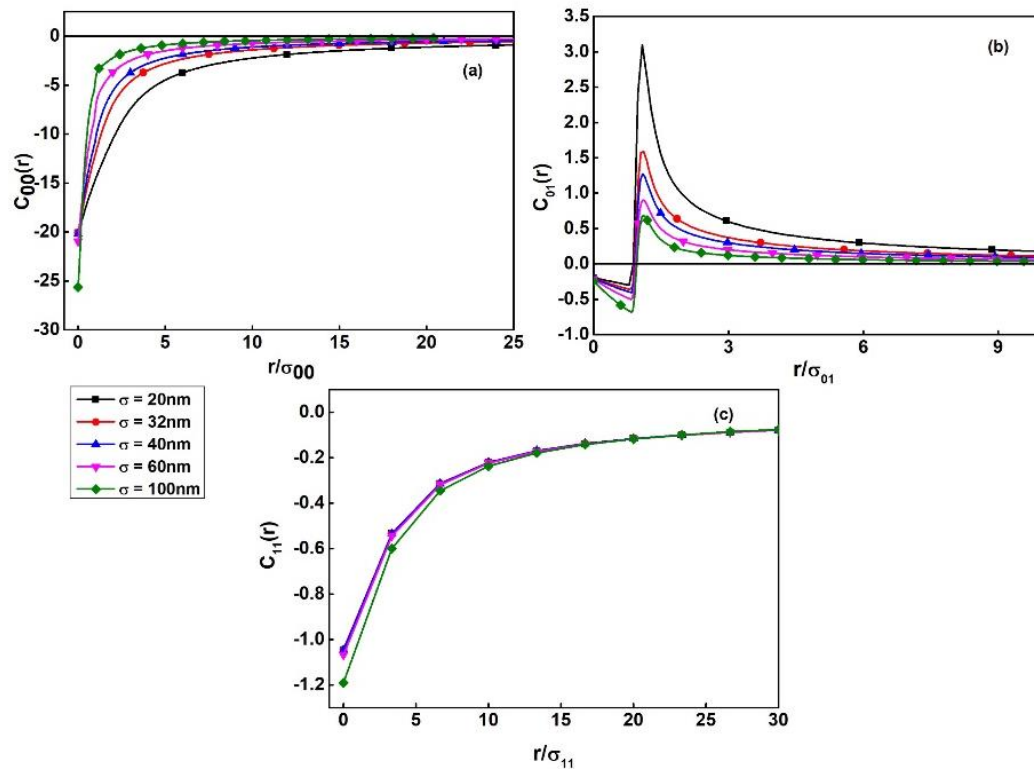


Figure 4.2: Plots of direct correlation functions (a) colloid-colloid $c_{00}(r)$, (b) colloid-counterion $c_{01}(r)$ and (c) counterion-counterion $c_{11}(r)$, as a function of colloidal diameter at a fixed $Z_0 = -25e$ and $C_0 = 0.968 \mu\text{M}$.

The colloid-colloid direct correlation function $c_{00}(r)$ in Figure 4.2(a) tends to increase with increase in diameter of colloid with the value -20.08 at $\sigma_0 = 20nm$ to -25.5 at $\sigma_0 = 100 nm$ at shorter interparticle distance with less oscillations. The $c_{00}(r)$ is negative at shorter interparticle distance and it level upto zero at larger interparticle distances. The colloid-counterion direct correlation function (Figure 4.2b) behave similar to $g_{0l}(r)$, however starting with negative values and leveling to zero at larger interparticle distances. The counterion-counterion direct correlation function $c_{11}(r)$ steadily increases from negative value as the colloid diameter increases.

4.3.1.1.3. Effective potential and potential of mean force

The effective interactions between the colloid-colloid shows repulsions in Figure 4.3(a) for all the diameters of the colloids. The $\beta V^{eff}(r)$ shifts towards the lower interparticle distance with increase in diameter of the colloid. The $\beta W_{00}(r)$ displayed in Figure 4.3(b) with increase in diameter of colloid becomes negative at $\sigma_0 = 60nm$ and $\sigma_0 = 100nm$ shows less repulsions and eventually becomes attractive. The $\beta W_{00}(r)$ shifts towards lower interparticle distance with increase in diameter of colloid. The magnitude of $\beta W_{00}(r)$ decreases from $\sigma_0 = 20nm$ and $\sigma_0 = 100nm$.

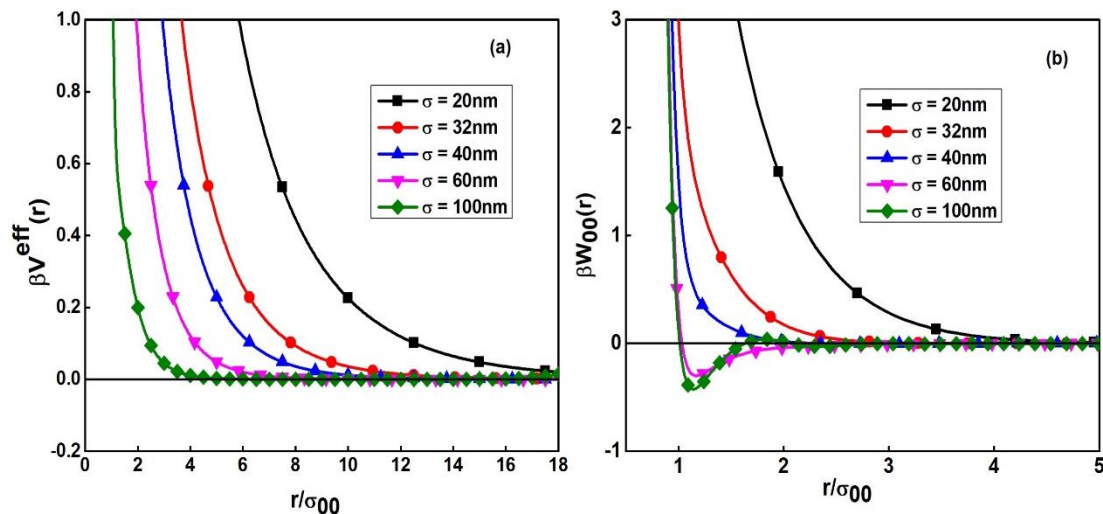


Figure 4.3: Plots of (a) $\beta V^{eff}(r)$ and (b) $\beta W_{00}(r)$, as a function of colloid diameter at fixed $Z_0 = -25e$ and $C_0 = 0.968 \mu M$.

4.3.1.1.4. Effective direct correlation functions

We studied the $c_{00}^{eff}(r)$ with increasing diameter of the colloidal particle. Figure 4.4 shows that $c_{00}^{eff}(r)$ for $\sigma_0 = 20nm$ is -20.04 and for $\sigma_0 = 100nm$ it is -25.6. The values become negative at short inter particle distance.

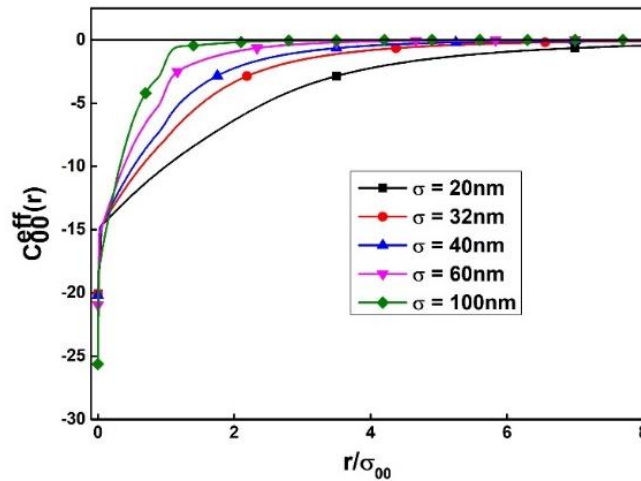


Figure 4.4: Plot of $c_{00}^{eff}(r)$, as a function of colloid diameter at fixed $Z_0 = -25e$ and $C_0 = 0.968 \mu M$.

4.3.1.2. Variation of colloid charge

4.3.1.2.1. Pair correlation functions

The effect of increasing colloidal charge was studied at fixed $\sigma_0 = 32nm$ and $C_0 = 0.968 \mu M$ and shown in Figure 4.5. The peak height of $g_{00}(r)$ (Figure 4.5a) increases with increase in charge of the colloid. The probability of finding a colloid around another colloid occurs at $r/\sigma_{00} = 1$ and nearly same for all cases. With increase in charge of colloid, the magnitude of colloid-counterion correlation function $g_{01}(r)$ (Figure 4.5b) decreases and peak position is at $r/\sigma_{00} = 1$. The $g_{11}(r)$ (Figure 4.5c) correlation function increases with increase in charge of the colloidal particle and it is broader.

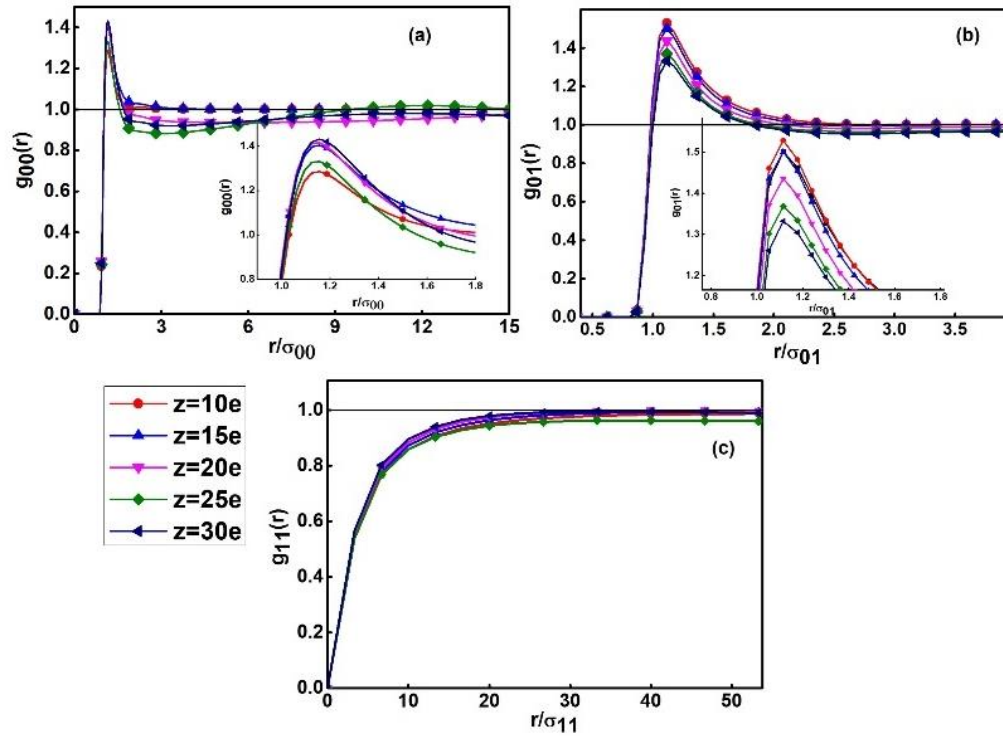


Figure 4.5: Plots of pair correlation functions (a) colloid-colloid $g_{00}(r)$, (b) colloid-counterion $g_{01}(r)$, (c) counterion-counterion $g_{11}(r)$, as a function of colloidal charge at fixed $\sigma_0 = 32\text{nm}$ and $C_0 = 0.968 \mu\text{M}$.

4.3.1.2.2. Direct Correlation functions

The direct correlation functions $c_{00}(r)$, $c_{01}(r)$, $c_{11}(r)$ as a function of colloidal charge was studied and shown in Figure 4.6. With increasing charge of the colloid, the values of $c_{00}(r)$ increases from -6.0 at $Z_0 = -10e$ to -101.2 at $Z_0 = -30e$. The values of colloid-counterion direct correlation functions (Figure 4.6b) ranges from -0.56 at $Z_0 = -10e$ to 2.5 at $Z_0 = -30e$. The variations are more at shorter interparticle distance. The $c_{11}(r)$ behaves similar to size variation.

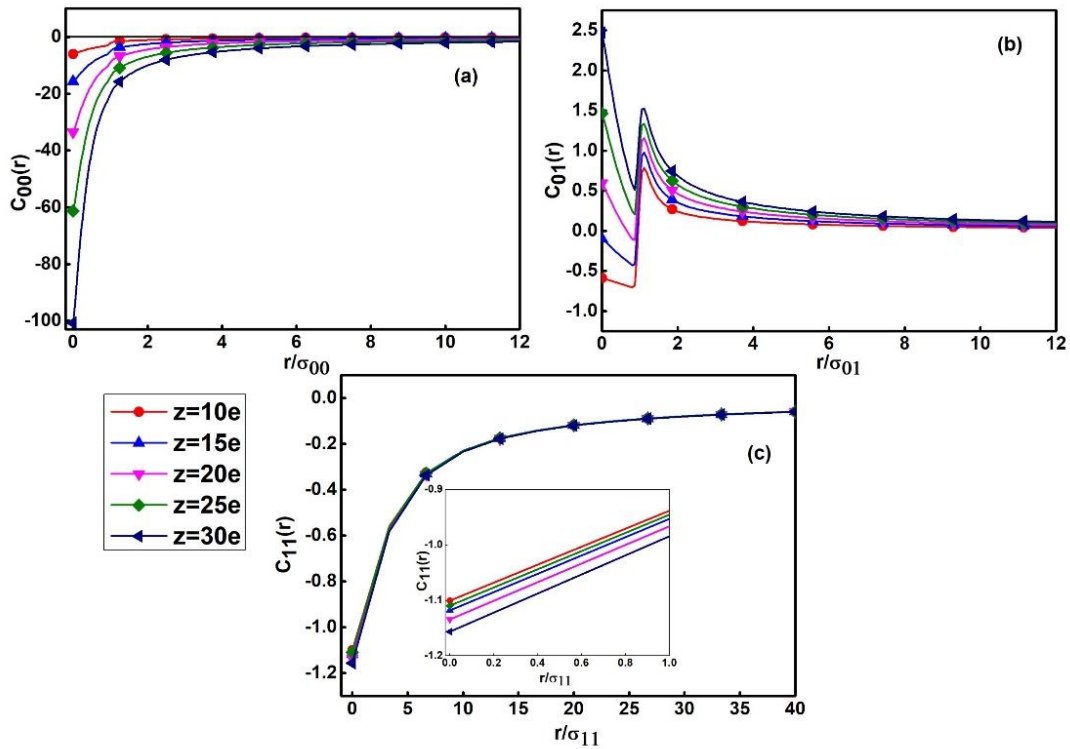


Figure 4.6: Plots of direct correlation functions (a) colloid-colloid $c_{00}(r)$, (b) colloid-counterion $c_{01}(r)$ and (c) counterion-counterion $c_{11}(r)$, as a function of colloid charge at fixed $\sigma_0 = 32\text{nm}$ and $C_0 = 0.968 \mu\text{M}$

4.3.1.2.3. Effective potential and potential of mean force

The magnitude of $\beta V^{\text{eff}}(r)$ (Figure 4.7a) increases as Z_0 increases and becomes negative for $Z_0 = 25e, 30e$. The effective colloid-colloid interactions increase with increase in charge of the colloidal particle and shows repulsive behavior at $Z_0 = 10e, 15e$ and $20e$ and eventually becomes attractive at $Z_0 = 25e, 30e$. The $\beta V^{\text{eff}}(r)$ is negative for $Z_0 = 25e, 30e$ at all r . This might be because with increase in Z_0 , the repulsion between the colloidal particles increases and the meanwhile the counterion condensation on the colloidal particles also increases. The $\beta W_{00}(r)$ (Figure 4.7b) becomes negative with all the cases of colloidal charge. The depth of attractive minima increases with increase in charge of the colloid. The attractive HNC minima is found at lower interparticle distance i.e. $r/\sigma_{00} \sim 1.0$.

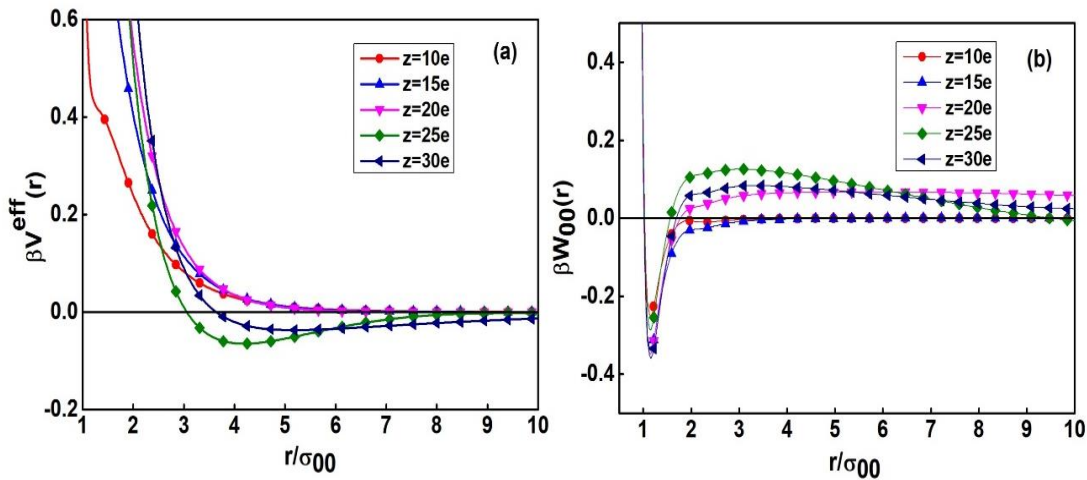


Figure 4.7: Variation of (a) $\beta V^{\text{eff}}(r)$ and (b) $\beta W_{00}(r)$ as a function of colloid charge at fixed $\sigma_0 = 32\text{nm}$ and $C_0 = 0.968 \mu\text{M}$.

4.3.1.2.4. Effective direct correlation functions

With increase in charge of colloid, the $c_{00}^{\text{eff}}(r)$ at short interparticle distances becomes negative and tends to zero at larger interparticle distance (Figure 4.8). The value at $Z_0 = -10e$ is -5.57 and at $Z_0 = -30e$ is -100.56 .

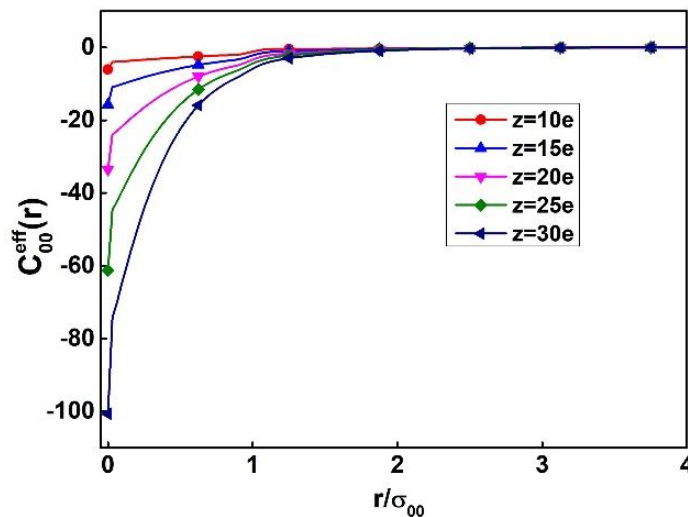


Figure 4.8: Plot of $c_{00}^{\text{eff}}(r)$ as function of colloid charge at fixed $\sigma_0 = 32\text{nm}$ and $C_0 = 0.968 \mu\text{M}$.

4.3.1.3. Variation in colloid concentration

4.3.1.3.1. Pair correlation functions

The variation of colloid concentration on pair correlation functions was studied at fixed $\sigma_0 = 32\text{nm}$ and $Z_0 = -25e$. As colloid concentration increases, the peak height of the colloid-colloid ($g_{00}(r)$) correlation function in Figure 4.9(a) increases and the peak position shifts towards shorter interparticle distance. This indicates the repulsion between the similarly charged colloids and it has been observed in several studies [14–16]. The colloid concentrations of $0.968\mu\text{M}$ and $1.936\mu\text{M}$ does not show any structure. The colloid-counterion correlation function $g_{01}(r)$ in Figure 4.9(b) decreases with increase in colloid concentration. The counterion-counterion correlation function $g_{11}(r)$ is structure less at low colloid concentration and shows structure with a broader peak only at $12.091\mu\text{M}$.

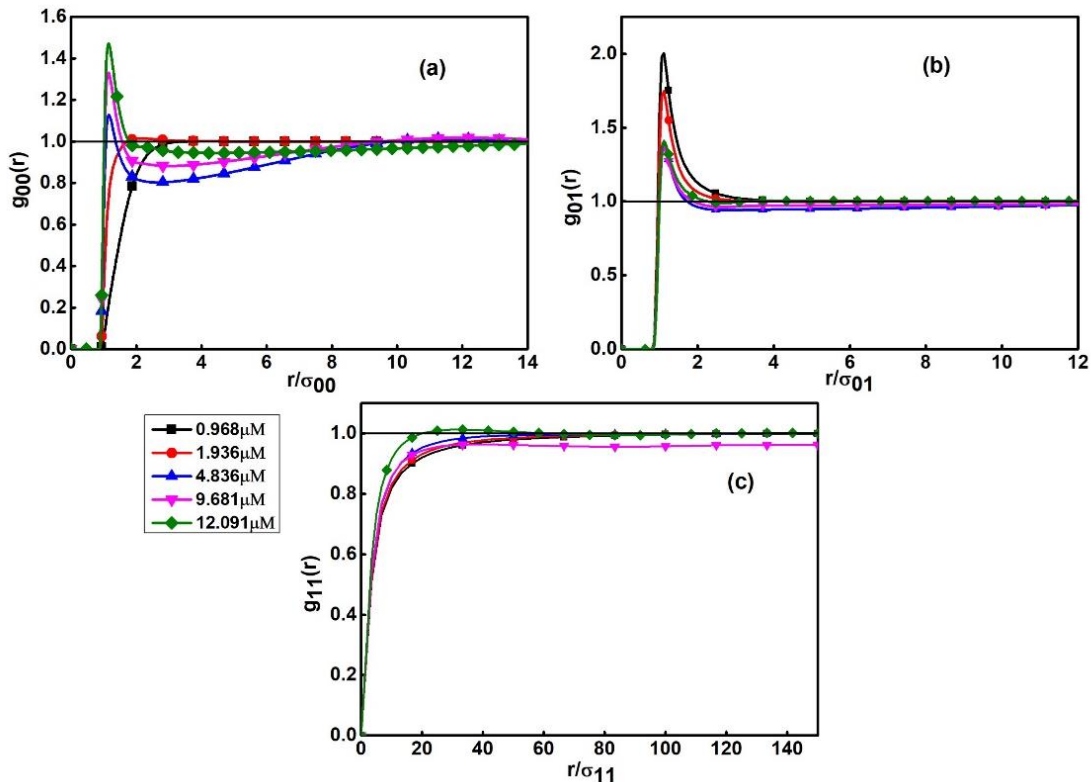


Figure 4.9: Plots of pair correlation functions (a) $g_{00}(r)$, (b) $g_{01}(r)$, (c) $g_{11}(r)$, as a function of colloid concentration at fixed $\sigma_0 = 32\text{nm}$ and $Z_0 = -25e$.

4.3.1.3.2. Direct correlation functions:

We studied the direct correlation functions $c_{00}(r)$, $c_{01}(r)$, $c_{11}(r)$ as a function of colloid concentration and displayed in Figure 4.10. With increasing concentration of the colloid, the values of $c_{00}(r)$ (Figure 4.10a) increases systematically from -20 at $C_0 = 0.968\mu\text{M}$ to -66.0 at $C_0 = 12.091\mu\text{M}$. The values differ more at lower interparticle distance and become indistinguishable at larger distance. The values of $c_{01}(r)$ (Figure 4.10b) ranges from -0.2 at $C_0 = 0.968\mu\text{M}$ to 1.7 at $C_0 = 12.091\mu\text{M}$. It shows the structure at shorter interparticle distance. The $c_{11}(r)$ behaves similar to size variation.

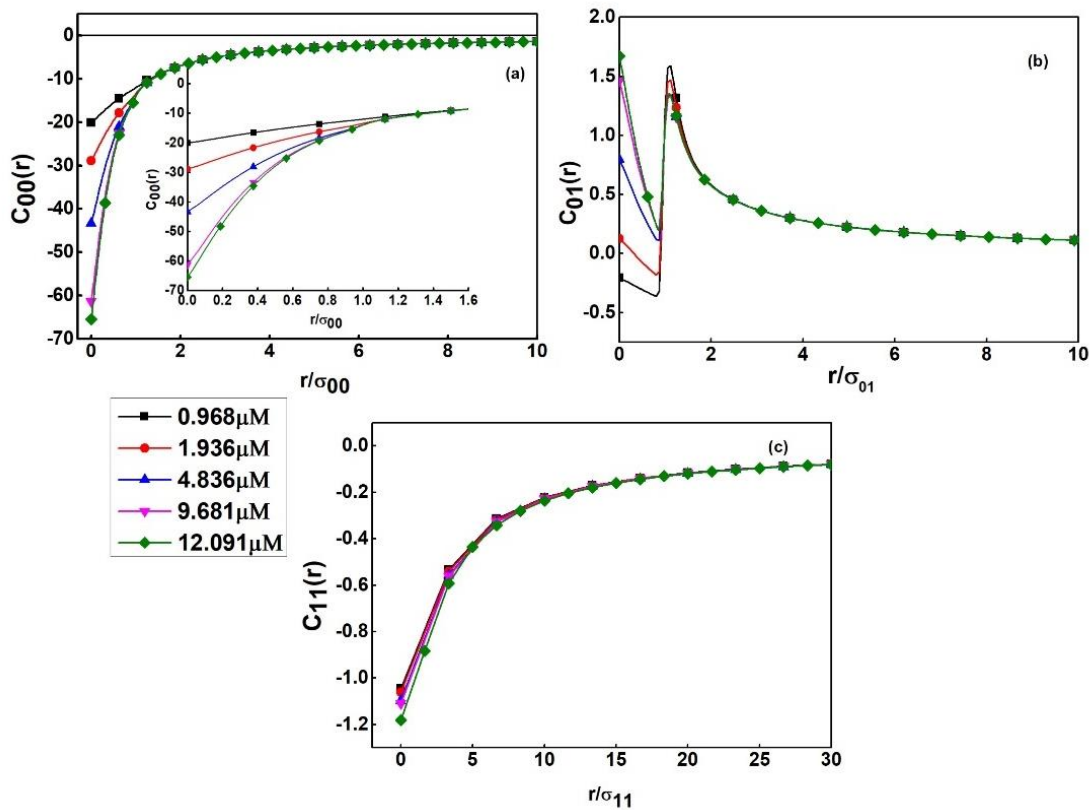


Figure 4.10: Plots of direct correlation functions (a) colloid-colloid $c_{00}(r)$, (b) colloid-counterion $c_{01}(r)$, (c) counterion-counterion $c_{11}(r)$, as a function of colloid concentration at fixed $\sigma_0 = 32\text{nm}$ and $Z_0 = -25e$.

4.3.1.3.3. Effective potential and potential of mean force

With increasing colloid concentration, the magnitude of $\beta V^{eff}(r)$ (Figure 4.11a) increases and becomes negative at $C_0 = 12.091 \mu\text{M}$. With colloid concentrations of $0.968 \mu\text{M}$, $1.936 \mu\text{M}$, $4.836 \mu\text{M}$ and $9.681 \mu\text{M}$ the effective colloid-colloid interaction shows repulsive behavior and eventually becomes attractive at $C_0 = 12.091 \mu\text{M}$ near $r/\sigma_{00} = 4.4$. The HNC $\beta W_{00}(r)$ (Figure 4.11b) is repulsive at $0.968 \mu\text{M}$ and it becomes negative with increase in colloidal concentration. The depth of $\beta W_{00}(r)$ increases from -0.1 at $4.836 \mu\text{M}$ to -0.4 at $12.091 \mu\text{M}$. The position of minima in $\beta W_{00}(r)$ shift towards lower interparticle distance around $r/\sigma_{00} \sim 1.0$.

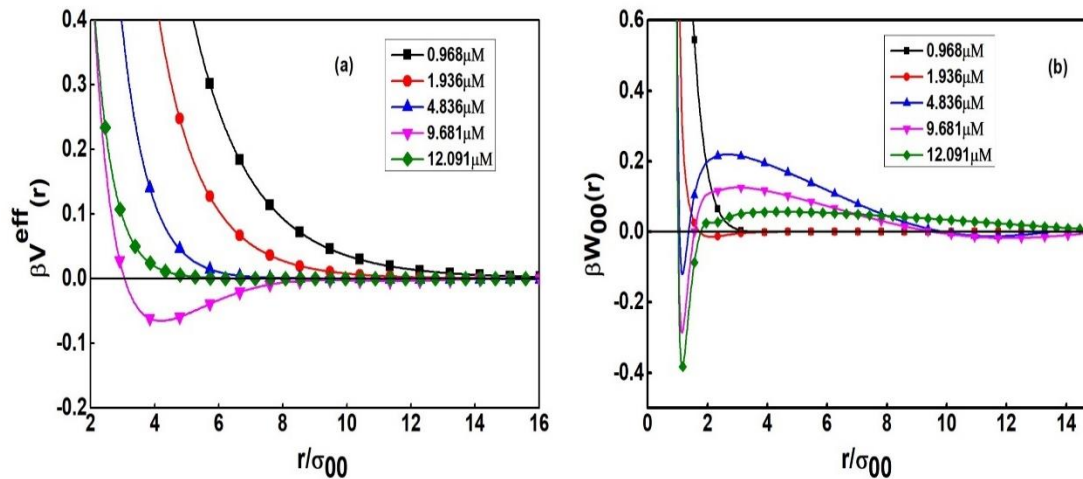


Figure 4.11: Plots of (a) $\beta V^{eff}(r)$ and (b) $\beta W_{00}(r)$, as a function of colloid concentration at fixed $\sigma_0 = 32\text{nm}$ and $Z_0 = -25e$.

4.3.1.3.4. Effective direct correlation functions

With increase in concentration of colloid, the $c_{00}^{eff}(r)$ becomes negative at short interparticle distances (Figure 4.12) and become negative. The value at $C_0 = 0.968 \mu\text{M}$ is -20.0 and at $C_0 = 12.091 \mu\text{M}$ is -62.0 .

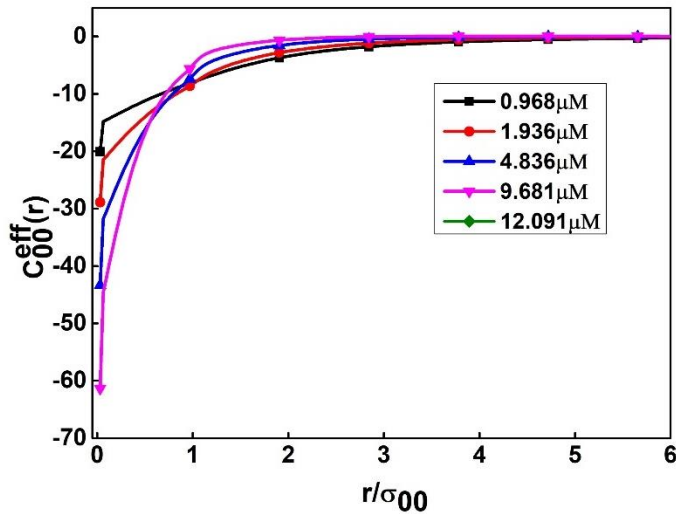


Figure 4.12: Plot of $c_{00}^{eff}(r)$ as a function of colloid concentration at fixed $\sigma_0 = 32\text{nm}$ and $Z_0 = -25e$.

4.3.2. Comparison of different closure approximations and molecular dynamics (MD) result in two-component colloidal system:

In this section, we have compared the results of Hypernetted chain (HNC), Percus Yevick (PY) Martynov Sarkisov (MS) approximations and MD result for two-component systems.

4.3.2.1. Size variation

Here we compare the results of various closures and MD results for two colloid diameters $\sigma_0 = 20\text{nm}$ and 100nm .

4.3.2.1.1 Effective potential

We varied the colloid diameter at fixed $Z_0 = -25e$ and $C_0 = 0.9681\mu\text{M}$. We have compared the $\beta V^{eff}(r)$ obtained from various closure relations and MD simulation with $\sigma_0 = 20\text{nm}$ and 100nm in Figure 4.13. The HNC shows repulsive interactions and shifts towards lower interparticle distance. MD result shows attractive behavior. The order of repulsive behavior of $\beta V^{eff}(r)$ looks like HNC > PY > MS for $\sigma_0 = 20\text{nm}$. When diameter is increased to $\sigma_0 = 100\text{nm}$ (Figure 4.13b) the order of repulsive behavior of closures changes to HNC > PY = MS. The MD result shows attractive behavior.

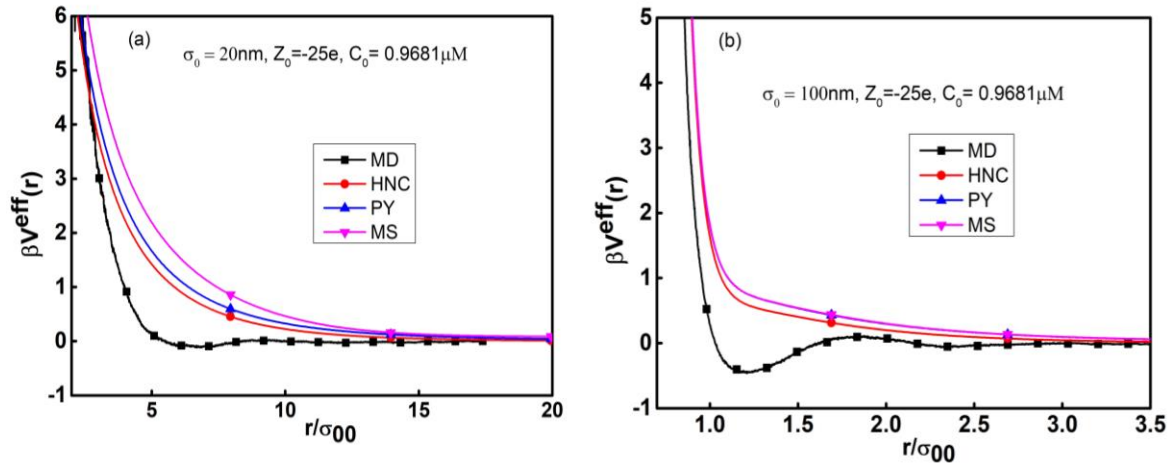


Figure 4.13: Comparison of $\beta V^{\text{eff}}(r)$ with different closures: HNC, PY, MS and MD result for two-component system at fixed $Z_0 = -25e$ and $C_0 = 0.9681 \mu\text{M}$. (a) $\sigma_0 = 20 \text{ nm}$ (b) $\sigma_0 = 100 \text{ nm}$.

4.3.2.1.2. Potential of mean force

We have studied the $\beta W_{00}(r)$ (Figure 4.14a) of the system with same parameters as mentioned in Figure 4.13. $\beta W_{00}(r)$ HNC at $\sigma_0 = 20 \text{ nm}$ shows more repulsive behavior compared to the $\beta V^{\text{eff}}(r)$ HNC and shifts towards lower interparticle distance. PY and MS closures tend to

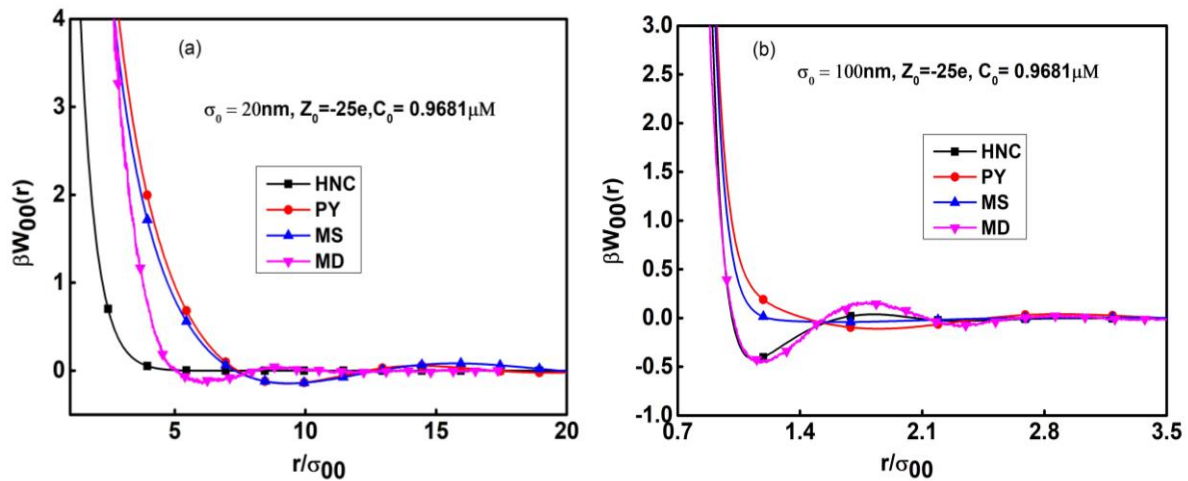


Figure 4.14: Comparison of $\beta W_{00}(r)$ with different closures: HNC, PY, MS and MD result for two-component system. Other parameters are same as in Figure 4.13.

become negative and attractive at $r/\sigma_{00} \approx 10.0$. The MD result shows attractive behavior.

The attractive minima for $\beta W_{00}(r)$ HNC is nearly -0.2. MS and PY closures also show secondary peaks which indicates long range interactions at $r/\sigma_{00} \approx 16.0$. In Figure 4.14(b) the HNC shows good agreement with MD result as the diameter of the colloidal particle increased to $\sigma_0 = 100nm$ and shows attractive minima (magnitude -0.5) with secondary peaks.

4.3.2.1.3. Effective direct correlation function

The effective colloid-colloid direct correlation functions for different closures are plotted in Figure 4.15. The value of $c_{00}^{eff}(r)$ HNC at $\sigma_0 = 20nm$ is -20.0 and at $\sigma_0 = 100nm$ is -25.0. The value of $c_{00}^{eff}(r)$ PY at $\sigma_0 = 20nm$ is -64.0 and at $\sigma_0 = 100nm$ is -60.0. The value of $c_{00}^{eff}(r)$ MS at $\sigma_0 = 20nm$ is -30.0 and at $\sigma_0 = 100nm$ is -34.0. The variation of $c_{00}^{eff}(r)$ with colloid diameter varies in the order $PY > MS > HNC > MD$.

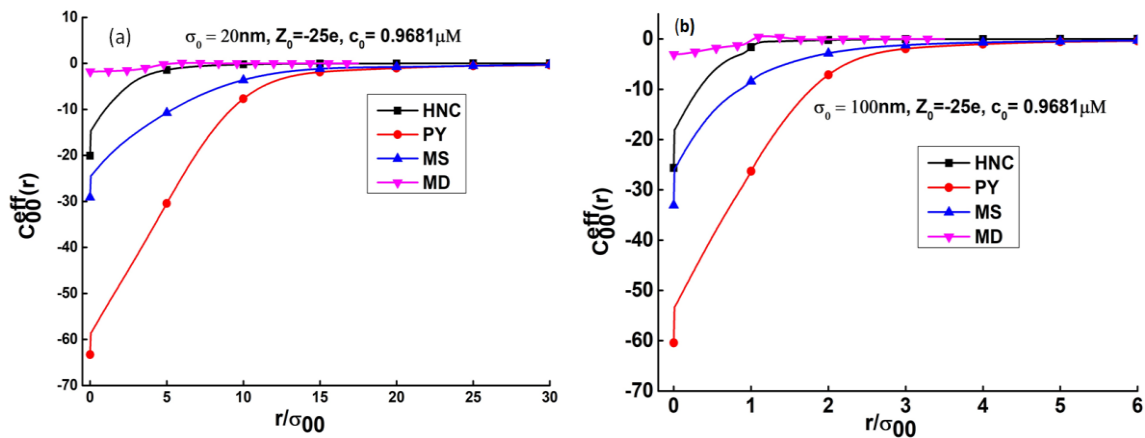


Figure 4.15: Comparison of $c_{00}^{eff}(r)$ with different closures: HNC, PY, MS and MD result for two-component system. Other parameters are same as in Figure 4.13.

4.3.2.2. Charge variation

4.3.2.2.1 Effective potential

We have compared the closures with variation of colloid charge at fixed $\sigma_0 = 32nm$ and $C_0 = 0.9681\mu M$. $\beta V^{eff}(r)$ was studied for $Z_0 = -10e$ and $Z_0 = -25e$ using different closures. All the closures overlap and shows similar behavior at $Z_0 = -10e$ (Figure 4.16(a)). The MD result

shows attractive minima for larger r . As the charge of the colloid increased to $-25e$ (Figure 4.16b) the $\beta V^{eff}(r)$ HNC shows repulsive interactions and shifts towards lower interparticle distance which is prominent in charged colloidal suspensions in case of HNC. The order of repulsive behavior is similar as in size variation (Figure 4.13a).

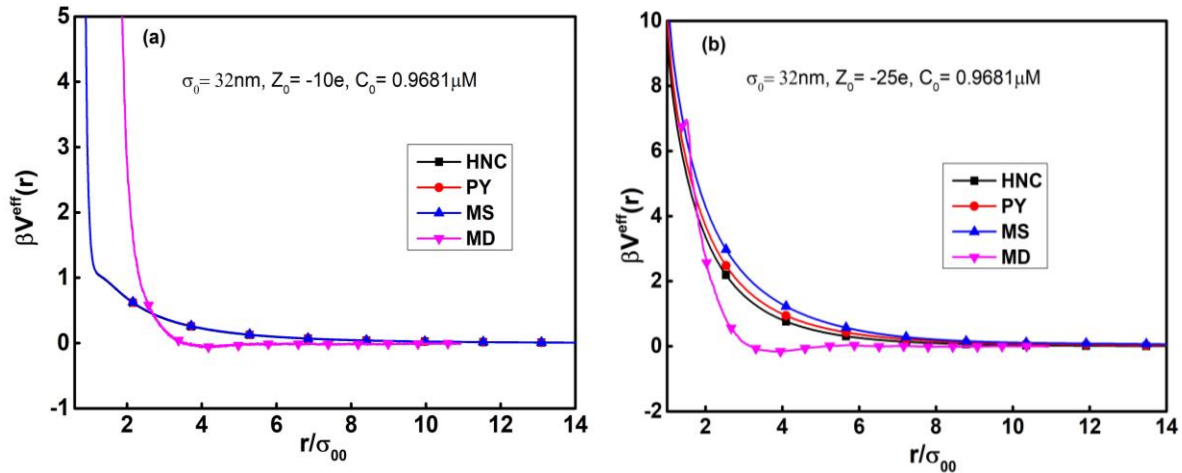


Figure 4.16: Comparison of $\beta V^{eff}(r)$ with different closures: HNC, PY, MS and MD result for two-component system at fixed $\sigma_0 = 32\text{nm}$ and $C_0 = 0.9681\mu\text{M}$. (a) $Z_0 = -10e$ and (b) $Z_0 = -25e$.

4.3.2.2.2 Potential of mean force

The effective interactions between colloid-colloid $\beta W_{00}(r)$ of the system with same parameters as mentioned in Figure 4.16 was studied. $\beta W_{00}(r)$ PY and MS behaves exactly same at $Z_0 = -10e$. $\beta V^{eff}(r)$ HNC shifts towards lower interparticle distance. When the charge of the colloid increased to $Z_0 = -25e$ the PY and MS closures becomes negative and shows attractive behavior at long range compared to HNC which shows short range repulsive interactions.

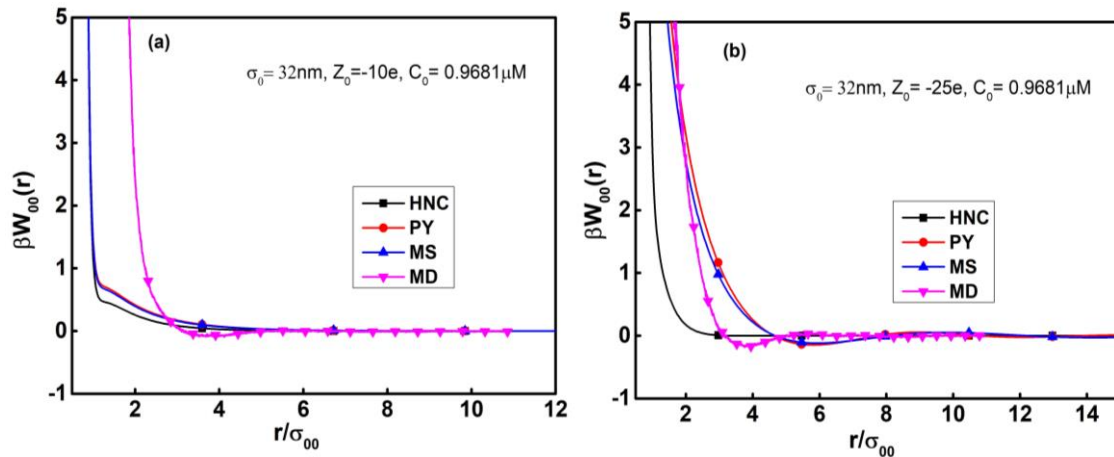


Figure 4.17: Comparison of $\beta W_{00}(r)$ with different closures: HNC, PY and MS for two-component system. Other parameters are same as in Figure 4.16.

4.3.2.2.3. Effective direct correlation function

The effective direct correlation function of colloid-colloid $c_{00}^{\text{eff}}(r)$ was plotted in Figure 4.18. The values of $c_{00}^{\text{eff}}(r)$ HNC, $c_{00}^{\text{eff}}(r)$ PY and $c_{00}^{\text{eff}}(r)$ MS at $Z_0 = -10e$ is nearly -2.5. The magnitude of the potential is less at short range. When the charge of the colloid increased to $Z_0 = -25e$ the magnitude of effective direct interactions between colloid-colloid increases and value of $c_{00}^{\text{eff}}(r)$ HNC is -64.0, $c_{00}^{\text{eff}}(r)$ PY is -29.0 and $c_{00}^{\text{eff}}(r)$ MS is -11.0.

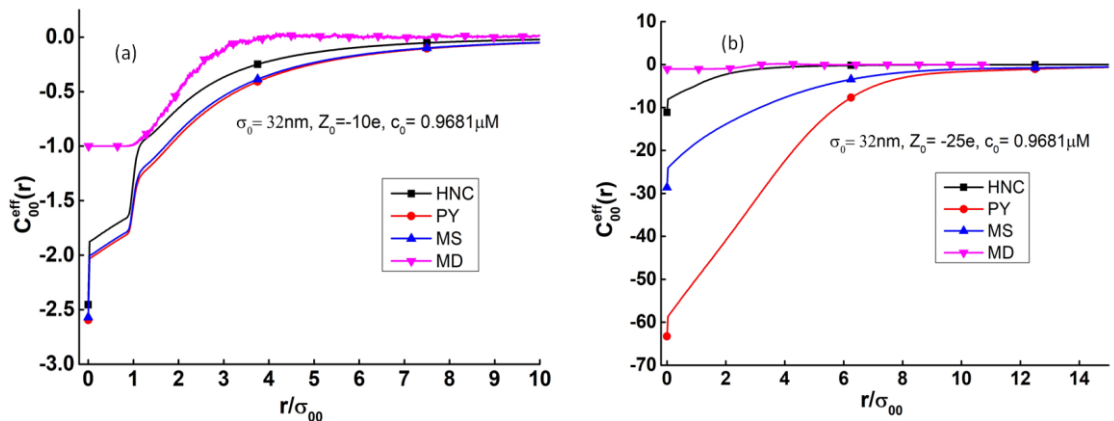


Figure 4.18: Comparison of $c_{00}^{\text{eff}}(r)$ with different closures: HNC, PY and MS for two-component system. Other parameters are same as in Figure 4.16.

4.3.2.3. Concentration variation

4.3.2.3.1 Effective potential

In this section we have discussed different closures at fixed $\sigma_0 = 32nm$, $Z_0 = -25e$ with variation in colloid concentration. The effective potential $\beta V^{eff}(r)$ (Figure 4.19(a)) shows that the closures behave similar to the system with $\sigma_0 = 20nm$, $Z_0 = -25e$ and $C_0 = 0.9681\mu M$ with lesser in magnitude compared to it. As the concentration of colloid increased to $4.84\mu M$ (Figure 4.19b) the $\beta V^{eff}(r)$ MS and $\beta V^{eff}(r)$ PY becomes negative at larger r/σ_{00} and repulsive at smaller r/σ_{00} . HNC shows repulsive interactions at shorter interparticle distance.

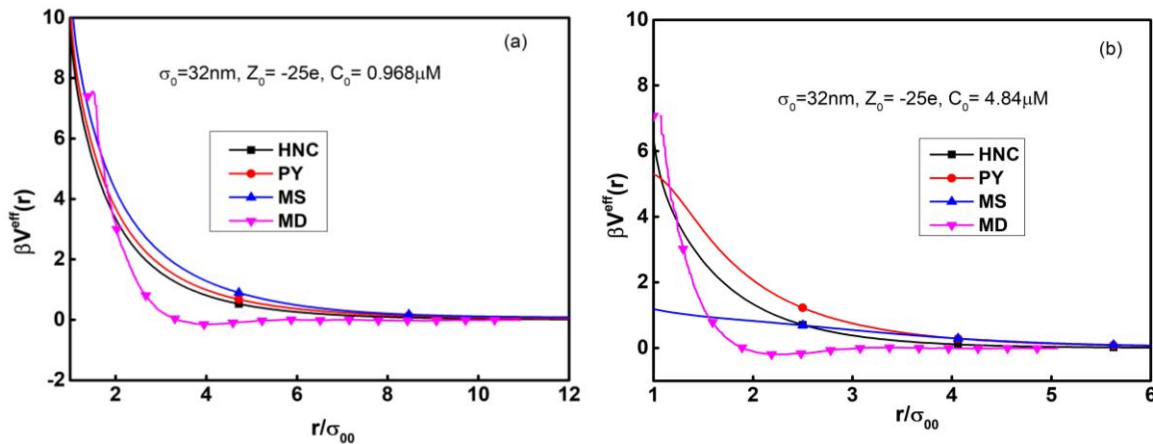


Figure 4.19: Comparison of $\beta V^{eff}(r)$ with different closures: HNC, PY and MS for two-component system at fixed $\sigma_0 = 32nm$ and $Z_0 = -25e$. (a) $C_0 = 0.9681\mu M$ (b) $C_0 = 4.84\mu M$

4.3.2.3.2. Effective direct correlation function

The $c_{00}^{eff}(r)$ of colloid-colloid was plotted in Figure 4.20. The values of $c_{00}^{eff}(r)$ HNC, $c_{00}^{eff}(r)$ PY and $c_{00}^{eff}(r)$ MS at $C_0 = 0.9681\mu M$ is -20.0 , -64.0 and -28.0 . The magnitude of the potential is larger and short range. When the concentration of the colloid increased to $C_0 = 4.84\mu M$ the magnitude of effective direct interactions between colloid-colloid decreases and value of $c_{00}^{eff}(r)$ HNC is -44.0 , $c_{00}^{eff}(r)$ PY is -51.0 and $c_{00}^{eff}(r)$ MS is -30.0 .

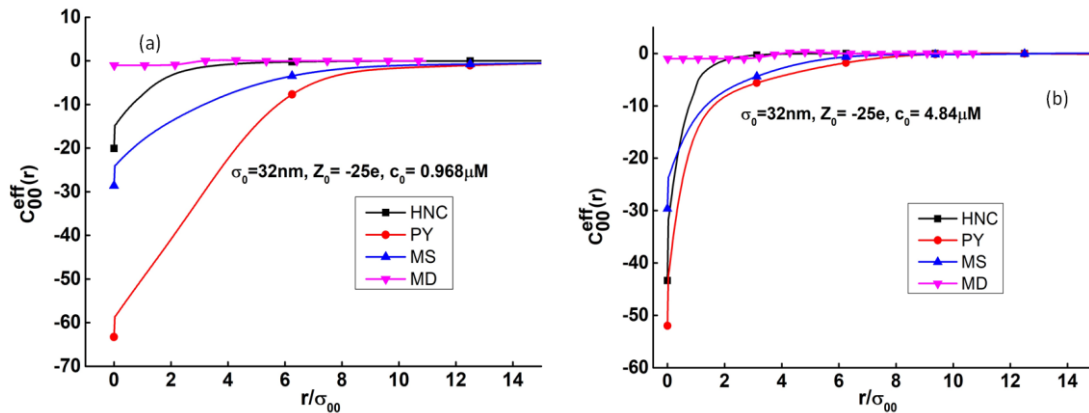


Figure 4.20: Comparison of $c_{00}^{eff}(r)$ with different closures: HNC, PY and MS for two-component system. Other parameters are same as in Figure 4.19.

4.3.3. Three-component system: HNC Results

4.3.3.1. Variation in colloid size:

4.3.3.1.1. Pair correlation functions:

The diameter of the colloid particle is varied from $\sigma_0 = 20$ to 100 nm at a fixed $Z_0 = -25e$, $C_0 = 0.968$ μM and $C_s = 4.84$ μM . The pair correlation functions are plotted in Figure 4.21 as a function of colloidal diameter. The peak height increases with increase in the diameter of the colloidal particle and the peak position shift towards lower interparticle distance Figure 4.21a. There is no structure in case of $\sigma_0 = 20\text{nm}$ and $\sigma_0 = 40\text{nm}$. The colloid-colloid repulsion is reduced with increase in diameter of the colloid. These results are very similar to those obtained for two-component systems. The effect of salt concentration ($C_s = 4.84$ μM) seems to be negligible in this case. The contact value of colloid-counterion (Figure 4.21b) decreases as the diameter of the colloid increases. This indicates the accumulation of counterions on the surface decreases. The counterion-counterion (Figure 4.21c) peaks are broader and peak height increases with increase in diameter of the colloid particle. The colloid-coion (Figure 4.21d) peak height increases steadily with increase in diameter of the colloid at $r/\sigma_{00} = 1.0$. The $g_{21}(r)$ i.e. counterion-coion (Figure 4.21e) peak height increases with increase in diameter of the colloid and the peaks are sharper. The $g_{22}(r)$ (Figure 4.21e) peak is broader and resembles $g_{11}(r)$.

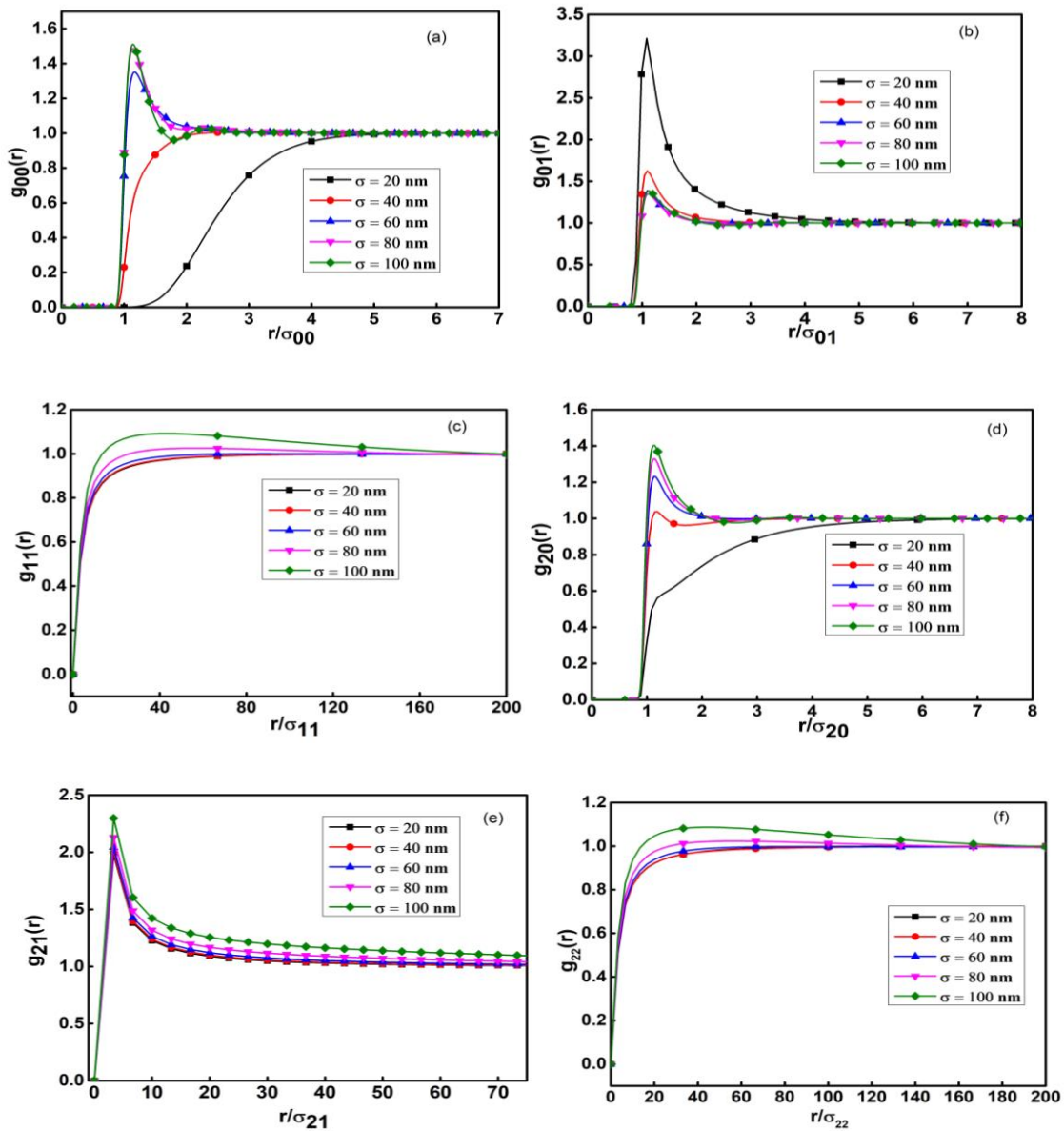


Figure 4.21: Variation of pair correlation functions (a) $g_{00}(r)$, (b) $g_{01}(r)$ and (c) $g_{11}(r)$ (d) $g_{20}(r)$, (e) $g_{21}(r)$ and (f) $g_{22}(r)$, as a function of colloid diameter at fixed $Z_0 = -25e$, $C_0 = 0.968 \mu\text{M}$ and $C_s = 4.84 \mu\text{M}$.

4.3.3.1.2. Direct correlation functions:

The direct correlation functions $c_{00}(r)$, $c_{01}(r)$, $c_{11}(r)$ were studied with variation in colloid diameter and presented in Figure 4.22. The colloid-colloid direct correlation function (Figure 4.22(a)) tends to increase with increase in diameter of colloid (-27.5 at $\sigma_0 = 100\text{nm}$ to -20.08

at $\sigma_0 = 20 \text{ nm}$). The colloid-counterion direct correlation functions $c_{01}(r)$ (Figure 4.22b) as well as counterion-counterion direct correlation functions $c_{11}(r)$ (Figure 4.22c) behaves similar to those of respective two-component systems.

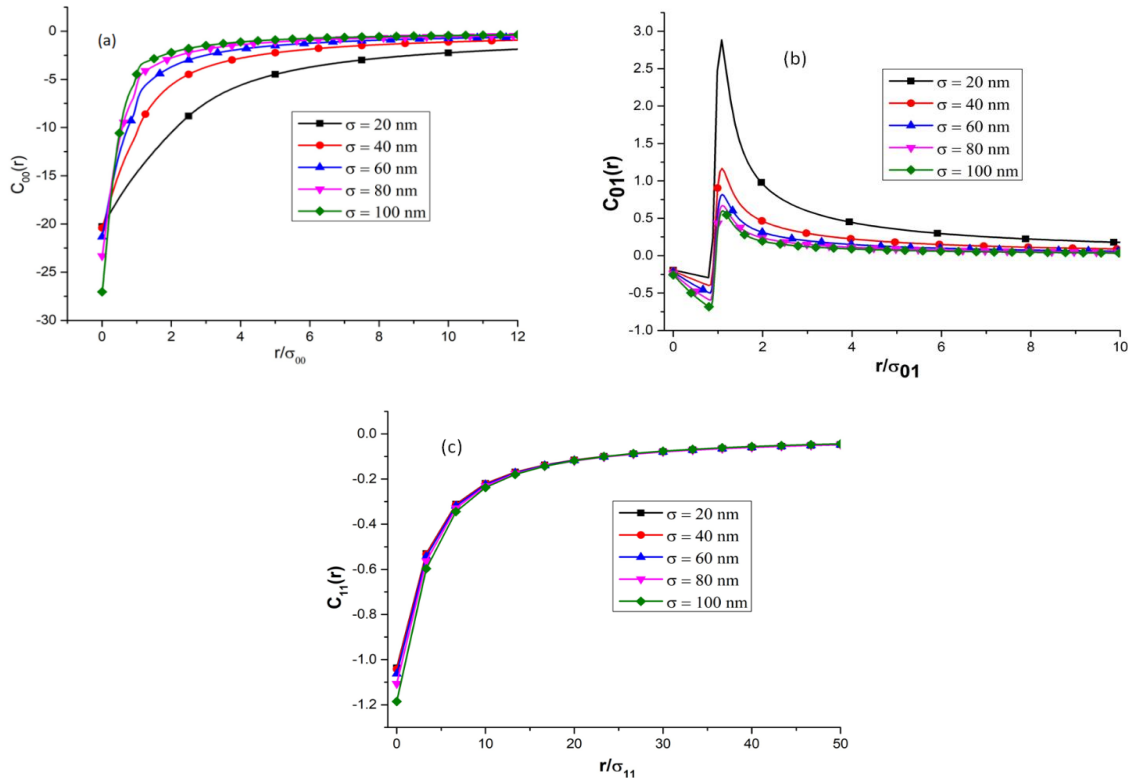


Figure 4.22: Plots of direct correlation functions (a) $c_{00}(r)$, (b) $c_{01}(r)$ and (c) $c_{11}(r)$, as a function of colloid diameter. Other parameters are same as in Figure 4.21.

4.3.3.1.3. Effective direct correlation functions:

The variation of $c_{00}^{eff}(r)$ with increasing colloid diameter is shown in Figure 4.23. The $c_{00}^{eff}(r)$ start from -20.04 for $\sigma_0 = 20 \text{ nm}$ (-27.6 for $\sigma_0 = 100 \text{ nm}$) and increases with inter-colloid distance and tends to zero. The feature is similar to the effective direct correlation functions of two-component system.

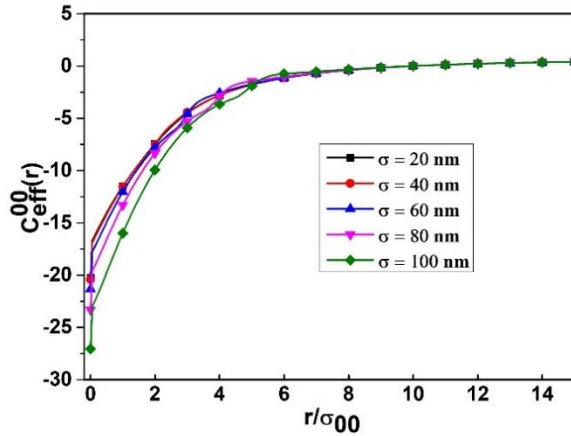


Figure 4.23: Plot of $c_{00}^{eff}(r)$ as a function of colloid diameter. Other parameters are same as in Figure 4.21

4.3.3.1.4. Effective potential and potential of mean force

The $\beta V^{eff}(r)$ shows attractive minima for all the diameters of the colloids (Figure 4.24a). The $\beta V^{eff}(r)$ shifts towards the lower interparticle distance with increase in diameter of the colloid. We noticed here that the $\beta V^{eff}(r)$ HNC of three-component colloidal system shows attractive behavior whereas $\beta V^{eff}(r)$ HNC of two-component colloidal system shows repulsive behavior. The salt concentration plays an important role for these attractive interactions in three-component colloidal system.

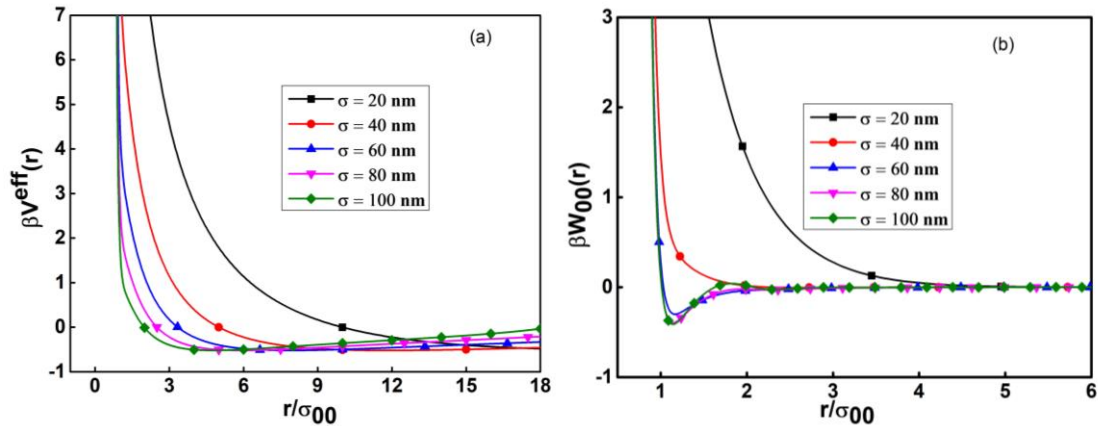


Figure 4.24: Plots of (a) $\beta V^{eff}(r)$ and (b) $\beta W_{00}(r)$, as function of colloid diameter. Other system parameters are same as in Figure 4.21.

The $\beta W_{00}(r)$ displayed in Figure 4.24(b) with increase in diameter of colloid becomes negative at $\sigma_0 = 60nm$, $\sigma_0 = 80nm$ and $\sigma_0 = 100nm$ shows less repulsions and eventually

becomes attractive. The $\beta W_{00}(r)$ shifts towards lower interparticle distance with increase in diameter of colloid.

4.3.3.2. Variation in colloid charge:

4.3.3.2.1. Pair correlation functions:

The effect of increasing colloidal charge was studied at fixed $\sigma_0 = 32\text{nm}$, $C_0 = 0.968\ \mu\text{M}$, $C_s = 4.84\ \mu\text{M}$ and shown in Figure 4.25. The $g_{00}(r)$ (Figure 4.25a) of three-component system is structureless and broad compared to the two-component systems. The peaks slightly shift to larger interparticle distance with increase in charge of the colloidal particle. With increase in charge of colloid, the magnitude of colloid-counterion correlation function $g_{01}(r)$ (Figure 4.25b) increases and peak position is at $r/\sigma_{00} = 1$ whose trend is opposite to the two-component colloidal system. The $g_{11}(r)$ (Figure 4.25c) correlation function is broader without any structure.

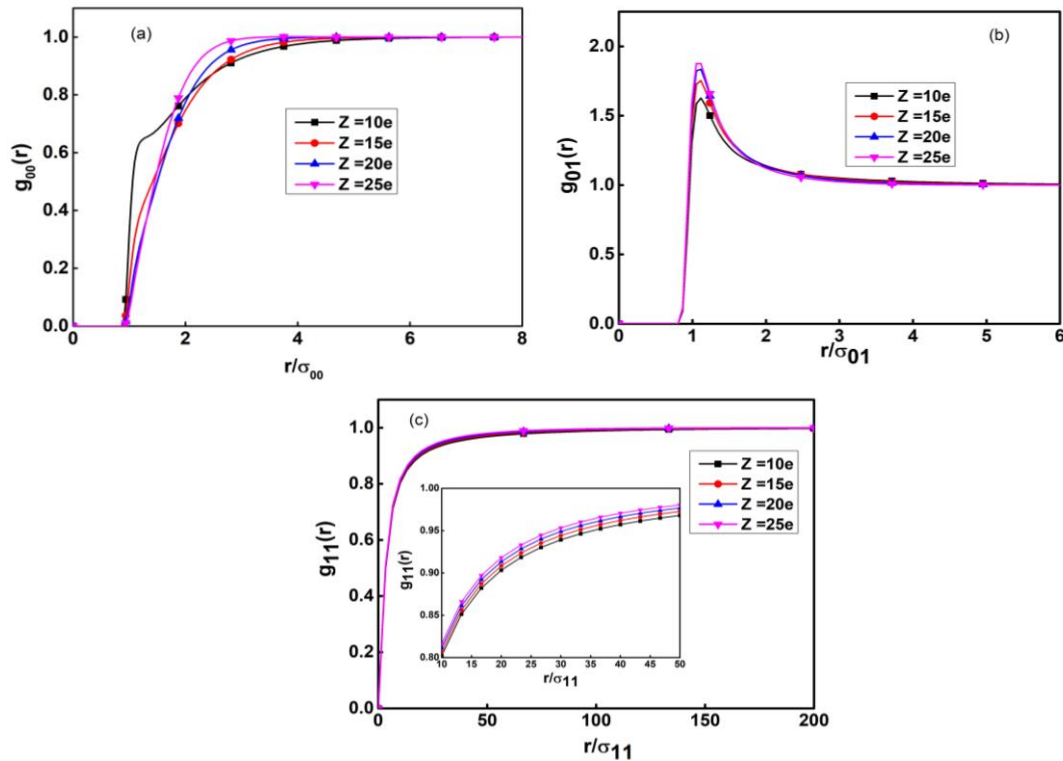


Figure 4.25: Plots of pair correlation functions (a) $g_{00}(r)$, (b) $g_{01}(r)$, (c) $g_{11}(r)$, as a function of colloid charge at fixed $\sigma_0 = 32\text{nm}$, $C_0 = 0.968\ \mu\text{M}$ and $C_s = 4.84\ \mu\text{M}$.

4.3.3.2.2. Direct correlation functions and effective direct correlation function

The direct correlation functions $c_{00}(r)$, $c_{01}(r)$, $c_{11}(r)$ with varying colloidal charge was studied and shown in Figure 4.26. With increasing charge of the colloid, the values of $c_{00}(r)$ systematically increases from -2.5 at $Z_0 = -10e$ to -20.6 at $Z_0 = -25e$.

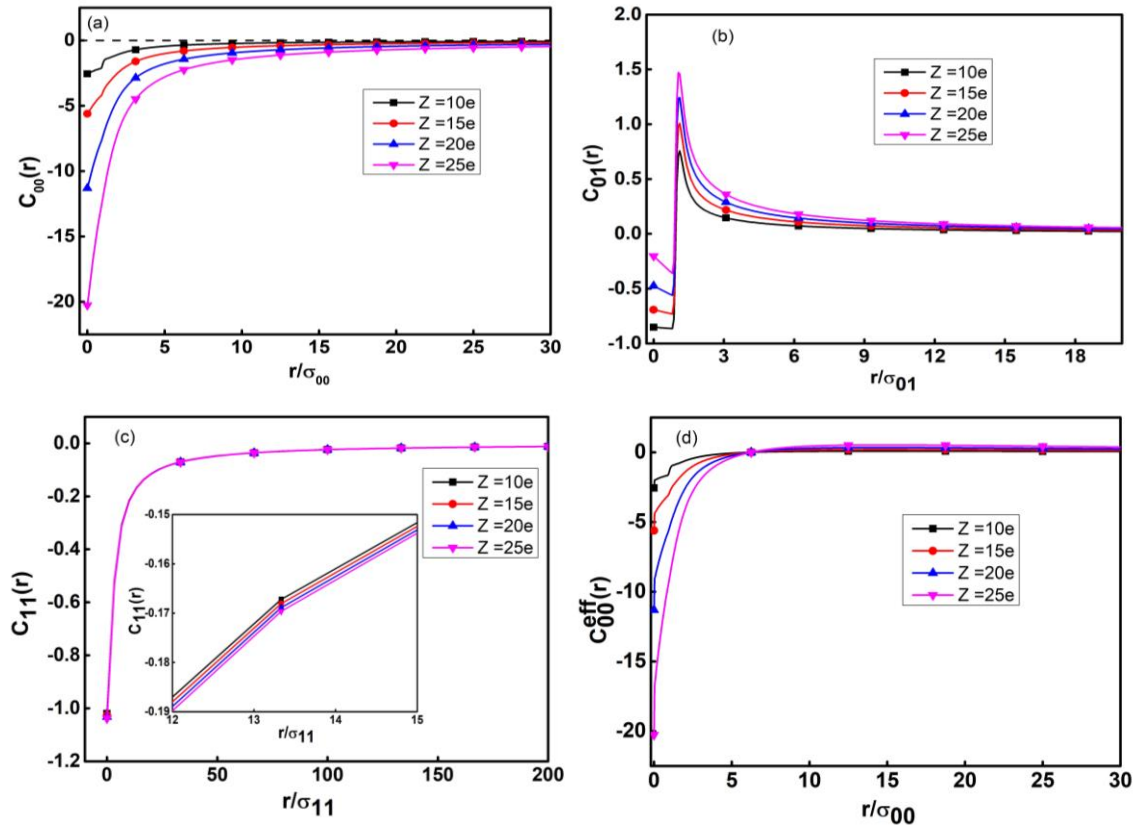


Figure 4.26: Plots of direct correlation functions (a) $c_{00}(r)$, (b) $c_{01}(r)$, (c) $c_{11}(r)$ and (d) $c_{00}^{eff}(r)$, as a function of colloid charge. Other parameters are same as in Figure 4.25.

The values of colloid-counterion direct correlation functions (Figure 4.26b) ranges from -0.8 at $Z_0 = -10e$ to -0.25 at $Z_0 = -25e$. The variation is prominent at shorter interparticle distance. The $c_{11}(r)$ (Figure 4.26c) doesn't show any variation with increase in charge of the colloidal particle. With increase in charge of colloid, the $c_{00}^{eff}(r)$ at short interparticle distances becomes negative with the values -5.57 (at $Z_0 = -10e$) to -20.56 (at $Z_0 = -25e$) (Figure 4.26d). The magnitude of potential decreases, becomes negative at smaller r and approaches to zero at larger r .

4.3.3.2.3. Effective potential and potential of mean force

The magnitude of $\beta V^{\text{eff}}(r)$ (Figure 4.27a) becomes more negative (attractive) with increase in charge. This might be because with increase in Z_0 , the coulomb repulsion between the colloidal particles increases and meanwhile the counterion condensation on the colloidal particles also increases. The depth of the minima are smaller compared to the corresponding two-component system. The $\beta W_{00}(r)$ (Figure 4.27b) shows repulsive behavior with all the cases of colloidal charge.

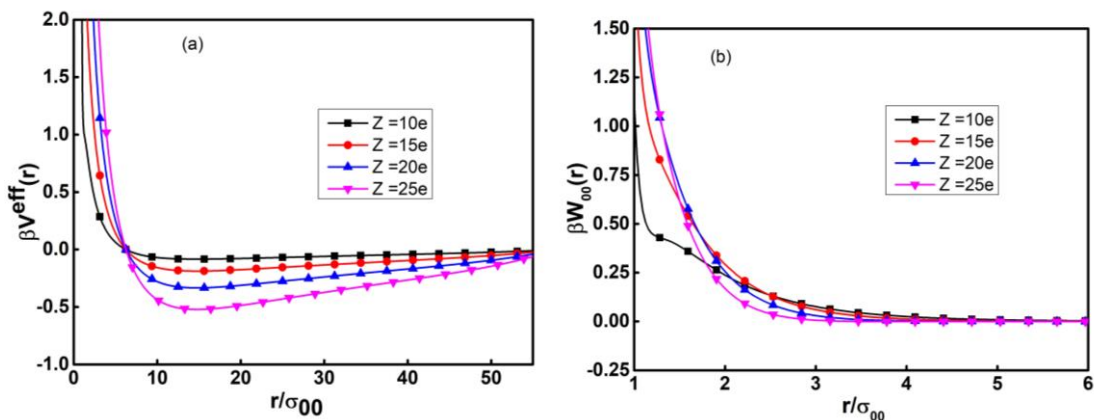


Figure 4.27: Plots of (a) $\beta V^{\text{eff}}(r)$ and (b) $\beta W_{00}(r)$, as a function of colloid charge. Other parameters are same as in Figure 4.25.

4.3.3.3. Variation in colloid concentration

4.3.3.3.1. Pair correlation functions

We have studied the pair correlation function with variation of colloid concentration at fixed $\sigma_0 = 32\text{nm}$ and $Z_0 = -25e$. The peak height of colloid-colloid ($g_{00}(r)$) correlation function displayed in Figure 4.28(a) increases with increase in colloid concentration. The peak position shifts towards shorter interparticle distance. On addition of salt, the peak heights become smaller compared to the corresponding two-component system. The $g_{00}(r)$ for colloid concentrations of $0.484\ \mu\text{M}$, $0.968\ \mu\text{M}$ and $1.936\ \mu\text{M}$ does not show any peak, similar to the two-component system. The contact values of colloid-counterion correlation function decreases (Figure 4.28(b)) with increase in colloid concentration. The $g_{11}(r)$ (Figure 4.28c) is structureless with broad peak for all colloid concentrations.

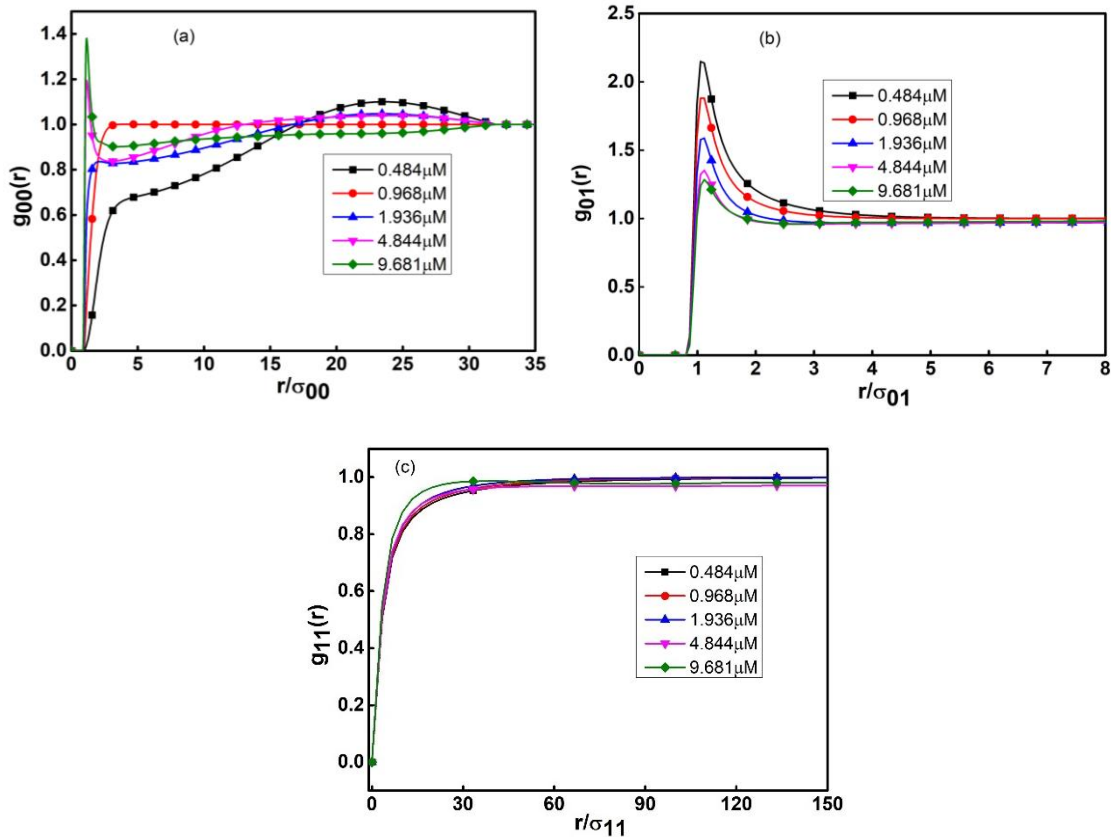


Figure 4.28: Plots of pair correlation functions (a) $g_{00}(r)$, (b) $g_{01}(r)$, (c) $g_{11}(r)$, as a function of colloid concentration at fixed $\sigma_0 = 32\text{nm}$ and $Z_0 = -25e$.

4.3.3.3.2. Direct correlation functions and effective direct correlation functions

We have studied the direct correlation functions $c_{00}(r)$, $c_{01}(r)$, $c_{11}(r)$ with varying colloid concentration and presented in Figure 4.29. The values of $c_{00}(r)$ (Figure 4.29a) increases from -15.0 at $C_0 = 0.484\mu\text{M}$ to -62.0 at $C_0 = 9.681\mu\text{M}$. The values of $c_{01}(r)$ (Figure 4.29b) ranges from -0.48 at $C_0 = 0.484\mu\text{M}$ to 1.5 at $C_0 = 9.681\mu\text{M}$. The prominent variations are observed at short interparticle distance. The $c_{11}(r)$ behaves similar to size variation. With increase in concentration of colloid, the HNC $C_{00}^{eff}(r)$ becomes negative at short interparticle distances (Figure 4.29(d)). With values -15.0 at $C_0 = 0.484\mu\text{M}$ and -62.0 at $C_0 = 9.681\mu\text{M}$. On addition of salt concentration, the $c_{00}^{eff}(r)$ behaves similar to the two-component colloidal system with concentration variation. The effect of salt seems to be negligible. The potential is negative at smaller r .

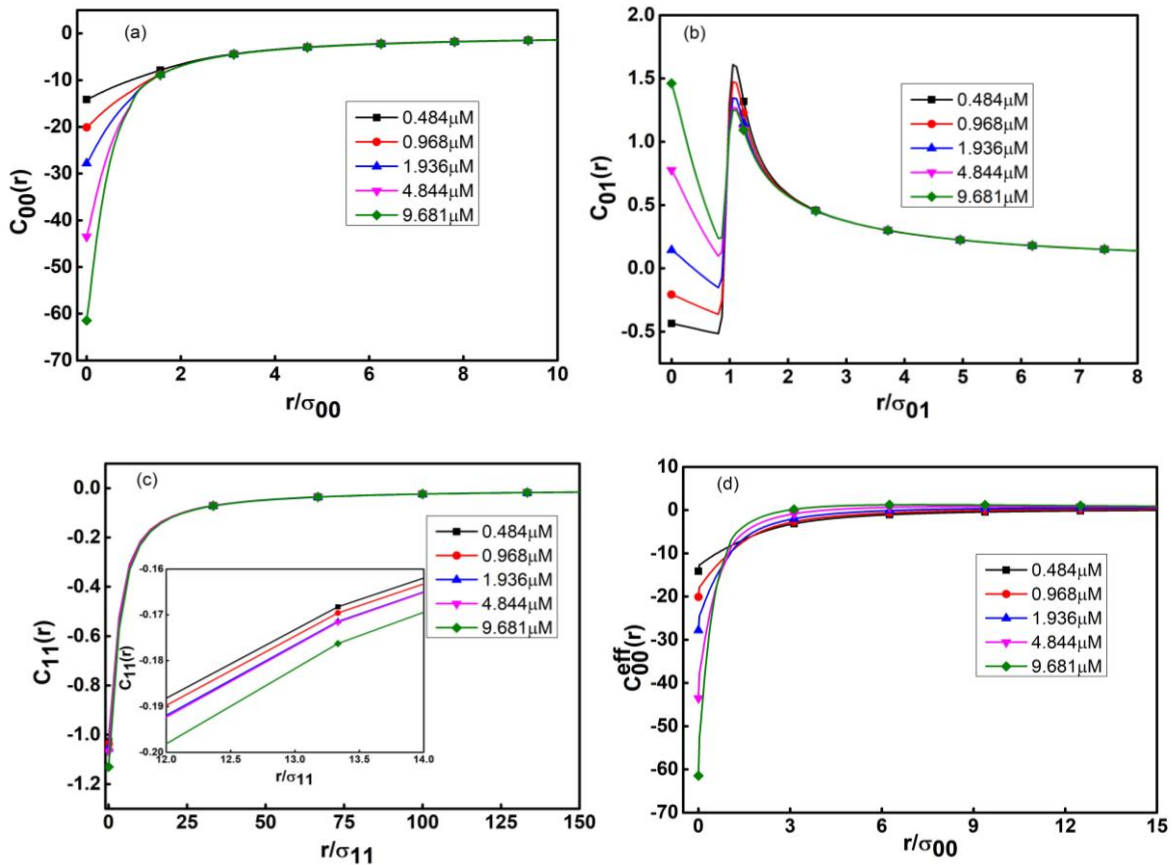


Figure 4.29: Plot of direct correlation functions (a) $c_{00}(r)$, (b) $c_{01}(r)$, (c) $c_{11}(r)$, and effective direct correlation function (d) $c_{00}^{\text{eff}}(r)$ as a function of colloid concentration. Other parameters are same as in Figure 4.28.

4.3.3.3.3. Effective potential and potential of mean force

The magnitude of $\beta V^{\text{eff}}(r)$ (Figure 4.30a) increases with increase in concentration of colloid and becomes negative at $C_0 = 0.9681 \mu\text{M}$, $1.936 \mu\text{M}$, $4.84 \mu\text{M}$, $9.681 \mu\text{M}$. The attractive minima increase with increase in colloid concentration and reaches -1.2 at $r/\sigma_{00} = 6.0$. With the colloid concentration of $0.484 \mu\text{M}$ the effective colloid-colloid interaction shows repulsive behavior. The $\beta V^{\text{eff}}(r)$ shifts towards lower inter-particle distance with increase in colloid concentration. The HNC $\beta W_{00}(r)$ (Figure 4.30b) is repulsive at $0.484 \mu\text{M}$, $0.968 \mu\text{M}$ and $1.936 \mu\text{M}$ and becomes attractive with increase in colloidal concentration ($C_0 = 4.84 \mu\text{M}$, $9.681 \mu\text{M}$) at shorter interparticle distance and becomes repulsive at larger interparticle

distance. The position of minima of $\beta W_{00}(r)$ shifts towards lower interparticle distance and the attractive HNC minima is found at $r/\sigma_{00} \sim 1.0$.

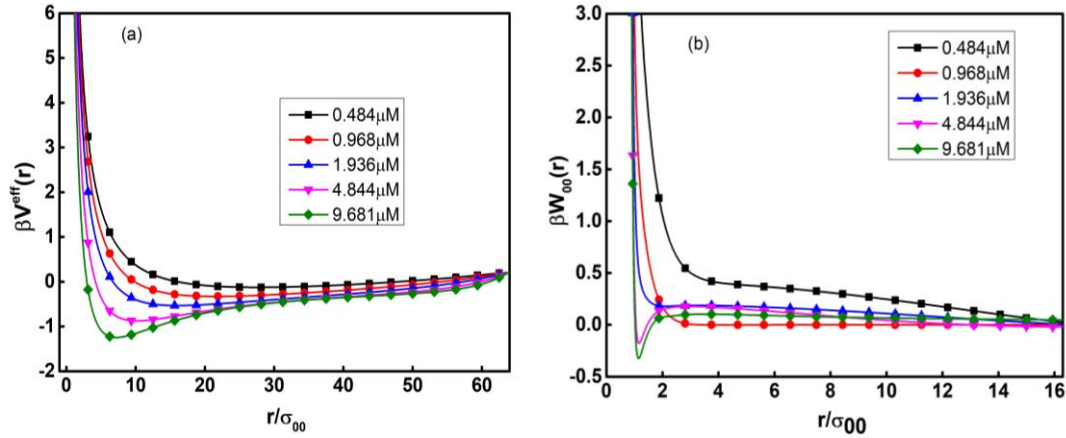


Figure 4.30: Plots of (a) $\beta V^{eff}(r)$ and (b) $\beta W_{00}(r)$ as function of colloid concentration. Other parameters are same as in Figure 4.28.

4.3.4. Comparison of different closures and MD results in three-component colloidal system:

We have studied the effect of different closure approximations on three-component colloidal systems as mentioned in section 4.3.2.

4.3.4.1. Size variation

4.3.4.1.1. Effective direct correlation functions

The colloid-colloid effective direct correlation function was studied and plotted in Figure 4.31. The colloid-colloid effective direct interactions for all three closures merge together (HNC=PY=MS). However, the MD results are different from this.

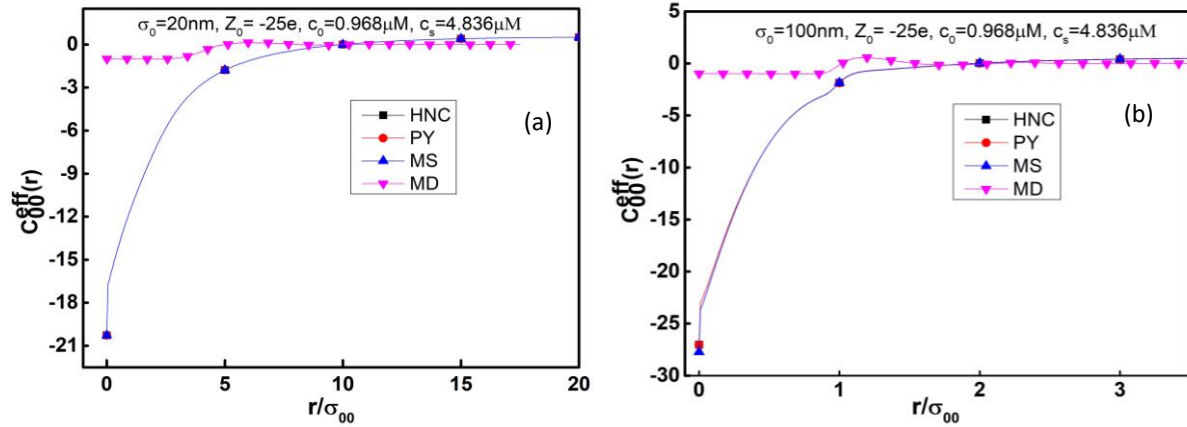


Figure 4.31: Comparison of $c_{00}^{eff}(r)$ with different closures: HNC, PY and MS for three-component system at fixed $Z_0 = -25e$, $C_0 = 0.968\mu\text{M}$ and $C_s = 4.836\mu\text{M}$. (a) $\sigma_0 = 20\text{nm}$ (b) $\sigma_0 = 100\text{nm}$

4.3.4.1.2. Effective potential

We have compared different closures with variation of colloid diameter at fixed $Z_0 = -25e$, $C_0 = 0.9681\mu\text{M}$ and $C_s = 4.836\mu\text{M}$. We studied the $\beta V^{eff}(r)$ for $\sigma_0 = 20\text{nm}$ and 100nm using

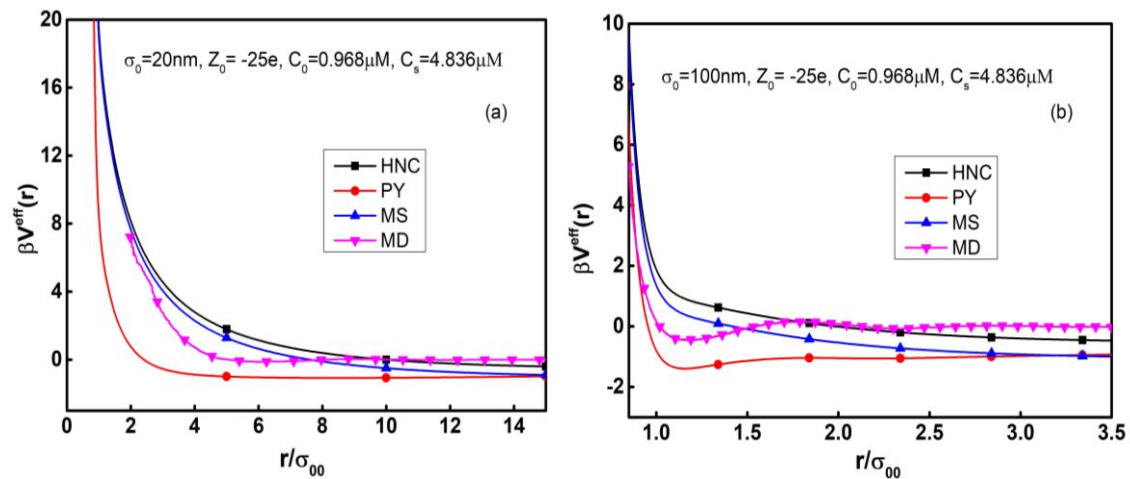


Figure 4.32: Comparison of $\beta V^{eff}(r)$ with different closures: HNC, PY and MS for three-component system. Other system parameters are same as mentioned in Figure 4.31.

different closures. Figure 4.32(a) shows that PY shifts towards lower interparticle distance and becomes attractive for larger r . The attractive minima for PY holds for larger r . For the

closures like HNC and MS the $\beta V^{eff}(r)$ is repulsive at lower interparticle distance and becomes attractive at larger interparticle distance. As the diameter of colloid is increased to $\sigma_0 = 100nm$ (Figure 4.32b), the attractive minima for PY $\beta V^{eff}(r)$ increases at lower interparticle distance i.e. $r/\sigma_{00} = 1.0$. On addition of salt, the closure becomes negative at larger interparticle distance and the order in the depth of the minima becomes PY > MS > HNC.

4.3.4.1.3. Potential of mean force

We have studied the $\beta W_{00}(r)$ (Figure 4.33a) of the system with same parameters as mentioned in Figure 4.32. For $\sigma_0 = 20nm$, the $\beta W_{00}(r)$ merges for all the closures and become purely repulsive. On addition of salt at $\sigma_0 = 20nm$, the PY and MS results becomes repulsive. There is no change with HNC approximation. When the diameter of colloid increased to $\sigma_0 = 100nm$ (Figure 4.33b) all the closures overlap and shows attractive minima.

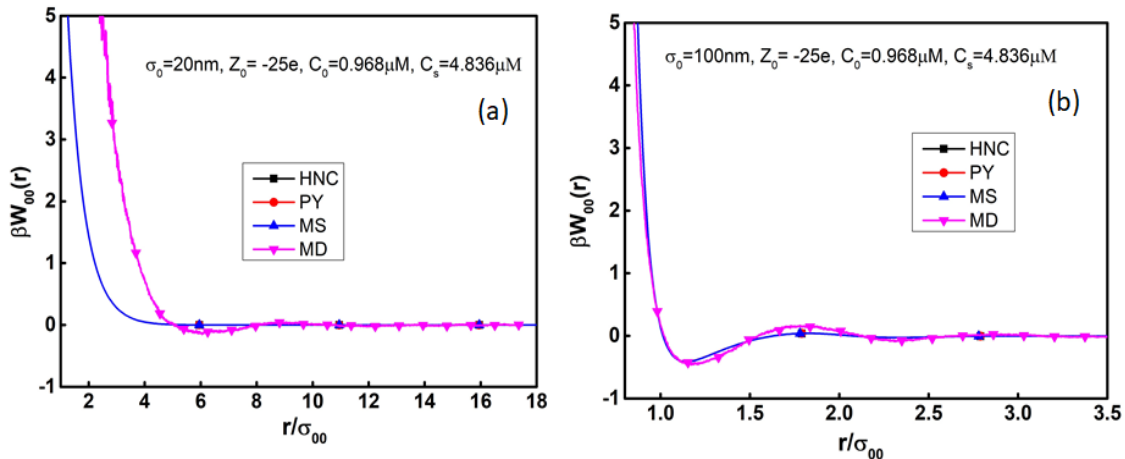


Figure 4.33: Comparison of $\beta W_{00}(r)$ with different closures: HNC, PY and MS for three-component system. Other parameters are same as in Figure 4.31.

4.3.4.2. Charge variation

4.3.4.2.1 Effective potential

We have studied the effect of closures with variation of colloid charge at fixed $\sigma_0 = 32nm$ and $C_0 = 0.9681\mu M$ and $C_s = 4.836\mu M$. The effective potential between the colloids $\beta V^{eff}(r)$ was studied for $Z_0 = -10e$ and $Z_0 = -25e$ using different closures. All the closures show

attractive behavior at $Z_0 = -10e$ (Figure 4.34(a)) at larger r . In presence of salt, the HNC, PY and MS becomes attractive. When the charge of the colloid increased to $-25e$ (Figure 4.34b), the HNC, PY and MS shows attractive interactions and the minima shift towards lower interparticle distance. The magnitude of $\beta V^{eff}(r)$ decreases and becomes negative. On addition of salt to the colloidal system, the PY becomes more attractive at lower interparticle distance which is opposite to two-component system. The order of attractive behavior is similar as the case of size variation (Figure 4.32a).

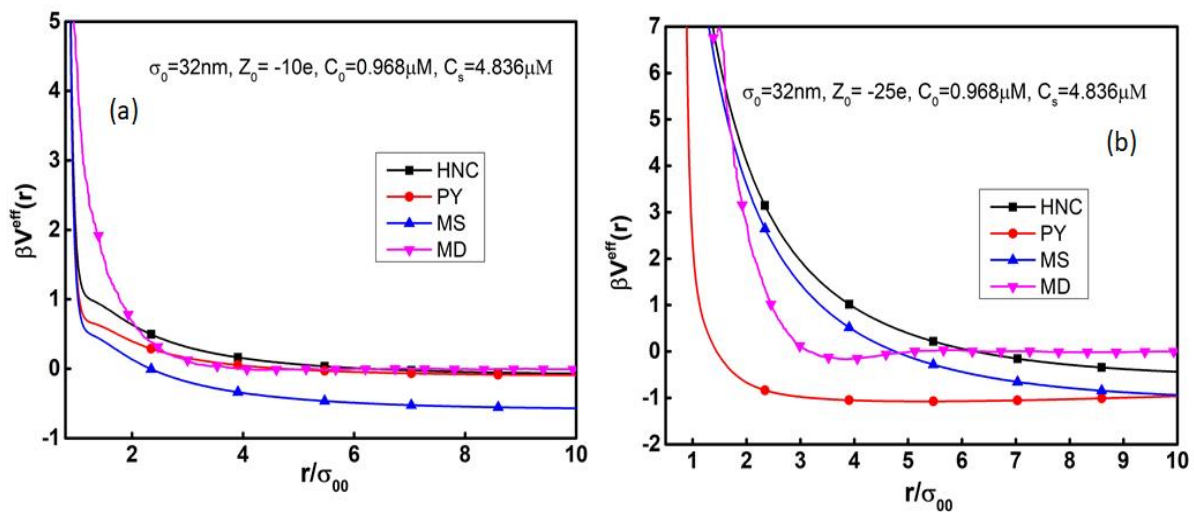


Figure 4.34: Comparison of $\beta V^{eff}(r)$ with different closures: HNC, PY and MS for three-component system at fixed $\sigma_0 = 32\text{nm}$, $C_0 = 0.9681\mu\text{M}$ and $C_s = 4.836\mu\text{M}$. (a) $Z_0 = -10e$ and (b) $Z_0 = -25e$

4.3.4.2.2 Potential of mean force

The colloid-colloid $\beta W_{00}(r)$ of the system with same parameters as mentioned in Figure 4.35 was studied. All the closures overlap and shows repulsive behavior with both charges $Z_0 = -10e$ and $Z_0 = -25e$. The PY and MS closures which showed attractive behavior in case of two-component colloidal system now shows repulsive interactions on addition of salt concentration $C_s = 4.836\mu\text{M}$.

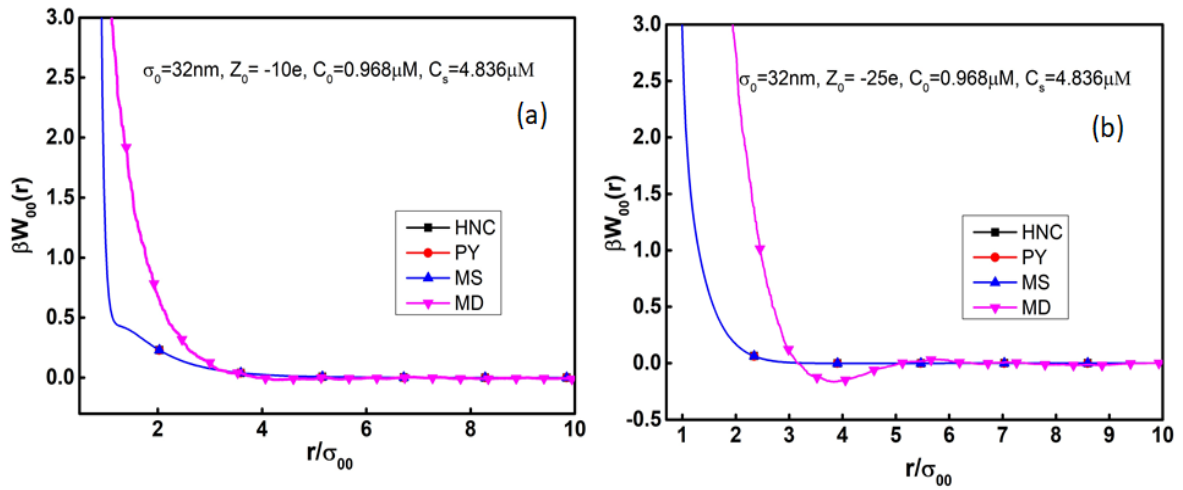


Figure 4.35: Comparison of $\beta W_{00}(r)$ with different closures: HNC, PY and MS for three-component system. Other parameters are same as in Figure 4.34.

4.3.4.2.3. Effective direct correlation function

The colloid-colloid $c_{00}^{eff}(r)$ was displayed in Figure 4.36. The $c_{00}^{eff}(r)$ for all the closures is same even when the charge of the colloid increased to $Z_0 = -25e$.

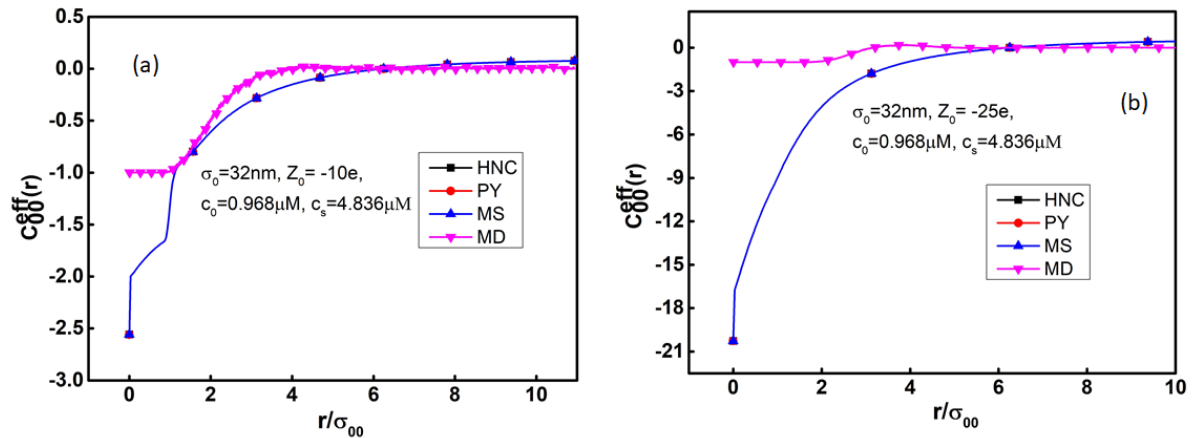


Figure 4.36: Comparison of $c_{00}^{eff}(r)$ with different closures: HNC, PY and MS for three-component system. Other parameters are same as in Figure 4.34.

4.3.4.3. Concentration variation:

4.3.4.3.1 Effective potential

We have studied different closures at fixed $\sigma_0 = 32\text{nm}$, $Z_0 = -25e$ with variation in colloid concentration. The effective potential $\beta V^{\text{eff}}(r)$ (Figure 4.37(a)) shows similar behavior as that of system with $\sigma_0 = 32\text{nm}$, $Z_0 = -25e$, $C_0 = 0.9681\mu\text{M}$, $C_s = 9.68\mu\text{M}$. As the concentration of colloid increased to $9.68\mu\text{M}$ (Figure 4.37b) all three closures becomes negative. The PY $\beta V^{\text{eff}}(r)$ becomes negative at $r/\sigma_{00} = 1.25$. The PY closure shifts towards shorter interparticle distance.

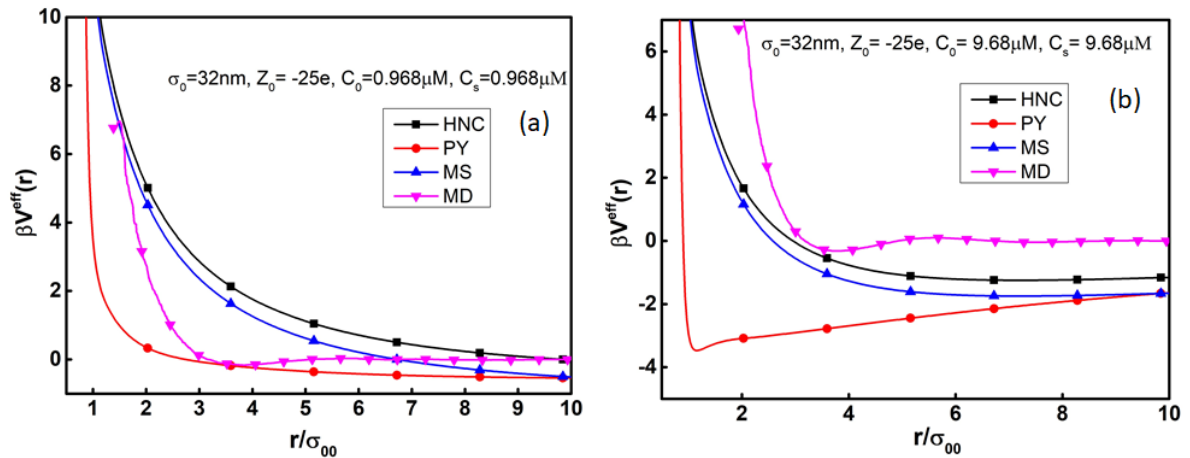


Figure 4.37: Comparison of $\beta V^{\text{eff}}(r)$ with different closures: HNC, PY and MS for three-component system at fixed $\sigma_0 = 32\text{nm}$ and $Z_0 = -25e$. (a) $C_0 = 0.9681\mu\text{M}$ (b) $C_0 = 9.681\mu\text{M}$.

4.3.2.3.2. Effective direct correlation function

The colloid-colloid $c_{00}^{\text{eff}}(r)$ was plotted in Figure 4.38. All the closures behave same irrespective of the concentration of colloid. As the concentration of colloid increased to $9.68\mu\text{M}$ (Figure 4.38b). In presence of salt concentration, the $c_{00}^{\text{eff}}(r)$ for all the closures behaves same without any deviation. However, the MD results are different from integral equation results.

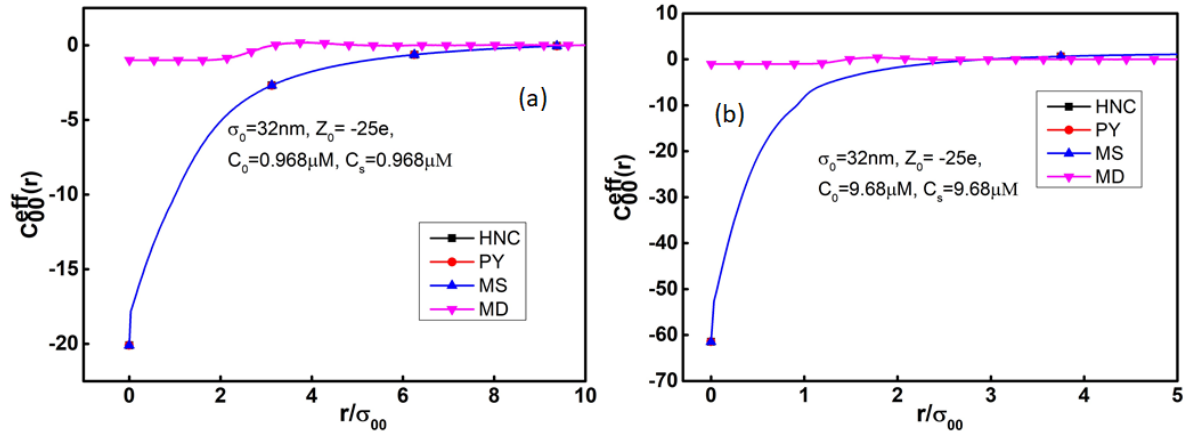


Figure 4.38: Comparison of $c_{00}^{eff}(r)$ with different closures: HNC, PY and MS for three-component system. Other parameters are same as in Figure 4.37.

4.3.2.3.3. Potential of mean force

The $\beta W_{00}(r)$ for colloid-colloid interaction was studied and plotted in Figure 4.39. At $C_0 = 0.9681\mu\text{M}$ and $C_s = 9.681\mu\text{M}$, all the closures show repulsive interactions and merged together. As the concentration of colloid and salt increased to $C_0 = 9.681\mu\text{M}$ and $C_s = 9.681\mu\text{M}$ (Figure 4.39b), all the closures become negative with attractive minima.

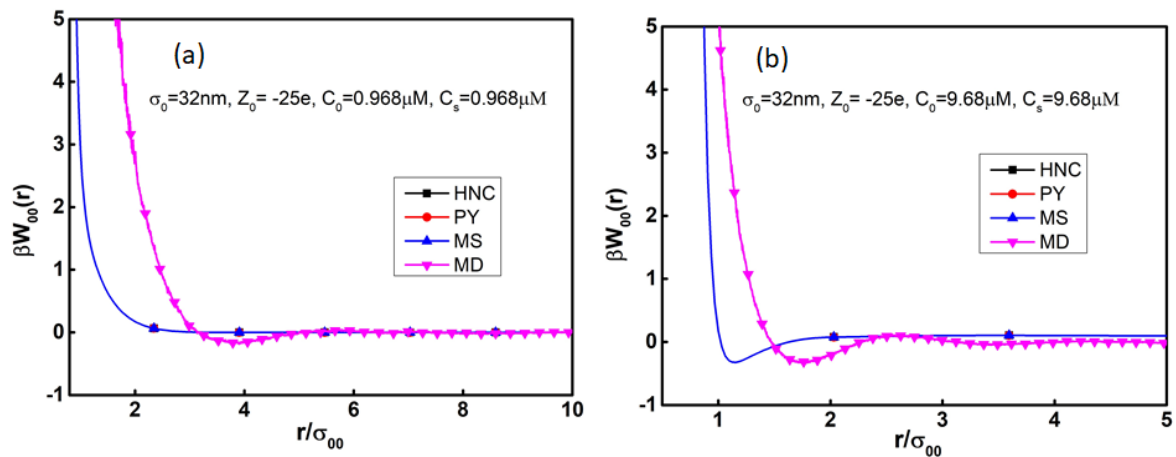


Figure 4.39: Comparison of $\beta W_{00}(r)$ with different closures: HNC, PY and MS for three-component system. Other parameters are same as in Figure 4.37.

4.4. Conclusion:

We used the integral equation formalism i.e. Ornstein Zernike Equation and solve it using Newton-GMRES algorithm for colloidal suspensions. The pair correlation functions, effective colloid potential of colloidal suspensions was studied with three different approximations: HNC, PY and MS. The performance of these approximations was analyzed with variation in size, charge and concentration of colloid. The pair correlation functions show systematic variations with size, charge and concentration of colloid with HNC theory. The effective colloid potential becomes repulsive with colloid size in a two-component system whereas it becomes attractive in three-component system. With increase in colloid charge and concentration, attractive behavior with both two-component and three-component colloidal systems were found. The potential of mean force becomes attractive with increase in size, charge and concentration of colloid in HNC theory for two-component system. The three-component systems behave similar to two-component systems with variation in size and concentration of colloid; opposite trends were found with charge variation. With increase in size, charge and concentration of the colloidal particle, the performance of HNC theory is better than those PY and MS theory. Few cases we compared with the molecular dynamics simulation results. HNC shows good agreement with MD simulation results for $\sigma_0 = 100\text{nm}$ and $Z_0 = -25e$ both for two-component and three-component systems. But PY shows good agreement only in three-component (added salt) systems. Generally, the integral equation results deviate substantially from that of simulation results. Among the studied closures, HNC seems to be closer to simulation than PY and MS for the studied systems.

4.5. References

- [1] J.A. Barker and D. Henderson, *What is "liquid"?* *Understanding the states of matter*, Rev. Mod. Phys. 48 (1976), pp. 587–671.
- [2] Z.-M. Chen and B.M. Pettitt, *Non-isotropic solution of an OZ equation: matrix methods for integral equations*, Comput. Phys. Commun. 85 (1995), pp. 239–250.
- [3] H.H.H. Homeier, S. Rast and H. Krienke, *Iterative solution of the Ornstein-Zernike*

- equation with various closures using vector extrapolation, *Comput. Phys. Commun.* 92 (1995), pp. 188–202.
- [4] G. Zerah, *An efficient Newton's method for the numerical solution of fluid integral equations*, *J. Comput. Phys.* 61 (1985), pp. 280–285.
- [5] C.T. Kelley, *Iterative Methods for Linear and Nonlinear Equations (Frontiers in Applied Mathematics vol 16)(Philadelphia: SIAM), (1995), .*
- [6] G.J. Ojeda-Mendoza, A. Moncho-Jordá, P. González-Mozuelos, C. Haro-Pérez and L.F. Rojas-Ochoa, *Evidence of electrostatic-enhanced depletion attraction in the structural properties and phase behavior of binary charged colloidal suspensions*, *Soft Matter* 14 (2018), pp. 1355–1364.
- [7] Y. Saad and M.H. Schultz, *GMRES: A generalized minimal residual algorithm for solving nonsymmetric linear systems*, *SIAM J. Sci. Stat. Comput.* 7 (1986), pp. 856–869.
- [8] L.S. Ornstein and F. Zernike, *Integral equation in liquid state theory*, in *Proc. Acad. Sci. Amsterdam*, 17 (1914), pp. 793.
- [9] J.M.J. Van Leeuwen, J. Groeneveld and J. De Boer, *New method for the calculation of the pair correlation function. I*, *Physica* 25 (1959), pp. 792–808.
- [10] J.K. Percus and G.J. Yevick, *Analysis of classical statistical mechanics by means of collective coordinates*, *Phys. Rev.* 110 (1958), pp. 1.
- [11] G.A. Martynov and G.N. Sarkisov, *Exact equations and the theory of liquids. V*, *Mol. Phys.* 49 (1983), pp. 1495–1504.
- [12] C.T. Kelley, *Solving Nonlinear Equations with Newton's Method*, Vol. 1, Siam, 2003.
- [13] C.T. Kelley and B.M. Pettitt, *A fast solver for the Ornstein--Zernike equations*, *J. Comput. Phys.* 197 (2004), pp. 491–501.
- [14] Y.V. Kalyuzhnyi and V. Vlachy, *Integral equation theory for highly asymmetric electrolyte solutions*, *Chem. Phys. Lett.* 215 (1993), pp. 518–522.

- [15] Y. V Kalyuzhnyi, V. Vlachy, M.F. Holovko and G. Stell, *Multidensity integral equation theory for highly asymmetric electrolyte solutions*, J. Chem. Phys. 102 (1995), pp. 5770–5780.
- [16] B. Hribar, Y. V. Kalyuzhnyi and V. Vlachy, *Ion-ion correlations in highly asymmetrical electrolytes*, Mol. Phys. 87 (1996), pp. 1317–1331.

Chapter 5
Conclusions and future scope

In this work, we studied the asymmetric binary mixtures with asymmetry in size, charge and mass ratio. The structural, thermodynamic properties and self-diffusion coefficient of these mixtures were studied using molecular dynamic simulations in chapter 2. These considerations were extended to model colloidal suspensions which mimic the realistic colloids in size, charge and concentration. The effective interactions between the colloids were discussed and compared the interactions between the two-component colloidal systems and three-component colloidal systems. We have investigated the structure, thermodynamic properties and self-diffusion coefficients of charged colloidal suspensions in bulk solutions in chapter 3. We have introduced the confinement in bulk solutions to study the influence of confinement on colloidal density and diffusion coefficient in chapter 3. In chapter 4, the model colloidal suspensions were investigated with formalism of integral equation theory i.e. Ornstein Zernike equation which is generalized using Newton-GMRES algorithm. Three different closure approximations were employed, and the performance of these approximations were analyzed with variation in size, charge and concentration of the colloid particle. These closures were compared with the MD results which were obtained in chapter 3.

We have reported the molecular dynamics simulation results for binary fluid mixtures having asymmetry in size, mass, charge and their combinations in chapter 2. A systematic variations in different properties as a function of charge, size and mass asymmetries have been observed. Possible explanation for these trends is presented in many cases. The pair correlation functions shift to larger inter-particle distances as the size and/or charge increases indicating increase in repulsion between particles. The mass variation has practically no effect. This may be due to the fact that mass doesn't appear explicitly in the expression for pair potential. With increase in size asymmetry, both the energy and pressure of the neutral systems decreases, an effect similar to decrease in density of the system. As the charge asymmetry increases, the interactions between the particles become long ranged and the magnitude of excess free energy increases. For a given charge asymmetry, higher excess free energy is found for size symmetric mixture than those of size symmetric case, possibly due to reduction in charge density. The self-diffusion coefficients are found to decrease with increase in size, charge and mass asymmetries. Arrhenius-type behavior is found for the diffusion coefficient. Empirical relations expressing diffusion coefficient of systems having more than one type of asymmetry

in terms of diffusion coefficient of systems having asymmetry of only one type, have been presented.

In chapter 3, we have studied model colloidal suspensions in bulk solutions as well as in between two walls using molecular dynamics simulations. The studies are carried out in a wide range of charge ($10e$ - $100e$), diameter (20 nm-100 nm), colloid concentrations ($0.484 \mu\text{M}$ - $2.42 \mu\text{M}$) and salt concentrations ($0 \mu\text{M}$ - $7.7 \mu\text{M}$). The correlation functions, effective colloid potential and different properties were determined using two-component and three-component primitive model. With increase in colloid charge, size and concentration, the peak height in $g_{00}(r)$ systematically increases. The depth of minima in the effective colloid-colloid potential are found to increase with increase in colloid charge, size and concentration. However, the position of the minima shifts to lower inter-colloid distance with increase in colloid size and concentration but remain more or less unaltered with increase in colloid charge. The effect of salt (in the range investigated) has very little effect. With the increase in counterion valency, the effective colloid-colloid potential becomes less attractive. For the cases of colloid suspensions in between two parallel walls, the density profiles functions for colloid become oscillatory indicating ordering/layering of particles. The oscillatory behavior is found to be pronounced for colloid with neutral walls or one positive and one negative wall. A systematic variation in the density profile of small particle/ion is also observed. The self-diffusion coefficient of neutral colloid is found to be higher than that of charged one irrespective of the nature of walls.

We used the integral equation formalism i.e. Ornstein Zernike Equation and solve it using Newton-GMRES algorithm for colloidal suspensions. The pair correlation functions, effective interactions of colloidal suspensions were studied with three different approximations: HNC, PY and MS. The performance of these approximations was analyzed with variation in size, charge and concentration of colloid. The pair correlation functions show systematic variations with size, charge and concentration of colloid with HNC theory. The effective potential becomes repulsive with colloid size in a two-component system whereas it becomes attractive in three-component system. With charge and concentration variation, attractive behavior with both two-component and three-component colloidal systems are found. The potential of mean force becomes attractive with increase in size, charge and

concentration of colloid in HNC theory for two-component system. The three-component systems behave similar to two-component systems with variation in size and concentration of colloid; opposite trends were found with charge variation. With increase in size, charge and concentration of the colloidal particle, the performance of HNC theory is better than those PY and MS theory. Few cases we compared with the molecular dynamics simulation results. HNC shows good agreement with MD simulation results for $\sigma_0 = 100\text{nm}$ and $Z_0 = -25e$ both for two-component and three-component systems. But PY shows good agreement only in three-component (added salt) systems. Generally, the integral equation results deviate substantially from that of simulation results. Among the studied closures, HNC seems to be closer to simulation than PY and MS for the studied systems.

Overall, with respect to “gaps in existing research” identified in chapter 1, we have carried out extensive molecular dynamics simulation data on model colloidal suspensions using primitive model with range of parameters: charge $Z_0 = 1e - 100e$, size $\sigma_0 = 0.6 \text{ nm} - 100 \text{ nm}$, colloid concentration $C_0 = 0.484 - 2.42 \mu\text{M}$, salt concentration $C_s = 0 - 7.7 \mu\text{M}$. Variations of effective colloid potential as a function of colloid charge, size and concentration have been studied. The effective potential becomes attractive as the charge/size/concentration of colloid increases. The trends in position and magnitude of the potential minima with system parameters have been identified. Alternatively, the structure and effective colloid potential have been calculated using Integral equation theories under HNC, PY and MS approximations. Using the recently developed Newton GMRES algorithm, we could able to increase the range of convergence substantially; e.g. colloid diameter upto 100 nm, concentration upto 12 μM . The results of different integral equation theories have been compared with MD simulation results.

Future Scope:

MD simulations of colloidal suspensions can be extended to wide range of system parameters (colloid charge, size, colloid concentration and salt concentration) and properties (e.g. thermal conductivity, heat coefficient, viscosity etc.)

Behavior of colloidal suspensions under confinement can be extended by varying the (i) charge on the confinement, (ii) confinement length, etc. Furthermore, it would be worthwhile to study the freezing phenomena in charged as well as uncharged confinement as a future work.

The quality and performance of the closure approximations can be improved (considering different closures, including bridge diagram sum etc, as well as developing robust algorithm).

LIST OF PUBLICATIONS AND CONFERENCES**List of publications**

- 1) Uday Kumar Padidela and Raghu Nath Behera, "Structure and effective interactions in model colloidal suspensions: A molecular dynamics simulation study", *Physics and Chemistry of Liquids*, (Under Review Manuscript ID: GPCH-2018-0212)
- 2) P. Udaykumar, R. N. Behera, "Molecular dynamics simulation study of colloidal suspensions under confinement", *Asian Journal of Chemistry*, 30(11), 2450-2454, 2018.
- 3) Uday Kumar Padidela, Tarun Khanna, and Raghu Nath Behera, "Structure, thermodynamics and diffusion in asymmetric binary mixtures: A molecular dynamics simulation study", *Physics and Chemistry of Liquids*, *Physics and Chemistry of Liquids*, 56 (5), 685-701, 2018.
- 4) Uday Kumar Padidela and Raghu Nath Behera, "Interactions in charged colloidal suspensions: A molecular dynamic simulation study", *AIP Conference Proceedings*, 1859:020111, 2017.
- 5) P. Udaykumar, T. Khanna and R. N. Behera, "Equilibrium structure and properties of model colloidal suspensions", *Research Journal of Recent Sciences*, 2(ISC-2012), 61-66, 2013. (Not part of thesis)

Conferences attended

- 1) Uday Kumar Padidela and Raghu Nath Behera. "Interactions in Charged Colloidal Suspensions: A Molecular Dynamic Simulation Study" in International Conference on Functional Materials, Characterization, Solid State Physics, Power, Thermal and Combustion Energy (FCSPTC)-2017 organized by Ramachandra College of Engineering, Eluru, Andhra Pradesh, 7th-8th April 2017.
- 2) Uday Kumar Padidela and Raghu Nath Behera, Integral equation studies of model colloidal suspensions: Comparison of different closure approximations, National Conference on NEW FRONTIERS IN CHEMISTRY- FROM FUNDAMENTALS TO APPLICATIONS (NFCFA 2015), BITS, Pilani-K. K. Birla Goa Campus, December 18-19, 2015.
- 3) Uday Kumar Padidela, Tarun Khanna and Raghu Nath Behera, "Structure and properties of model colloidal suspensions: Molecular Dynamics Simulation Study". One Day State Level Seminar on Advances in Colloid Chemistry sponsored by

UGC and organised by Department of Chemistry, Parvatibai Chowgule College of Arts and Science, Margao, Goa on 14th Feb 2015. (Second Prize).

- 4) P. Uday Kumar, T. Khanna and R. N. Behera, “Molecular Dynamics Simulation Study of Model Colloidal Suspensions”, Two Day Symposium on Chemistry with Computers, January 18-19, 2014, CSIR-IICT and IIIT, Hyderabad, India.
- 5) P. Udaykumar, T. Khanna and R. N. Behera, “Equilibrium Structure and Properties of model Colloidal suspensions”, 2nd International Science Congress, 8 – 9 December 2012, Mathura (UP), India.

Brief Biography of the Candidate

Name	Mr. Uday Kumar Padidela
Education	M.S. (Pharm), NIPER, Kolkata, 2011 B. Pharmacy, St. Peter's Institute of Pharmaceutical Sciences, (Kakatiya University), 2009
Email	padidelakumar@gmail.com

Academic Achievements:

- i) Qualified GATE–2009 (Pharmaceutical sciences).
- ii) Qualified NIPER JEE – 2009.

Professional Experience:

1. Senior Research Fellow in a CSIR sponsored project entitled “Study of Effective interactions in charged colloidal suspensions” at Department of Chemistry, BITS Pilani K.K. Birla Goa Campus; from May 2012 to Feb 2015.

Research Publications

03 publications in peer reviewed journals, 01 conference proceeding (Listed in Appendix-I)

Conferences/workshop attended during PhD

05 conferences (Listed in Appendix-I)

Brief Biography of Supervisor

Name	Dr. Raghu Nath Behera
Designation	Associate Professor, Department of Chemistry BITS-Pilani K. K. Birla Goa Campus
Education	PhD Chemistry, IIT Kanpur, 2001. Post-doctoral Fellow, Univ. of California, Davis, USA (Dec 1999 - Jun 2002). Scientific coworker, Univ. of Heidelberg, Germany (Aug 2002 - Nov 2003).
Email	rbehera@goa.bits-pilani.ac.in, raghu_behera@yahoo.com
Web Page	http://universe.bits-pilani.ac.in/goa/rbehera/profile
Areas of Research Interest	Theoretical and computational chemistry particularly, Statistical mechanics of macroionic solution Integral equation theory of fluid Molecular modeling & simulation Combining Quantum-Classical Calculations in studying Enzyme function Electronic structure calculations, Secondary Interactions, Atom-transfer radical polymerization
No of Sponsored Research Projects	Ongoing Project : 02, (SERB, DST) Completed Project : 01, (CSIR)

Our Ref: JB/GPCH/P18/1412

19 July 2018

Dear Uday Kumar Padidela,

Material requested: 'Structure, thermodynamics and diffusion in asymmetric binary mixtures: a molecular dynamics simulation study' by Uday Kumar Padidela, Tarun Khanna & Raghunath Behera *Physics and Chemistry of Liquids* (2017).

Thank you for your correspondence requesting permission to reproduce the above mentioned material from our Journal in your printed thesis and to be posted in the university's repository – Birla Institute of Technology and Science.

'This is the authors accepted manuscript of an article published as the version of record in *Physics and Chemistry of Liquids* © Taylor & Francis <https://doi.org/10.1080/00319104.2017.1407932> '

This permission does not cover any third party copyrighted work which may appear in the material requested.

Please note that this license does not allow you to post our content on any third party websites or repositories.

Yours sincerely

Jo Bateman – Permissions Administrator, Journals

Taylor & Francis Group

3 Park Square, Milton Park, Abingdon, Oxon, OX14 4RN, UK.

Tel: +44 (0)20 7017 7617

Fax: +44 (0)20 7017 6336

Web: www.tandfonline.com

e-mail: joanne.bateman@tandf.co.uk



Taylor & Francis Group
an informa business

**ROYAL SOCIETY OF CHEMISTRY LICENSE
TERMS AND CONDITIONS**

Jul 10, 2018

This Agreement between BITS Pilani KK Birla Goa Campus -- Uday Padidela ("You") and Royal Society of Chemistry ("Royal Society of Chemistry") consists of your license details and the terms and conditions provided by Royal Society of Chemistry and Copyright Clearance Center.

License Number	4385230190344
License date	Jul 10, 2018
Licensed Content Publisher	Royal Society of Chemistry
Licensed Content Publication	Faraday Discussions of the Chemical Society
Licensed Content Title	Properties of concentrated polystyrene latex dispersions
Licensed Content Author	Deryck J. Cebula,James W. Goodwin,G. Charles Jeffrey,Ronald H. Ottewill,Anthony Parentich,Rachel A. Richardson
Licensed Content Date	Dec 31, 1969
Licensed Content Volume	76
Licensed Content Issue	0
Type of Use	Thesis/Dissertation
Requestor type	academic/educational
Portion	figures/tables/images
Number of figures/tables/images	1
Format	print and electronic
Distribution quantity	1
Will you be translating?	no
Order reference number	
Title of the thesis/dissertation	Effective interactions and properties of model colloidal suspensions:Integral Equation theory and molecular dynamics simulation study
Expected completion date	Jul 2018
Estimated size	168
Requestor Location	BITS Pilani KK Birla Goa Campus NH 17B Road Zuarinagar Vascodagama Goa, Goa 403726 India Attn: BITS Pilani KK Birla Goa Campus
Billing Type	Invoice
Billing Address	BITS Pilani KK Birla Goa Campus

[Print This Page](#)